Accurate characterisation of seafloor acoustic response to improve seabed identification

Irène Mopin

THESE DE DOCTORAT DE

L'ECOLE NATIONALE SUPERIEURE
DE TECHNIQUES AVANCEES BRETAGNE

ECOLE DOCTORALE N° 648
Sciences pour l'Ingénieur et le Numérique
Spécialité : Signal, Image et Vision

Par

Irène MOPIN

Accurate characterisation of seafloor acoustic response to improve seabed identification

Thèse présentée et soutenue à Brest, le 15 mars 2023
Unité de recherche : Lab-STICC UMR6285

Rapporteurs avant soutenance :

Luciano FONSECA	Professeur, Université de Brasilia (Brésil)
François OLLIVIER	Maître de conférences HDR, Sorbonne Université (France)

Composition du Jury :

Président :	Jérôme MARS	Professeur, INP Grenoble (France)
Examinateurs :	Isabelle QUIDU	Maître de conférences HDR, ENSTA Bretagne (France)
Dir. de thèse :	Benoît ZERR	Professeur, ENSTA Bretagne (France)
Co-dir. de thèse :	Philippe BLONDEL	Professeur, Université de Bath (Royaume-Uni)

Invité(s)

Gilles LE CHENADEC	Enseignant-chercheur, ENSTA Bretagne (France)
Jacques MARCHAL	Maître de conférences, Sorbonne Université (France)
Michel LEGRIS	Enseignant-chercheur, ENSTA Bretagne (France)

Accurate characterisation of seafloor acoustic response to improve seabed identification

Irène Mopin

15/03/2023

À ma grand-mère,

et tous ceux partis durant ces trois années...

Acknowledgments

Les premiers mots de ce manuscrit sont aussi les derniers, rédigés loin de l'effervescence de la soutenance. Sérénité. Je suis heureuse de clore ce manuscrit, de marquer la fin de cette aventure scientifique et humaine de trois ans qui a su se frayer un chemin entre pandémie, guerre en Ukraine, réchauffement climatique, perte d'une partie de bâtiment, et grève SNCF. Vient le moment de faire le point, de ranger ses cahiers manuscrits, d'effacer le tableau. Et aussi de se souvenir et rembobiner pour remercier tous ceux qui ont compté.

Il va donc sans dire que je souhaite en premier lieu remercier mes directeurs de thèse et encadrants. Merci à Benoît d'avoir insisté pendant plusieurs années et de m'avoir soutenue coûte que coûte. Merci à Philippe de m'avoir accueillie si gentillement à Bath et de m'avoir accompagnée dans tous mes périples Outre-Manche. Merci à Gilles de m'avoir fait confiance et de m'avoir supportée trois ans ! Merci à Jacques pour son soutien technique au top. Et merci... à Michel pour m'avoir si bien non-encadrée en discutant, corrigeant, relisant mes productions tout au long de ces trois années.

Un immense merci à tous les membre du jury. En particulier à Luciano et François pour avoir accepté de relire ce gros manuscrit. Et aussi à Jérôme et Isabelle pour s'être prêtés aux rôles d'examinateurs. Merci à vous tous pour vos remarques et vos conseils pour la suite. J'espère vous retrouver bientôt pour discuter et collaborer sur ces sujets d'acoustique sous-marine passionnants. Et puisqu'on évoque la soutenance, merci à tous ceux qui sont venus, nombreux, y assister !

Cette thèse n'aurait pas eu lieu sans le soutien de l'AID, de la DGA et de DSTL que je remercie fortement pour leur confiance. De même, je tiens à remercier l'ENSTA Bretagne, l'université de Bath, le Lab-STICC et Sorbonne Université pour leur accueil dans leurs équipes et leurs locaux. Une grande partie du matériel technique utilisé durant cette thèse a aussi été financé par l'Union Européenne (FEDER/Bretagne). Merci au GT SISO de l'ENSTA Bretagne de m'avoir transmis cette opportunité.

Les travaux présentés dans ce manuscrit n'auraient pas pu se faire sans les équipes du département STIC de l'ENSTA Bretagne. Je les remercie amplement pour leur bienveillance, leur soutien scientifique, technique et moral, et leur enthousiasme. Chercheurs, enseignants, ingénieurs, techniciens, thésards, et administratifs, tous ont contribués au bon déroulement

de mes recherches. Je ne les cite pas individuellement, mais chacun se reconnaîtra, à sa manière, dans ces courts mots, j'espère. Je remercie aussi tous les autres collègues de l'ENSTA Bretagne qui ont pu m'aider dans mon parcours d'apprentie-chercheure : direction, administratifs, communication, gestions... Merci à vous.

De même, je remercie les équipes de Sorbonne Université et de l'université de Bath qui m'ont accueillie et ont travaillé avec moi pendant de courtes – mais intenses – périodes ! En particulier, merci à Christian, Hélène, Anne, Shaula, Gianluca, Zuhayr, et Alfie.

La recherche allant de pair avec l'enseignement, je profite de ces mots pour remercier les étudiants ayant participé aux projets sur la rétro-diffusion – du fond et de la colonne d'eau – : étudiants de l'ENSTA Bretagne, de l'IUEM, et élèves des classes préparatoires venus pour leurs TIPEs.

Enfin, merci à ma famille pour leur soutien. Merci à ceux qui ne sont plus là pour la fin, mais qui étaient au rendez-vous au début. Merci aux amis, proches, moins proches, et lointains. Et surtout, merci à Grégoire sans qui rien ne serait possible.

Contents

List of Symbols

Media characteristics

$\alpha_{\mathbf{s}}$ Attenuation coefficient of compressional waves in sediment. 22, 23, 34, 37, 43
$\alpha_{\mathbf{w}}$ Attenuation coefficient of compressional waves in water. 23, 37, 58, 75
$c_{\mathbf{s}}$ Sound speed in a fluid seafloor. 7, 12, 24
$c_{\mathbf{sw}}$ Ratio of sound speed of the seafloor over sound speed of the water. 33, 40
$c_{\mathbf{w}}$ Sound speed in the sea water. 4, 7, 12, 24, 56
$\rho_{\mathbf{s}}$ Density of the seafloor. 7, 12, 24, 37
$\rho_{\mathbf{sw}}$ Ratio of density of the seafloor over density of the water. 33, 40
$\rho_{\mathbf{w}}$ Density of the sea water. 7, 12, 24, 37, 56
$Z_{\mathbf{s}}$ Acoustic characteristic impedance of the seafloor as an homogeneous medium. 22–24
$Z_{\mathbf{w}}$ Acoustic characteristic impedance of the sea water. 22–24

Seafloor acoustic response

R Pressure reflection coefficient at a fluid/fluid plane interface. 24, 26, 32, 43
s Scattering strength. 37
S Scattering strength in decibels. 25
$\mu_{\mathbf{L}}$ Lambert parameter. 22, 28–31
σ Parameter of the Rayleigh probability density function. 27, 103, 110, 111, 113, 114, 128, 161, 162, 235
BS Backscattering strength in decibels. 25, 72, 73, 75, 82, 110, 111, 114, 118, 124, 128, 153, 165, 232, 235, 236
bs Backscattering strength. 28, 39, 40, 66, 83, 110, 111, 118
$\mathbf{bs}$ Backscattering strength as a random variable. 83, 111, 124, 128, 232, 233
$\widehat{\mathrm{BS}}$ Backscattering strength estimate in decibels. 118, 119
a_i Backscattering index amplitude (complex) of a i^{th} scatterer on the seafloor. 84
a Scattering index amplitude of one scatterer of the seafloor (complex). 83, 101, 232, 233
A Complex backscattering index amplitude of the seafloor. 100, 110
$A_{\mathbf{dB}}$ Amplitude of the backscattering index of the seafloor in decibels. 104
$|A|$ Modulus of the complex backscattering index amplitude of the seafloor. 84
$\mathbf{A}$ Amplitude of the backscattering index of the seafloor as a random variable. 124
$\mathbf{A_{dB}}$ Amplitudes of the backscattering index of the seafloor as a random variable in decibels. 104
$\mathbf{A}^{(i)}$ Imaginary parts of the backscattering index amplitude of the seafloor as a random variable. 103, 110

$|\mathbf{A}|$ Modulus of the complex backscattering index amplitude of the seafloor as a random variable. 103, 105–107, 109–111, 114, 115, 119, 121–124, 198, 233, 236

$\mathbf{A}^{(r)}$ Real part of the backscattering index amplitude of the seafloor as a random variable. 103, 110

φ Phase of the complex backscattering index of the seafloor. 100

$\boldsymbol{\varphi}$ Phases of the complex backscattering index of the seafloor as a random variable. 103, 110

ϕ Phase of one scatterer of the seafloor. 84, 101, 102, 232, 233

Echosounder directivity

ϑ_x Angle inside the directivity pattern or directivity function in direction x. 59

ϑ_y Angle inside the directivity pattern or directivity function in direction y. 59

$\mathcal{D}$ Directivity pattern or directivity function. 54, 57, 59, 68, 83, 84

$\theta_{\mathbf{-3dB}}$ Main beam angular half-aperture defined at -3dB. 68

Φ 2D equivalent beam width. 67, 68

Ψ 3D beam equivalent solid aperture. 68

Geometry

$\mathcal{A}$ Area of the seafloor insonified by an acoustic source. 38, 51, 66, 67, 75, 100, 153, 161, 162

h Height of the echosounder above the seafloor or height at nadir. 68

M Number of scatterers in the insonified area. 101, 102

θ Any angle of the scattered acoustic wave from the seafloor with respect to the vertical axis. 25, 37, 38

$\theta_{\mathbf{i}}$ Angle of the incident acoustic wave on the seafloor with respect to the vertical axis. 22–24, 26, 27, 34, 35, 40, 44, 72, 75, 85, 118, 232

$\theta_{\mathbf{r}}$ Angle of the reflected acoustic wave on the seafloor with respect to the vertical axis. 24

$\theta_{\mathbf{t}}$ Angle of the transmit acoustic wave on the seafloor with respect to the vertical axis. 24, 43

Interface characteristics

$\vec{k}$ Two-dimensional spatial wave-number of the surface roughness. 33

$k_{\mathbf{c}}$ Spatial cut-off wave number of the seafloor relief. 23, 33, 39–41

$\zeta_{\mathbf{ss}}$ Bottom small-scale roughness or microroughness. 31, 40

$\sigma_{\zeta_{\mathbf{ss}}}$ Root mean square Root mean square (RMS) of small-scale roughness or microroughness. 32, 33, 40–42

σ_ψ Root mean square RMS slope of the seabed interface. 22, 31–34, 41

σ_ζ Root mean square RMS of the interface roughness $\zeta(\vec{x})$. 22, 27

$\mathcal{R}$ Rayleigh roughness parameter. 27, 32

ψ Local slope of the seabed interface. 33, 41, 77

ζ Bottom roughness function $z = \zeta(x, y)$. 26, 31, 38, 40, 42

σ_ζ^2 Spatial variance of the interface roughness $\zeta(\vec{x})$. 38, 42

$W(\vec{k})$ Two-dimensional roughness spectrum (Power spectra describing the seafloor roughness). 33, 38, 40, 112, 113

Mathematical tools

$J_0(.)$ Zero-order Bessel function of the first kind. 42, 105

$I_0(.)$ Modified zero-order Bessel function of the first kind. 106
$K(.)$ Modified Bessel function of the second kind. 107

Signals characteristics

$A_{\mathbf{i}}$ Amplitude of the incident signal on the seafloor. 23, 38, 100, 110
$A_{\mathbf{s}}$ Amplitude of the scattered signal from the seafloor. 38, 39, 100, 110
ƒ Frequency of an acoustic signal. 4, 22, 30, 35, 44, 72, 85, 118, 174, 232
$I_{\mathbf{bs}}$ Backscattered intensity of an incident acoustic wave from the seafloor. 24
$I_{\mathbf{i}}$ Intensity of the incident acoustic wave on the seafloor. 24, 110
$I_{\mathbf{s}}$ Scattered intensity of an incident acoustic wave from the seafloor in all directions. 25, 27, 110
$k_{\mathbf{i}}$ Wave number of the incident acoustic wave on the seafloor. 22, 23, 26, 27, 32
λ Wavelength of the incident signal. 6, 40
τ Transmit pulse length. 4, 8, 66–68, 174

Transducer and electronics

$\beta_{\mathbf{Tx}}$ Efficiency of the transmitting transducer. 57
$V_{\mathbf{Tx}}$ Input voltage given to the transmitting transducer. 57

Acronyms

ARC Angular Response Curves. 72, 80, 81, 89, 215–218, 226, 236, 238

CW Continuous Wave. 4, 50, 51, 64–67, 69, 70, 114, 188

DTM Digital Terrain Model. 76, 86, 95, 96, 116, 158, 223, 226, 230, 237

FLS Forward Looking Sonar. 3

GeoHab Marine Geological and Biological Habitat mapping conference. 35
GESMA *Groupe d'étude sous-marine de l'Atlantique (France).* 35
GNSS Global Navigation Satellite System. 2
GSAB Generic Seafloor Acoustic Backscatter. 35, 72, 76

IHO International Hydrographic Organisation. 5

LBL Long Base Line. 2

MBES MultiBeam EchoSounder. 3, 12, 77, 220, 230
MLE Maximum Likelihood Estimation. 118, 128, 130–132, 137, 138, 234

NRE Naval Research Establishment, Dartmouth, Nova Scotia, Canada. 42

PDF Cumulative Density Function. 135
PDF Probability Density Function. 27, 100, 103–108, 119, 120, 122, 135
PZT Lead zirconate titanate. 169, 172, 173

RFM Rough Facet Model. 32
RMS Root Mean Square. 23, 26, 27, 31, 32, 40–42, 50, 53, 56, 61, 62, 83, 110, 112, 124

SBES SingleBeam EchoSounder. 3, 12, 230
Shom *Service Hydrographique et Océanographique de la Marine (France).* 10, 82
SNR Signal to Noise Ratio. 49–51, 62, 64
SSS Side-Scan Sonar. 3

TPU Total Propagated Uncertainty. 238

USBL Ultra Short Base Line. 2

Chapter 1

Introduction

The majority of remote sensing systems is currently using electromagnetic waves or optical waves as vectors for information in various applications. Sound waves are also employed but less democratized in particular in domains such as cartography or positioning. That is why acoustics is mostly used for specific usages such as communication (e.g. speech, telephony) and art (e.g. music). Underwater, issues are different because the only physical phenomenon that can transport information without being rapidly absorbed by the medium is sound. Consequently, all remote sensing applications have developed a subaquatic equivalent using acoustic waves. For example, Global Navigation Satellite System (GNSS) underwater counterparts are systems called Long Base Line (LBL) or Ultra Short Base Line (USBL) [Audric, 2004], and optical cameras are replaced by acoustic cameras.

As with other types of waves, a large variety of wavelengths or frequencies are available. A subjective classification of frequencies will be used in this manuscript considering that our works only involve underwater active systems (see figure 1.1). The underwater acoustics frequency range is thus divided in three domains:

- Low frequencies: [10, 80] kHz
- High frequencies: [80, 400] kHz
- Very high frequencies: [400, 700] kHz

Only frequencies between 10 kHz and ∼700 kHz are considered in the following works, especially during discussions about applications and systems.

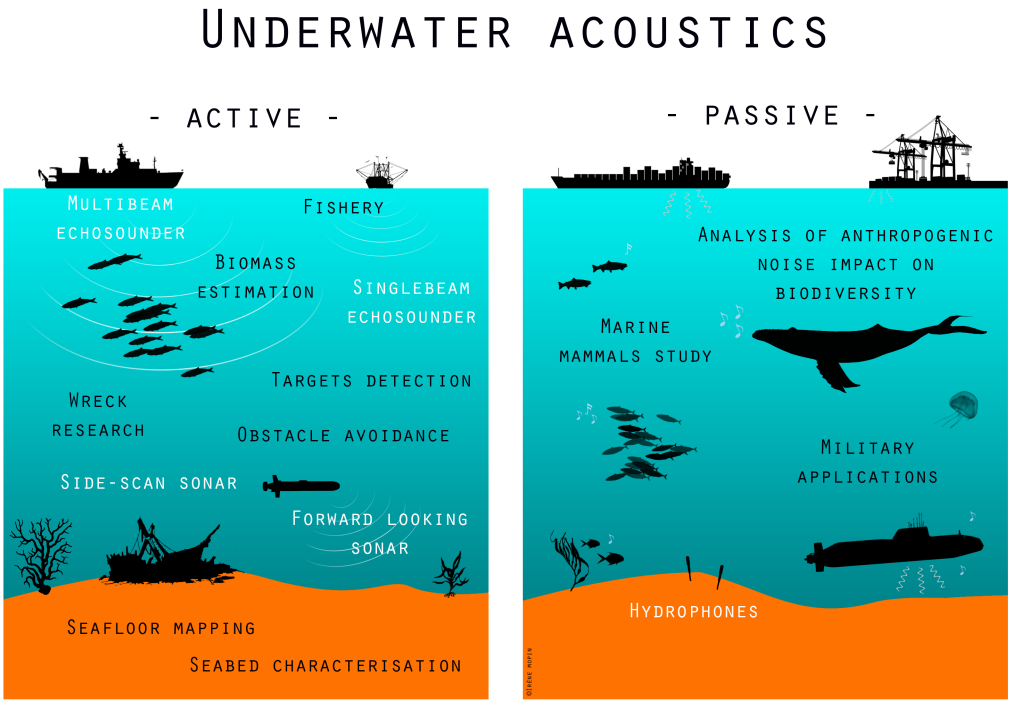

Figure 1.1 – Examples of underwater acoustics applications (black) and systems (white)

Because it relays for several scientific domains that happen to be less appropriate in the seawater complex medium, underwater acoustics is a wide field that regroups many activities such as research, development, survey, monitoring or control. Acoustics systems are used underwater equally for civilian and military applications and each specific purpose has its particular system. Beyond this division, all underwater acoustics usages and systems are classified in two large categories: active and passive (see figure 1.1). On the one hand, the active class includes systems that use both transmitters and receivers. Using the reciprocity of piezoelectric materials which are the dominant components of underwater acoustic transducers, transmitters and receivers can be separated (multi-static measurements) or combined in one transducer (mono-static measurements). Some examples of common active systems are shown in figure 1.1 such as singlebeam echosounder (SBES), multibeam echosounder (MBES), side-scan sonar (SSS) or forward looking sonar (FLS). On the other hand, the passive class includes systems that use only receivers. In the vast majority of applications, systems employed are hydrophones, as shown in figure 1.1. Table 1.1 presents a non-exhaustive list of applications corresponding to the passive and active categories. Each application is associated to a reference publication [1] and an example of system.

Applications	Reference publication	Ex. of system used
Active		
Fishery	[Simmonds and MacLennan, 2008]	SBES
Biomass estimation	[Stanton et al., 1994]	SBES
Target detection	[Petillot et al., 2010]	SAS
Obstacle avoidance	[Petillot et al., 2001]	FLS
Target tracking	[Karoui et al., 2015]	FLS
Wreck research	[Majcher et al., 2021]	MBES, SBP
Seafloor mapping	[Mayer, 2006]	MBES
Dredging	[Velegrakis et al., 2010]	MBES, SBP
Positioning	[Vickery, 1998]	Pingers
Navigation	[Zerr et al., 2005]	SSS
Localization	[Rohou et al., 2019]	SBES
Passive		
Marine mammal study	[Samaran et al., 2019]	Hydrophones
Noise impact analysis	[Chou et al., 2021]	Hydrophones
Target detection	[Bouffaut, 2019]	Hydrophones
Environment monitoring	[Mansour et al., 2013]	Hydrophones
Discretion	[Listewnik, 2013]	-

Table 1.1 – Applications of underwater acoustics associated to examples of related publications and systems used (SBES = SingleBeam EchoSounder, SAS = Synthetic Aperture Sonar, FLS = Forward Looking Sonar, MBES = MultiBeam EchoSounder, SBP = Sub-Bottom Profiler, SSS = Side Scan Sonar)

1. Arguably not the first or the best in this field, but the one considered by the author to best present the system and application.

1.1 Context of the thesis

The subject of research in this PhD is the seabed acoustic response which, by definition, can only be obtained by using active systems. Two particular active systems are considered in the following works: singlebeam echosounders (SBES) and multibeam echosounders (MBES). Table 1.1 shows that they are employed for many applications including some whose object is the seafloor such as seafloor mapping. Historically, SBES can be considered as the antecedent of MBES. One of their authentic applications has been to detect the seabed for navigation safety. For this purpose the echosounder is mounted under the ship, on the hull. It transmits an acoustic signal toward the sea bottom and records its echo (see figure 1.2). The two-way travel time of the signal is used to derive the water height H as:

$$H = \frac{c_{\mathrm{w}} t}{2} \tag{1.1}$$

where c_{w} is the sound speed in the water and t is the propagation time of the signal. In the context of this PhD, the transmitted signal is a truncated sinusoid of central frequency ƒ and duration τ. It is called in the following a pulse or countinuous wave (CW) pulse. The recorded cycle between two transmissions of this pulse (i.e. coupled transmission and reception) is called a ping.

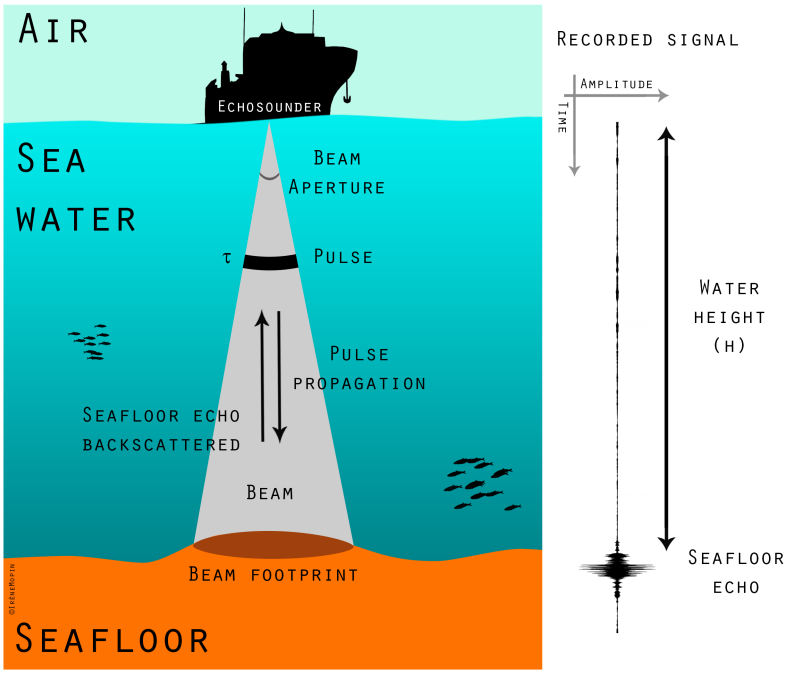

Figure 1.2 – Singlebeam echosounder used for water height measurement

As illustrated in figure 1.2 the acoustic energy transmitted by the singlebeam echosounder is focused in a specific direction i.e. toward the seafloor. Variations of the transmitted energy level according the directions are described by the directivity function of the echosounder. The

main directions in which the SBES transmits the maximum of acoustic energy are generally grouped around its axis and called its main beam. This beam is mostly modelled as a cone as shown in figure 1.2. The intersection between the cone and the seafloor is called the beam footprint.

Multibeam echosounders are used the same way to detect the sea bottom but, as their name suggests, they have multiple beams. These beams are located on a fan athwartship and they all provide one or several measurements of the two-way travel time t. One ping of a MBES provides therefore at least as many sea bottom detections as beams. Using this system therefore considerably increases the number of measurements compared to singlebeam echosounder surveys.

Among the applications presented in table 1.1, some have the seafloor as main interest (seafloor mapping), and some use it as a boundary (positioning) or a reference (navigation). The first set directly matches the subject of this PhD. Indeed, it deals with the description and analysis of the seafloor itself by acoustics. In detail, the theme 'seafloor mapping' can be otherwise defined as cartography, which includes measuring the bathymetry i.e. measuring the topography of the seafloor. It is an essential part of hydrography whose aim is to map the sea bottom following accurate standards specified by the International Hydrographic Organisation (IHO). The PhD works presented in this manuscript will be restricted to this hydrography/bathymetry context where SBES and MBES are operated following IHO criteria.

1.2 What is the seafloor?

Before discussing the seafloor acoustic response, it is important to define what the seafloor is and how it is considered in this manuscript. First of all, a basic definition [2] identifies it as "the bottom of the ocean" and adds that it can be named "seafloor", "seabed", or "sea bottom". In this description, the depth under the seabed surface is described as the "depth below seafloor". Based on these information, we can define the seafloor as an interface between the ocean (water) and the bedrock (mineral) (see figure 1.3). In term of acoustic propagation, it corresponds to a fluid/solid interface.

The fluid medium i.e. the sea water, is composed of different layers of water with various sound speeds (or temperatures) that can vary in time due to currents or other oceanic phenomena. It contains fauna and flora (*pelagos*) such as fish, plankton, and also suspended matter of diverse origins.

On the other side, the solid medium is composed of several types of geological structures made of different materials according to the location. Due to this complex constitution, its surface could hardly be perfectly flat. The interface between the water medium and the geophysical substrate can thus be considered rough. This roughness has various scales:

2. From Wikipedia `https://en.wikipedia.org/wiki/Seabed` (August 2022)

- the large scale which corresponds to the bathymetric scale i.e. much larger that the echosounder beam footprint. It is generally described using global slopes of the interface.
- the medium scale which is of the order of the beam footprint.
- the fine scale which is of the order of the acoustic wavelength λ of the transmitted pulse.

Without any external contribution, the seafloor could have been modelled as a perfect rough interface between a fluid and a solid. However, in the ocean, the bottom is often affected by external phenomena that blur this interface (see figure 1.3). Some of them are listed below:

- **Sedimentation** All suspended matter in the water column eventually ends falling with gravity on the bottom. This effect leads to deposits of diverse sizes of particles which potentially aggregate with time. Several layers of sediments are created this way above the geophysical substrate. The deepest become purely mineral as the pressure rises, ejecting the water between particles. The other layers include more and more water as getting increasingly closer to the water medium (e.g. porous sand filled with water).
- **Benthos** The bottom of the ocean is also the habitat of a wide quantity of marine species, fauna (zoobenthos) and flora (phytobenthos). The benthos is composed of different sizes of organisms, from micro (<1mm) such as bacteria to macro (>1mm) such as crustaceans or corals. All theses organisms are organised differently according to the location (deep sea, coastal areas, etc.) and at a smaller scale they are not distributed homogeneously on the ocean bottom (bioturbation).
- **Anthropogenic interventions** Human activities impact the ocean in multiple ways. For examples, building marine infrastructures such as harbour, platforms, or pipe laying changes permanently or temporary the bottom structure. Fishery, and especially trawling, modifies the bottom configuration at large scale. Waste products spilled in the ocean also affect the constitution of the seabed after sinking and mixing.
- **Ocean current** Movements of the water mass induced by oceanic currents can modify the composition of the bottom. Sediments can be transported, according to their grain size and the current strength, by rolling, saltating or suspension. The roughness of the seafloor can then be changed at all scales discussed previously. Oceanic currents also impact the *benthos*. On the one hand they apply constraints on the environment of the habitat that restrict the number of species in an area (e.g. strong current limiting access to slight animals). On the other hand, they facilitate transport between habitat areas (e.g. larvae transport, pollination, settlement).
- **Geological processes** Displacements of mineralogical systems generate large scales modification of the bottom of the ocean. For example, plate tectonics force the seafloor constitution to change and can also provoke drastic changes of *benthos* (e.g. hydrothermal vents). In coastal areas, landslides due to erosion or weathering are also examples of major modification of the seabed.

Variations of these five phenomena can be observed in space and time at different scales. They can be episodic (e.g. earthquake, human construction) but also periodic. For example, displacement and modification of sediment deposits can be generated by tide currents. In

areas where tides are periodic (e.g. diurnal), variations of the seafloor composition will follow this cycle. Fauna and flora can also have a cyclic impact on the seafloor (e.g. diurnal and seasonal behaviour).

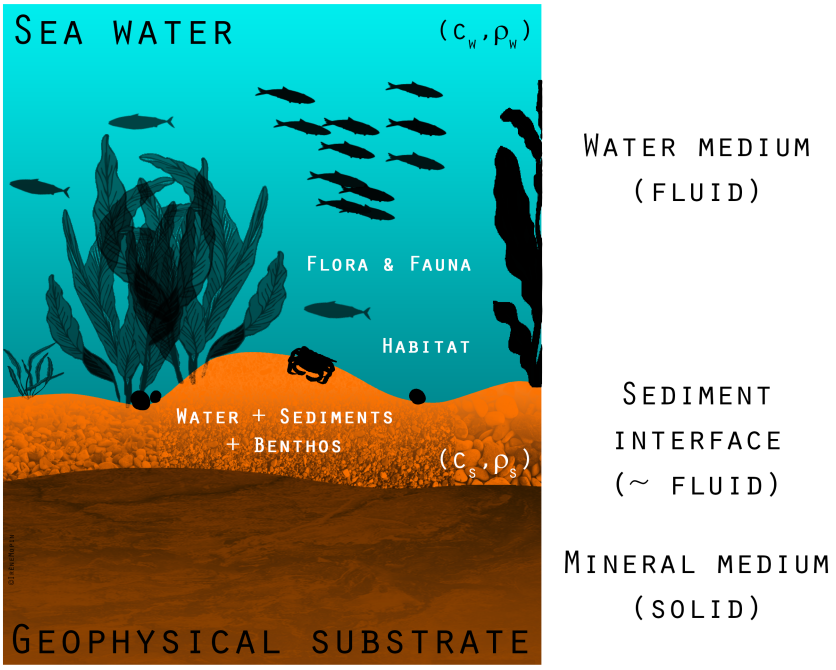

Figure 1.3 – What is the seafloor? Examples of typical systems, of different densities ρ and where sound travels at velocity c.

All these phenomena combined contribute to make less clear the interface between the sea water and the geophysical subsoil. The seafloor can then be identify as a the fuzzy interface between these two media. It is thus composed of multiple elements (e.g. sand grains, shells, algae, crabs, plastics[3]) that have different acoustic responses and are not perfectly located neither in the horizontal plane (xy) nor along the vertical axis z. This diversity of components separated in space also implies that the sea water is a component of this intangible interface. This makes the seabed a mixture of water and other constituents, mineral, organic or anthropogenic. It can therefore be modelled as a rough interface between two fluids: the sea water and the sediment (composed of all types of materials and organisms) filled with water.

A strong hypothesis is made in the high frequency context of this PhD that the two fluid media are perfectly homogeneous with sound speed c_w for the water medium and c_s for the sediment medium, and respectively with ρ_w and ρ_s their densities. No layering is then taken into account in any of the media, neither changes in their composition in time or presence of targets i.e. the interface is supposed permanent in time. In addition, because the two media are fluids, only compressional acoustics waves are then considered in the following.

3. See [Nurlatifah et al., 2021], [Barrett et al., 2020]

From the acoustic measurement point of view, the seafloor corresponds to an echo which is a long and energetic signal received by the echosounder as shown in figure 1.2. If the seafloor was a perfect plane interface, this echo would be an exact replica of the transmitted signal with less energy because of attenuation with range and geometrical spreading. However, in practice, it is found mostly longer than the transmitted pulse length τ. This stretch effect is mainly due to the geometry of acquisition and the system parameters. Indeed, when the pulse first interacts with the seafloor it takes a short time after this start date for the entire pulse to reach it. Then, according to the pulse length and the beam aperture, the travelling signal is scattered from the seafloor for a certain amount of time. In particular, for oblique beams, the echo length is directly correlated to the beam footprint size as illustrated in figure 1.4. This effect is purely geometrical and can therefore be predicted. Nevertheless, measured echo lengths are sometimes longer than predicted. This effect is usually related to the roughness of the interface that generates diffuse scattered signals arriving later to the receiver, or to the penetrability of the interface leading to multiple scattered signals inside the sediment medium that inevitably arrive after the interface echo. These observations demonstrate the observability of the water/sediment interface fuzziness by acoustics systems.

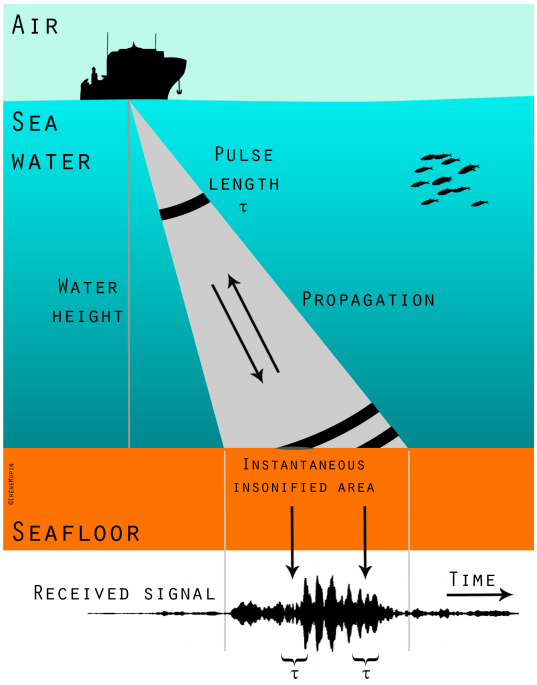

Figure 1.4 – Elongation of the seafloor echo due to geometry of acquisition (oblique angle, pulse length and beamwidth)

In the context of seabed mapping, the topography of the seafloor (bathymetry) is derived from measurements of the water height under the echosounder (see figure 1.2). This height corresponds to the two-way travel time spent by the transmitted signal to propagate from the echosounder to the seafloor (see equation 1.1. In hydrography, the range (or time) on which is based the height measurement is called the sounding. Usually it is detected from the seafloor

acoustic echo at the range (or time) of the maximum seafloor echo magnitude and/or at the range (or time) corresponding to the center of the echosounder beam (for oblique beams). In literature, these methods of detection are respectively called amplitude detection and phase detection (as reference to the angle of the target inside the beam). Using these methods, echosounders provide one sounding per beam which leads to several soundings per ping for multibeam echosounders. Nowadays, latest-generation echosounders, especially multibeam echosounders, can provide several soundings per beam using upgraded detection methods such as multi-detection or extra-detection.

In this PhD, we choose to only focus on the basic method of one sounding per beam, one of the main problematic being to define the seafloor acoustic response value that can be associated to this sounding. In other words, which time-sample(s) of the long seafloor echo corresponds to the acoustic response, each having its own value?

1.3 Purposes of the seafloor acoustic response

From the fundamental use of detecting the sea bottom for navigation safety emerged the necessity to create maps of marine hazards. On these maps, illustrated by figure 1.5, sounding measurements are gathered to obtained intelligible features of the sea bottom topography. These nautical charts have been employed for many decades to avoid marine dangers and also to locate ships during navigation. For this purpose, sea marks and water heights are essential, but they can be reinforce with another feature: the seafloor type (sand, rock, mud, etc.). Indeed, the type of seafloor is a useful information to add when approaching from the coasts where the bathymetry is complex. The nature of the seafloor has then appeared on nautical maps for centuries and are still part of actual charts as shown in figure 1.5.

Historically, the seabed type was measured manually, most of the time simultaneously with the sounding. At that time the water height was estimated using a lead line cast from the ship toward the seabed. Leads of different shapes existed, but specific leads were used to sample the seafloor while making the sounding measurement. They were covered by suet or designed to bring back parts of the seafloor onboard. This method was efficient to measure sand, mud or other fine sediments. But sometimes, when results were not reliable, young seamen were asked to dive to get seabed samples such as described by E. Jurien, lieutenant-commander, in his report of exploring the approach of Julia Island (Italy) in 1841:

> "La plus grande longueur du plateau est d'environ 40 mètres; il est formé d'une pierre très-dure, à arêtes vives, d'un aspect jaunâtre. Les plombs de sonde revenaient mâchés et le suif ne rapportait ni sable ni scorie. Un matelot que nous fimes plonger dans le but de rapporter quelques échantillons de la roche, ne put parvenir à en détacher. Ce plateau est coupé à pic, et, dès qu'on tombe dans les fonds de 15 mètres, on trouve un sable noir et très-fin ressemblant à de la poussière de charbon." [4]

In this report, we can observe that the seafloor nature is identified by its material (sand, slag, rock), its grain size (fine, very fine, dust), its hardness (very hard) and its color.

4. E. Jurien, Capitaine de corvette, commandant le brick la Comète, 1841, Annales maritimes et coloniales : publiées avec l'approbation du ministre de la marine et des colonies par M. Bajot.

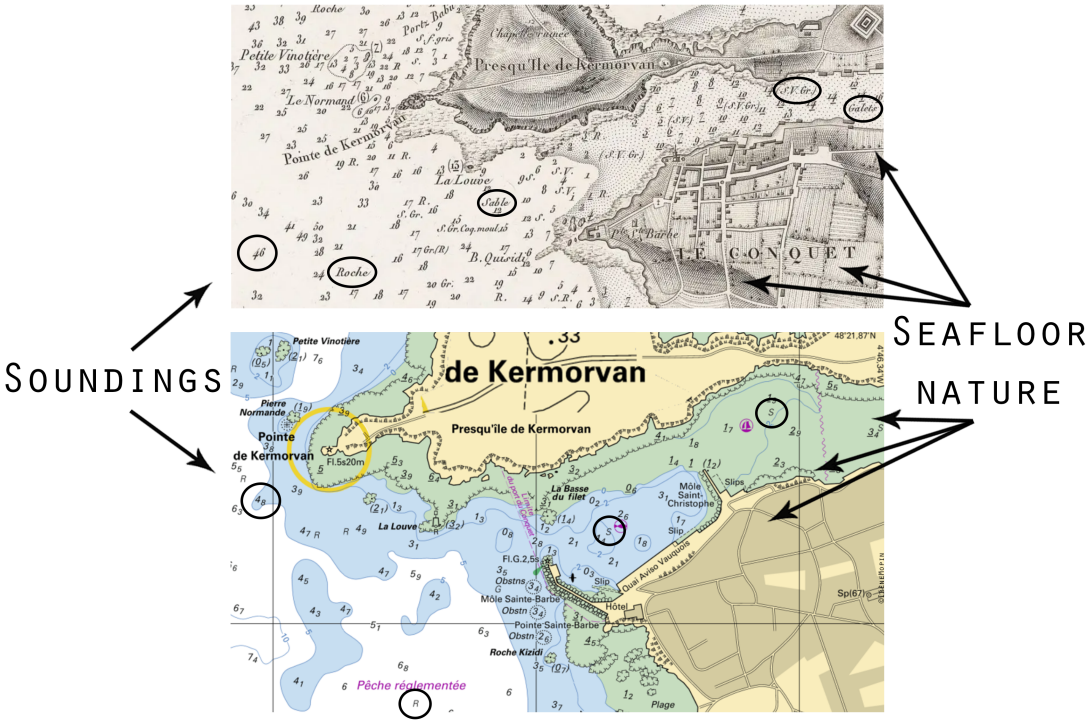

Figure 1.5 – Extract of nautical charts of the harbour of Le Conquet (France) of 1.5km x 900m. Up: Archive of survey made in 1816, from M. Beautemps-Beaupré, Pilote français, vol. 1 Environs de Brest, 1822. Circled seafloor natures are: *Roche* = rock, *Sable* = sand, *Galets* = pebbles, *S.V.Gr* = sand, mud, gravel. Down: current map of the area from the French marine hydrographic institute (Shom) (`data.shom.fr`). Circled seafloor natures are: R = rock, S = Sand.

Nowadays, sounding measurements are mainly made using echosounders. The major benefits of these systems are the high increase of the soundings density and of the efficiency of the survey, especially using multibeam echosounders. However, seafloor samplings can no longer be made simultaneously to the acoustic measurement except by stopping the vessel which is time consuming and provides very sparse results compared to the number of soundings. Being able to link echosounder data, i.e. acoustic echoes of the seabed, to its constitution is thus of primary interest for applications such as seafloor mapping and marine cartography. In literature and in practice, this connection is generally made by an acoustic attribute of the seafloor called its acoustic response. It is directly linked to the characteristics of the seabed (composition, roughness, etc.) and its variations can be discriminating.

More precisely, the seafloor acoustic response is an essential parameter for a broad list of applications. Some of them are listed below:

- **Seabed characterisation** The objective of this application is to relate sedimentological information with acoustic features in order to derive the seafloor type from survey

measurements. The seabed acoustic response is used in addition to the bathymetry at different scales (slope, roughness, etc.).

- **Seabed classification** In this application, the relation with geological features is not necessary. The main objective is to group the different seabed attributes measured and to label these ensembles. The seabed acoustic response is used here as a parameter in the classification algorithm. Sometimes it can also lead to several complementary parameters.
- **Habitat mapping** This application is strongly connected to the previous ones. In addition to classify and characterise the seabed, a marine habitat (e.g. coral reef, seagrass land, maerl...) is also inferred. Ecological an biological information are then added to derive a map of areas that support the survival and reproduction of specific species.
- **Seafloor monitoring** The aim of this application is to measure and control modifications in the seabed in time. They can appear at different time-scales such as years (e.g. anthropogenic constructions), months (e.g. variations in sediments location due to tides), days (e.g. movements of fauna and flora), etc. They can also be due to input of materials intentionally (e.g. wind farm) or non-intentionally (e.g. mines). The seabed acoustic response is used as one of the parameters that provide information on the seafloor changes.
- **Sonar performance models** The objective of this application is to evaluate performances of a system such as its ability to detect a target. Targets can be biological (e.g. fish, marine mammals), geological (e.g. seabed, obstacles), or anthropogenic (e.g. mines, submarines). The seabed acoustic response is in this case a part of an energetic balance between the signal of interest and all type of noises that can hide the target echo. It can also be used to calibrate systems.
- **Propagation models** The loss of energy of an acoustic signal transmitted in the sea water is here of main interest. During its propagation, this signal, in most of the cases, encounters boundaries of the model which can be the sea surface or the seabed. It is then reflected (or scattered) and looses acoustic energy in the process (transmission). This loss of energy is taken into account at the interface between sea water and seabed by using the seafloor acoustic response.

In the first four applications of this list, the seafloor acoustic response is increasingly used because of the echosounders improvements, especially their ability to be calibrated in magnitude. This way, absolute variations of the seafloor response can be studied according to time and space. For example, these variations can be enlightening of certain types of seafloors such as time variations of sand ripples (displacement and modification of roughness).

From this short summary, we can observe that the seafloor acoustic response is sometimes the principal subject of interest (mostly in seabed characterisation and classification) but some other times it is considered as undesirable (target detection) or as a loss (propagation model). This PhD is not especially associated to a particular application. The aim to characterise precisely the seabed acoustic response, the results and the methods developed are relevant for any application using this parameter.

1.4 Work hypotheses and problem statement

A summary of the main hypotheses discussed previously in which this PhD take place are listed in table 1.2. Acoustic systems employed are singlebeam and multibeam echosounders with a high frequency range. They are used in a hydrographic context i.e. to measure bathymetry. Estimation of the seabed acoustic response is therefore based on bathymetric-like data provided by these echosounders. In acoustic models, the seafloor is defined as a still (no movement in time) interface between two homogeneous fluid media: the sea water and the bottom sediment layer.

System	Active, SBES or MBES
Frequency range	High frequencies (10 kHz - 700 kHz)
Context	Hydrography, bathymetry
Seafloor	Stable interface between two homogeneous fluid media of celerities c_w and c_s and densities ρ_w and ρ_s
Applications	E.g. seafloor mapping, seabed characterisation and classification...

Table 1.2 – General hypotheses and characteristics considered in this PhD

The objective of the PhD is to characterise accurately the seabed acoustic response in this context. The first question that has to be solved is therefore the definition of the seabed acoustic response. The answer is discussed based on previous works on the seabed acoustic response found in literature. The study relies on four analyses:

1. Analysis of the **semantics** used in literature to name the seabed acoustic response
2. Analysis of basic, physical and empirical **models** of the seabed acoustic response
3. Analysis of the **sonar equations** in which the seabed acoustics response is a parameter,
4. Analysis of the **variability** of the seabed acoustics response and its modelling

From the results of this study and based on a scattering model, a definition of the seabed acoustic response is determined.

The second step of the PhD is then to derived an accurate estimate of this seafloor acoustic response. Based on literature and on practical usages in hydrography and particularly in bathymetry, different estimators are studied. In order to identify the best (i.e. accurate) estimator, their bias, variances, and speed of convergence are compared. At the end, characteristics (expected value and variance) of the best estimate are derived analytically according to the number of pings and time-samples of the seafloor echo used to estimate seafloor response.

The next step is then to define a measure of the estimation accuracy. It is made using the uncertainty. From the analytical results of the best seafloor response estimator, a theoretical formulation of its associated uncertainty is derived. In practice, it can be seen as an *a priori* evaluation of the accuracy of a planned survey.

In a last step, theoretical hypotheses under which analytical calculations were made are verified using singlebeam echosounder data. Because one of these hypotheses implies that echosounder characteristics should be perfectly known, a dedicated singlebeam echosounder is designed, manufactured, and calibrated during the PhD (at Sorbonne University (Paris, France) and ENSTA Bretagne (Brest, France)). Measurements are made with it on sediment bottoms in the tank of the university of Bath (United Kingdom) and in the harbour of Brest (France). Finally, after the validation of the hypotheses, the seafloor response estimation is applied to different singlebeam and multibeam echosounder survey data. The *a priori* uncertainty levels associated to these results are then compared to *a posteriori* uncertainty results i.e. the uncertainty levels calculated from echosounders measurements.

This manuscript is divided in three parts. The first part discusses the definition of the seabed acoustic response. It is divided in three chapters: theoretical models of the seafloor acoustic response (chapter 2), practical measurements (chapter 3), and study of the variability of the seafloor response (chapter 4). The second part introduces the scattering model based on the results of the first part and derives the definition of the seabed acoustic response (chapter 5). Then several estimators of the seafloor response are calculated and compared (chapter 6). At the end of this part, the best estimator of the seafloor acoustic response is identified and a model of it and its uncertainty is derived analytically. The last part of this manuscript describes the design and manufacture of the splitbeam and singlebeam echosounder (chapter 7). Then the theoretical hypotheses are discussed based on *in situ* data. Finally, the seafloor acoustic response estimation method is applied to singlebeam and multibeam data and perspectives for seafloor identification and detection of seabed changes are proposed (chapter 8).

Part I

What is the acoustic response of the seafloor?

Preamble

The definition of the seafloor acoustic response is not unequivocal. An overview of the state of the art informs us that depending on authors' point of view, as they can have different science backgrounds (acoustician, mathematician, physicist, sedimentologist, etc.), this response is grasped differently. Indeed, it can be viewed as a loss of acoustic energy by the acoustic propagation modeller, or as a transfer function by the mathematician, or even as an inherent characteristic of the seafloor that can inform the sedimentologist on its composition. All these definitions are attached to the same desire to define the acoustic response of the seabed, but can lead to totally different models. The perspective from which the scientist is considering the issue is therefore important to be clarified before studying the models.

The analysis of the seafloor acoustic response is a common and historical subject in underwater acoustics. It has been of interest in the military sector for almost a century, and has gradually become a public research topic more recently. Because of these two major contexts in which it has been studied, the vocabulary employed to discuss and present works on the seabed acoustic response is diverse. Depending on the authors, and their originating fields of interest, the lexicon used in publications could have different descriptions and connotations.

A non-exhaustive consultation of the state of the art regarding the seabed acoustic response permits to identify dozen of phrases that are or had been used in publications and monographs to describe the phenomenon. They are listed in appendix A. A first analysis of the vocabulary employed by authors shows that phrases used are mostly composed of two parts: 1) the type of variable it is related to, i.e. its physical or mathematical denomination; 2) what produce the phenomenon, i.e. its physical cause. Examples of phrases are given in table 1.3. We can note that the physical causes could be designated as the physical mechanism itself (e.g. 'scattering') or meant implicitly by the name of the model author (e.g. 'Lambert'). Sometimes, the physical part is not given and only remains the subject of the phenomenon, i.e. the seafloor (e.g. 'bottom').

Types of the variables can be analysed independently. Even if they are part of the same semantic field, several words are used to describe the seabed acoustic response. Those found in the state of the art are listed in table 1.4. They are supported by two kinds of definition: their literal sense i.e. denotation, and their implied meaning i.e. connotation. We observe that, whilst the words are describing the same phenomenon, several denotations are employed and they lead to multiple interpretations and undertones. For example, the word 'strength'

Physical cause	Type of variable
Backscattering	Strength
Scattering	Cross-section
Bottom	Loss
Plane wave scattering	Amplitude
Lambert	Coefficient
Reverberation	Strength

Table 1.3 – Examples of phrases employed in the literature to describe the acoustic response of the seafloor

refers usually to the power of an acoustic source where the source is the principal object of interest in the statement, whereas the word 'loss' is mostly used to describe a decrease of energy that affect the phenomenon of interest. Those two words are therefore antonyms in the common language, however they are both used to present the acoustic response of the seabed in literature. As said earlier, the difference takes place in the context namely the application(s) targeted and the working field of the authors. The word 'loss' is as a matter of fact mostly found in publications and monographs about underwater target detection or acoustic propagation models where the main subject is not the seabed. The word 'strength' is, in contrast, found in topics dealing with the seafloor acoustic response as the primary matter.

Type of variable	Denotation	Connotation
Strength	Acoustic power	Positive, quality of the seabed
Loss	Reduction of acoustic energy	Negative, unwanted phenomenon
Constant	Fixed value	Immutable, never changes
Cross-section	Detectability, signature of the target	Contrast with the acoustic environment
Response	Ratio	Reaction to stimuli
Coefficient	Ratio	Proportionality
Amplitude	Absolute value	Physical acoustic signal
Degree	Measure	Value from a scale
Signal	Propagative wave	Temporality, duration
Function	Dependence in parameters	Evolution, changing
Parameter	Specific value	Associated to a model
Index	No unit	Characteristic, specific

Table 1.4 – Words employed in the literature to describe the seafloor acoustic response variable

Couples of other contradictory words can be found in the list of table 1.4 if we look in details at the words connotations, like 'parameter'≠'function' or 'amplitude'≠'signal'. From a mathematical point of view, a majority of the words seem to have a commonality: they all describe a single value (like 'amplitude' or 'parameter'). Indeed, in most of the physical or heuristic models developed in literature and in the useful and practical sonar equation, the

seabed acoustic response is mainly considered as a deterministic value. In seldom publications, the words describe rather a process that varies with external parameter(s). Terms like 'function' are in this case employed.

In this first part of the thesis, both the constant single value underlying meaning and the variable one are discussed in order to understand the mechanisms and the reasons of their usage. It begins with physical and heuristic models that are depicted and compared. Each of them depends on the application requested, the system (sonar) used, the processing capacity and a certain number of parameters. Second chapter presents the usual practical processing of the seabed acoustic response based on the sonar equation. Finally, the last chapter brings to light the randomness of the seabed acoustic response and discusses the reasons of its variability.

Chapter 2

Analytical models of the acoustic seafloor response

State of the art of seafloor acoustic response embraces a large number of models whose aims are to describe analytically the phenomenon. According to the application where it is used, the model could be basic i.e. with a unique parameter, or highly complex i.e. up to 13 parameters. Some authors wish their model to be as close as possible to the seabed features, typically in order to retrieve sediment characteristics (grain size, rugosity, porosity) from the acoustic measurements. These types of models are based on geo-acoustics principles. On the contrary, some models aims at being flexible and adaptable to the measurement diversity. In this case, they can have no relation with physical parameters of the seabed. They are sometimes purely phenomenological or mathematical. We name this class of models 'heuristic' in this chapter. Table 2.1 synthesizes some of the principal models found in the literature (non-exhaustive) together with the number and description of their parameters. We specify also if the model is heuristic or based on physical developments, and parameters employed.

In the following, models that derive the seafloor acoustic response are introduced. It begins with definitions of the scattering strength and then we present different approaches to compute it from completely heuristic models to physical ones.

Authors or reference publications	Model short name	Model type	Nb. of param.	List of parameters
[Dosso and Holland, 2006]	Pressure reflection coefficient	Ph	3	θ_{i}, Z_{s},Z_{w}
[Clay and Medwin, 1977]	Amount of coherent reflection	Ph	3	θ_{i}, k_{i}, σ_ζ
[Ishimaru, 1977][Lurton, 2010]	Lambert's law	H	2	θ_{i}, μ_{L}
[Sevaldsen, 2002]	THALES / Lambert's law	H+ Php	5	θ_{i}, $\mathfrak{f}$,b_1,b_2,b_ϕ
[Mackenzie, 1961]	Lambert-Mackenzie's law	H	3	θ_{i}, $\mu_{\text{L-M}}$, $\mathfrak{n}$
[Jenserud et al., 2001]	-	H	4	θ_{i}, $\mu_{\text{L-M}}$, $\mathfrak{n}$, b_0
[Del Balzo et al., 1997]	-	H+ Php	4	θ_{i}, b_0, b_Φ, $\mu_{\text{L-DB}}$
[Ellis and Crowe, 1991]	-	H + Php	4	θ_{i}, μ_{L}, b_a, σ_ψ
[Caruthers and Novarini, 1993]	-	H Phφ + Php	12	θ_{i}, k_{i}, Z_{s}, Z_{w}, k_L, k_h, k_c, α_{s}, m_0, σ_ψ
[Patterson, 1963]	-	H + Php	3	θ_{i}, Z_{s}, Z_{w},
[McKinney and Anderson, 1964]	-	H	3	θ_{i}, $\mathfrak{f}$, b_b

[Caprais and Lombardi, 1996]	GESMA model	H	3	θ_i, B_1, B_2
[Lurton et al., 2015]	GSAB model	H	7	θ_i, b_A, b_B, b_C, b_D, b_E, b_F
[Nolle et al., 1963]	-	H Phφ	9	θ_i, k_i, Z_s, Z_w, α_s, α_w, d_corr, Υ_0, δ
[Essen, 1994]	-	H Phφ	7	θ_i, k_i, Z_s, Z_w, A_i, k_c, W_0
[Jackson et al., 1986]	Jackson model	H Phφ	8	θ_i, k_i, Z_s, Z_w, α_s, σ_φ, b_h, b_a

Table 2.1: Characteristics of seafloor acoustic response models. 'Ph' = Physical,'H' = Heuristic, 'Phφ' = Based on physical phenomena, 'Php' = Physical parameters.

In this chapter and more generally in all the manuscript, parameters are sometimes written in decibels for convenience. In that case, they require references (see table 2.2). The reference pressure in underwater acoustics is $p_\mathrm{ref} = 1\mu$Pa which lead to a reference acoustic intensity (for a monochromatic plane wave of RMS pressure $\underline{p_\mathrm{ref}}$) of $\underline{I_\mathrm{ref}} \approx 6.7 \cdot 10^{-19}\mathrm{W/m^2}$. Note that the reference distance is currently one meter, but could be found in literature (generally historical) at one yard. A correction of $20\log_{10}(1\mathrm{meter}/1\mathrm{yard}) = 0.78\mathrm{dB}$ can be added or subtracted to the equation when necessary for coherence.

References	Values
Pressure	$\underline{p_\mathrm{ref}} = \frac{p_\mathrm{ref}}{\sqrt{2}} = 1\mu\mathrm{Pa}$
Intensity	$\underline{I_\mathrm{ref}} = \frac{{p_\mathrm{ref}}^2}{\rho_\mathrm{w} c_\mathrm{w}} \approx 6.7 \cdot 10^{-19}\mathrm{W/m^2}$
Range	$r_\mathrm{1m} = 1\mathrm{m}$
Area	$\mathcal{A}_1 = 1\mathrm{m}^2$
Voltage	$\underline{V_\mathrm{ref}} = \frac{V_\mathrm{ref}}{\sqrt{2}} = 1\mathrm{V}$

Table 2.2 – References values in underwater acoustics

The underlining of parameters $\underline{\bullet}$ stands for its RMS value defined as:

$$\underline{\bullet} = \lim_{T\to\infty} \sqrt{\frac{1}{2T}\int_{-T}^{T} [\bullet(t)]^2 dt} \tag{2.1}$$

In the particular case of the monochromatic sinusoidal signal supposed in this PhD, this RMS value is equal to the 0-peak value of the parameter divided by $\sqrt{2}$ i.e.:

$$\underline{\bullet} = \frac{\bullet}{\sqrt{2}} \tag{2.2}$$

2.1 From a flat interface to a more realistic rough seabed

In this section, the seafloor acoustic response is derived from its basic definition as a reflection coefficient from a plane interface between two media to a more sophisticated model representing the seafloor as a rough surface. Presence of a roughness induce two phenomena in the scattering: a coherent part and an incoherent part. Models dealing with one or both theses representations are described in the following. At the end, the issue of the volume scattering is briefly addressed.

2.1.1 First definitions

The basic definition of the seabed acoustic response is a simple plane interface model. The seafloor is depicted as an interface between two media of different compositions (see figure 2.1). Above the interface the medium is the sea water, of acoustic characteristic impedance Z_{w}, and beneath the interface is the seafloor compose of sediment, of constant acoustic characteristic impedance Z_{s}. Both are supposed fluid and of constant sound speeds respectively c_{w} and c_{s} and density ρ_{w} and ρ_{s}. In this configuration, [Dosso and Holland, 2006] show that the acoustic energy release from the seabed corresponds to what they called 'bottom loss', and is defined as the pressure reflection coefficient R i.e.:

$$R = \left| \frac{Z_{\mathrm{s}} - Z_{\mathrm{w}}}{Z_{\mathrm{s}} + Z_{\mathrm{w}}} \right| \tag{2.3}$$

with $Z_{\mathrm{w}} = c_{\mathrm{w}}\rho_{\mathrm{w}}$, $Z_{\mathrm{s}} = c_{\mathrm{s}}\rho_{\mathrm{s}}$. This model was applied for an acoustic wave that arrived perpendicularly on the interface (see figure 2.1). The incident wave is reflected in the same direction i.e. perpendicularly to the interface.

This model can be modified to take into account the incidence angle of the incoming acoustic wave on the interface. This configuration appears when the acoustic source (e.g. sonar) transmits a signal to the seabed with a tilt angle. The pressure reflection coefficient R becomes in this case:

$$R(\theta_{\mathrm{i}}) = \left| \frac{Z_{\mathrm{s}} \cos\theta_{\mathrm{i}} - Z_{\mathrm{w}} \cos\theta_{\mathrm{t}}}{Z_{\mathrm{s}} \cos\theta_{\mathrm{i}} + Z_{\mathrm{w}} \cos\theta_{\mathrm{t}}} \right| \tag{2.4}$$

with θ_{i}, θ_{r} and θ_{t} respectively the angle of the incident, reflected and transmitted acoustic waves with respect to the vertical axis (see figure 2.1). In the case of a plane interface θ_{r} is the only direction where acoustic energy is reflected, and:

$$\begin{aligned} \theta_{\mathrm{r}} &= -\theta_{\mathrm{i}} \\ \sin\theta_{\mathrm{t}} &= \frac{c_{\mathrm{s}}}{c_{\mathrm{w}}} \sin\theta_{\mathrm{i}} \end{aligned} \tag{2.5}$$

This model of seabed acoustic response has two main parameters which are the characteristic impedances of the media constituting the interface. It is considered as a physical model as shown in table 2.1.

When the interface water/sediment is rough, acoustic energy is reflected in all directions. This phenomenon is called 'scattering'. In term of acoustic intensity, a portion of the incident wave intensity I_{i} is scattered in every directions θ. If the source is placed at an incident angle

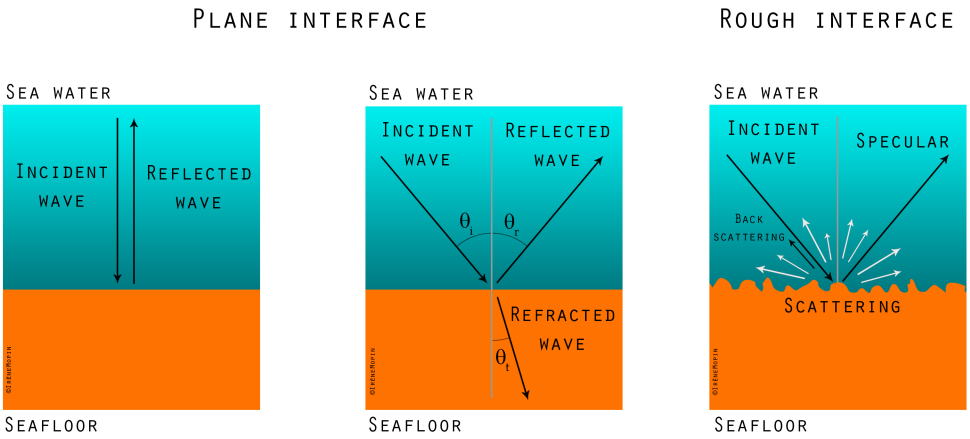

Figure 2.1 – Basic flat and rough interface modelling of the seabed

θ_i above the seabed (see figure 2.1), the specific amount of intensity I_bs that comes back in the direction θ_i is named backscattered intensity. In contrast, the intensity that goes away by reflection at the angle $\theta_\mathrm{r} = -\theta_\mathrm{i}$ is named the specular intensity. It is usually the greater amount of intensity scattered.

The acoustic level (in decibels) that corresponds to the ratio of intensity I_s reflected in any directions θ on the incident intensity arrived on a small interface area $\mathcal{A}_1$ is called scattering strength and noted S. It is defined by [Urick, 1954] in decibels as:

$$\mathrm{S}(\theta, \theta_\mathrm{i}) = 10 \log_{10} \mathrm{s}(\theta, \theta_\mathrm{i}) = 10 \log_{10} \left(\frac{I_\mathrm{s}(\theta)}{I_\mathrm{i}(\theta_\mathrm{i})} \mathcal{A}_1 \right) \tag{2.6}$$

where $I_\mathrm{i}(\theta_\mathrm{i})$ is the intensity incident on a small area $d\mathcal{A}$ and $I_\mathrm{s}(\theta)$ is the scattered intensity measured at one meter back from $d\mathcal{A}$ toward the source. The backscattering strength BS can be therefore derived as:

$$\mathrm{BS}(\theta = \theta_\mathrm{i}) = 10 \log_{10} \mathrm{bs}(\theta = \theta_\mathrm{i}) = 10 \log_{10} \left(\frac{I_\mathrm{s}(\theta_\mathrm{i})}{I_\mathrm{i}(\theta_\mathrm{i})} \mathcal{A}_1 \right) \tag{2.7}$$

Considering the intensity scattered by a unit area $\mathcal{A}_1 = 1\mathrm{m}^2$ the backscattering strength, as a surface index, is consequently defined as:

$$\mathrm{BS}(\theta_\mathrm{i}) = 10 \log_{10} \left(\frac{I_\mathrm{s}(\theta_\mathrm{i})}{I_\mathrm{i}(\theta_\mathrm{i})} \right) \tag{2.8}$$

For an infinite interface, the total acoustic pressure p_s scattered by the rough surface can be written as the sum of a coherent part (its mean) and a fluctuating part [Tsang and Kong, 2004], i.e.:

$$p_\mathrm{s} = \langle p_\mathrm{s} \rangle + \delta p_\mathrm{s} \text{ with } \langle \delta p_\mathrm{s} \rangle = 0 \tag{2.9}$$

with $\langle p_s \rangle$ the reflected pressure statistical average and δp_s the pressure variations. The total intensity scattered by the surface can then be expressed as [Ogilvy and Merklinger, 1991]:

$$I_s = \frac{\langle |p_s|^2 \rangle}{Z_s} = \frac{|\langle p_s \rangle|^2 + \langle \delta |p_s|^2 \rangle}{Z_s} \tag{2.10}$$

with $|\langle p_s \rangle|^2$ the coherent part corresponding to the specular reflection from a perfectly flat and infinite interface, and $\langle \delta |p_s|^2 \rangle = \langle |p_s|^2 \rangle - |\langle p_s \rangle|^2$ the incoherent part (angular spreading and weak correlation with the incident wave) corresponding to the scattering from a very rough interface.
If the interface is perfectly flat, the coherent term is maximum and the incoherent term vanishes, the latter could therefore be neglected. On the contrary, if the roughness of the interface increases, the coherent term decrease and the incoherent term becomes predominant. For a very rough interface, the coherent term can be totally neglected.

Using this representation of scattering, different models of seabed acoustic response are derived. Some of them are discussed in the following subsections.

2.1.2 Modelling coherent scattering

Assuming that all points of the rough seabed interface have the same reflection coefficient R, and that the interface has a large mean curvature radius and gentle RMS slope (equivalent to Kirchhoff approximation), each ray incident on this surface is reflected with a phase shift depending on its wavenumber k_i, its angle of incidence θ_i, and the surface roughness $\zeta = z(x, y)$. Figure 2.2 shows that this spatial phase difference equals $k_i 2\zeta \cos(\theta_i)$.

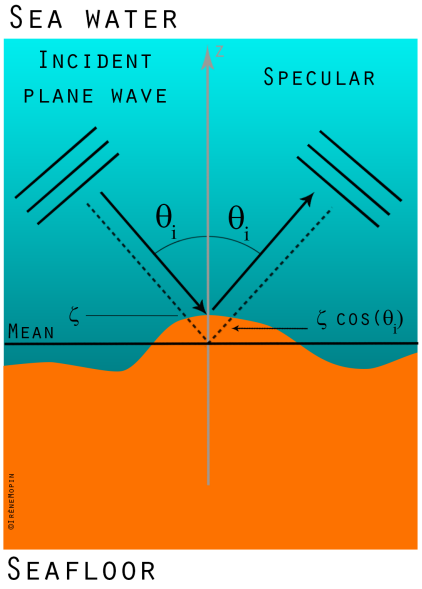

Figure 2.2 – Path differences for specular scatter from a horizontal facet of a rough surface. Inspired from [Clay and Medwin, 1977].

In this model, only the specular scatter contribution coming from insonified horizontal facets is taken into account. At any instant, the amplitude of the pressure p_r reflected at a facet of the rough surface is given by [Clay and Medwin, 1977] as:

$$p_\mathrm{r} = Rp_0 \cos\left(2k_\mathrm{i}\zeta\cos\theta_\mathrm{i}\right) \tag{2.11}$$

with p_0 the reflected amplitude in the zero roughness case (mirror). For a given surface configuration, the sum of the contributing pressures produces a coherent reflection $\langle p_\mathrm{r}\rangle$. This average pressure depends on the statistics of the surface. The authors derive the case where the surface Probability Density Function (PDF) is Gaussian. It gives the average ratio of the coherent, specularly scattered pressure to the mirror-reflected pressure from the mean interface as:

$$\left\langle \frac{p_\mathrm{r}}{p_0} \right\rangle = R\int_{-\infty}^{\infty} \left[\cos\left(2k_\mathrm{i}\zeta\cos\theta_\mathrm{i}\right)\right] \left[\frac{1}{\sigma_\zeta\sqrt{2\pi}} \exp\left\{-\frac{1}{2}\left(\frac{\zeta}{\sigma_\zeta}\right)^2\right\}\right] d\zeta \tag{2.12}$$

where σ_ζ is the RMS surface roughness. The integration is made on an infinite surface and defines the coherent reflection coefficient for a Gaussian rough surface $\langle R\rangle$ [Clay and Medwin, 1977]:

$$\langle R\rangle = \left\langle \frac{p_\mathrm{r}}{p_0} \right\rangle = Re^{-\left(2k_\mathrm{i}\sigma_\zeta\cos\theta_\mathrm{i}\right)^2/2} \tag{2.13}$$

Equivalently, the specularly scattered coherent intensity relative to the mirror-reflected intensity is given by:

$$\langle R\rangle^2 = R^2 e^{-\mathcal{R}^2} \tag{2.14}$$

where the roughness of the interface is commonly quantified by a parameter $\mathcal{R}$ called the Rayleigh roughness parameter [1] because it was studied by Rayleigh [Rayleigh, 1907, Strutt and Rayleigh, 1945]. It is defined [Stanton and Clay, 1986] as:

$$\mathcal{R} = 2k_\mathrm{i}\sigma_\zeta\cos\theta_\mathrm{i} \tag{2.15}$$

Figure 2.3 shows the variations of importance of the coherent part of the scattered field according to the Rayleigh parameter $\mathcal{R}$. We observe that a strong coherent reflection coefficient can be found for small Rayleigh parameters which implies an incident wavelength larger than the seafloor roughness or an incident angle close to 90°. On the contrary, when the roughness is larger than the wavelength (i.e. large $\mathcal{R}$) the scattering dominates and its coherent component is diminished exponentially.

This model defines the seabed acoustic response as a coherent reflection coefficient for a Gaussian rough surface $\langle R\rangle$ which main parameter is the Rayleigh coefficient $\mathcal{R}$ composed of three parameters: the incident wavenumber k_i, its angle of incidence θ_i, and the surface RMS roughness σ_ζ. It is considered as a physical model as shown in table 2.1.

1. Not to be confused with the parameter of the Rayleigh probability density function σ mostly used in the following parts of this manuscript.

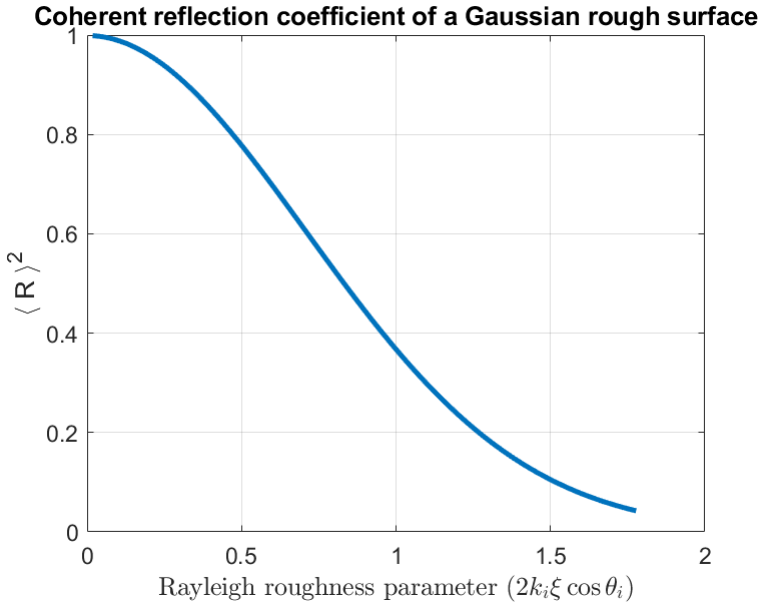

Figure 2.3 – Coherent reflection from the rough seafloor as a function of $k_i\sigma_\zeta \cos\theta_i$. Adapted from [Stanton and Clay, 1986]

2.1.3 Modelling incoherent scattering

We first consider in this section the seabed as a rough interface where a portion of the incident power $P_\mathrm{i} = I_\mathrm{i}\mathcal{A}\cos\theta_\mathrm{i}$ is scattered into the half-space above the interface (the transmitting and reflected powers are not considered). This scattering phenomenon is characterized in space by an angular function $g(\theta_\mathrm{i}, \theta)$ (see figure 2.4). It can have different patterns depending on the specificities of the seafloor interface. The function is normalized so that $\int g(\theta_\mathrm{i}, \theta)d\theta = \eta(\theta_\mathrm{i})$. In this case, the scattered intensity I_s at a reference distance of $r_\mathrm{1m} = 1\mathrm{m}$ (and with no absorption) can be written as [Lurton, 2010]:

$$I_\mathrm{s} = P_\mathrm{i} g(\theta_\mathrm{i}, \theta) = I_\mathrm{i}\mathcal{A}_1 \cos(\theta_\mathrm{i}) \frac{g(\theta_\mathrm{i}, \theta)}{r_\mathrm{1m}^2} \tag{2.16}$$

where $\mathcal{A}_1$ is a unit area of $1\mathrm{m}^2$ from which the intensity is scattered. The scattering strength is then defined as:

$$\mathrm{s}(\theta_\mathrm{i}, \theta) = \frac{I_\mathrm{s}}{I_\mathrm{i}} r_\mathrm{1m}^2 = \mathcal{A}_1 \cos(\theta_\mathrm{i}) g(\theta_\mathrm{i}, \theta) \tag{2.17}$$

This expression leads to the backscattering strength, defined at $r_\mathrm{1m} = 1\mathrm{m}$ and with $\mathcal{A}_1 = 1\mathrm{m}^2$, as:

$$\mathrm{bs}(\theta = \theta_\mathrm{i}) = \cos(\theta_\mathrm{i}) g(\theta_\mathrm{i}, \theta_\mathrm{i}) \tag{2.18}$$

If the scattering is perfectly isotropic i.e. functions $g(\theta_\mathrm{i}, \theta)$ and $\eta(\theta_i)$ are independent of angles (see figure 2.4) and if the scattered transmit intensity is null, we can define $\eta(\theta_i) = \eta_0$ and $g = \eta_0/2\pi$, and the backscattering cross-section becomes:

$$\mathrm{bs}(\theta = \theta_\mathrm{i}) = \mu_\mathrm{LS} \cos(\theta_\mathrm{i}) \tag{2.19}$$

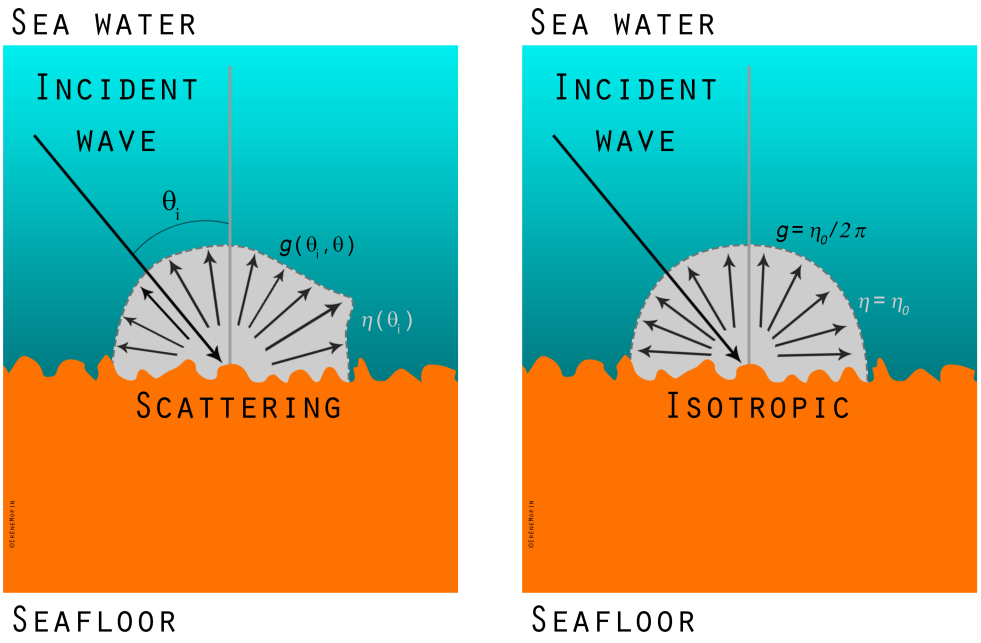

Figure 2.4 – Scattering phenomenon at a rough and non-penetrable interface

where $\mu_{\mathrm{LS}} = \eta_0/2\pi$ is the Lommel-Seeliger constant [Fromm, 2020]. If the scattering is depending on the roughness of the seafloor, the scattered intensity depends on the interface slope distribution [Lurton, 2010]. A relation commonly named 'Lambert's cosine law' or 'Lambert's law' defines in this case the seafloor characteristic function $g(\theta_{\mathrm{i}}, \theta)$ as a constant times $\cos\theta$ [Ishimaru, 1977]. The constant is called the 'Lambert parameter' and noted μ_{L}. The resulting backscattering cross-section bs is [Ishimaru, 1978, Jenserud et al., 2001]:

$$\mathrm{bs}(\theta = \theta_{\mathrm{i}}) = \cos(\theta_{\mathrm{i}}) g(\theta_{\mathrm{i}}, \theta_{\mathrm{i}}) = \mu_{\mathrm{L}} \cos^2(\theta_{\mathrm{i}}) \tag{2.20}$$

where $\mu_{\mathrm{L}} = \eta_0/\pi$. It gives in decibels [Howell, 2000]:

$$\mathrm{BS} = 10\log_{10}(\mu_{\mathrm{L}}) + 10\log_{10}\left(\cos^2\theta_{\mathrm{i}}\right) \tag{2.21}$$

An upper limit of $10\log_{10}(\mu_{\mathrm{L}})$ can be derived considering a perfectly reflecting interface where $\eta_0 = 1$ [Lurton, 2010]. It gives $10\log_{10}(\mu_{\mathrm{L,max}}) = -5$dB ref. $1\mathrm{m}^2$. In literature, several *in situ* measurements of this parameter were carried out by numbers of authors, e.g.:

— [Desharnais and Ellis, 1997] who processed data from SACLANT Undersea Research Center from 50 Hz to 1000 Hz. They found values of Lambert coefficient from -36 dB for a silt-clay seabed to -11 dB for a flat sand seabed;

— [Mackenzie, 1961] who made measurements at 530 Hz and 1030 Hz on a clay bottom and found that a value of $10\log_{10}\mu_{\mathrm{L}} = -27$ dB fits his data well for incident angles from 0° to 60°;

— [Garlan and Demoulin, 1997] who found in their cases three values of $10\log_{10}\mu_{\mathrm{L}}$ that fit with three types of seabed: rock = -18 dB, sand= -31 dB, and silt= -37 dB;

— [Gensane, 1989] who found $10\log_{10}\mu_{\mathrm{L}} = -29$ dB for mud, -22 dB for sand, -15 dB for gravel and rock [Caprais and Lombardi, 1996].

In conclusion, Lambert model defines the seabed acoustic response as an heuristic coefficient balanced by an angular function of the incident angle on the seafloor. It is considered as an heuristic model as shown in table 2.1.

An improvement on Lambert's law was developed by Thales [2] in [Sevaldsen, 2002] where the constant μ_{L} became dependent on the porosity b_ϕ of the seafloor and the frequency of the incident acoustic wave $\mathfrak{f}$. The model is assumed to be valid in the frequency range $1 - 10$ kHz and is given by:

$$\mathrm{BS} = 10\log_{10}\left(\mu_{\text{L-T}}\right) + 10\log_{10}\left(\cos^2\theta_{\mathrm{i}}\right) \tag{2.22}$$

$$\mu_{\text{L-T}} = 0.84 \cdot \mathfrak{f}_{(\mathrm{kHz})} \cdot 10^{-b_\alpha} \tag{2.23}$$

$$b_\alpha = 0.1(b_1 + b_2 \cdot b_\phi) \tag{2.24}$$

where b_1 and b_2 are constants, and values of b_α are given for some sediment types as mud = 3.7, sand = 3.1, and rock = 1.8. The seafloor response is in this model dependent on five parameters (see table 2.1)

A generalization of the Lambert's rule was developed by [Mackenzie, 1961] and is often called 'Lambert-Mackenzie's law' in the literature. The model depends on μ_{L} but also on an exponent $\mathfrak{n}$ on the cosine function. For backscattering strength it gives [Jenserud et al., 2001]:

$$\mathrm{bs} = \mu_{\text{L-M}}\cos^{\mathfrak{n}}\theta_{\mathrm{i}} \tag{2.25}$$

The two parameters are used as adjustable coefficients to help characterize the sites and frequency dependence of the seafloor response [Desharnais and Ellis, 1997]. The seafloor response is in this model dependent on two parameters (see table 2.1)

According to this generalised Lambert's rule (equation 2.25), the backscattering strength approaches zero for high incidence angles ($\theta_{\mathrm{i}} \to 90°$). For some terrains, a different behaviour is observed [Urick, 1983] where the backscattering strength approaches a threshold for incidence angles above 80°. To account for this effect, the Lambert-Mackenzie rule can be modified by adding a threshold b_0 [Jenserud et al., 2001]:

$$\mathrm{bs} = b_0 + \mu_{\text{L-M}}\cos^{\mathfrak{n}}\theta_{\mathrm{i}} \tag{2.26}$$

This model depends therefore on three parameters: the Lambert-Mackenzie constant $\mu_{\text{L-M}}$, the threshold b_0 and the exponent $\mathfrak{n}$ (see table 2.1). It is assumed frequency independent.

2. Thales: ex-Thomson Marconi Sonar

Based on the models of equations 2.20 and 2.26, [Del Balzo et al., 1997] modified the Lambert's rule to include a correction at high incidence angles to account for the scattering-strength plateau caused by scattering inside the sediment (considered coming from volume inhomogeneities). The threshold b_0 added in the Del Bazo model is not a free parameter but is connected to the Lambert constant μ_{L} by the seabed type. The rule is formulated as [Sevaldsen, 2002]:

$$\mathrm{bs} = b_0(b_\Phi) + \mu_{\text{L-DB}}(b_\Phi)\cos^2\theta_i \tag{2.27}$$

where b_0 is the high incidence angle plateau threshold, and where both b_0 and $\mu_{\text{L-DB}}$ depend on bottom type through a parameter b_Φ. This parameter is related to the mean sediment grain-size b_δ in millimetres by $b_\delta = (1/2)b_\Phi$. Consequently the model is characterized by one geo-physical parameter: the grain-size b_δ in addition to the three other heuristic parameters (see table 2.1).

2.1.4 Merging incoherent and coherent components

In this section, both of the incoherent and coherent components of the scattering strength are taken into account. The total backscattering strength can be written in this manner as:

$$\mathrm{bs} = \mathrm{bs}_{\mathrm{coh}} + \mathrm{bs}_{\mathrm{scat}} \tag{2.28}$$

with $\mathrm{bs}_{\mathrm{coh}}$ modelling the specular reflection of the incident acoustic wave on the rough interface, and bs_{scat} modelling the diffuse scattering.

A first model using two components was developed by [Ellis and Crowe, 1991]. They combined Lambert's rule for diffuse scattering to a strong scattering process concentrated near the specular direction. The latter is not using coherent field but has the same purpose. It can be found in [Beckmann and Spizzichino, 1987] and [Lysanov and Brekhovskikh, 1982] and is derived in the Kirchhoff approximation from the Helmholtz integral for a two-dimensions isotropically rough surface of RMS slope σ_ψ described by a Gaussian distribution. It is commonly named facet scattering because it assumes reflections from a statistical distribution of facets inclined with respect to the horizontal. The combination of the two models gives a backscattering strength as [Ellis and Crowe, 1991][Jenserud et al., 2001]:

$$\mathrm{bs} = \mu_{\mathrm{L}}\cos^2(\theta_{\mathrm{i}}) + b_a\frac{1}{\cos^4\theta_{\mathrm{i}}}\exp\left(-\frac{\tan^2\theta_{\mathrm{i}}}{2\sigma_\psi^2}\right) \tag{2.29}$$

where μ_{L} is the Lambert constant, b_a the facet strength and σ_ψ the RMS facet slope, also called the facet width since it describes a measure of the angular width near normal incidence over which the facet reflection is important. A backscattering strength function similar but with the $\cos^4\theta_{\mathrm{i}}$ term missing has been used in [Ellis and Franklin, 1987]. This was a generalization of the function proposed by [Watson and McGirr, 1972] who used a constant for σ_ψ and chose b_a to be either 1 or equal to the magnitude of the seafloor reflection coefficient at normal incidence. A fit to real measurements was done by [Ellis and Crowe, 1991] and gives $10\log_{10}\mu_{\mathrm{L}} = -32\,\mathrm{dB}$, $10\log_{10}b_a = -12\,\mathrm{dB}$, and $(180°/\pi)\sigma_\psi = 10°$ (the transmitted frequency and the seabed type are not specified in the article, except that it is at low frequency).
This model is included in table 2.1 as an heuristic model with four parameters.

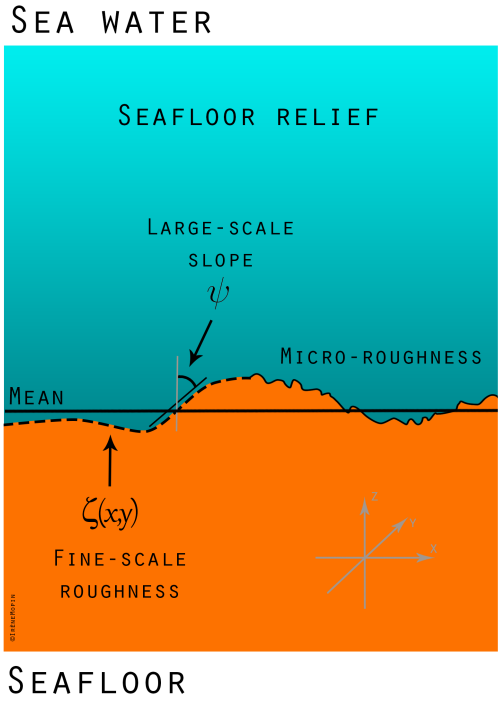

Figure 2.5 – Model of the interface relief or bottom roughness ζ. Heights z are function of the two space dimensions $\vec{x} = (x, y)$ so that $z = \zeta(\vec{x})$. They are measured according to the mean of ζ. Two regimes of the relief below the large scale bathymetry are illustrated: the fine-scale roughness and the micro-roughness (see their spectrum in figure 5.6)

Another model, developed by [Novarini and Caruther, 1998], assumed the backscattering strength to be composed of three contributions:

- $\mathrm{bs}_{\mathrm{RFM}}$: the scattering from fine-scale components of the bottom roughness ζ i.e. from geomorphology at a scale below large-scale deterministic bathymetry but larger than the incident wavelength (see figure 2.5);
- $\mathrm{bs}_{\mathrm{scat}}$: the scattering from the small-scale roughness, also called micro-roughness ζ_{ss} (see figure 2.5);
- $\mathrm{bs}_{\mathrm{vol}}$: the scattering from the inhomogeneities in the volume of sediment (with due regard to the fact that it comes through the rough interface).

The authors gives:

$$\mathrm{bs} = \mathrm{bs}_{\mathrm{RFM}} + \mathrm{bs}_{\mathrm{scat}} + \mathrm{bs}_{\mathrm{vol}} \tag{2.30}$$

The first term $\mathrm{bs}_{\mathrm{RFM}}$ is handled by the Rough Facet Model (RFM) [Novarini and Caruthers, 1994]. It represents the collective contribution from reflections at the fine-scale facets containing micro-roughness, i.e. it is controlled by a facet reflection process which is partially coherent for individual facets but collectively incoherent when summed over the sonar insonified area. (Note that the facet slopes are supposed random variables and assumed Gaussian distributed, and the measurement is made in far field (see definition in section 3.2.1)). The

$\mathrm{bs}_{\mathrm{RFM}}$ term is then defined as:

$$\mathrm{bs}_{\mathrm{RFM}} = |R|^2 e^{-\mathcal{R}^2_{\zeta_{\mathrm{ss}}}} \frac{1}{8\pi\sigma^2_\psi \cos^2\theta_{\mathrm{i}}} \exp\left(-\frac{\tan^2\theta_{\mathrm{i}}}{2\sigma^2_\psi}\right) \tag{2.31}$$

where R is the the pressure reflection coefficient for smooth surface, σ_ψ is the RMS slope of the fine scale facets and $\mathcal{R}_{\zeta_{\mathrm{ss}}}$ is the Rayleigh roughness parameter of the micro-roughness, given by:

$$\mathcal{R}_{\zeta_{\mathrm{ss}}} = 2\sigma_{\zeta_{\mathrm{ss}}} k_{\mathrm{i}} \cos\theta_{\mathrm{i}} \tag{2.32}$$

with $\sigma_{\zeta_{\mathrm{ss}}}$ the RMS height of the micro-roughness and k_{i} the incident acoustic wavenumber. The first two terms $|R|^2 e^{-\mathcal{R}^2_{\zeta_{\mathrm{ss}}}}$ correspond to the coherent reflection coefficient due to the micro-roughness on a facet. The last two terms correspond to the contribution of the fine-scale slopes of the facets, which is also the high-frequency limit of the Helmholtz-Kirchhoff theory [Brekhovskikh et al., 1991] for backscattering.

The two interface parameters ($\sigma_{\zeta_{\mathrm{ss}}}$ and σ_ψ) are band-limited quantities. The variance of the micro-roughness for a two-dimensional isotropic interface is given as:

$$\sigma^2_{\zeta_{\mathrm{ss}}} = 2\pi \int_{\vec{k}_c}^{\vec{k}_h} W(\vec{k}) \vec{k} d\vec{k} \tag{2.33}$$

and the variance of the slopes of the fine-scale interface:

$$\sigma^2_\psi = 2\pi \int_{\vec{k}_L}^{\vec{k}_h} W(\vec{k}) \vec{k}^3 d\vec{k} \tag{2.34}$$

with $\vec{k}$ the spatial frequency of the surface roughness, $W(\vec{k})$ the power spectra describing the seafloor roughness (often chosen as an isotropic power law $W(\vec{k}) = b^2_3 \vec{k}^{-2b_4}$, see section 2.3.3), $\vec{k}_L$ and $\vec{k}_h$ respectively the low and high spatial frequencies present in the relief, and k_{c} denotes the cut-off spatial frequency (see figure 5.6). These spatial frequencies are determined by the size of the footprint and the sampling of the bottom roughness. $\vec{k}_h$ can approach infinity, but $\vec{k}_L$ approaching zero is not physical because the footprint of a sonar is always limited in size.

In equation 2.31, the micro-roughness is only represented by $|R|^2 e^{-g_{\zeta_{\mathrm{ss}}}}$ as a loss mechanism in the specular direction. However, the micro-roughness also scatters energy in all directions, and its contribution to the total backscattering strength have to be taken into account. [Novarini and Caruther, 1998] chose to evaluate this contribution through the perturbation theory (acoustically smooth interface, [Brekhovskikh et al., 1991]), leading to resonant (Bragg) scattering. For Bragg scattering due to the micro-roughness and isotropic penetrable interface, the backscattering strength can be written as:

$$\mathrm{bs}_{\mathrm{scat}} = R^2 k^4_{\mathrm{i}} \cos^4\theta_{\mathrm{i}} W\left(\frac{k_{\mathrm{i}}}{\pi}\sin\theta_{\mathrm{i}}\right)\frac{1}{\pi^2} \tag{2.35}$$

where the power density spectrum $W(\vec{k})$ is evaluated at the resonant wavenumber $k_{\mathrm{i}}\sin(\theta_{\mathrm{i}})/\pi$.

To model the contribution of $\mathrm{bs_{vol}}$, the authors choose to use the [Ivakin and Lysanov, 1981] formalism (volume contributions taking into account the rough boundary). For monostatic backscattering and isotropic, weak, volume scattering, the volume contribution to the backscattering strength is given as [Ivakin and Lysanov, 1981]:

$$\mathrm{bs_{vol}} = \frac{m_0}{4k_\mathrm{i} b_\delta \frac{\rho_\mathrm{sw}^2}{c_\mathrm{sw}}} \left\langle \frac{T^4(\theta_\mathrm{i}')[\frac{1}{c_\mathrm{sw}^2} - \sin^2\theta_\mathrm{i}']^{1/2}}{\frac{1}{c_\mathrm{sw}}\cos\psi} \right\rangle \tag{2.36}$$

where the local incidence angle θ_i is replaced by the incidence angle $\theta_\mathrm{i}' = \theta_\mathrm{i} - \psi$, ψ is the local slope angle of the interface, m_0 is a free parameter called volume scattering coefficient, the angle brackets represent an average over fine-scale slopes in the footprint of the sonar, c_sw= $c_\mathrm{s}/c_\mathrm{w}$, ρ_sw= $\rho_\mathrm{s}/\rho_\mathrm{w}$, and $T(\theta_\mathrm{i}')$ is the local amplitude transmission coefficient given by:

$$T(\theta_\mathrm{i}') = \frac{2\rho_\mathrm{sw}\cos\theta_i'}{\rho_\mathrm{sw}\cos\theta_\mathrm{i}' + (\frac{1}{c_\mathrm{sw}^2} - \sin^2\theta_\mathrm{i}')^{1/2}} \tag{2.37}$$

and b_δ is a loss parameter given by:

$$b_\delta = \frac{\alpha_\mathrm{s} c_\mathrm{s}\log(10)}{\mathfrak{f}_\mathrm{kHz}\pi} \tag{2.38}$$

where α_s is the attenuation coefficient in the sediment and $\mathfrak{f}_\mathrm{kHz}$ the frequency in kilo-Hertz. In their publication, [Novarini and Caruther, 1998] simplify and rearrange equation 2.36 to get:

$$\mathrm{bs_{vol}} = \mu_\mathrm{NC} V(\theta_\mathrm{i} - \sigma_\psi) \tag{2.39}$$

where

$$V(\theta_\mathrm{i} - \sigma_\psi) = \frac{\cos^4(\theta_\mathrm{i} - \sigma_\psi)[1 - \sin^2(\theta_\mathrm{i} - \sigma_\psi)c_\mathrm{sw}^2]^{1/2}\left(\rho_\mathrm{sw} + \frac{1}{c_\mathrm{sw}}\right)^4}{\left\{\rho_\mathrm{sw}\cos(\theta_\mathrm{i} - \sigma_\psi) + \left[\frac{1}{c_\mathrm{sw}^2} - \sin^2(\theta_\mathrm{i} - \sigma_\psi)\right]^{1/2}\right\}^4} \tag{2.40}$$

and

$$\mu_\mathrm{NC} = \frac{8\rho_\mathrm{sw}^2 m_0}{2k_\mathrm{i}\frac{1}{c_\mathrm{sw}} b_\delta \cos(\sigma_\psi)\left[\rho_\mathrm{sw} + \frac{1}{c_\mathrm{sw}}\right]^4} \tag{2.41}$$

where σ_ψ is the RMS slope of the surface within the fine-scale portion as prescribed by the rough facet model [Novarini and Caruthers, 1994]. The constant μ_NC is a surface scattering constant attributed to volume scattering. The functional form $V(\theta_\mathrm{i})$ goes to unity as θ_i goes to zero (normal incidence). It can vary between cosine (Lommel-Seeliger law [3]) at normal incidence through cosine squared (Lambert's law) at moderate grazing angles, to higher powers of cosine for near grazing angles.

This model is finally one of the seabed acoustic response that has the most parameters (12 parameters are needed, see table 2.1). It is heuristic but based on physical phenomena and uses physical parameters characteristic of the seabed sediment or the water medium.

3. The Lommel–Seeliger law is often cited in the literature of the former Soviet Union, e.g., [Ivakin and Lysanov, 1981], but we have not found the original reference to this form in translated scientific literature.

2.2 Empirical models

Several models of scattering (or backscattering) strength have been developed purely mathematically in order to describe measurements made at sea. These models sometimes refer retrospectively to some physical principles but remain eventually empirical. In the following, examples of mathematical models are given.

2.2.1 Patterson model

[Patterson, 1963] proposed a mathematical model for the backscattering strength of a rough interface as, in decibels:

$$\mathrm{BS} = 10\log_{10}\left[R^2(b_B + b_C)\right] \tag{2.42}$$

In this formula, the term R refers to the reflection coefficient, b_B is weighting constant times some type of a random distribution density function, and b_C is a constant times the cosine of the incident angle θ_i raised to a constant power. In details it gives:

$$R = \frac{\rho_\mathrm{sw} c_\mathrm{sw}\cos\theta_\mathrm{i} - \sqrt{1 - c_\mathrm{sw}^2\sin^2\theta_\mathrm{i}}}{\rho_\mathrm{sw} c_\mathrm{sw}\cos\theta_\mathrm{i} + \sqrt{1 - c_\mathrm{sw}^2\sin^2\theta_\mathrm{i}}} \tag{2.43}$$

for $c_\mathrm{s}/c_\mathrm{w}\sin\theta_\mathrm{i} \leq 1$.

$$b_B = 16(1 + 11.9\tan^2\theta_\mathrm{i})^{-2.9} \tag{2.44}$$

$$b_C = 0.04\cos\theta_\mathrm{i} \tag{2.45}$$

These empirical coefficients were fitted to data at 2.5 kHz described in [Patterson, 1963]. In total, three parameters are used in this model (see table 2.1) including two physical ones (seafloor and water impedancies).

2.2.2 McKinney and Anderson model

Based on measurements of backscattering strength in 16 locations around the coast of the US, McKinney and Anderson [4] computed a model for frequencies $\mathfrak{f}$ from 12.5 kHz to 290 kHz. Their model has two parts according to the incidence angle θ_i [Jenserud et al., 2001]:
For $50° < \theta_\mathrm{i} \leq 90°$, which can be linked to a diffuse scattering:

$$\mathrm{bs}(\theta_\mathrm{i}) = 1.196[(\cos\theta_\mathrm{i} + 0.19)^{b_b(\sin\theta_\mathrm{i})^{16}} \cdot 2.53\mathfrak{f}_\mathrm{kHz}^{(3.2-0.8b_b)}10^{(2.8b_b-12)} + 3.162278.10^{-5}] \tag{2.46}$$

And for $0° < \theta_i \leq 50°$, which can be linked to the near-nadir scattering:

$$\mathrm{bs}(\theta_\mathrm{i}) = 1.196\Big\{(\cos\theta_\mathrm{i} + 0.19)^{b_b(\sin\theta_\mathrm{i})^{16}} \cdot \left[1 + 125e^{(-2.64(b_b-1.75)^2 - 50/(\cot^2\theta_\mathrm{i} b_b))}\right] \cdot 2.53\mathfrak{f}_\mathrm{kHz}^{(3.2-0.8b_b)}10^{(2.8b_b-12)} + 3.162278.10^{-5}\Big\} \tag{2.47}$$

The scalar b_b correspond to the bottom type (1=mud; 2=sand; 3=gravel; 4=rock) and can be interpolated e.g. 1.5 for mud and sand [Caprais and Lombardi, 1996], 2.5 for coarse sand [Bouvet, 1992]. Three parameters are then used in this model (see table 2.1)

4. The reference publication could not be found. Only [McKinney and Anderson, 1964] is cited to be the reference but the model doesn't appears in it.

2.2.3 GESMA model

The French underwater study group of the Atlantic (*Groupe d'étude sous-marine de l'Atlantique* (GESMA)) developped its own model, frequency independent, with two parameters B_1 and B_2 depending on the seafloor type [Bouvet, 1992]. It gives the backscattering strength, in decibels, as:

$$\mathrm{BS}(\theta_\mathrm{i}) = B_1 + B_2 \log_{10}\left(\frac{\pi}{2} - \theta_\mathrm{i}\right) \tag{2.48}$$

with θ_i the incident angle, and: (B_1=-60, B_2=13) for mud, (B_1=-67, B_2=28) for fine sand or sandy mud, (B_1=-47, B_2=21) for hard sand, (B_1=-37, B_2=21) for gravel, (B_1=-16, B_2=7) for rock.

2.2.4 GSAB model

More recently, the Generic Seafloor Acoustic Backscatter (GSAB) working group supported by the Marine Geological and Biological Habitat mapping conference (GeoHab) developed an empirical model for the backscattering strength. It is a combination of a Gaussian law for specular angles, a Lambert-like law for grazing angles, and an intermediate term to account for the smooth transition between specular and lateral modes. The backscattering strength is given, in decibels [Lurton et al., 2015] [Lamarche et al., 2011], as:

$$\mathrm{BS}(\theta_\mathrm{i}) = 10\log_{10}[b_A \exp(-\theta_\mathrm{i}^2/2b_B^2) + b_C \cos_D^b \theta_\mathrm{i} + b_E \exp(-\theta_\mathrm{i}/2b_F^2)] \tag{2.49}$$

where :

- b_A quantifies the specular maximum amplitude. In the tangent-plane approach ([Brekhovskikh et al., 1991]), b_A is related to the coherent reflection coefficient at the water–seabed interface, and is therefore high for smooth sediment interfaces (at the acoustic wavelength scale) and for strong water–sediment impedance contrasts.
- b_B quantifies the angular extent of the specular regime. In the tangent-plane model, it represents the facet slope variance and is therefore an interface roughness descriptor.
- b_C quantifies the average BS level at oblique incidence. It is the offset associated with Lambert's law describing BS at intermediate angles for rough interfaces, and includes the contribution of the volume inhomogeneity backscatter. b_C increases with frequency, seafloor roughness and impedance, and heterogeneities present inside the sediment volume. The constant $10\log_{10} b_C$ ranges from -20 to -30 dB, but values between -15 and -40 dB are commonly observed.
- b_D is the backscatter angular decrement, commanding the fall-off at grazing angles. It is high for soft and smooth sediment interfaces. According to the laws of Lommel-Seeliger and Lambert, b_D is equal to 1 and 2, respectively.
- b_E is the transitory maximum level (dB) where the transitory function (i.e. the last term of equation 2.49) aims at linking smoothly the specular function and the grazing angle function (i.e. the two first terms of equation 2.49).
- b_F is the transitory maximum angular half-extent (in degrees)

This model has therefore seven parameters (see table 2.1) which makes it the most sophisticated empirical model of this section. Sometimes, for simplicity, only five parameters are used (removing b_E and b_F as in [Augustin and Lurton, 2005]).

2.3 Increasing model complexity to get closer to physical phenomena

The aim of this section is to present scattering models which objectives are to be closer to the physical phenomena leading to the backscattering strength. Three examples are chosen arbitrarily with different modelling of the seafloor: the sediment is penetrable or not, the roughness of the interface has different scales, etc.

2.3.1 Nolle model: incoherent scattering by water-filled sand

[Nolle et al., 1963] assumed a water-filled sand medium, containing a distribution of scatterers positions not completely uniform. If these scatterers were given an orderly arrangement, the scattering would consist largely of the coherent reflection. Since the scatterers are irregularly placed, much of the scattered acoustical energy is incoherent and distributed broadly in angle. In order to compute the incoherent scattering, the authors express the random properties of the distribution of the scatterers positions using an average scattering amplitude factor per unit volume Υ. Specifically, on the average, when a volume element dV is affected by the pressure field $p(x, y)$, the scattered pressure at unit distance in the medium is $\Upsilon_0 p(x, y)dV$. The actual value of the scattering amplitude factor at (x, y, z) is then denoted by:

$$\Upsilon(x, y, z) = \Upsilon_0[1 + \delta(x, y, z)] \tag{2.50}$$

The quantity δ is a measure of local deviation from the average scattering amplitude factor. The quantity Υ_0 is a measure of the average amplitude of the re-radiated signal from an element of volume, as considered in Huygens' principle. The effect of scattering corresponds to the integrated result of deviations of local re-radiation from this average. $\delta(x, y, z)$ is defined as a random function. For large volume $\int \delta(x, y, z)dV = 0$. The mean-square value of $\delta(x, y, z)$ is $\langle\delta^2\rangle$.

Using this scattering concept, the calculation of the total scattering from a semi-infinite medium is derived by [Nolle et al., 1963]. Under the assumption that the correlation distance d_{corr} is of the order of the sand particle radius i.e. much smaller than the wavelength, the surface scattering coefficient becomes:

$$\mathrm{s}(\theta_\mathrm{i}, \theta, \theta_\mathrm{t}) = 16\pi \left[\Upsilon_0 e^{\alpha_\mathrm{s}}\right]^2 \langle\delta^2\rangle \left(\frac{\rho_\mathrm{w}}{\rho_\mathrm{s}}\right)^3 d_{\text{corr}}^3 \left[-\Re(U)\right]^{-1} \left|\frac{2q_1}{(1+q_1)}\right|^2 \left|\frac{2q_2}{(1+q_2)}\right|^2 \tag{2.51}$$

with

$$U \equiv (-\alpha_\mathrm{s} + j\omega/c_\mathrm{s})(\cos\theta + \cos\theta_\mathrm{t}) \tag{2.52}$$

$$q_1 = \frac{(-\alpha_\mathrm{w} + j\omega/c_\mathrm{w})\rho_\mathrm{s}}{(-\alpha_\mathrm{s} + j\omega/c_\mathrm{s})\rho_\mathrm{w}} \cdot \frac{\cos\theta}{(1 - \left[\frac{-\alpha_\mathrm{w}+j\omega/c_\mathrm{w}}{-\alpha_\mathrm{s}+j\omega/c_\mathrm{s}}\right]^2 \sin^2\theta)^{1/2}} \tag{2.53}$$

$$q_2 = \frac{(-\alpha_\mathrm{w} + j\omega/c_\mathrm{w})\rho_\mathrm{s}\cos\theta_\mathrm{i}}{(-\alpha_\mathrm{s} + j\omega/c_\mathrm{s})\rho_\mathrm{w}\cos\theta_\mathrm{t}} \tag{2.54}$$

Where θ is the angle for detection of scattering (in the case of backscattering $\theta = \theta_\mathrm{i}$). The different parameters are listed below:

- α_{w} and α_{s} are respectively attenuation coefficients of water and sediment;
- ρ_{w} and ρ_{s} are respectively acoustical densities of water and sediment;
- d_{corr} is a characteristic distance that may be considered as a radius of correlation. If d_{corr} is assumed to be proportional to the particle radius d_a, then equation 2.51 predicts that s varies as d_a^4 if the grazing angle of incidence exceeds the critical value. This comes about through the factors d_{corr}^3 and $[-\Re(U)]^{-1}$ that vary as d_a. The exact value of d_{corr} is unimportant in both the frequency characteristic and the variation with angle, provided only that d_{corr} is small compared to the wavelength;

The frequency dependence of the scattering coefficient s for angles under the critical angle is governed largely by the factors $\Upsilon_0^2\langle\delta^2\rangle$ and $[-\Re(U)]^{-1}$. The first one describes the variations in scattering power per unit volume and is expected to vary as ω^4 which corresponds to the characteristic frequency effect in Rayleigh scattering. The second one is approximately a reciprocal measure of the amplitude attenuation constant α_{s} for the sand medium, varying as $\omega^{-1/2}$. Thus, s varies, for the lower incident angles, approximately as $\omega^{7/2}$.

2.3.2 Essen model: case of shear waves presence in sediment

[Essen, 1994] propose a simplified perturbation approach which directly determines the scattered acoustic field. No account is taken for larger scale roughness, which may modulate the angle dependence or cause shadowing. Essen's approach reproduces the backscattering coefficient as a function of incident angle as given by [Dacol and Berman, 1988] without accounting for multiple scattering.

The fist-order perturbation theory is applied to acoustic scattering from a rough seafloor. The incident acoustic wave is assumed to be a plane wave of amplitude A_{i}. The bottom roughness is described by $z = \zeta(x, y)$ (see figure 2.5) and is represented by a two-dimensional Fourier integral:

$$\zeta(\vec{x}) = \int W_z(\vec{k}) e^{j(\vec{k}\,\cdot\,\vec{x})} d\vec{k} \tag{2.55}$$

where $W_z(-\vec{k}) = W_z^*(\vec{k})$ i.e. W_z is constrained to give real values of $\zeta(\vec{x})$, $\vec{x} = (x, y)$, and $\vec{k} = (k_x, k_y)$ is the horizontal wave-number vector components. This mathematical representation is appropriate for a frozen seafloor. The seafloor interface is assumed to be a zero-mean homogeneous random process, i.e.:

$$\left| \begin{array}{l} \langle W_z(\vec{k})\rangle = 0 \\ \langle W_z(\vec{k}) W_z^*(\vec{k'})\rangle = W(\vec{k})\delta(\vec{k} - \vec{k'}) \end{array} \right. \tag{2.56}$$

where the angle brackets indicate expected values (estimated by means), and $W(\vec{k})$ is the roughness spectrum of the interface. If the seabed is supposed homogeneous, Fourier amplitudes are supposed decorrelated. In this case, the spatial covariance function of $\zeta(\vec{x})$ depends only on the spatial lag between positions $\vec{x}$ and not on the positions itself. It is also equal to the two-dimensional Fourier transform of the spectrum $W(\vec{k})$. The total variance of the roughness σ_ζ^2 is determined from equations 2.55 and 2.56 as:

$$\sigma_\zeta^2 = \int W(\vec{k}) d\vec{k} \tag{2.57}$$

In the publication, ensemble averaging are replaced by spatial averaging, assuming that different parts of the insonified area $\mathcal{A}$ yield statistically independent contributions of the scattered field. Thus, the insonification has to respect the hypothesis of being extend over areas with diameters large compared to the correlation lengths of bottom roughness.

Considering approximate solutions for the scattered field (means of perturbations theory), and applying boundary conditions (an undistributed seafloor yields a specular reflected wave, and non-linear terms yield quadratic coupling between zero-order acoustic variables and bottom roughness), [Essen, 1994] found a scattering coefficient as:

$$\mathrm{s}(\omega, \theta_\mathrm{i}, \theta) = \frac{\omega^2}{c_\mathrm{w}^2} \frac{|A_\mathrm{s}|^2}{|A_\mathrm{i}|^2} W(\vec{k}_\mathrm{s} - \vec{k}_\mathrm{i}) \cos^2\theta \tag{2.58}$$

where A_s is the scattered amplitude from the interface and depends on the seafloor model and solutions, θ the scattering angle, $\vec{k}_\mathrm{s}$ is the scattered wave-vector, and $\vec{k}_\mathrm{i}$ is the incident wave-vector. Note that only angles in the plane $(\theta_\mathrm{i}, \theta)$ are kept here for notation simplicity whereas equation 2.58 is actually in three dimensions.

For a seafloor represented as an elastic medium containing compressional and shear waves, and in the limiting case of an existing vanishing shear-wave velocity, A_s becomes:

$$A_\mathrm{s} = 2j\gamma_{\omega 0} A_\mathrm{i} \frac{(b_\alpha - 1)(b_\alpha(\vec{k}_\mathrm{i} \cdot \vec{k}_\mathrm{s} - k_\mathrm{i}^2) - \gamma_{p0}\gamma_{ps}) - b_\alpha(b_\alpha\gamma_{\omega 0}^2 - \gamma_{p0}^2)}{(b_\alpha\gamma_{\omega 0} + \gamma_{p0})(b_\alpha\gamma_{\omega s} + \gamma_{ps})} \tag{2.59}$$

with

$$\begin{aligned} b_\alpha &= \rho_\mathrm{s}/\rho_\mathrm{w} \\ \gamma_{\omega 0} &= (\omega/c_\mathrm{w})\cos\theta_\mathrm{i} \\ \vec{k}_\mathrm{s} &= \vec{k}_\mathrm{i} + \vec{k} \\ \gamma_{p0} &= \sqrt{(\omega/c_\mathrm{s})^2 - k_\mathrm{i}^2} \end{aligned} \tag{2.60}$$

In the backscattering case, $\vec{k}_\mathrm{r} = -\vec{k}_\mathrm{i}$ i.e. $\theta = \theta_\mathrm{i}$, and $W(-\vec{k}) = W(\vec{k})$. Therefore, the backscattering strength can be derived as:

$$\mathrm{bs}(\omega, \theta = \theta_\mathrm{i}) = \left(\frac{\omega}{c_\mathrm{w}}\cos\theta_\mathrm{i}\right)^4 \frac{|A_\mathrm{s}|^2}{|A_\mathrm{i}\frac{\omega}{c_\mathrm{w}}\cos\theta_\mathrm{i}|^2} W(2\vec{k}_\mathrm{i}) \tag{2.61}$$

Inserting A_s from 2.59 for the limiting case of vanishing shear wave velocity gives bs identical to the formula used by [Jackson et al., 1986] (see section 2.3.3).

The transfer function $\mathcal{H}_\mathrm{T} = \frac{|A_\mathrm{s}|^2}{|A_\mathrm{i}\frac{\omega}{c_\mathrm{w}}\cos\theta_\mathrm{i}|^2}$ depends on the geophysical properties of the sediment seafloor which are characterized by the velocity and attenuation of compressional and shear waves in the medium, and its density.

The two-dimensional roughness spectrum $W(\vec{k})$ depends on the absolute value and the direction of the wave vector $\vec{k}$. With respect to the directional dependence, [Essen, 1994] assumes for simplicity that the spectrum is isotropic, i.e.:

$$W(\vec{k}) = \frac{W_{1\mathrm{D}}(k)}{2\pi k} \tag{2.62}$$

where $W_{1\mathrm{D}}(k)$ is the one-dimensional wave-number spectrum which is normalized by $\sigma_\zeta^2 = \int W_{1\mathrm{D}}(k)dk$. This yields:

$$\mathrm{bs}(\omega, \theta_\mathrm{i}) = \frac{\gamma_{\omega 0}^4 \mathcal{H}_\mathrm{T}}{4\pi k_\mathrm{i}} W_{1\mathrm{D}}(2k_\mathrm{i}) \tag{2.63}$$

To compute scattering strength the author considered two different spectra:

$$W_{1\mathrm{D}}(k) = W_0 k^{-3} \text{ if } k \geq k_\mathrm{c}, \text{ and} = 0 \text{ otherwise} \tag{2.64}$$

and

$$W_{1\mathrm{D}}(k) = \frac{W_0}{2k_\mathrm{c}} k^{-2} \text{ if } k \geq k_\mathrm{c}, \text{ and} = 0 \text{ otherwise} \tag{2.65}$$

In both spectra, W_0 is a dimensionless constant, and k_c is a cut-off wave-number. Both spectra contain the same total variance:

$$\sigma_\zeta^2 = \frac{W_0^2}{2} k_\mathrm{c}^{-2} \tag{2.66}$$

In [Essen, 1994], $W_0 = 0.04$ and $k_\mathrm{c} = 20\mathrm{m}^{-1}$ are chosen to describe realistic values of backscattering strength for incident angles above 15° and frequencies above 10 kHz. As $\mathcal{H}_\mathrm{T}$ is independent of frequency, bs frequency dependence is determined by $\gamma_{\omega 0}^4$ and $W(\vec{k})$. The first gives a ω^4 dependence, reduced to ω^3 assuming an isotropic spectrum. With spectrum of equation 2.64, bs becomes independent of frequency, in accordance with most of the data presented by [Bunchuk and Zhitkovskii, 1980]. Spectrum of equation 2.65 yields a linear increase of backscatter with frequency, which can also be found on measurements of [Urick, 1983].

Essen model is then using 7 parameters, some empirical and some physical (see table 2.1).

2.3.3 Jackson: combination of composite roughness, Kirchhoff approximation, and volume scattering

In order to model seafloor scattering, [Jackson et al., 1986] compute separately the scattering from interface roughness and the sediment volume scattering. The first one is computed using to two different models according to the incident angle: the composite roughness for large incident angles ($\theta_\mathrm{i} > 20°$) and the Kirchhoff approximation for angles close to the nadir. The volume scattering is added for every angle, with account taken of refraction and reflection at the randomly sloping interface.

In the model, the seafloor relief is divided in two scales of roughness (see figure 2.5):

- the large-scale roughness ζ
- the small-scale relief, noted ζ_ss

These scales are separated in term of spatial frequency by the cut-off wave-number k_c. A scheme of the roughness spectrum divided in these two part is given figure 5.6.

Composite roughness

The composite roughness model applies the Rayleigh-Rice perturbation approximation to the small-scale portion of the interface. This approximation is valid when the small-scale RMS relief $\sigma_{\zeta_{ss}}$ is much smaller than the incident signal wavelength λ i.e. for high spatial frequencies of the roughness. A penetrable two-fluid interface is assumed.

The small-scale backscattering cross section $\mathrm{bs}_{\mathrm{ss}}(\theta_{\mathrm{i}})$ depends upon the ratio c_{sw} and ρ_{sw} as well as upon the incident angle θ_{i} and the acoustic wave-number in water $k_{\mathrm{i}} = 2\pi \mathrm{f}_{\mathrm{i}}/c_{\mathrm{w}}$. It can be expressed as Kuo's backscattering cross section [Kuo, 1964] i.e.:

$$\mathrm{bs}_{\mathrm{ss}}(\theta_{\mathrm{i}}) = 4k_{\mathrm{i}}^4 \cos^4\theta_{\mathrm{i}} F(\theta, c_{\mathrm{sw}}, \rho_{\mathrm{sw}}) W(2k_{\mathrm{i}} \sin\theta_{\mathrm{i}}, 0) \tag{2.67}$$

with $W(\vec{k})= W(k_x, k_y)$ the two-dimensional roughness spectrum, considered Gaussian and isotropic i.e. of the form $W(\vec{k}) = b_\beta^2 \vec{k}^{-b_\gamma}$, and $2k_{\mathrm{i}} \sin\theta$ the Bragg wave-number. In this expression and in the following, the incident wave-vector is supposed in the plane (xz), therefore the second parameter of the spectrum is omitted (i.e. $W(\vec{k}) = W(k) = W(k_x, 0)$). The presence of the Bragg wave-number does not implies a periodic seafloor interface but that in the spectrum of wavelets, those having the Bragg wave-number dominate the backscattering strength when the interface relief is much smaller than the acoustic wavelength. The form of the function $F(\theta_{\mathrm{i}}, v_{\mathrm{sw}}, \rho_{\mathrm{sw}})$ changes as the incident angle passes the critical angle $\theta_{\mathrm{c}} = \sin^{-1}(c_{\mathrm{w}}/c_{\mathrm{s}})$:

$$F(\theta_{\mathrm{i}}, v_{\mathrm{sw}}, \rho_{\mathrm{sw}}) = \frac{[(\rho_{\mathrm{sw}} - 1)^2 \sin^2\theta_{\mathrm{i}} + \rho_{\mathrm{sw}}^2 - v^{-2}]^2}{[\rho_{\mathrm{sw}} \cos\theta_{\mathrm{i}} + (v_{\mathrm{sw}}^{-2} - \sin^2\theta_{\mathrm{i}})^{1/2}]^4} \text{ if } \theta_{\mathrm{i}} > \theta_{\mathrm{c}} \tag{2.68}$$

$$F(\theta_{\mathrm{i}}, v_{\mathrm{sw}}, \rho_{\mathrm{sw}}) = \frac{[(\rho_{\mathrm{sw}} - 1)^2 \sin^2\theta_{\mathrm{i}} + \rho_{\mathrm{sw}}^2 - v^{-2}]^2}{[(1 - \rho_{\mathrm{sw}}^2) \sin^2\theta_{\mathrm{i}} + \rho_{\mathrm{sw}}^2 - v_{\mathrm{sw}}^{-2}]^2} \text{ if } \theta_{\mathrm{i}} < \theta_{\mathrm{c}} \tag{2.69}$$

[Jackson et al., 1986] assume that the slopes of the large-scale surface ψ are statistically small i.e. the RMS slope σ_ψ is small:

$$\sigma_\psi < 0.1 \tag{2.70}$$

In addition, a restriction to incident angles larger than 20° is made so that the local incident angle can be approximated by $\theta_{\mathrm{p}} + \psi$ with θ_{p} the pointing angle or the incidence angle for a flat seabed. Assuming that the slope of the large scale surface ψ is a Gaussian-distributed random variable, the backscattering cross section for incident angles 20^o and more is obtained by averaging the small-scale backscattering cross section as follows:

$$\mathrm{bs}(\theta_{\mathrm{i}}) = \frac{F_1(\theta_{\mathrm{i}}, \sigma_\psi)}{\pi^{\frac{1}{2}} \sigma_\psi} \int_{-\theta_{\mathrm{i}}}^{\infty} \mathrm{bs}_{\mathrm{ss}}(\theta_{\mathrm{p}} - \psi) \exp\left[\frac{\psi^2}{\sigma_\psi^2}\right] d\psi \tag{2.71}$$

where the function $F_1(\theta_\mathrm{i}, \sigma_\psi)$ accounts for shadowing by the large-scale surface and is chosen to be the shadowing function derived by [Beckmann, 1965] as:

$$\begin{aligned} F_1(\theta_\mathrm{i}, \sigma_\psi) &= (2b_q)^{-1}\left(1 - e^{-2b_q}\right) \\ &\text{with} \\ b_t &= \frac{1}{\sigma_\psi \tan\theta_\mathrm{i}} \\ b_q &= \frac{1}{4b_t}\left[\pi^{1/2}e^{-b_t^2} - b_t(1 - \mathrm{erf}(b_t))\right] \end{aligned} \tag{2.72}$$

In Jackson's model, the roughness spectrum is partitioned in two parts: large and small scale. The cutoff wave number k_c marks the boundary between those parts and is chosen so that the small scale interface satisfies the Rayleigh-Rice approximation (i.e. the condition of validity or perturbation model). The cut-off frequency is also chosen so that the large-scale interface can be treated as locally flat. Depending on authors, the condition on the small-scale surface is written as:

$$2k_\mathrm{i}\sigma_{\zeta_\mathrm{ss}} < 1 \tag{2.73}$$

or

$$2k_\mathrm{i}\sigma_{\zeta_\mathrm{ss}}\cos\theta_\mathrm{i} < 1 \tag{2.74}$$

where $\sigma_{\zeta_\mathrm{ss}}$ is the RMS relief of the small-scale surface.

Supposing the two-dimensional relief $\zeta(\vec{x})$ is a stationary process having a null expected value i.e. $E[\zeta(\vec{x})] = 0$ with $\vec{x}$ the two-dimensional vector giving horizontal positions (x, y) (see figure 2.5), its covariance is:

$$C(\vec{x}) = E[\zeta(\vec{x} - \vec{x}_0)\zeta(\vec{x})] \tag{2.75}$$

where $\vec{x}_0$ is an arbitrary horizontal displacement. The small-scale roughness spectrum can be calculated in this case as its Fourier transform:

$$W(\vec{k}) = \frac{1}{(2\pi)^2}\iint_{-\infty}^{\infty} C(\vec{x})e^{j\vec{k}\vec{x}}d^2\vec{x} \tag{2.76}$$

and it is normalized as:

$$\iint_{-\infty}^{\infty} W(\vec{k})d^2k = \sigma_\zeta^2 = C(0) \tag{2.77}$$

where σ_ζ^2 is the variance of the roughness. Given this normalisation, the small-scale RMS relief $\sigma_{\zeta_\mathrm{ss}}$ appearing in the Rayleigh-Rice criteria can be calculated in terms of the spectrum:

$$\sigma_{\zeta_\mathrm{ss}}^2 = 2\pi\int_{k_c}^{\infty} W(\vec{k})kdk \tag{2.78}$$

This expression defines the small-scale interface relief ζ_ss as a filtered version of the true interface relief ζ.

Kirchhoff approximation

At incident angles close to 0°, the entire composite roughness model is replaced by the Kirchhoff approximation. Assuming the rough surface relief is comparable to or greater than the acoustic wavelength, the coherent intensity becomes a negligible part of the total intensity. In that case, in the Kirchhoff approximation, the backscattering strength is given by [Jackson et al., 1986]:

$$\mathrm{bs}(\theta_\mathrm{i}) = \frac{R^2(0)}{8\pi \cos^2\theta_\mathrm{i} \sin^2\theta_\mathrm{i}} \int_0^\infty e^{-b_q u^{2b_a}} J_0(u) u du \tag{2.79}$$

where $R(0)$ is the plane wave reflection coefficient at normal incidence defined in equation 2.3, and

$$b_q = \cos^2\theta_\mathrm{i} \sin^{-2b_a}(\theta_\mathrm{i})\, b_h^2 2^{1-2b_a} k_\mathrm{i}^{2(1-b_a)} \tag{2.80}$$

and where $J_0(.)$ is the zero-order Bessel function of the first kind. b_h and b_a are constant that can be chosen arbitrarily. [Jackson et al., 1986] give examples of backscattering strength curves for $b_h = 0.1$ at a frequency of 30 kHz for values of b_a from 0.5 to 1. Links between b_a and the spectrum parameter b_γ when supposed isotropic (i.e. $W(\vec{k}) = b_\beta^2 \vec{k}^{-b_\gamma}$) are made such as $b_a = 0.5$ corresponds to $b_\gamma = 3.0$ (a spectrum of high frequencies), or $b_a = 1.0$ corresponds to $b_\gamma = 4.0$ (a smooth surface).

Volume scattering

[Jackson et al., 1986] based their volume scattering part on the Naval Research Establishment (NRE) [Stockhausen, 1963] volume scattering model. It includes refraction and attenuation in a statistically homogeneous sediment with perfectly flat interface. The acoustic energy incident upon each elemental volume is computed by considering transmission and refraction of the incident energy at the interface, as well as attenuation in the sediment, but energy scattered by the rest of the sediment is assumed negligible (no multiple scattering). The resulting surface scattering cross-section bs_vs is derived as:

$$\mathrm{bs}_\mathrm{vs}(\theta_\mathrm{i}) = \frac{5\,\mathrm{bs}_\mathrm{v}[1 - R^2(\theta_\mathrm{i})]^2 \cos^2\theta_\mathrm{i}}{\alpha_\mathrm{s} \log(10) \cos\theta_\mathrm{t}} \text{ for } \theta_\mathrm{i} > \theta_\mathrm{c} \tag{2.81}$$

$$\mathrm{bs}_\mathrm{vs}(\theta_\mathrm{i}) = 0 \text{ for } \theta_\mathrm{i} < \theta_\mathrm{c} \tag{2.82}$$

where the subscript v stands for volume, s for small scale as previously, θ_t is the angle of refraction from a flat interface such as $\cos\theta_\mathrm{t} = \sqrt{1 - (v\cos\theta_\mathrm{i})^2}$ providing incident angles lower than the critical angle, R is the plane wave reflection coefficient, and α_s the compressional wave attenuation coefficient in sediment. bs_v is defined as the scattering cross-section per unit solid angle per unit sediment volume.

From equation 2.81 we see that the surface scattering cross-section $\mathrm{bs}_\mathrm{vs}(\theta_\mathrm{i})$ depends on the ration $\mathrm{bs}_\mathrm{v}/\alpha_\mathrm{s}$. The authors choose to treat this ratio as a free parameter which is not related to any specific scattering mechanism. They determined it by fitting backscattering strength data, with the constraint $\mathrm{bs}_\mathrm{v}/\alpha_\mathrm{s} < 0.004$

Complete model

Finally, the complete model of backscattering strength from [Jackson et al., 1986] has two parts:

- Interface scattering: computed by numerical integration of equation 2.71 for incident angles greater than 20° and equation 2.79 for angles smaller than 20°;
- Volume sediment scattering: computed by numerical integration of equation 2.71 with bs_{vs} (equation 2.81) in place of bs_{ss} for all incident angles.

In total, 8 parameters are used in this model with some of them perfectly empirical (see table 2.1). In the publication, [Jackson et al., 1986] say themselves that their approach for the penetrable two-fluid boundary is heuristic and "without rigorous justification".

2.4 Summary

All the models of scattering or backscattering strength detailed in this chapter are listed in tables 2.1 and 2.3 with their characteristics. They are all making the hypothesis that the seafloor is an interface between two media: sea water and sediment. Both these media are mainly represented as homogeneous fluids, even the sediment which is supposed filled with water. Table 2.3 sums up the types of surface used to represent the interface water/sediment. Except for basic models, all of them depicted the seafloor as a rough interface. Their differences are in the characteristics of this interface: how is the roughness described (spectrum, etc.)? Is the interface penetrable i.e. is volume scattering involved? What is the impedance difference between the two media? In addition, there are also differences in the characteristics of the second medium: is there any scattering inside the sediment? Are inhomogeneities or layering taken into account? Etc. The list of models could be endless if we choose to study the diverse possibilities, that is why we limited this chapter to certain current models.

Authors	Type of interface	Type of reflection taken into account	Validity domain
[Dosso and Holland, 2006]	Flat, infinite, penetrable	Coherent	Angles < critical angle
[Clay and Medwin, 1977]	Rough, random	Coherent	-
[Ishimaru, 1978]	Rough	Incoherent	Grazing angles
[Sevaldsen, 2002]	Rough, porous	Incoherent	1 to 10 kHz, grazing angles
[Mackenzie, 1961]	Rough	Incoherent	530 and 1030Hz, grazing angles
[Jenserud et al., 2001]	Rough	Incoherent	-
[Del Balzo et al., 1997]	Rough, penetrable	Incoherent	-
[Ellis and Crowe, 1991]	Rough, random	Incoherent	-
[Caruthers and Novarini, 1993]	Rough on 2 levels, penetrable	Coherent + incoherent	365 Hz - 5 kHz
[Nolle et al., 1963]	Rough, penetrable	Incoherent	400-1100 kHz
[Essen, 1994]	Rough, random, penetrable	Incoherent	10-100 kHz

[Jackson et al., 1986]	Rough on 2 levels, random, penetrable, shadow	Incoherent	10-100 kHz

Table 2.3: Characteristics of seafloor response models

The main observation from this chapter is to note that the response of the seafloor, or backscattering strength, is always defined in all the models studied as a deterministic value, even if the roughness of the interface is described as random, with facets, multi-scales, random slopes or inhomogeneities. This assumption supposed that, for a given seafloor, only a given absolute value of backscattering strength (BS) exists. This value, in the majority of the models, is reliant on the angle of the incident acoustic wave on the seafloor (θ_i). This second assumption presumes that each type of seafloor has its own specific BS(θ_i) curve. At the end, depending on the model, this curve is supposed varying with the frequency ($\mathfrak{f}$) of the incident acoustic wave. This assumption is not taken into account in all models because frequency variations of the BS can appear to be negligible in some cases. Indeed, the predictable behaviour suggested by Lambert's law applies only to what Urick [Urick, 1954] refers to as a Type III acoustic seafloor (i.e. a heavily dissected bottom with underwater ridges) for which Lambert's law is invariant in frequency. However, various data suggest a definite frequency dependency for smoother (mud, clay and sand) seafloor [Urick, 1954]. This difference can be attributed to penetration of the incident acoustic wave, but Urick defines it also as possibly due to differences in the scales of bottom roughness. Bottoms with large roughness compared to the incident wavelength have, according to him, a backscattering strength independent of frequency. Bottoms with an appreciable portion of their roughness spectrum at roughness less than the incident acoustic wavelength have a scattering strength which increases with frequency. Under the context of this PhD (incident frequency around 100 kHz, see next parts), the backscattering strength is assumed to vary with angles and frequencies, therefore we write BS = BS($\theta_\mathrm{i}, \mathfrak{f}$).

The acoustic seafloor response BS = BS($\theta_\mathrm{i}, \mathfrak{f}$) is computed for many applications (see Introduction) but models cited in this chapter are particularly useful in simulations such as acoustic propagation models [Weinberg, 1982] or sonar performance models [Savage and Meredith, 1996]. In effect, to simulate the loss due to the reflection of an incident acoustic wave on the seafloor during its propagation, it is necessary to use a scattering or backscattering strength model. Lambert's model has been widely employed in this context, namely because propagation models are mostly carried out in low frequency, but other models can be used according to the precision wished by the user and the accurateness of the simulation.

It was shown previously that some of the BS($\theta_\mathrm{i}, \mathfrak{f}$) models are using geophysical parameters i.e. seabed characteristics like the grain size of the sediment, its porosity, density, or acoustics sound speed (see table 2.1). However these models are not necessarily physical models because they are not always based on a physical framework but on physical assumptions (perturbation theory, etc.). This is why we named in table 2.1 that last kind of models heuristic but inspired from physical phenomena. These physically based models can be used, for example, to extrapolate measured data to unmeasured angles, frequencies or bottom types. An other

example of application is the geophysical parameters estimation. In that case, results can be sometimes ambiguous as different input parameters may provide similar BS curves. In the worst case, an accurate inversion may be technically impossible. The higher the complexity, the greater the specialisation of a model for a given seafloor type.
The other part of models are those that are absolutely not related to geoacoustic parameters. In that case they are called heuristic in the sense of mathematical or empirical. They only derived from knowledge of previous measurements and expertise of the authors on the subject. Sometimes they are related *a posteriori* to physical phenomena (specular, grazing angles, etc.), but they remain parameterized by non-physical variables. These purely mathematical models can be employed, for example, to classify seabed terrains using their $\mathrm{BS}(\theta_\mathrm{i}, \mathrm{f})$ curves.

Chapter 3

The sonar equation: a tool between theory and practice to measure the seafloor acoustic response

Models detailed in the previous chapter are employed to estimate without measurement the seabed acoustic response for computer simulations, analytical analyses, or as benchmarks for classification and characterisation. Yet, a number of marine applications need to process the seafloor response from acoustic measurements, either because it is the main interest of the survey (e.g. habitats mapping [Ierodiaconou et al., 2018] or seabed classification [Biffard et al., 2007]) or because it represents an essential parameter in the analysis (e.g. sonar performance models [Scanlon et al., 1996]). In order to retrieve the seafloor response BS from *in situ* measurements, a calculation method was developed historically, called 'sonar equation'. Written commonly in decibels, it can be seen as an energetic balance of the loss and gain that impact the transmitted signal intensity during its propagation. Each phenomenon affecting the signal is parametrised independently in a decibel variable, providing a convenient way to sum them up. The seafloor acoustic response, or backscattering strength BS is one of the parameters involved therefore it can be calculated by inverting the equation.
In this chapter, different manners to write the sonar equation are presented, based on the state of the art. In particular, sonar equations allowing to compute the seafloor response are discussed. Every parameters of sonar equations are detailed.

3.1 Sonar equations

According to the circumstances of use and the authors' objectives, the sonar equation can be of several forms. The main purpose of the equation is to relate the acoustic echo level received by the sonar with its transmit level. However, the user point of view and the application decide the list of parameters involved in the process. The basic sonar equation [1] that can be found in literature is relating the echo level EL from an underwater target to the source level SL transmitted by the echosounder corrected from the directivity index at transmission DI_{Tx}, transmission losses TL and the target strength TS (see figure 3.1):

$$EL = SL + DI_{\text{Tx}} - 2TL + TS \tag{3.1}$$

The echo level is calculated from the received amplitude voltage of the target echo V_{Rx} as (see equation 3.59):

$$EL = 10 \log_{10} \left(\frac{1}{2} V_{\text{Rx}}^2 \right) - S_{\text{Rx}} \tag{3.2}$$

where S_{Rx} is the sensitivity of the receiver (see definition in section 3.2.6).

This kind of equation has been adapted to various situations depending on which application is of interest. These adaptation can be grouped in three main classes that are discussed in this section:

1. **Echosounder performances assessment** The sonar equation is in this situation uses to infer the performances of an echosounder to detect targets in a specific underwater environment. At first to detect the seabed for navigation safety, it is also used for military purposes (mine countermeasure, etc.) or civil applications (obstacle detection, etc.).

1. For an active mono-static system.

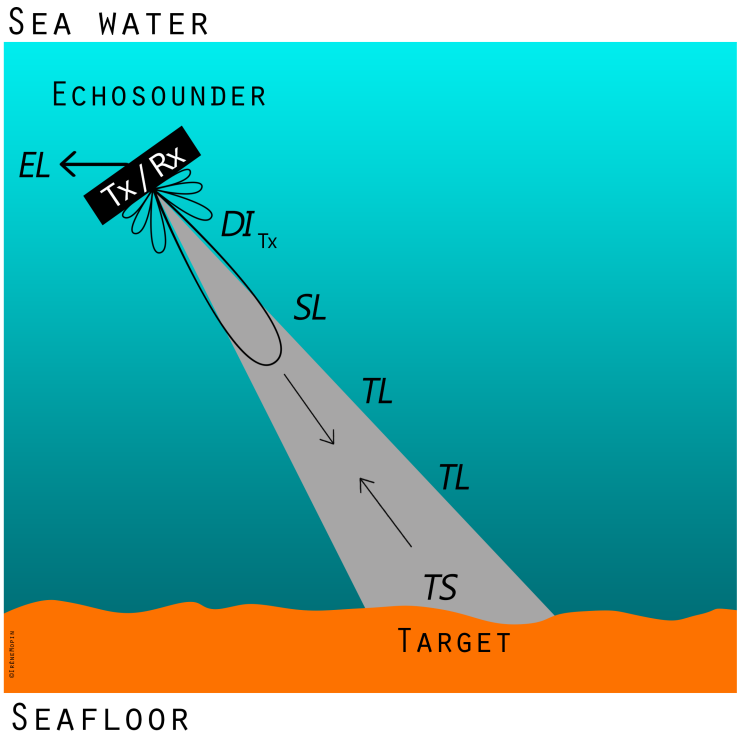

Figure 3.1 – Illustration of the basic components of the sonar equation parameters. In this example the target is the seafloor. The notation Tx stands for transmitter and Rx for receiver.

2. **Specific parameter estimation** In this context, one parameter value of the sonar equation is of interest. In most of the cases it is the target strength such as fish responses, or in our case the seabed response.
3. **Echosounder design and operation** The objective in this situation is to estimate the system characteristics before building it. In that case, the sonar equation is used to predict all parameters values given the material and design chosen. After the set up of the system, it is then used to calibrate all parameters.

3.1.1 Echosounder performances assessment

The interest is here to detect a target over ambient or source noises. The equation is therefore used to analyse the performances of the echosounder to detect the target. The noise level is noted NL and the detection threshold specific to the echosounder (level above which detection is available) is noted DT. In this type of equation generally appears the characteristics of the system such as its receiving directivity index DI_{Rx}. The sonar equation then follows [Urick, 1983]:

$$SL + DI_{\mathrm{Tx}} - 2TL + TS - (NL - DI_{Rx}) = DT \tag{3.3}$$

This equation has the form of a signal to noise ratio (SNR), useful to estimate the sonar capacity of detecting a target. The combination $NL - DI_{\mathrm{Rx}} + DT$ is sometimes called the

minimum detectable echo level [Urick, 1983]. When the background is reverberation instead of noise, [Urick, 1983] replaces $NL - DI_{Rx}$ by an equivalent plane-wave reverberation level RL [Urick, 1983]. Then the sonar equation becomes:

$$SL + DI_{\mathrm{Tx}} - 2TL + TS = RL + DT \tag{3.4}$$

Still in the SNR representation context, the sonar equation is also found in literature written as an inequality. In addition to previous parameters, the signal part includes a processing gain PG of the system which corresponds to an additional gain due to diverse effects (see section 3.2.10 for details) such as to the use of frequency modulated signals (FM) instead of classical sinusoidal signals named CW [Lurton, 2010]. The sonar equation is this way:

$$SL + DI_{\mathrm{Tx}} - 2TL + TS - NL + DI_{Rx} + PG > DT \tag{3.5}$$

The signal to noise ratio can also be seen as a signal excess SE related to the probability of detection of a target. In some applications such as sonar performance calculations, it is assumed that $SE = 0$dB corresponds to a probability of detection of 50%. In his report, [Dawe, 1997] defines this excess as:

$$SE = SL + DI_{\mathrm{Tx}} - 2TL - NL + AG - DT - DF_0 \tag{3.6}$$

where AG is the echosounder antenna array gain and measures the ability of the receiving array to pick up and discriminate incoming sounds in a background of non-isotropic noise. In practice, the array beamformer is usually included in the echosounder processor. However, for the purpose of simplifying the system model, the effect of the beamformer is combined with the one of the receiving array that gives a directivity index DI_{Rx} when the ambient noise is isotropic, or an array gain AG when the ambient noise is not isotropic. DI is a function of the number of receivers, the array geometry and the frequency, whereas AG also accounts for the statistical properties of the input signal and ambient noise. The last parameter DF_0 represents the operational degradation of the received level and is a catch-all for several cumulative imperfections in modelling all the other terms in the sonar equation (except for imperfections in the model of DT which have their own cumulative loss term). DF_0 varies according to the echosounder: recommended values for various sonars can be found in the Sonar Modelling Handbook [2]. Arbitrary values where given to 4 dB for all active sonars in [Dawe, 1997].

3.1.2 Parameter estimation: the seafloor acoustic response

In order to estimate one parameter value, the other parameters of the sonar equation have to be detailed. Depending on the resulting precision necessary, more or less details are taken into account. At first, the echo level can be substituted by the sum of the received RMS voltage $\frac{1}{2}V_{\mathrm{Rx}}^2$ in decibels (where V_{Rx} is the 0-peak voltage of a narrow band signal) and the receiver sensitivity S_{Rx} as shown in equation 3.2. Considering a target of target strength TS located on the axis of the echosounder, it gives a sonar equation of the form [Jackson and Richardson, 2007]:

$$10\log_{10}\left(\frac{1}{2}V_{\mathrm{Rx}}^2\right) = SL + S_{\mathrm{Rx}} - 2TL + TS + DI_{\mathrm{Tx}} \tag{3.7}$$

2. This reference hasn't been found even if it is widely cited by [Dawe, 1997] and discussed in [Holden, 2014].

This equation deliberately shows the directivity indices DI_{Tx}. According to authors, it can be chosen to be included or not in the source level parameter SL. In this manuscript DI_{Tx} is always separated from SL.

Equation 3.7 is not of the SNR form, and manages to describe the environment in which the pulse propagate. This type of sonar equation is currently used to estimate targets responses such as fish, scattering layers (plankton, sediment in suspension), or sea bottom. These responses are the center of interest and their values have to be precisely measured. It implies that all the equation parameters have to be known or able to be measured and calibrated. In the context of this manuscript the target of interest is the seafloor. Its target strength can be written as $TS = \mathrm{BS} + 10\log_{10}(\mathcal{A})$ with $\mathcal{A}$ the insonified area and BS its backscattering strength i.e. its response. The sonar equation then becomes [Malik et al., 2018]:

$$10\log_{10}\left(\frac{1}{2}V_{\mathrm{Rx}}^2\right) = 10\log_{10}\left(\frac{1}{2}V_{\mathrm{Tx}}^2\right) + S_{\mathrm{Rx}} + S_{\mathrm{Tx}} - 2TL + \mathrm{BS} + 10\log_{10}(\mathcal{A}) \tag{3.8}$$

where V_{Tx} is the transmit voltage of the CW signal, S_{Rx} is the receiver sensitivity, and S_{Tx} is the transmitter sensitivity (brought back to 1 m of the source). When the target is not on the axis of the beam, the directivity function at the angle of the target has to be add to the equation to consider the loss of energy due to the directivity pattern.

Another formulation of equation 3.8 using the echo and source level as in equation 3.1 can be used as:

$$EL = SL + DI_{\mathrm{Tx}} - 2TL + \mathrm{BS} + 10\log_{10}(\mathcal{A}) \tag{3.9}$$

The backscattering strength of the seafloor BS, or seabed acoustic response, can therefore be derived from *in situ* measurements by processing echosounder data and calculating:

$$\mathrm{BS} = EL - SL - DI_{\mathrm{Tx}} + 2TL - 10\log_{10}(\mathcal{A}) \tag{3.10}$$

It is important to note that in the SNR point of view, when the background masking the target is considered to be the reverberation (e.g. equation 3.4), the latter is composed of scattering from the water surface, the water volume, and also the sea bottom. The term 'reverberation' is also associated, in this particular context, to the seafloor response.

3.1.3 Echosounder design and operation

In order to design a new echosounder, it is important to be able to evaluate *a priori* its characteristics. For example, if the echosounder is produced to estimate fish biomass, the target strength has to be precisely calculated therefore all the sonar equation parameters must be known and calibrated. One of the parameters that corresponds to a specific characteristic of the echosounder is its receiving sensitivity S_{Rx}. As shown in equation 3.2, it is needed to evaluate the received echo level. A method to measure in water this sensitivity is to use a standard hydrophone which sensitivity at transmission S_{v} is perfectly calibrated and then to transmit a known pulse to the echosounder. This measurement can be done at sea but is generally made in tanks for convenience. The sonar equation in this situation is derived from the definitions of the sensitivities (see section 3.2.6 for details) which give in decibels:

$$S_{\mathrm{Rx}} = 10\log_{10}\left(\frac{\frac{1}{2}V_{\mathrm{Rx}}^2}{\frac{1}{2}V_{\mathrm{ref}}^2}\right) - 10\log_{10}\left(\frac{\frac{1}{2}p_{\mathrm{Rx}}^2}{\frac{1}{2}p_{\mathrm{ref}}^2}\right) \tag{3.11}$$

and

$$S_{\mathrm{v}} = 10\log_{10}\left(\frac{\frac{1}{2}p_{\mathrm{Tx}}^2}{\frac{1}{2}p_{\mathrm{ref}}^2}\right) - 10\log_{10}\left(\frac{\frac{1}{2}V_{\mathrm{Tx}}^2}{\frac{1}{2}V_{\mathrm{ref}}^2}\right) \tag{3.12}$$

where V_{Rx} is the 0-peak received voltage delivered by the echosounder, V_{Tx} is the 0-peak transmitted voltage given to the hydrophone, p_{Rx} is the acoustic pressure received by the echosounder, and p_{Tx} is the transmitted pressure delivered by the hydrophone brought back to 1 m of the source. Figure 3.2 summarize the different parameters involved and their locations.

The link between the two previous equations is the pressures. Indeed, the pressure at the entrance of the echosounder is the pressure delivered by the hydrophone minus the transmission loss TL due to propagation in water. Therefore, supposing that the hydrophone is placed on the axis of the echosounder, it can be written:

$$10\log_{10}\left(\frac{\frac{1}{2}p_{\mathrm{Rx}}^2}{\frac{1}{2}p_{\mathrm{ref}}^2}\right) = 10\log_{10}\left(\frac{\frac{1}{2}p_{\mathrm{Tx}}^2}{\frac{1}{2}p_{\mathrm{ref}}^2}\right) - TL \tag{3.13}$$

Consequently, the sonar equation that permits to measure the receiving sensitivity of the echosounder S_{Rx} is:

$$S_{\mathrm{Rx}} = 10\log_{10}\left(\frac{V_{\mathrm{Rx}}^2}{V_{\mathrm{Tx}}^2}\right) - S_{\mathrm{v}} + TL \tag{3.14}$$

This equation is an example of parameter calculation for echosounder design. Other parameters can be calculated and other methods can be of course employed.

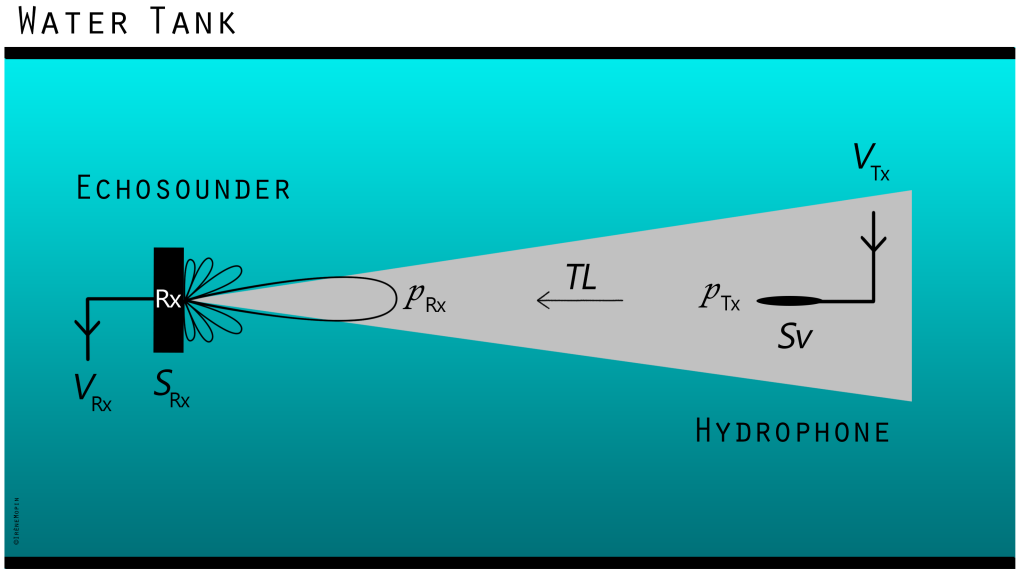

Figure 3.2 – Illustration of the components of the sonar equation for echosounder receiving sensitivity measurement S_{Rx} in tank. The hydrophone is centred on the echosounder axis.

Nowadays, commercial systems have their own sonar equation included in their real time data process. From a manufacturer to another, this equation can be written differently. Below are presented two examples of sonar equations supposed [3] implemented in two Kongsberg mono-static singlebeam echosounders: the EA400 used for bathymetric purposes and the EK60 used for fishery. Because the seafloor backscattering strength is of main interest in this PhD, sonar equations are written to calculate this parameter.

The sonar equation used to infer the backscattering strength of the seafloor is chosen as a baseline to be equation 3.10. In this equation, Kongsberg uses a different paradigm to define the parameters. Source and echo levels are derived from the acoustic powers respectively transmitted and received by the echosounder [Fuhs, 1982]. This approach is known in the literature as used by the radar community (radar cross section calculation)[Davies, 1954]. However, because the sonar equation is a balance in acoustic intensity, powers has to be corrected to retrieve intensities.
For an omnidirectional source, the link between RMS acoustic power transmitted and propagating on a sphere of radius r and the RMS transmitted intensity is:

$$\underline{P_{\mathrm{Tx}}} = 4\pi r^2 \underline{I_{\mathrm{Tx}}} \tag{3.15}$$

The spatial reference generally used for an acoustic source is 1m therefore $r = 1\mathrm{m}$ and $\underline{P_{\mathrm{Tx}}} = 4\pi \underline{I_{\mathrm{Tx}}}$. The source level in Kongsberg paradigm is consequently calculated as:

$$SL_{\mathrm{K}} = 10\log_{10}\left(\frac{\underline{P_{\mathrm{Tx}}}}{4\pi}\right) + G_{\mathrm{Tx}} \tag{3.16}$$

where $\underline{P_{\mathrm{Tx}}}$ is the RMS transmitted power and G_{Tx} is a gain (in decibels) added to compensate from the transducer omnidirectionality hypothesis made to define the RMS transmitted power from the RMS transmitted intensity [Fuhs, 1982]. Indeed, the echosounder antenna is by definition directional, so the acoustic energy is focused. This effect is taken into account by adding a directivity index parameter noted previously DI_{Tx} but named G_{Tx} in the radar equation context.
On the other side, the RMS received power $\underline{P_{\mathrm{Rx}}}$ has to be corrected by the equivalent surface area of the receiving antenna $\mathcal{A}_{\mathrm{ant}}$ to obtain an intensity value. This correction is derived as the antenna gain G_{Rx}. It corresponds to the approximation of the antenna directivity index [Stutzman, 1998] for $L \gg \lambda$ with L the length of the size of the antenna. It is given as [Foldy, 1946] [4]:

$$G_{\mathrm{Rx}} = \frac{4\pi}{\lambda^2}\mathcal{A}_{\mathrm{ant}} \tag{3.17}$$

Consequently the echo level in Kongsberg paradigm is:

$$EL_{\mathrm{K}} = 10\log_{10}\left(\underline{P_{\mathrm{Rx}}}\frac{4\pi}{\lambda^2}\right) - G_{\mathrm{Rx}} \tag{3.18}$$

3. i.e. reverse engineered and inspired from Kongberg EM technical note available online (Link)

4. This result is commonly found in radar literature that the radar cross-section of flat plate is equal to $\frac{4\pi}{\lambda^2}\mathcal{A}_{\mathrm{plate}}$ [Nicolaescu and Oroian, 2001]. The echosounder received antenna being flat, it can be considered as a flat plate. Therefore its antenna gain corresponds to the flat plate radar cross-section [Fuhs, 1982][Appel-Hansen, 1979].

Finally, the sonar equation that is employed to calculate the seafloor acoustic response in Kongsberg EA400 is:

$$\mathrm{BS}_{\mathrm{EA400}} = 10\log_{10}\left(\underline{P_{\mathrm{Rx}}}\right) - 10\log_{10}\left(\underline{P_{\mathrm{Tx}}}\right) - 10\log_{10}\left(\frac{\lambda^2}{16\pi^2}\right) + 2TL - 10\log_{10}\left(\mathcal{A}\right) - G_{\mathrm{Tx}} - G_{\mathrm{Rx}} \tag{3.19}$$

For the other singlebeam echosounder, the sonar equation is based on the same assumptions with two other parameters added to increase accuracy in the acoustic response measurements. Kongsberg EK60 were created to measure fish or fish schools backscattering strength to estimate species biomass across a large area. They were designed differently as the bathymetric echosounder (ex: EA400) to be able to detect fish positions inside the beam. For this purpose, the transducer is separated in four quadrants that permits, at reception, to derive phase difference information of the signal backscattered by the target. With this information, the echo level of the target can be corrected from the loss due to its position $(\vartheta_x, \vartheta_y)$ in the directivity pattern $\mathcal{D}$. The sonar equation for fish target target strength TS estimation is given in Kongsberg paradigm as [Ona et al., 2009]:

$$TS_{\mathrm{K}} = 10\log_{10}\left(\underline{P_{\mathrm{Rx}}}\right) - 10\log_{10}\left(\underline{P_{\mathrm{Tx}}}\right) - 10\log_{10}\left(\frac{\lambda^2}{16\pi^2}\right) + 2TL - 10\log_{10}\left(\mathcal{D}(\vartheta_x, \vartheta_y)\right) - G_{\mathrm{Tx}} - G_{\mathrm{Rx}} \tag{3.20}$$

In the case of fish schools, the target position cannot be estimated because the echo represents an entire volume that scattered the incident energy. The target strength is then called volume backscattering strength and noted BV (see details in section 3.2.12). Because the target is a volume, this target strength is a volume index. The volume insonified by the beam v has therefore to be added to the equation as:

$$v = \mathcal{A}\frac{c\tau}{2} \tag{3.21}$$

where $\mathcal{A}$ is the surface insonified at a given range and τ the pulse length. The sonar equation used to calculate BV in Kongsberg paradigm is then given as [Ona et al., 2009]:

$$\begin{aligned} BV_{\mathrm{K}} = {} & 10\log_{10}\left(\underline{P_{\mathrm{Rx}}}\right) - 10\log_{10}\left(\underline{P_{\mathrm{Tx}}}\right) - 10\log_{10}\left(\frac{\lambda^2}{16\pi^2}\right) + 2TL - 10\log_{10}\left(\mathcal{A}\right) \\ & - 10\log_{10}\left(\frac{c}{2}\right) - \left(10\log_{10}\left(\tau\right) + 2S_{\mathrm{acorr}}\right) - G_{\mathrm{Tx}} - G_{\mathrm{Rx}} \end{aligned} \tag{3.22}$$

where S_{acorr} is a parameter used to compensate from the pulse energy difference between the square shape pulse desired and the effective pulse shape transmitted by the echosounder [Ona et al., 2009] (see details in section 3.2.15). The notation S_{acorr} probably comes from the parameter S_{a} which is the area backscattering strength calculated as the integral of BV over a range interval [MacLennan et al., 2002]. It is widely used in fishery acoustics to created maps of acoustic response that are easier to read than 3D data. In equation 3.22, there is two S_{acorr} because it is considered forward in backward as the system is mono-static.

When using Kongsberg EK60 for seafloor backscattering strength measurements, the two parameters shown previously have to be included in the equation. In effect, the seafloor echo,

if the echosounder is tilted, can come from different angles in the beam so the directivity pattern amplitude can be corrected; and because the insonified area is calculated, the pulse length is used and can also be corrected. Consequently $\mathcal{D}(\vartheta_x, \vartheta_y)$ and $2S_{\text{acorr}}$ are added to the sonar equation 3.19 to obtain the calculation of the seafloor response from Kongsberg EK60 echosounder [Eleftherakis et al., 2018]:

$$\begin{aligned} \text{BS}_{\text{EK60}} = {} & 10\log_{10}\left(\underline{P_{\text{Rx}}}\right) - 10\log_{10}\left(\underline{P_{\text{Tx}}}\right) - 10\log_{10}\left(\frac{\lambda^2}{16\pi^2}\right) + 2TL - 10\log_{10}\left(\mathcal{A}\right) \\ & - G_{\text{Tx}} - G_{\text{Rx}} - 2S_{\text{acorr}} - 10\log_{10}\left(\mathcal{D}(\vartheta_x, \vartheta_y)\right) \end{aligned} \tag{3.23}$$

3.1.4 Summary

In summary, three major types of sonar equations were presented in this section:

- **Signal to noise ratio** The sonar equation is in this case written as a ratio between parameters or phenomena that are considered noises (i.e. can cover the signal of interest) and others that are of interest. It can have the form of an equation but is commonly employed as an inequation (e.g. equation 3.5).
- **Parameter estimate equation** This sonar equation described only the different phenomena that affect the energy of the transmitted signal. The parameter of interest can be any parameter of the equation. It has the form of an equation (e.g. equation 3.10).
- **Manufacturer specific equation** The sonar equation is here of the same type as the previous case, however its form is dependent on the manufacturer. They can therefore be inspired from various signal processing methods. In addition, some equations can be basic because of real-time necessity, or very precise for accurate estimations in post-processing (e.g. equation 3.23).

What is common between the three types of equation is that they correspond to a balance in acoustic intensity that describes phenomena applied to an acoustic signal during its propagation, and they are written in decibels.

3.2 Details of sonar equations parameters

Multiple parameters have been introduced in the previous section to present the different sonar equations. Some of them are commonly used because they are part of the basic components of the sonar equation, but some others are more rare. Depending on the precision needed for the sonar equation usage, parameters are used or not. In the following, they are presented to describe their roles.

Inspired from the global hypotheses described in the introduction of this manuscript, we recall that the sea water medium is homogeneous and has no boundary except the seafloor (open sea).

3.2.1 Far field condition

Every directional transducer or antenna has a typical range before which the transmitted acoustic field is not perfectly modelled. Energy variations along the transducer axis is in

this area not stable because of interferences between signal transmitted from the different area elements that structure the transducer. After a certain distance on axis called Fresnel or Fraunhofer distance, the acoustic field is stable and the loss of energy on axis can be modelled by the parameter TL of the sonar equation (see details in section 3.2.4) [Bobber, 1970][Foote, 2014]. All ranges after this distance are defined as the far field of the transducer or the antenna. Every echosounder measurements in this manuscript are made in far field. It is also a strong hypothesis of many parameter calculation in the following.

In literature, the far field distance is approximated analytically by several methods which lead to several ranges which are multiples of the range below [Foote, 2014][Ocheltree and Frizzel, 1989][Williams, 1951]:

$$r_{\text{Far field}} = \frac{L^2}{\lambda} \tag{3.24}$$

with L the size of the antenna of the echosounder and λ the transmitted wavelength. The value by which this range is multiplied in literature depends on the precision desired of the transmitted signal phase. In practice, the formulation of equation 3.24 is mainly chosen directly as the far field distance [Lurton, 2010] without any multiplicative constant.

3.2.2 Source Level SL

The source level SL specifies the amount of sound radiated by a transmitter. It is defined as the RMS intensity of the source $\underline{I_{\text{Tx}}}$, in decibels, relative to the intensity of a plane wave of RMS pressure 1μPa, calculated in far field and brought back to the reference distance of one meter from the acoustic center of the transmitter in the direction of the target. The reference point of the source level is generally located along the axis of the transmitter beam pattern. Then [Urick, 1983]:

$$SL = 10\log_{10}\frac{\underline{I_{\text{Tx}}}}{\underline{I_{\text{ref}}}} \tag{3.25}$$

The acoustic intensity $\underline{I_{\text{Tx}}}$ transmitted by the source is by definition:

$$\underline{I_{\text{Tx}}} = \frac{\underline{p_{\text{Tx}}^2}}{\rho_{\text{w}} c_{\text{w}}} \tag{3.26}$$

where $\underline{p_{\text{Tx}}}$ is the RMS acoustic pressure transmitted by the source [5], ρ_{w} the water density, and c_{w} the water sound speed. Similarly, the reference intensity can be written in function of the reference pressure $\underline{p_{\text{ref}}}$ as:

$$\underline{I_{\text{ref}}} = \frac{\underline{p_{\text{ref}}^2}}{\rho_{\text{w}} c_{\text{w}}} \tag{3.27}$$

Consequently, the source level becomes:

$$SL = 10\log_{10}\left(\frac{\underline{I_{\text{Tx}}}}{\underline{I_{\text{ref}}}}\right) \simeq 10\log_{10}\left(\underline{I_{\text{Tx}}}\right) + 181.8 \tag{3.28}$$

5. Calculated in far field and brought back to the reference distance of one meter from the acoustic center of the transmitter.

Using the link between RMS acoustic power $\underline{P_{\text{Tx}}}$ and RMS acoustic intensity of equation 3.15, it gives, at the reference :

$$10\log_{10}\left(\underline{P_{\text{Tx}}}\right) = 10\log_{10}(4\pi) + 10\log_{10}(\underline{I_{\text{Tx}}}) = SL - 170.8 \tag{3.29}$$

This gives a formulation of SL in function of the acoustic power generated by an omnidirectional source. In the case of a directional source, the directivity index at transmission is found in some monograph (e.g. [Lurton, 2010]) included in the term SL to account for the gain on the transmitter axis due to its directivity pattern. In this manuscript, DI_{Tx} is taken out, and SL is always defined as:

$$SL = 170.8 + 10\log_{10}\left(\underline{P_{\text{Tx}}}\right) \tag{3.30}$$

In a more practical way, the source level can be calculated in function of the electrical power $\underline{P_{\text{elec}}}$ given to transducer for transmission. This involves using the efficiency of the transducer β_{Tx} which is defined as [Urick, 1983]:

$$\beta_{\text{Tx}} = \frac{\underline{P_{\text{Tx}}}}{\underline{P_{\text{elec}}}} \tag{3.31}$$

The source level then becomes:

$$SL = 170.8 + 10\log\left(\underline{P_{\text{elec}}}\right) + 10\log\left(\beta_{\text{Tx}}\right) \tag{3.32}$$

The electrical power can also be written in function of the input voltage V_{Tx} (0-peak) given to the transmitter and the conductance G (the real part of the transducer electric admittance) such as [Sherman and Butler, 2007]:

$$\underline{P_{\text{elec}}} = \frac{1}{2}V_{\text{Tx}}^2 G \tag{3.33}$$

which gives SL as:

$$SL = 170.8 + 10\log\left(\frac{1}{2}V_{\text{Tx}}^2\right) + 10\log\left(G\right) + 10\log\left(\beta_{\text{Tx}}\right) \tag{3.34}$$

3.2.3 Transmitter Directivity Index DI_{Tx}

The transmitter directivity index is associated to a source. It defined as the difference between the intensity generated by the directional transmitter on its axis I_{direct} and the intensity that would be produced in the same direction by an omnidirectional source radiating the same total amount of acoustic power I_{omni}, i.e. [Lurton, 2010]:

$$DI_{\text{Tx}} = 10\log_{10}\frac{I_{\text{direct}}}{I_{\text{omni}}} \tag{3.35}$$

I_{direct} is calculated by integrating the directivity pattern $\mathcal{D}$ of the transmitter over the entire space, and I_{omni} is by definition equal to 4π. Then, the directivity index at transmission can be derived as:

$$DI_{\text{Tx}} = 10\log_{10}\frac{4\pi}{\iint \mathcal{D}(\vartheta_x,\vartheta_y)\cos\vartheta_x d\vartheta_x d\vartheta_y} \tag{3.36}$$

3.2.4 Transmission Loss TL

The transmission loss parameter TL quantitatively describes the weakening of sound between a point one meter from the source and a point at a distance r in the sea, i.e.:

$$TL = 10\log_{10}\frac{\text{signal intensity at 1m}}{\text{signal intensity at target or receiver}} = 10\log_{10}\left(\frac{\underline{I_{\text{Tx}}}}{\underline{I_r}}\right) \tag{3.37}$$

with $\underline{I_{\text{Tx}}}$ the intensity at the reference range located one meter from the source and $\underline{I_r}$ the intensity at a distant point r from the source.

In practice, TL is considered as the sum of losses due to geometrical spreading and losses due to attenuation of the sound wave during propagation. Geometrical spreading represents the regular weakening of a signal amplitude as it spreads outward from the source. In an homogeneous medium, which is the case here as defined in the introduction of this manuscript, the spreading of an omnidirectional source has a spherical form. Likewise, in far field, the spreading of a directional source is by definition also spherical [Bobber, 1970]. In this case, the total power P_r at the range r spreads by the source is the same as the power $P_{r'}$ at the range r'. It can then be written:

$$\underline{P_r} = \underline{P_{r'}} = 4\pi r^2 \underline{I_r} = 4\pi r'^2 \underline{I_{r'}} \tag{3.38}$$

with I_r the intensity at the range r, and $I_{r'}$ the intensity at the range r'. Therefore the geometrical loss part of the TL parameter becomes in open sea:

$$10\log_{10}\left(\frac{I_{\text{Tx}}}{I_r}\right) = 10\log_{10}\left(\frac{I_{\text{r=1m}}}{I_r}\right) = 10\log_{10}(r^2) = 20\log_{10}(r) \tag{3.39}$$

The second part of TL (attenuation) includes the effects of absorption and scattering. It represents a loss of acoustic energy during the propagation. Indeed, when a plane wave travels through an absorbing medium, a certain fraction of its intensity is lost in each small unit distance travelled. If the intensity at some range r is noted I_r, the loss of intensity dI when travelling a small distance dr is given by [Urick, 1983]:

$$\frac{dI}{I_r} = -\eta_0 dr \tag{3.40}$$

where η_0 is a proportionality constant and the minus sign indicates that dI is a negative change of intensity. Integrating between ranges r and r', we find that the intensity $I_{r'}$ at range r' is related to the intensity I_r at range r by

$$I_{r'} = I_r e^{-\eta_0(r'-r)} \tag{3.41}$$

In decibels it becomes:

$$10\log_{10} I_{r'} - 10\log I_r = -10\eta_0(r'-r)\log_{10}(e) \tag{3.42}$$

We can therefore define the absorption coefficient of the sound in water by $\alpha_{\text{w}} = 10\eta_0\log_{10}(e)$, in decibels per meters:

$$\alpha_{\text{w}} = \frac{10\log_{10} I_r - 10\log_{10} I_{r'}}{r'-r} \tag{3.43}$$

As the attenuation part of the TL is taken from the transmitter face (i.e. at $r = 0m$), it becomes:

$$10\log\left(\frac{I_{\text{Transmitter face}}}{I_r}\right) = \alpha_{\text{w}} r \tag{3.44}$$

Under the assumption of spherical spreading, the total transmission loss TL is then:

$$TL = 20\log_{10}(r) + \alpha_{\text{w}} r \tag{3.45}$$

Note that, when absorption is taken into account in natural value (not decibels), it is commonly quantified by a parameter γ_{w} expressed in Neper per meter, and represented as a an exponential decrease of the sound pressure p, i.e. [Lurton, 2010]:

$$p(r,t) = \frac{p_0}{r^2} e^{j(\omega t - kr)} e^{-\gamma_{\text{w}} r} \tag{3.46}$$

γ_{w} is related to the absorption coefficient α_{w} by $\alpha_{\text{w}} = 20\gamma_{\text{w}}\log_{10}(e) \approx 8.686\gamma_{\text{w}}$.

3.2.5 Receiver Array Gain AG and Directivity Index $DI_{\mathbf{Rx}}$

The array gain parameter only employed at reception. It is an evaluation of the benefit gained by using an antenna of omnidirectional transducers instead of one elementary transducer on the signal to noise ratio. It is defined by [Urick, 1983] as:

$$AG = 10\log_{10}\frac{(\text{signal/noise})_{\text{array}}}{(\text{signal/noise})_{\text{one element}}} \tag{3.47}$$

where the numerator is the signal to noise ratio at the array terminal and the denominator is the signal to noise ratio at a single transducer of the antenna.

A first approach to derive AG is to involve the directional patterns of the signal and noise fields together with the beam pattern of the array. The signal and noise fields are characterized by the directional functions $S(\vartheta_x, \varphi)$ and $N(\vartheta_x, \vartheta_y)$, representing the signal and noise power per unit solid angle, respectively, incident on the array from the polar directions ϑ_x and ϑ_y. The array gain becomes with these definitions [Urick, 1983]:

$$AG = 10\log_{10}\frac{\int_{4\pi} S(\vartheta_x,\vartheta_y)\mathcal{D}(\vartheta_x,\vartheta_y)d\Omega / \int_{4\pi} N(\vartheta_x,\vartheta_y)\mathcal{D}(\vartheta_x,\vartheta_y)d\Omega}{\int_{4\pi} S(\vartheta_x,\vartheta_y)d\Omega / \int_{4\pi} N(\vartheta_x,\vartheta_y)d\Omega} \tag{3.48}$$

where $\mathcal{D}(\vartheta_x, \vartheta_y)$ is the beam pattern of the array.

Another approach to derive AG is to involve the coherence of signal and noise across the dimensions of the antenna. The coherence defines the degree of similarity of the signal waveform and the noise between any pair of elements. It is measured by the cross-correlation coefficient of the outputs of different elements of the array. This calculation is valid only on the following conditions:

— linear additive antenna array with all elements of equal sensitivities;

— individual output voltages, as functions of time, including any phase shifts or delays incorporated for steering;

— elements of the array in series.

The array gain is then defined as the ratio, in decibels, of the signal to noise of the array to the signal to noise of a single element [Urick, 1983][Urick, 1966]:

$$AG = 10\log_{10}\frac{\sum_i \sum_j (\rho_{\text{sig}})_{ij}}{\sum_i \sum_j (\rho_{\text{n}})_{ij}} \tag{3.49}$$

where ρ_{sig} and ρ_{n} are the cross-correlation coefficients between the ith array element and the jth element of the signal and of the noise respectively. They are properties of the signal and noise acoustic field in which the array is placed. Indeed, the same sonar antenna can have a different array gain in different signal and noise fields. Both ρ_{sig} and ρ_{n} depend also on the delays introduced into the array for steering.

Commonly, the array gain degrades as the signal coherence decreases and as the noise coherence increases. When the water in which the array operates is not statistically time-stationary i.e. causes amplitude and phase fluctuations in the received signal, the array performance is consequently degraded [Bourret, 1961, Berman and Berman, 1962, Brown, 1962, Lord and Murphy, 1964]. Table 3.1 summarizes different cases of signal and noise characteristics and the corresponding array gain in these conditions.

Signal	Noise	AG
Completely coherent	Completely coherent	0dB
Completely incoherent	Completely incoherent	0dB
Perfectly coherent	Incoherent	$10\log_{10}(n)$
Perfectly coherent	Partly coherent	$10\log_{10}\left(\frac{n}{1+(n-1)\rho}\right)$

Table 3.1 – Summary of common array gain AG computing cases from [Urick, 1983]. n is the number of elementary transducers of the antenna and ρ the cross-correlation coefficient of the noise when the signal is perfectly coherent signal and a partly coherent noise, i.e. $(\rho_{\text{n}})_{ij} = \rho$ for $i \neq j$ and $(\rho_{\text{n}})_{ij} = 1$ for $i = j$.

In the particular case where the signal is an unidirectionnal plane wave and perfectly coherent and the noise is isotropic (i.e. when the noise power per unit solid angle is the same in all directions, so that $N(\vartheta_x, \vartheta_y) = 1$), the array gain AG reduces to the quantity called directivity index at reception DI_{Rx}. In that case, and for an array steered in the direction of the signal arrival, the array gain becomes [Urick, 1983]:

$$AG = DI_{\text{Rx}} = 10\log_{10}\frac{\int_{4\pi} d\Omega}{\int_{4\pi} \mathcal{D}(\vartheta_x, \vartheta_y) d\Omega} = 10\log\frac{4\pi}{\int_0^{2\pi}\int_{-\frac{\pi}{2}}^{\frac{\pi}{2}} \mathcal{D}(\vartheta_x, \vartheta_y)\cos\vartheta_x d\vartheta_x d\vartheta_y} \tag{3.50}$$

DI_{Rx} is always a positive number, except in literature before 1948 where it was considered as a negative quantity e.g. [Christensen et al., 1943]. It is also a useful parameter to estimate quickly in practice the array gain, however users have to be aware of the particular conditions in which DI_{Rx} applies (coherent signal in an isotropic additive noise). Sometimes, in a real ocean environment, AG is better to be directly employed. The choice between the two parameters should be made knowing the noise characteristics.

Equation 3.50 shows that the receiver directivity index DI_{Rx} can be defined the same way as DI_{Tx} (see equation 3.36) i.e.

$$DI_{\mathrm{Rx}} = DI_{\mathrm{Tx}} = 10 \log \frac{I_{\mathrm{direct}}}{I_{\mathrm{omni}}} \tag{3.51}$$

At reception, the directivity index represents the decrease in noise perceived by the receiver due to the directivity of the antenna (assuming the ambient noise is isotropic). At transmission, it expresses the increase of acoustic energy concentration along the main direction. Consequently, the directivity index at reception is not employed in the type of sonar equations that are not of the signal to noise ratio form.

Computed values of directivity indexes are proposed in literature for classical geometry of antennae [Lurton, 2010] at high frequency. For example, for a linear antenna of length L with $L \gg \lambda$:

$$DI_{\mathrm{Rx}} \approx \log_{10} \left(\frac{2L}{\lambda} \right) \tag{3.52}$$

If the antenna is made of N omnidirectional transducers spaced by $\lambda/2$ its directivity index becomes equal to $10 \log_{10} n$. This corresponds to the gain in signal to noise ratio obtained by summing n independent realizations of a stable signal superposed with Gaussian noise.
For an antenna of surface S with its diameter $\gg \lambda$:

$$DI_{\mathrm{Rx}} \approx \log_{10} \left(\frac{4\pi S}{\lambda^2} \right) \tag{3.53}$$

For a hull-mounted point-like hydrophone (omnidirectional), the directivity pattern is one half-space and its directivity index is $DI_{\mathrm{Rx}} = 10 \log_{10} 2 = 3\mathrm{dB}$.

3.2.6 Transmitter and receiver sensitivities $S_{\mathbf{Tx}}$ and $S_{\mathbf{Rx}}$

The sensitivity of a transducer in underwater acoustics describes its quality to transform voltage in acoustic pressure and inversely. Echosounders transducers have two separated sensitivities: one in transmission S_{Tx} and one in reception S_{Rx}.

The transmitter sensitivity corresponds to the ratio of the RMS sound pressure transmitted in water on the front of the transducer $\underline{p_{\mathrm{Tx}}}$ to the RMS voltage given to the transducer $\underline{V_{\mathrm{Tx}}}$.

$$S_{\mathrm{Tx}} = 10 \log_{10} \left(\frac{\underline{p_{\mathrm{Tx}}}^2}{\underline{p_{\mathrm{ref}}}^2} \right) - 10 \log_{10} \left(\frac{\underline{V_{\mathrm{Tx}}}^2}{\underline{V_{\mathrm{ref}}}^2} \right) \tag{3.54}$$

where the reference RMS voltage is $\underline{V_{\mathrm{ref}}} = 1\mathrm{V}$. By definition (e.g. [Lurton, 2010]), the transmitter sensitivity is brought back to 1 m of the echosounder and given for a RMS voltage of 1 V i.e. $\underline{V_{\mathrm{Tx}}} = 1\,\mathrm{V}$. Therefore, the transmitter sensitivity is:

$$S_{\mathrm{Tx}} = 10 \log_{10} \left(\frac{\underline{p^2_{\mathrm{Tx}}}_{(\underline{V_{\mathrm{Tx}}}=1\mathrm{V})}}{\underline{p^2_{\mathrm{ref}}}} \right) \tag{3.55}$$

These hypotheses explain why unit values taken to define the sensitivity are always specified as dB ref. $1\mu\,\mathrm{Pa}/1\,\mathrm{m}/1\,\mathrm{V}$. From equation 3.55 and the definition of the source level SL (see equation 3.25), the relation between them is:

$$S_{\mathrm{Tx}} = SL - 10\log_{10}\left(\frac{1}{2}V_{\mathrm{Tx}}^2\right) + DI_{\mathrm{Tx}} \tag{3.56}$$

with V_{Tx} the 0-peak voltage transmitted to the transducer. The directivity index at transmission needs to be added here because the measurement (in far field and brought back at 1 m) is made on axis and the sensitivity includes by default DI_{Tx}.

Inversely, the receiver sensitivity is defined as the RMS voltage generated by the transducer $\underline{V_{\mathrm{Rx}}}$ when it receives a a RMS acoustic pressure $\underline{p_{\mathrm{Rx}}}$, i.e.

$$S_{\mathrm{Rx}} = 10\log_{10}\left(\frac{\underline{V_{\mathrm{Rx}}}^2}{\underline{V_{\mathrm{ref}}}^2}\right) - 10\log_{10}\left(\frac{\underline{p_{\mathrm{Rx}}}^2}{\underline{p_{\mathrm{ref}}}^2}\right) \tag{3.57}$$

where the reference RMS pressure is $\underline{p_{\mathrm{ref}}} = 1\mu\mathrm{Pa}$. By definition (e.g. [Lurton, 2010]), the receiver sensitivity is given for an incoming pressure of 1μPa i.e. $\underline{p_{\mathrm{Rx}}} = 1\mu\mathrm{Pa}$. Therefore, the receiver sensitivity is:

$$S_{\mathrm{Rx}} = 10\log_{10}\left(\frac{\underline{V_{\mathrm{Rx}}^2}_{(\underline{p_{\mathrm{Rx}}}=1\mu\mathrm{Pa})}}{\underline{V_{\mathrm{ref}}^2}}\right) \tag{3.58}$$

Unit of this sensitivity is specified as dB ref. $1\mathrm{V}/1\mu\mathrm{Pa}$. From equation 3.58 the received sensitivity can be linked to the echo level EL received by a transduceras:

$$S_{\mathrm{Rx}} = 10\log_{10}\left(\frac{1}{2}V_{\mathrm{Rx}}^2\right) - EL \tag{3.59}$$

with V_{Rx} the 0-peak voltage generated by the transducer.

3.2.7 Noise Level NL

The noise, in the sonar equation, can originate from the receiver itself (i.e. its electrical self-noise) or from the environment of the receiver. The latter is called ambient noise. It corresponds to the total noise background observed with an omnidirectional receiver which is not due to the receiver itself or to some identifiable and localized sources. It is defined by [Urick, 1983] as the intensity of the ambient background measured with a non-directional receiver and referred to the intensity of a plane wave having a RMS pressure of 1μPa :

$$NL = 10\log_{10}\frac{\text{noise intensity}}{\text{reference intensity}} \tag{3.60}$$

The parameter NL takes into account the noise in the frequency band of the receiver B_{Rx}. As ambient levels NL_0 are given for a reference band of 1Hz, NL is generally defined in practice as [Lurton, 2010]:

$$NL = NL_0 + 10\log(B_{\mathrm{Rx}}) \tag{3.61}$$

with NL_0 constant in the band of interest.

Ambient noise has been found by probability density analyses of data in one deep- and two shallow-water areas [Calderon, 1964] to have a Gaussian amplitude distribution at moderate depths. Near the surface, however, ambient noise has been observed to be more spiky than Gaussian and to contain individual spikes or crashes of sound originating from nearby sources such as breaking wavelets. In addition, although ambient noise is Gaussian over short time periods, it is clearly non-stationary over longer time periods because of the variability of the noise source [Urick, 1983].

3.2.8 Reverberation Level RL

The sea is composed of a lot of different kinds of inhomogeneities from small particles (dust, mud, etc.) to macro particles (fish, schools of fish, etc.). All this content induces sound scattering and the sum of all scattering contributions is sometimes called "reverberation" in the literature . For example, scattering from the sea surface becomes surface reverberation. Mainly employed in the SNR version of the sonar equation (e.g. equation 3.4) the term RL is defined by [Urick, 1983] as:

$$RL = 10\log_{10}\frac{\text{reverberation intensity at the receiver terminals}}{\text{intensity generated by signal of reference pressure}} \tag{3.62}$$

RL is therefore directly analogous to the echo level EL, with which it may be compared to obtain the echo-to-reverberation ratio. To do so, the echo level EL from the target is written $EL = SL + DI_{\text{Tx}} - 2TL_{\text{target}} + TS_{\text{target}}$ and the reverberation level is written:

$$RL = SL + DI_{\text{Tx}} - 2TL_{\text{reverb}} + SS_{\text{reverb}} \tag{3.63}$$

with SS_{reverb} the scattering strength of the sea inhomogeneities. The echo-to-reverberation ratio at the target distance in an homogeneous medium (i.e. $TL_{\text{reverb}} = TL_{\text{target}}$) is then:

$$EL - RL = TS_{\text{target}} - SS_{\text{reverb}} \tag{3.64}$$

Depending on what is considered to be the target of interest, the reverberation scattering takes into account the rest i.e. what is not scattered by the target. For example, if the target is a sphere lying on the seafloor, the reverberation level contains the seafloor scattering, volume scatterings from water and seafloor (if penetration or if the target is smaller than the insonified area) and sea surface scattering. Note that in this example the different sources of scattering are not all on the axis receiver-target. Therefore a directivity function correction should be added for each scattering direction to account for the level modification. When the seafloor is the main interest target, its scattering is excluded from the reverberation level parameter.

3.2.9 Detection threshold DT

The detection threshold is the decision level at which an observer decides if a signal (or an echo) is present in data based upon two criteria: 1) the probability of making a correct detection and 2) the probability of having a false alarm. This implies that the detection threshold value is always supported by a value of probability of detection PD and a value of probability of false alarm PFA. Values of these parameters differ according to mission objectives, but common values are given in [Dawe, 1997] as $PD = 10\log_{10}(50\%)$ and $PFA = 10\log_{10}(10^{-2})$ or $PFA = 10\log_{10}(10^{-5})$.

From the received signal, detection can be made directly on the time-samples amplitude [6], the echosounder is in this case called an amplitude detector. On the contrary, when the detection is done on the square of the input signal amplitude, it is called a power detector. In term of performance of the sonar, the lower the detection threshold, the better is the system. It is important to note that DT is recommended to be measured as a statistical quantity to have a valid meaning [Dawe, 1997] i.e. multiple detections from different received signals are suitable.

Several definitions of the detection threshold exist in the literature. Three of them are presented in the following. In [Urick, 1983] the detection threshold is defined at the receiver terminal as as the ratio of the signal power in the receiver frequency bandwidth to the noise power in a 1Hz frequency band:

$$DT_{1\text{Hz}} = 10\log_{10}\frac{\text{signal power to just perform a certain function}}{\text{noise power at the receiver terminal}} \tag{3.65}$$

This definition is mostly used in passive sonars, even if it is not specify in [Urick, 1983], but [Burdic and Bartram, 1984] imply that it can be used also for active sonars. However, a second definition is given in [Dawe, 1997] and the Sonar Modelling Handbook [7] where the noise power is taken in the entire receiver frequency bandwidth. This definition is mostly used for active sonars. It is possible to write the relationship between the two definitions of DT. The proportional coefficient being the receiver frequency bandwidth B_{Rx}, i.e.:

$$DT_{1\text{Hz}} = DT_B + 10\log_{10}(B_{\text{Rx}}) \tag{3.66}$$

with respectively $DT_{1\text{Hz}}$ and DT_B the detection thresholds taken into account the noise power in a 1Hz frequency band or in the receiver frequency bandwidth.

Another definition of the detection threshold is given by [Lurton, 2010] as the minimum signal to noise ratio value at the receiver output making possible a given level of target detection. It is then called reception threshold and is linked to the output signal to noise ratio SNR (for a linear receiver, after processing) by:

$$DT = 10\log_{10}(\text{SNR}) \tag{3.67}$$

In order to evaluate DT in practice, [Dawe, 1997] proposes two equations according to the type of processing employed on the signal. The first applied for sonars that use cross-correlation with an exactly known signal (a single pulse being detected in a background of Gaussian noise) and is:

$$DT_B = 10\log_{10}(d) - 10\log_{10}(B_{\text{Rx}}) - 10\log_{10}(2t) + OL - CG \tag{3.68}$$

and the second applies to sonars that use incoherent summation of power and is:

$$DT_B = 5\log_{10}(d) - 5\log_{10}(B_{\text{Rx}}) - 5\log_{10}(t) - 5\log_{10}(n_p) + OL - CG \tag{3.69}$$

6. Often on the envelope.

7. This reference is not available in the open literature but is widely cited e.g [Dawe, 1997] and discussed at length in [Holden, 2014].

where d is the detection index determined from receiver operative characteristic (ROC) curves according to the sonar application, t is the total length of time history used by the observer to make a decision, n_p is the number of sonar pulses that are incoherently summed, CG is the colour gain, and OL is the operational processor loss also known as the processor degradation factor. We can note that in these equations, the effects of a human observer are considered by taking into account the influence of the time t they has to make a decision and the colours of the display (e.g. gray scale or coloured scale). It was shown by [Buratti et al., 1989] and [Dawe and Galbreath, 1997] that the detection threshold can be improved by 1.5dB with appropriate colour coding. This corresponds to $CG = 1.5$dB.

The parameter OL corresponds to the cumulative losses associated specifically with the detection threshold. Values of this parameter are completely arbitrary and are chosen according to the type of sonar being used, e.g. [Dawe, 1997] gives values of 4dB for CW active sonars or 1dB to 3dB from sonar manufacturers. Additional losses can also be taken into account in OL as, for example, [Dawe, 1997]:

- Equipment misalignments and display losses: Conley [8] has described the various possible equipment misalignments for an active sonar which cause losses in performance. Loss mechanisms can occur in the filters, modulate frequency signals replications, display controls, servos, drifting of the transmitter drive and drifting of analogue circuits. According to Conley, measurements of existing active sonar systems give typical values for losses due to equipment misalignments as 5dB for displays, 2dB for receivers and 2dB for transmitters. In addition, the display loss due to the equipment misalignment mentioned by Conley was possibly due to a cumulative contribution of human factors effects.
- Doppler mismatch: in the case of frequency modulated pulse compression processing, a loss is incurred when the frequency of the received signal is shifted off the reference frequency, thereby reducing the overlap of the signal and the reference [9]. This loss can be evaluated as $20\log_{10}(1 - \delta f/B)$ where δf is the frequency shift and B is the original bandwidth of the waveform.
- Receiver position error: usual echosounders operate on the assumption that the positions of the receiving array elements are known exactly. In practice positions of the transducers are known approximately in many cases. Conventional echosounders can generally tolerate a positional error of up to about one quarter of the signal wavelength, while adaptive echosounders can generally only tolerate a positional error of about one tenth of the wavelength throughout the data integration period, before significant performance degradation will occur. For a rigid array this is not a significant problem (e.g. hull mounted active and passive sonars). However, for towed arrays the effect can be important. Sonar processors in this case employ array shape estimation algorithms to compensate for the effects of array distortion. For practical modelling purposes the effect of any receiver positional error can either be subsumed into the operational loss term OL, or supposed as negligible.

8. Unfound reference even if cited by [Dawe, 1997] as R. Conley (1994). *'Sources of Sonar System Losses'*, talk presented to the 15th Annual Meeting of TTCP Panel GTP-2, held at DRA Portland, UK.

9. R. Conley (1994). *'Sources of Sonar System Losses'*, talk presented to the 15th Annual Meeting of TTCP Panel GTP-2, held at DRA Portland, UK.

3.2.10 Processing Gain PG

The processing gain, in the sonar equations, generally corresponds to a gain value of signal echo level on the noise level obtained by processing the received signals. It mainly appears in active acoustics when using pulse compression. In this case it can be defined as the ratio of the signal to noise ratio of the current pulse compression on the signal to noise ratio of a CW pulse compression, i.e.:

$$PG = 10\log_{10}\left(\frac{\mathrm{SNR}}{\mathrm{SNR}_{\mathrm{CW}}}\right) \tag{3.70}$$

Because in this Phd work pulse compression is not employed and a CW pulse is transmitted, PG is not considered.

3.2.11 Operational degradation of the received level DF_0

The parameter DF_0 is an operational degradation term that is used as a catch-all for several cumulative imperfections in modelling terms of the sonar equation. It varies according to the system modelled. Certain types of imperfections can be found in the literature, in particular, [Dawe, 1997] mentioned a few of them such as:

- Scalloping losses: for an array of receivers, the sonar processor forms beams at regular intervals in azimuth. These beams are rounded in shape, often ellipsoidal in cross section, so that where their edges overlap there is a small dip in the array response. If the target is not central to one of the beams, or is crossing from one beam to the next due to high relative transverse motion, there is a dip in gain as the target moves through the dip in the array response where the beams overlap. The scalloping loss varies with the type of apodization window used [Harris, 1978]. It can vary up to 3dB or more at some frequencies if the beams are widely spaced [10]. For closely spaced beams, modern signal processing techniques can generally render this scalloping loss negligible [Blomqvist, 1979].
- Loss due to ship motion: as the receiving array moves during acquisition, sometimes beam stabilisation doesn't manage to keep the beam pointing in the proper direction. A performance loss is the added to account for this effect.
- Loss of signal coherence across the array: for relatively large apertures there is a loss in signal coherence across the receiving array aperture due to propagation effects. It depends on the frequency and the antenna length. According to Conley [11] losses can vary from 0.1 to 5.2 dB for frequency modulated pulses for a bottom bounce signal.

3.2.12 Target Strength TS

The target strength is the acoustic response of a target of interest. It is defined at one meter [12] from the acoustic center of the target as [Urick, 1983]:

$$TS = 10\log_{10}\frac{\text{echo intensity at one meter from target}}{\text{incident intensity}} \tag{3.71}$$

10. R. Conley (1994). *'Sources of Sonar System Losses'*, talk presented to the 15th Annual Meeting of TTCP Panel GTP-2, held at DRA Portland, UK.

11. R. Conley (1994). *'Sources of Sonar System Losses'*, talk presented to the 15th Annual Meeting of TTCP Panel GTP-2, held at DRA Portland, UK.

12. i.e. measured in far field and brought back to 1m.

Several types of target exist and are classified into three main categories in the literature:

— the point target whose dimension are very small compared to the beam aperture or the angular resolution.

— the volume target which is defined by the geometry of the echosounder. It is generally characterised by a parameter BV for volume backscattering strength. BV is a volume coefficient in decibels, therefore its target strength becomes: $TS = BV + 10\log_{10} v$ with v the insonified volume.

— the surface target, which is also defined by the geometry of the echosounder. It is generally characterised by a parameter bs for backscattering strength. $\mathrm{BS} = 10\log_{10}\mathrm{bs}$ is a surface coefficient, therefore its target strength becomes: $TS = \mathrm{BS} + 10\log_{10}\mathcal{A}$ with $\mathcal{A}$ the insonified area on the surface.

In this manuscript the target of interest is the seafloor, consequently, the target strength that is used is $TS = \mathrm{BS} + 10\log_{10}\mathcal{A}$.

3.2.13 The insonified area A

To derive the area $\mathcal{A}$ insonified by the echosounder, a CW pulse of length τ is considered i.e. a sinusoid over the time interval [0,τ]. At the observation time $t>\tau$, the propagation delay is delimited by t (for the pulse start, emitted at $t = 0$) and by $t - \tau$ (for the pulse end, emitted ar $t = \tau$). Therefore, the backscattered signal coming from a point target at ranges r verifies:

$$t - \tau < T(r) < t \tag{3.72}$$

where $T(r)$ is the two-way travel time between the sonar and a point at range r. Assuming the propagation is spherical in an homogeneous medium then $T(r) = \frac{2r}{c_\mathrm{w}}$. With this assumption and the hypothesis that the elementary scatterers simultaneously contributing at t are located at distances r, we can write [Lurton, 2010]:

$$\frac{c_\mathrm{w}(t-\tau)}{2} < r < \frac{c_\mathrm{w}t}{2} \tag{3.73}$$

The backscattered level can then be represented as a function of time or range equivalently when the previous conditions are validated.

The insonified area is mainly calculated geometrically in literature using a modelled beam as a cone and assuming the transmission of a CW pulse of length τ on a flat seafloor. Three different geometrical situations, illustrated in figure 3.3, are detailed in the following:

- When the echosounder (or the beam) is tilted at a angle θ_i and under the hypothesis of an equivalent beam width Φ (see definition in section 3.2.14), the insonified area $\mathcal{A}$ on a flat seafloor can be modelled as:

$$\mathcal{A} = \Phi r \frac{c_\mathrm{w}\tau}{2\sin\theta_\mathrm{i}} \tag{3.74}$$

  In this formula, the sound wave propagation between the source and the seafloor is assumed to be spherical, the insonified surface at time t is then delimited by the two concentric circles of radii $\frac{c_\mathrm{w}(t-\tau)}{2\sin\theta}$ and $\frac{c_\mathrm{w}t}{2\sin\theta}$.

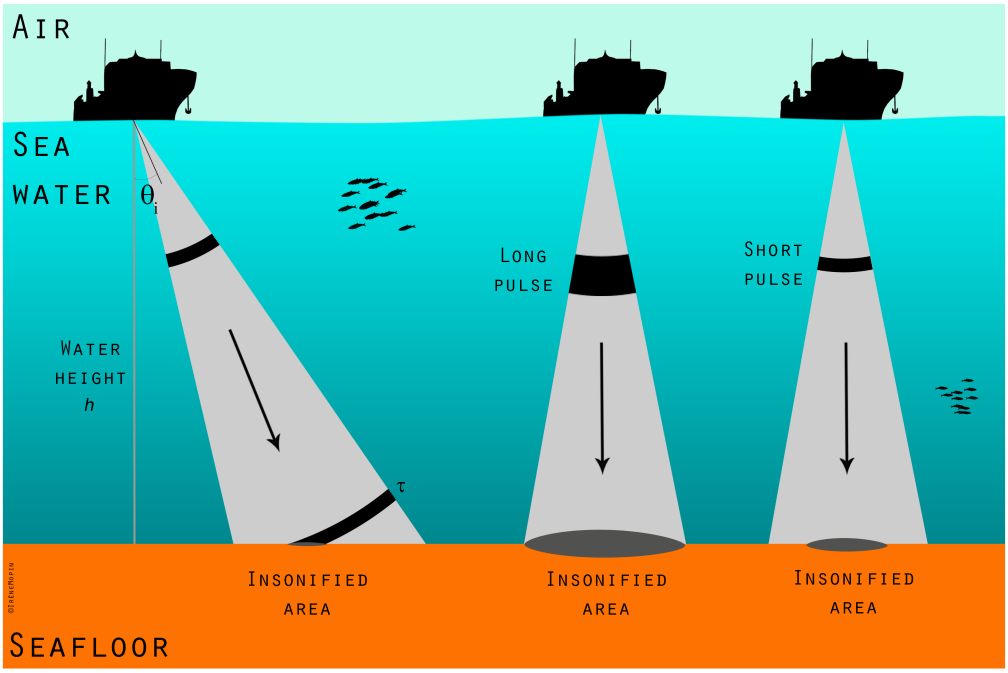

Figure 3.3 – Illustration of the three different model of insonified areas.

- When the echosounder is at normal incidence above the seafloor (i.e. $\theta_{\mathrm{i}} = 0°$), and the pulse is long enough for the beam footprint to be insonified at once, the insonified area becomes:

$$\mathcal{A} = \Psi h^2 \tag{3.75}$$

  where h is the height of the echosounder above the seafloor, and Ψ is the three-dimensional beam equivalent solid aperture in steradians (see definition in section 3.2.14). If the beam is conical, the insonified area can be expressed as a function of the angular half-aperture $\theta_{\text{-3dB}}$ [Lurton, 2010]:

$$\mathcal{A} = \pi(h\tan(\theta_{\text{-3dB}}))^2 \approx \pi h^2(\theta_{\text{-3dB}})^2 \tag{3.76}$$

- When the echosounder is at normal incidence above the seafloor (i.e. $\theta_{\mathrm{i}} = 0°$), and the pulse is short, the insonified area is not determined by the beam aperture but by the pulse duration τ. The pulse projection on the seafloor is a disk whose radius is given by the delay between the edge and the center. The oblique range between the echosounder and the disk edge is $r = h + \frac{c_{\mathrm{w}}\tau}{2}$. The disk radius equals $r_d = \sqrt{r^2 - h^2} \approx \sqrt{hc_{\mathrm{w}}\tau}$ (since $c_{\mathrm{w}}\tau/2 \ll h$), then

$$\mathcal{A} = \pi r_d^2 = \pi h c_{\mathrm{w}}\tau \tag{3.77}$$

In the above models of insonified area, the pulse envelope is considered to be perfectly rectangular. However, in practice, a rectangular envelope cannot be generated by the transducer because of its bandwidth, the actual pulse envelope has therefore a modified shape.

The difference of acoustic energy induced by this phenomena is taken into account in the sonar equation and in particular in the insonified area model by replacing the theoretical pulse length τ by an effective pulse length τ_{eff} defined in section 3.2.15.

3.2.14 Equivalent beam width Φ and equivalent solid angle Ψ

The equivalent beam width Φ is defined in two dimensions using an ideal rectangular directivity function (equal to 1 in the main lobe and 0 elsewhere) integrating the same amount of energy as the real directivity function $\mathcal{D}$. It is calculated as [Lurton, 2010]:

$$\Phi = \int_{-\pi}^{+\pi} \mathcal{D}(\vartheta) d\vartheta \tag{3.78}$$

The equivalent solid angle Ψ corresponds to the same idea but for a 3-dimensional beam function, such as:

$$\Psi = \int_{0}^{2\pi} \int_{-\frac{\pi}{2}}^{\frac{\pi}{2}} \mathcal{D}(\vartheta_x, \vartheta_y) \cos \vartheta_x d\vartheta_x d\vartheta_y \tag{3.79}$$

3.2.15 Equivalent pulse length τ_{eff} and energy factor correction S_{acorr}

When a CW pulse is transmitted by an echosounder, the transducer bandwidth creates transitory effects on the shape of the signal. The energy of the signal actually transmitted is therefore lower than the perfect rectangular pulse energy given electronically to the transducer. This difference of acoustic energy is taken into account by using an effective pulse length τ_{eff} whose amplitude is unity and whose energy is proportional to the theoretical pulse energy by a factor called S_{acorr} in [Eleftherakis et al., 2018] and [Ona et al., 2009] and defined in decibels as:

$$10 \log(\tau_{\text{eff}}) = 10 \log(\tau) + S_{\text{acorr}} \tag{3.80}$$

Figure 3.4 illustrates the pulse shape modification between the desired transmitted rectangular and the actual transmitted shape. In practice, the effective pulse length can be evaluated by measuring the difference of acoustic energy between the defined rectangular pulse and the pulse actually transmitted by the echosounder [Mopin et al., 2022] using a calibrated hydrophone. When the echosounder is used in mono-static, the effective pulse length includes the shape modification at transmission and reception, and S_{acorr} is noted in the sonar equation $2S_{\text{acorr}}$ to specify that it is considered both ways (see for example equation 3.23).

In literature, it can also be found that in order to reduce spectral sidelobes effects the transmitted signal is apodised, generally with usual windows as Hanning, Hamming, etc. This method is called waveform shading and implies also a loss of acoustic energy between a theoretical transmitted pulse and the actual transmitted pulse. [Dawe, 1997] proposes some coefficients that allows to derive the effective pulse length τ_{eff} from the theoretical pulse length τ according to the window employed [Harris, 1978]. For example, the author gives:

- Rectangle shading: $\tau_{\text{eff}} = 1.0\tau$
- Triangle shading: $\tau_{\text{eff}} = 0.5\tau$
- Hanning shading ($\cos^2$): $\tau_{\text{eff}} = 0.5\tau$
- Hamming shading: $\tau_{\text{eff}} = 0.54\tau$

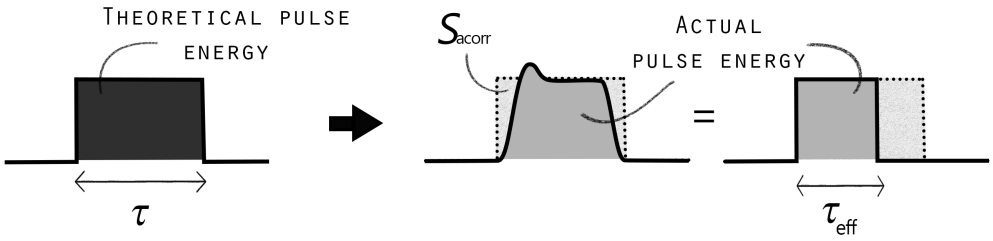

Figure 3.4 – Pulse shape modification between the theoretical transmitted rectangular pulse and the actual transmitted pulse. The energy loss between the two is included in parameter S_{acorr}.

- Blackman shading: $\tau_{\text{eff}} = 0.42\tau$
- Half cycle sine shading: $\tau_{\text{eff}} = 0.64\tau$

3.3 Summary

In this chapter, we saw that diverse type of sonar equations exist in literature, and various of them employ the seabed acoustic acoustic response as a parameter. The first kind is employed to evaluate echosounders performances and is written as a signal to noise ratio. The second kind is used to estimate a specific parameter among the equation parameters. The last kind is derived to design echosounders and used in real time operation. All parameters of these sonar equations are described in this chapter.

With the aim of evaluating the seafloor acoustic response, the work in this PhD restrict this ensemble to a sonar equation type having the seafloor for target of interest. The seabed response is then considered as the backscattering strength BS parameter. Currently, the form of the sonar equation used to estimate BS from *in situ* measurements is the intensity balance describing the loss of energy of a transmitted CW signal due to its propagation in the medium, its scattering from the target and due to other system components. Sonar equations 3.10, 3.19 and 3.23 are of this form. Parameters employed depend on those available (measured or given by the manufacturer) and on the precision desired on the BS measurement. It is important to note that similarly to the first chapter, the seafloor response is also in this chapter considered as a deterministic value (mainly employed in decibels) BS.

Chapter 4

From determinism to randomness: considering variability of the seafloor response measurements

In the previous chapters, models of the seafloor acoustic response and methods to compute it in practice (using sonar equations) were discussed. They consider mostly that the backscattering strength BS is a deterministic value depending on the transmitted frequency $\mathfrak{f}$ and the incidence angle on the seafloor θ_i. It came also to light that $\mathrm{BS}(\mathfrak{f}, \theta_\mathrm{i})$ is specific to a seafloor type and depends on the characteristics of the interface (roughness and impedance).

Following this hypothesis of a deterministic value, $\mathrm{BS}(\mathfrak{f}, \theta_\mathrm{i})$ values are used in literature for various applications such as seabed classification or characterisation [Hughes Clarke et al., 1997][Fonseca and Mayer, 2007]. They are often called angular response curves (ARC) [Huang et al., 2013][Trzcinska et al., 2021]. For some applications, a comparison is made between the measured ARC and models discussed in chapter 2, sometimes to derived the model parameters from *in situ* data, sometimes to classify the results. In most of the cases, this comparison is difficult because BS measurements show a large variability between pings for a given couple frequency and incidence angle on what is considered globally the same type of seafloor. In order to show this ping to ping variability, a survey was conducted during this PhD in the Bay of Brest (France) with a singlebeam echosounder (Kongsberg EA400). Measurements were part of a student project at ENSTA Bretagne which aim was to study seafloor classification using acoustic methods [1]. The echosounder was tilted at six different angles: 0°, 5°, 15°, 25°, 45°, and 65°. Measurements were done in survey mode i.e. following lines across areas where the terrain is supposed homogeneous on sedimentary map [Gregoire, 2016][Gregoire et al., 2016]. An example of resulting backscattering strength curves for $\mathfrak{f} = 38\,\mathrm{kHz}$ on one of the areas is given figure 4.1. On this graph, each BS values of each ping is plotted. Because of the vessel movements during acquisition, different angles around the angle of tilt of the echosounder are reached. This explains the dispersion in angles. However, the dispersion in amplitude is large and is observed even if the terrain is defined homogeneous.

This ping to ping variability can be due to two types of phenomena that are discussed in the two first sections of this chapter:

1. **External phenomena** that are not related to the seafloor. They include system parameters (sensitivities, directivity functions, etc.) that could not be perfectly known or can vary and environmental parameters that could not be measured every pings. See section 4.1.
2. **Terrain characteristics** which are specify to a type of seafloor. They are composed of different scale of properties that can induce variability in the seafloor response. See section 4.2.

In literature, the information contained in this ping to ping variability is described by a limited number of parameters depending on the application. For example, data of figure 4.1 are averaged to obtain one value per angle. To compare results from different terrains, value are then fitted to the GSAB model discussed section 2.2.4. The average is consequently used here as a mean to reduce information to one value per angle. In the last section of this chapter we present other methods and parameters that are commonly used to describe the seafloor response variability.

1. Project *Guerlédan* 2020-2021 at ENSTA Bretagne: `https://guerledan.ensta-bretagne.fr/`. Advisors: Irène Mopin (ENSTA Bretagne), Gilles Le Chenadec (ENSTA Bretagne), Olivier Morio (Shom), Julian Le Deunf (Shom). Students: Aelaïg Cournez, Flora Gues, Yann Lambrechts, Romain Safran.

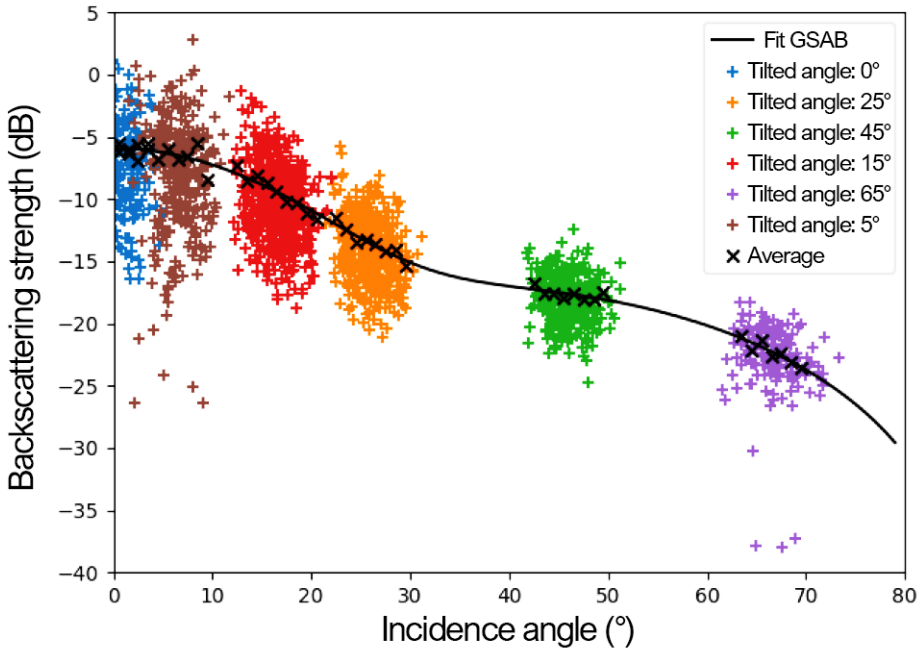

Figure 4.1 – Seafloor backscattering strength BS measured in the Bay of Brest (Area 3 of figure 4.2, France) with Kongsberg EA400 at 38 kHz tilted, following survey lines. From student report 2020-2021 [3].

4.1 Variability due to external phenomena

The seafloor acoustic response is computed in practice using sonar equations that were discussed in chapter 3. All the parameters that composed these sonar equations can be estimated theoretically, empirically, or measured with more or less accuracy depending on the precision the application required. They can be classified in two categories: 1) technical parameters that are specific to an echosounder system (e.g. apertures, sensitivities, directivities, etc.), and 2) environmental parameters that depend on the location of the measurement (e.g. absorption coefficient, terrain slope, etc.).
Technical parameters are commonly measured in tank before the survey (calibration) and are constant values. Even if measured in tank some of them can vary in time because of temporal modifications of the echosounder such as appearance of biofouling or deterioration of the transducers. Periodic calibrations *in situ* are carried out to detect and correct this kind of unintended effects. The first part of this section presents different methods of calibration and their requirements and constraints.
On the contrary, environmental parameters need to be evaluated during the survey and can vary from ping to ping. These measurements have their own uncertainties that lead to uncertainties on the measurement of the seafloor response. Using a sonar equation, these uncertainties can be estimated. Method and results from [Malik et al., 2018] are discussed in

3. Project *Guerlédan* 2020-2021 at ENSTA Bretagne: `https://guerledan.ensta-bretagne.fr/`. Advisors: Irène Mopin (ENSTA Bretagne), Gilles Le Chenadec (ENSTA Bretagne), Olivier Morio (Shom), Julian Le Deunf (Shom). Students: Aelaïg Cournez, Flora Gues, Yann Lambrechts, Romain Safran.

the second part of this section.
Finally, limits in parameter measurements accuracy can also appear when dealing with commercial echosounder especially when the use of the echosounder to provide a BS value is not its current usage. This point is discussed in the last part of this section.

4.1.1 Echosounder magnitude calibration

Several calibration methods exist to measure echosounder specifics parameters. The mostly employed technique is the use of a calibrated hydrophone in tank. This kind of measurement allows to derive the sensitivities at transmission and reception of the echosounder, and also its directivity functions and apertures at transmission and reception independently. Another calibration method using a perfectly known target [Vagle et al., 1996, Foote et al., 2005] permits to measure directly the two-way directivity and aperture, and also the distortion of the transmitted signal leading to the Sa_{corr} value and the effective pulse length τ_{eff} [Ona et al., 2009] (see section 3.2.15 for details). With this method an accuracy of 0.1 dB on the calibration results was demonstrated by [Foote, 1982] with a copper sphere as target.

Measurements in tank also inform of the echosounder particularities such as un-suspected gains due to electrical circuits or connections, transducer amplitude variations, etc. For example, for a calibration on a sphere target of known target strength TS_{sphere} [Manik, 2012], two parameters are added to the sonar equation 3.8 to take into account these features: a gain at transmission G_{Tx} and a gain at reception G_{Rx}, leading to:

$$10\log_{10}\left(\frac{1}{2}V_{\text{Rx}}^2\right) = 10\log_{10}\left(\frac{1}{2}V_{\text{Tx}}^2\right) + S_{\text{Rx}} + S_{\text{Tx}} - 2TL + TS_{\text{sphere}} + G_{\text{Tx}} + G_{\text{Rx}} \quad (4.1)$$

These gains are specific to a system and can be verified regularly.

In order to get the best accuracy on the system parameters (and because some echosounders cannot fit in a tank), calibration of the echosounder can in addition be made *in situ* on the sphere target. This method helps to identify residual effects that sometimes appear when the echosounder is mounted aboard (bump), or due to the marine environment (biofouling). It is also used to control the correct functioning of the echosounder in time (from one survey to another). During the *in situ* calibration, attention has to be made at the measurement conditions that may influence the resulting accuracy. Different parameters that can affect the results are discussed in [Foote, 1983] where they are classified in three categories:

- intrinsic parameters (sphere): diameter, density, sound speeds (for compressional and shear acoustic waves propagating in solid)
- extrinsic parameters (liquid medium): density, sound speed, temperature
- extrinsic parameters (equipment): transmitted frequency and pulse duration

Some of them can be neglected while others can be considered and corrected to maintain the 0.1 dB accuracy of the sphere calibration.

When a sphere calibration cannot be made, either in tank or *in situ*, a possible solution is to use the seafloor as a reference target [Ladroit et al., 2018]. The acoustic response of the reference terrain is measured beforehand with a calibrated echosounder on sphere (generally

a single-beam echosounder) [Eleftherakis et al., 2018] and then compared to the ongoing measurement of the seafloor backscattering strength. This method implies to know a terrain that has a constant acoustic response in time and space and which is perfectly flat in term of bathymetry. [Lurton et al., 2018] present an analysis of different terrain responses according to the incident angles and azimuths of the measurements. In their geographical area, the best terrain for calibration is shown to be the *Carré Renard* in the Bay of Brest (France).

From a technical point of view, the calibration on sphere requires, for being relevant, to be able to measure the position of the sphere in the echosounder beam. This measurement is not available with mono-transducer echosounder and in this case the reference terrain calibration is therefore recommended. Echosounders composed of several transducers are in contrast perfectly adapted to sphere target measurement and are called in the following split-beam echosounders [Brede et al., 1990].

Before calibration, technical parameters appearing in the sonar equation are considered by [Malik et al., 2018] to have an unpredictable uncertainty up to prohibitive. After calibration, this uncertainty falls to negligible to small according to the authors.

4.1.2 Environmental parameters uncertainties

Seafloor response BS can be affected by changes in the environment during measurements. For example, [Stanic and Kennedy, 1992] show that even in the measurements are made with an echosounder mounted on a stable platform (perfect compensation of system parameters), ping to ping variations still appear. The authors supposed that they are caused by random variations in the structure of the water column. Indeed, changes in the sea water characteristics lead to modifications of the position and size of the insonified area and therefore induce variability of BS. [Stanic and Kennedy, 1992] observed this effect increasing with range, as confirmed by [Chotiros et al., 1985].

In order to evaluate the magnitude of BS variations that can be generated by environment changes, the sonar equation is used. In sonar equation 3.10, two components are depending on environmental parameters: the transmission loss TL and the insonified area $\mathcal{A}$. They can vary according to the water absorption coefficient α_{w}, the range r, and the incident angle on the seafloor θ_{i} (considering the local slope of the seabed in 3D). In practice, these parameters are measured *in situ* as frequently as possible, with a probe (absorption and sound velocity) or using bathymetric data provided by the echosounder (slope and range). The latter can therefore be estimated for each ping, contrary to profiles of absorption and sound velocity that involve stopping the vessel during measurement or leaving probes in the ocean (e.g. expendable bathythermograph (XBT)). As they are evaluated *in situ*, uncertainties on these parameters measurements imply uncertainties on TL and $\mathcal{A}$ and finally on the seabed response BS. Analyses of these uncertainties are found in [Malik et al., 2018] and detailed below.

The first parameter to be measured is the incidence angle on the seafloor θ_{i}. Uncertainties on this parameter depends on three components:

1. the received angle which is function of the performance of the system and the platform motion measurement [Hare, 2001, Lurton and Augustin, 2010]. In [Malik et al., 2018] this component is neglected.
2. the effect of the beam steering and refraction during the wave propagation [Hare et al., 1995]. [Malik et al., 2018] suppose that the sound speed is continuously measured at the transducer head by a probe and that a complete sound speed profile provides an average value of the sound speed on the entire water column. Considering that sound speed uncertainties remain smaller than 0.1%, the authors infer that the effect of beam steering and refraction can be neglected.
3. the seafloor slope in the beam footprint. In some cases this slope is ignored and the seafloor assumed flat an horizontal in the footprint. However, it is not always the case, therefore the slope is generally determined combining a previous digital terrain model (DTM) measurement and geometry assumptions. This method gives accurate results but is subject to uncertainties. In addition, small-scale slopes in the bathymetry also affect the local incidence angle and can cause additional uncertainties [Dolan and Lucieer, 2014, Zhu et al., 2014].

These three components cannot be dissociated but uncertainties on the incidence angle impact the angle at which is reported the measured backscattering strength and the insonified area computation.

The influence of the incidence angle uncertainty on the BS measurement uncertainty is analysed in [Malik et al., 2018]. Based on the GSAB model (see section 2.2.4), the uncertainty $\delta\,\mathrm{BS}$ is derived in decibels as:

$$\delta_{\theta_\mathrm{i}}\,\mathrm{BS} = \frac{10}{\log 10}\left(\frac{\partial\,\mathrm{bs}}{\partial\theta_\mathrm{i}}\right)\frac{\delta\theta_\mathrm{i}}{\mathrm{bs}} \tag{4.2}$$

with BS the backscattering strength modelled with GSAB, and $\partial\,\mathrm{bs}\,/\partial\theta_\mathrm{i}$ its differential. The uncertainty is maximum for specular regime and is large at angles over 70°. Between angles from $10-20°$ to $50-60°$ (the "plateau") uncertainties are supposed negligible by the authors. This stability is an argument for using BS measurements in this angular range as a reference for comparison and classification.

The uncertainty on the incidence angle $\delta\theta_\mathrm{i}$ also leads to uncertainties on the insonified area $\delta\mathcal{A}$. For short pulse approximation, it is given by [Malik et al., 2018] as:

$$\mathcal{A} \propto \frac{1}{\sin\theta_\mathrm{i}} \Rightarrow \frac{\delta\mathcal{A}}{\mathcal{A}} = \frac{\delta\theta_\mathrm{i}}{\tan\theta_\mathrm{i}} \tag{4.3}$$

which yields to uncertainties on BS caused by angle variations in insonified area as:

$$\delta_{\mathcal{A},\theta_\mathrm{i}}(\mathrm{BS}) = 10\log_{10}\left(1+\frac{\delta\mathcal{A}}{\mathcal{A}}\right) = 10\log_{10}\left(1+\frac{\delta\theta_\mathrm{i}}{\tan\theta_\mathrm{i}}\right) \tag{4.4}$$

For long pulse approximation, it is given by [Malik et al., 2018]:

$$\mathcal{A} \propto \frac{1}{\cos\theta_\mathrm{i}} \Rightarrow \frac{\delta\mathcal{A}}{\mathcal{A}} = -\tan\theta_\mathrm{i}\delta\theta_\mathrm{i} \tag{4.5}$$

which yields:

$$\delta_{\mathcal{A},\theta_\mathrm{i}}(\mathrm{BS}) = 10\log_{10}\left(1+\frac{\delta\mathcal{A}}{\mathcal{A}}\right) = 10\log_{10}\left(1-\tan\theta_\mathrm{i}\delta\theta_\mathrm{i}\right) \tag{4.6}$$

These results apply only if the terrain actual slope is taken into account. In the case where no compensation of the seafloor topography is achieved (i.e. seafloor assumed flat and horizontal), the uncertainty depends on the incident angle θ_i for the assumed flat terrain and the actual terrain slope ψ. This leads to the short pulse approximation:

$$\delta_{\mathcal{A},\varphi}(\mathrm{BS}) = 10\log_{10}\left|\sin\theta_\mathrm{i}/\sin(\theta_\mathrm{i}-\psi)\right| \tag{4.7}$$

Reciprocally, the long pulse approximation uses cos(.). Values of uncertainties are given in [Malik et al., 2018] according to incidence angles (0° to 80°) and seafloor slope (−15° to 15°). Results shows that across-track [4] seafloor slope uncertainty is significant and more severe at mid-range incidence angles (20° - 50°). For along-track [5] angles and slopes, BS uncertainty result shows to be negligible for smooth terrain (< 0.1 dB for slope angles up to 15°) but increases significantly for steeper slopes (> 0.5 dB for slopes 30°-45°). In summary, BS measurement has been proved to be impacted significantly by the beam pointing angle uncertainty and the local seafloor slope uncertainty.

The transmission loss parameter includes the effects of geometrical divergence and absorption of the acoustic energy. Consequently, its uncertainties are related to measurements of the range and of the absorption coefficient.

- **Uncertainty due to range measurement.** The range r is commonly calculated as $r = \bar{c}_\mathrm{w}t/2$ with $\bar{c}_\mathrm{w}$ the average sound speed between the source and the target, idealy the harmonic mean sound speed profile [Charlot et al., 2019][Charlot, 2019]. The corresponding uncertainty δr is due to both uncertainties in time measurement and average sound speed, i.e. assuming t and $\bar{c}_\mathrm{w}$ independent [Malik et al., 2018]:

$$\frac{\delta r}{r} = \sqrt{\left(\frac{\delta t}{t}\right)^2 + \left(\frac{\delta\bar{c}_\mathrm{w}}{\bar{c}_\mathrm{w}}\right)^2} \tag{4.8}$$

  with δt the travel-time uncertainty bounded by the sampling step of the digitized time signal, and $\delta\bar{c}_\mathrm{w}$ the sound speed measurement uncertainty. [Malik et al., 2018] discuss the magnitude order of the uncertainties for multibeams echosounders and conclude to $\delta\bar{c}_\mathrm{w}/\bar{c}_\mathrm{w} = 0.1\%$, $\delta t/t = 0.1\%$, and therefore $\delta r/r = 0.18\%$, that gives a total uncertainty on the transmission loss due to spreading ($2TL_r = 40\log_{10} r$) equals to:

$$\delta_r(2TL_r) = 40\log_{10}\left(1+\frac{\delta r}{r}\right) \approx 0.035\mathrm{dB} \tag{4.9}$$

- **Uncertainty due to absorption loss.** The range impact on the absorption loss ($2TL_\alpha = 2\alpha r$) is given by:

$$\delta_r(2TL_\alpha) = 2\alpha r\frac{\delta r}{r} \tag{4.10}$$

4. In the pointing direction i.e. perpendicularly to the vessel axis.
5. Along the vessel axis.

Those two parts of transmission loss uncertainties are calculated in [Malik et al., 2018] for MBES and found negligible. However, the absorption coefficient uncertainty itself, derived as:

$$\delta_\alpha(2TL_\alpha) = 2\alpha r\frac{\delta\alpha}{\alpha} \tag{4.11}$$

can have a high magnitude (up to 10 dB in the worst case at oblique angles) and is therefore a major factor in the final backscattering strength uncertainty.

A summary of the uncertainty due to environmental sources has been made by [Malik et al., 2018] where the authors classify their magnitude from negligible to prohibitive. Table 4.1 shows their classification. A scale of values in decibels are given to classify the uncertainties:

- Negligible (N): 0.01-0.1 dB
- Small (S): 0.1-1 dB
- Moderate (M): 1-3 dB
- High (H): 3-6 dB
- Prohibitive (P): beyond 6 dB

We observe from table 4.1 that most of the parameters can have negligible or small uncertainties if the seafloor slope is taken into account and if water parameters are known and no anomalies appears.

Parameter	Uncertainty sources	Magnitude
Incidence angle	Seafloor slope (ignored)	N to P
	Seafloor slope (compensated)	N to M
Insonified area ($\mathcal{A}$)	Insonified area model	N to S
	Incidence angle (refraction, seafloor slope)	S to M
	- if seafloor slope ignored	H to P
	Propagation range	N
Transmission loss (TL)	Absorption coefficient	S to H
	Propagation range	N
	Frequency differences (ignored)	N to M
	Water column anomalies (e.g. bubbles)	N to P

Table 4.1 – Major sources of uncertainty on the backscattering strength measurement using sonar equation, from [Malik et al., 2018]. N is for negligible, S = small, M = moderate, H = high, and P = prohibitive.

4.1.3 Constraints due to manufacture and survey operation

Most of current and former echosounders process in real time a seafloor response i.e. backscattering strength $\mathrm{BS}_{\mathrm{sounder}}$ during the survey. It is a real asset because it allows to verify the proper functioning of the echosounder and it also provides a fast result of the seabed response map. However, in order to be efficient a fast signal processing and a robust seabed echo detection algorithm are employed. This leads to compromises either in the choice of the algorithms and in the form of sonar equation to be included in the echosounder software.

The seabed echo detection can be done by two methods providing the sounding i.e. the recorded time-sample corresponding to the range r between the echosounder and the seafloor:

- at oblique angles, the sounding can be detected using the phase difference between two received signal coming from the seafloor to two different transducers of the antenna [Eleftherakis et al., 2018]. The sounding corresponds in this case to the range where the phase difference is crossing zero i.e. on the center of the beam.
- at normal incident (nadir) or if no phase information is available, the sounding is detected on the maximum amplitude (or the center of gravity) of the received signal coming the seafloor [Eleftherakis et al., 2018].

According to the quality of the received data, ambiguities could obviously appeared (low signal to noise ratio, noise on the phase difference, etc.) and led to wrong soundings values. That is why data can be reviewed afterwards where what is considered as a wrong sounding can be deleted in post-processing by the user or a data processing algorithm [Le Deunf et al., 2020].

Associated to the sounding, echosounders provide in real time and store a processed value of the seafloor backscattering strength $BS_{sounder}$ (or other target strengths). This value is computed using a sonar equation specific to the echosounder as shown in section 3.1.3. Exploiting $BS_{sounder}$ values directly is useful when the echosounder is used for its main usage. However, for this PhD seabed response measurements are made at different incident angles on the seafloor with a singlebeam echosounder. The sonar equations employed by Kongsberg EA400 and EK60 (see equations 3.19 and 3.23) are only valid at nadir i.e. for an incidence of 0° (current use of singlebeam echosounders). Therefore, at the other angles the insonified area calculated by the echosounder is not valid and consequently so is the backscattering strength value. In order to re-calculate the backscattering strength with the good assumptions, raw data provided by the echosounder are needed. They are composed of all the parameters of the echosounder sonar equation parameters. Each parameter can therefore be re-derived and the seafloor response associated to the sounding re-estimated.

While re-computing the parameters in order to get the seafloor backscattering strength, uncertainties can appear, caused by shortcomings in the documentation provided by the manufacturer ([Malik et al., 2018]) or by unwanted modifications in the echosounder characteristics (e.g. failure of transducers or in motion compensation, [Gallaudet, 2001, Hiroji, 2016]). In addition, raw data provided by echosounders are not always suitable for post-processing, due to real time processing constraints and limitation in storage space. Indeed, raw data provided by the echosounder in the loggings are generally composed of the decimated received signal envelopes (from an unknown processing). For example, Kongsberg EA400 provides received signals with a sampling frequency corresponding to four samples per pulse length. Other examples are given for the last generation of fishery echosounders in [Demer et al., 2017]. Decimation factors are given together with the resulting sampling frequencies and summarised in table 4.2.

In the BS estimation process from survey data with commercial echosounders some accuracy can therefore be loss because of real-time and storage constraints. Even if some parameters can be re-calculated, decimation can't be undo most of the time.

Echosounder	Decimation	Resulting sampling frequency
ES18 - 18 kHz	6	23.4 kHz
ES38B - 38 kHz	6	187.5 kHz
ES70-7C - 70 kHz	6	250 kHz
ES120-7C - 120 kHz	12	125kHz
ES200-7C - 200 kHz	8	187.5 kHz
ES333-7C - 333 kHz	6	250 kHz

Table 4.2 – Simrad EK80 echosounders decimation factors and resulting sampling frequencies, from [Demer et al., 2017]

4.2 Variability due to terrain characteristics

Apart from external phenomena, the seafloor response can vary from ping to ping because of the seafloor variability itself. Theses changes are due to the terrain characteristics and the way the survey is conducted. They can have different origins that are classified in four categories based on their scales:

1. **Time scale** Temporal variabilities due to modifications of the seabed in time.
2. **Geographic scale** Spatial variabilities due to changes on the seabed type along survey lines.
3. **Echosounder scale** Spatial variabilities due inhomogeneities in the terrain inside the beam footprint
4. **Pulse scale** Intrinsic variability of the scattering mechanism inside the insonified area, also called speckle.

In the following, these four class are discussed and examples are given from literature.

4.2.1 Time scale

Temporal modifications of the seafloor can appear a different time scales. According to the surveys repeatability (years, months, days, or less), their impact can be observed on seafloor response measurements. Some examples of seafloor changes affecting the backscattering strength that are observed in literature are listed below:

- **Annual changes** [Urgeles et al., 2002] show modifications of the backscattering strength map (5 dB) between 1993, 1997 and 1999 after a major rainstorm and flood happened in 1996.
- **Tide-cycle changes** Modifications on the backscattering strength measurements (variability $>$ 3 dB over the full angular range) were observed by [Montereale-Gavazzi et al., 2019] in tidal environments. Tide cycles resulted in sedimentary changes due to deposition and erosion. These effects were mostly observed on terrain composed of soft sediments (e.g. sand).
- **Diurnal changes** [Gorska et al., 2018] show in tank the effect of micro-phyto-benthos photosynthetic activity on BS measurements between day and night. A variability up to 1.5 dB at 250 kHz was observed on sandy inhabited sediments.

- **Small and continuous changes** Biological activity, or bioturbation, was demonstrated to modify continuously the seafloor interface and therefore the backscattering strength by [Jackson et al., 2009][Jumars et al., 1996]. They observed changes on soft muddy seafloor at 40 kHz.

In time, the seabed acoustic response is consequently variable at different scales. These changes can lead to misinterpretation of the backscattering strength information if not taken into account.

For echosounder calibration on reference area (see details in section 4.1.1), the terrain used should be stable in time to avoid bias in the results. Different surveys should therefore be achieved to ensure that ARC variations are negligible in time [Lurton et al., 2018][Montereale-Gavazzi et al., 2019].

4.2.2 Geographic scale

Measurements of the seafloor acoustic response are usually associated to hydrographic surveys. Therefore, survey lines that can be kilometres long are followed. Along these lines, the seabed type can vary significantly from an area to another kilometres away. Consequently, when mapping backscattering strength measurements from survey lines, a large variability can be observed because of changes in the seabed type [Lamarche et al., 2011][Fezzani and Berger, 2018]. As an example, figure 4.2 from [Mopin et al., 2022] shows a sediment map of the Bay of Brest (France). Three areas are enlighten (sandy mud, gravel, gravelly coarse and maerl) for which measurements of the seafloor response were made by the authors. For each terrain, measured ARC were found different. Equivalent results are given in [Fezzani et al., 2021].

We have to note that even if sediment maps show sharp boundaries between terrains, limits of area are not in practice perfectly clear. Indeed, sediment are composed of multiple elements that can mix with the adjacent components creating a fuzzy interface between the two areas.

Even if the terrain is defined homogeneous in a area, variations can still appear on the seafloor backscattering strength. It has been shown by [Lurton et al., 2018] and [Montereale-Gavazzi et al., 2019] that seabed features such as sand ripples have an impact on BS measurements. According to the azimuth of the survey line, significant variabilities in the ARC are observed. Consequently, a terrain considered homogeneous from a geological point of view can have various acoustic signatures according to the survey method.

4.2.3 Echosounder scale

As discussed previously, seafloor backscattering strength variability from one ping to another can come from terrain changes at a large spatial scale. At a smaller scale, it can also originate from the terrain variability itself [Nolle et al., 1963][Becker, 2004][Goff et al., 2004]. In effect, a terrain is defined as homogeneous when its composition does not change spatially, however this composition can be made of different sediment types as long as they are statistically constantly represent.
As an example, sediment samplings were done on the terrain area 3 of figure 4.2 from which

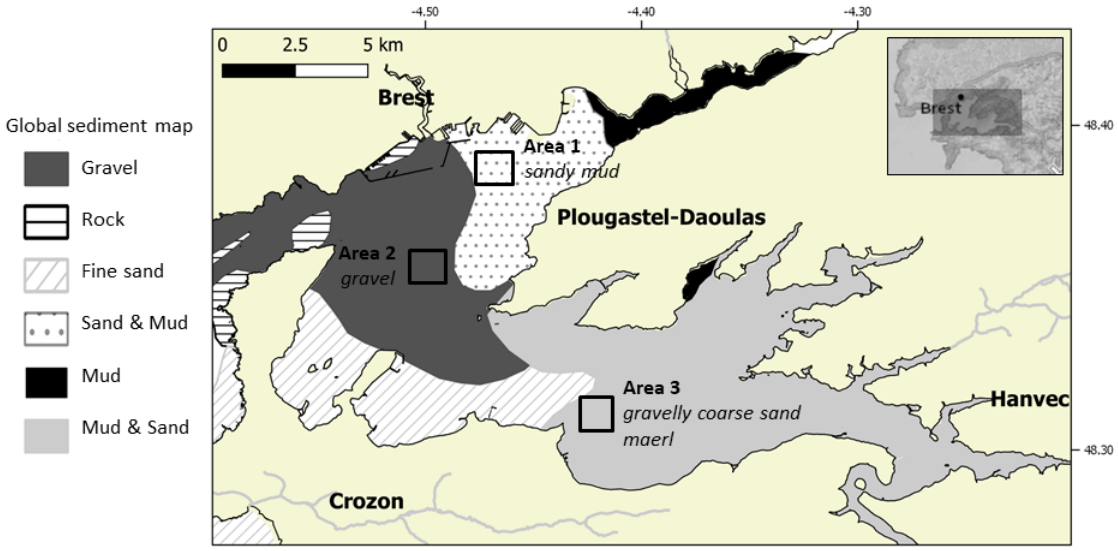

Figure 4.2 – Sediment map of the Bay of Brest (France) from [Mopin et al., 2022] with the three areas surveyed. The global sediment map comes from data.shom.fr (`www.shom.fr/HOM/GEOL_SEDIM_MONDIALE`) and land information come from `geo.data.gouv.fr`.

BS measurements of figure 4.1 come from [6]. Results are shown figure 4.3. Samplings were made with a Van Veen grab sampler [7] associated with underwater videos. Samples of sediment were photographed directly on-board and then a granulometric analysis was performed at Shom [8] (sifting and laser). Pictures, *in situ* samplings, and grain size analysis shows several components of the sediment: fauna (brittle-stars), shells of different sizes (broken or not), gravel, muddy sand, rocks from 2cm to 10cm, granules (2-4mm diameter) and gravels (4-11mm diameter). When watching the video it is also observed that a few soft sediments are present, they are also observed in the granulometric analysis (<1%). In addition, the seafloor looks quite hard on video.

Backscattering strength measurements of figure 4.1 were therefore made on what in considered an homogeneous terrain on the sediment map (area 3 in figure 4.2), however the terrain is composed of various elements spatially distributed. From the echosounder point of view, the spatial random layout of the terrain components induces a variability between one spatial distribution inside the footprint and another for the next ping. This spatial variability leads to variations in the received signal and therefore in the resulting BS. Each BS measured from each ping is consequently considered as the response of the same seafloor type but varies as observed in figure 4.1. The seafloor response variability is therefore characteristic of the sediment mixture.

6. Project *Guerlédan* 2020-2021 at ENSTA Bretagne: `https://guerledan.ensta-bretagne.fr/`. Advisors: Irène Mopin (ENSTA Bretagne), Gilles Le Chenadec (ENSTA Bretagne), Olivier Morio (Shom), Julian Le Deunf (Shom). Students: Aelaïg Cournez, Flora Gues, Yann Lambrechts, Romain Safran.

7. See details in the student report 2021-2022, or on `https://www.whoi.edu/what-we-do/explore/instruments/instruments-sensors-samplers/grab-sampler-van-veen/`.

8. Analyses were performed by Pierre Shute from the granulometry department of Shom.

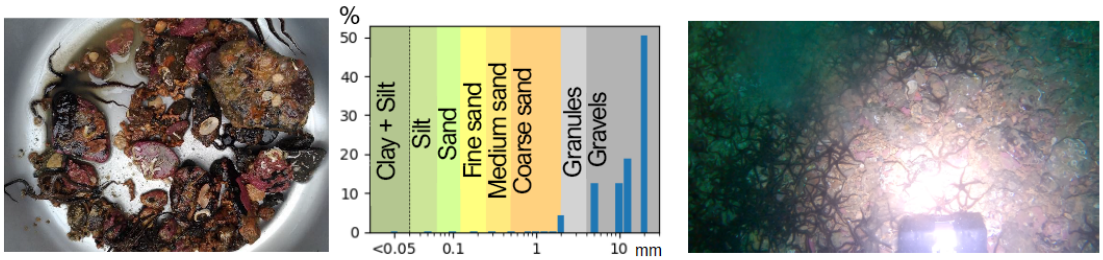

Figure 4.3 – Sediment composition of the terrain BS measurements of figure 4.1 come from (Bay of Brest, France). Left: composition of the sample made with a Van Veen grab sampler. Center: Granulometric analysis of the sample. Right: Video capture of the terrain. From from student report 2020-2021.

The terrain analysed in this section is also used in literature as a reference area for echosounder magnitude calibration [Eleftherakis et al., 2018]. Measurements with high frequency echosounders shows that the backscattering strength of the area is stable in time (at large scale) and independent of the azimuth [Lurton et al., 2018].

4.2.4 Pulse scale

The last scale at which variability of the backscattering strength is observed is at the origin of the backscattered signal i.e. where the transmitted pulse is backscattered from the seabed. Geometrically, the composition of the seabed can be modelled as a rough interface (see figure 2.5) which leads to different spatial positions of reflectors of the incident acoustic signal called scatterers. The insonified area being a surface, it can be modelled by several individual scatterers participating to the final scattered signal. Even if each scatterer reflects the same energy (i.e. they are from the same seabed type), their locations due to the roughness change their signal phases and they consequently interfere with each other [Stanton et al., 2018]. The total backscattered signal measured by the echosounder and composed of all the scatterers contributions becomes therefore random by definition. The deterministic value bs therefore become a random variable noted **bs**. Its variability is observed inside a ping, from a time-sample of the seafloor echo to another. Consequently, the seafloor acoustic response is intrinsically random because of the geometry of acquisition (insonified area) and the roughness of the seafloor (random positions of scatterers).

Models of the backscattering strength discussed in the previous chapters define bs as a deterministic value. In order to introduce its randomness, a stochastic approach is developed based on the sonar equation 3.8 and the multiple scatterers hypothesis from [Stanton et al., 2018]. The scattering process describes in the following accounts for a single ping and a mono-static echosounder geometry. The signal is assumed narrowband.

For a single scatterer, the RMS voltage $V_{\mathrm{Rx}}/\sqrt{2}$ received by the echosounder is given using the sonar equation in natural values, as (inspired by [Stanton et al., 2018]):

$$\frac{V_{\mathrm{Rx}}}{\sqrt{2}} = \frac{V_{\mathrm{Tx}}}{\sqrt{2}} 10^{S_{\mathrm{Rx}}/20} 10^{S_{\mathrm{Tx}}/20} e^{-j\omega t} \frac{1}{r^2} e^{2jkr} e^{-2\alpha_{\mathrm{w}} r} \mathcal{D}^2(\vartheta_x, \vartheta_y) a \tag{4.12}$$

where:

- $V_{\mathrm{Tx}}/\sqrt{2}$ is the RMS transmitted voltage,
- S_{Tx} is the transmitter response at a reference distance of 1m,
- S_{Rx} is the receiver sensitivity,
- r is the distance between the transducer and the scatterer,
- ω is the angular frequency of the incident and scattered sinusoidal signals,
- k is the wavenumber of the incident and scattered sinusoidal signals,
- α_{w} is the absorption coefficient of the water medium,
- $\mathcal{D}$ is the two-way beampattern of the echosounder whose values lie in the range [0,1],
- $(\vartheta_x, \vartheta_y)$ are the angular coordinates of the scatterer in the beam,
- a is the backscattering index amplitude of the scatterer which is a complex variable.

The voltage received by the echosounder for an aggregation of M scatterers constituting the insonified area of seafloor is therefore (inspired by [Stanton et al., 2018]):

$$\frac{V_{\mathrm{Rx}}}{\sqrt{2}} = \frac{V_{\mathrm{Tx}}}{\sqrt{2}} 10^{S_{\mathrm{Rx}}/20} 10^{S_{\mathrm{Tx}}/20} e^{-j\omega t} \sum_{i=1}^{M} \frac{e^{2jkr_i}}{r_i^2} e^{-2\alpha_{\mathrm{w}} r_i} \mathcal{D}^2(\vartheta_x^i, \vartheta_y^i) a_i \tag{4.13}$$

where r_i, a_i and $(\vartheta_x^i, \vartheta_y^i)$ are the range, backscattering index amplitude and angular location of the i$^{\mathrm{th}}$ scatterer respectively. The simple summation of echoes from individuals scatterers reflects the assumption that only single-order scattering is being considered and higher orders scattering (e.g. re-scattering of echoes between individuals) are assumed negligible.

Assuming that all systems and environment parameters of the sonar equation are constant and perfectly known, they can be included in a constant $C_{\mathrm{eq.so}}$ for simplicity of analysis. The backscattering index amplitude $|A|$ of an ensemble of M scatterers then becomes [Stanton et al., 2018]:

$$|A| = \frac{1}{C_{\mathrm{eq.so}}} \left| \sum_{i=1}^{M} |a_i| \mathcal{D}^2(\vartheta_x^i, \vartheta_y^i) e^{j\phi_i} \right| \tag{4.14}$$

where ϕ is the phase shift associated with the i$^{\mathrm{th}}$ scatterer. This phase shift can be induced by the locations of the scatterers which is directly linked to the roughness of the terrain. Consequently, random locations of the scatterers imply the randomness of $(\vartheta_x^i, \vartheta_y^i)$ and ϕ_i leading to stochastic magnitudes of the received echo voltage V_{Rx} (see equation 4.13) and therefore to the randomness of the measured seafloor response .

In this model, the range from the echosounder has been approximated constant regardless the scatterer in the insonified area i.e. $r_i^2 \sim r^2 = \mathrm{cst}$ and $e^{-2\alpha r_i} \sim e^{-2\alpha r} = \mathrm{cst}$. However, minor range differences can remain between scatterers especially when the acoustic wavelength is comparable to or smaller than the roughness [Stanton et al., 2018].

From this model, we observe the presence of an intrinsic randomness of the backscattering strength induced by the location of the scatterers in the insonified area (randomness of ϕ_i). But another variability is also generated by the scatterers locations inside the beam pattern $\mathcal{D}$ (randomness of $(\vartheta_x^i, \vartheta_y^i)$) [Stanton et al., 2018]. In the case of a multibeam echosounder or a titled singlebeam echosounder, when incidence angles on the seafloor are large (grazing angles), the effect of the directivity function across-track [9] can be compensated because each time of the recorded signal corresponds to an incidence angle. However, in the along-track direction [10] it is impossible to distinguish the position of a scatterer because the seafloor is a surface target. The impact of the directivity function then cannot be compensated in that direction. Consequently, in sonar equations that include the compensation of the directivity pattern $\mathcal{D}$, a bias is always present because of the non-compensation of the along-track effect (even if phase information are available - split-beam echosounders - because it only corresponds to the strongest scatterer in the surface insonified). The randomness of the backscattering strength due to the scatterer location inside the beam is therefore always present in this configuration of echosounders.

4.3 Representations of seafloor response information

For numerous applications, the seafloor response variability (ping to ping, or time-sample to time-sample) is inconvenient and it is preferred a single value summarizing the information (e.g. one value per incident angle). On the contrary, for some other applications such as seafloor classification, variability is a valuable and informative information. However, even in this case it needs to be described by a finite number of single values as inputs to classification algorithms. Consequently, in literature, the randomness of the backscattering strength is summarised as an ensemble of scalar values called features. In the following, some examples of this features are given with corresponding references publications.

4.3.1 Summarize information to reduce variability

The first way authors deal with the seafloor response variability is by reducing it which summarize the information in a single value. Several methods are employed in the literature to do so, but the most represented is the average [Fonseca et al., 2021], [Amiri-Simkooei et al., 2009], [Simons and Snellen, 2009]. For instance, in order to reduce ping to ping variability, [Eleftherakis et al., 2018] average all samples magnitude of the seabed echo that are located in the interval [-1°, +1°] around the center of the beam (time-sample corresponding to the sounding). It gives BS values per ping that are already means of raw BS data. Then, a second average is made with all pings values along the survey line. This method is repeated for each incident angle θ_i and frequency $\mathfrak{f}$ leading to a resulting seafloor angular response curve $\mathrm{BS}(\theta_\mathrm{i}, \mathfrak{f})$.

The decrease of BS variability is in most of the case measured by comparing standard deviations of the results. The standard deviation in decibels $\mathrm{std}_\mathrm{dB}[\,\bullet\,]$ is defined by [Nolle

9. i.e. in the direction perpendicular to the survey line.
10. i.e. in the direction of the survey line.

et al., 1963] as:

$$\mathrm{std}_{\mathrm{dB}}\left[\bullet\right] \equiv 10\log_{10}\left[1+\frac{\text{standard deviation of }\bullet}{\text{average value of }\bullet}\right] \tag{4.15}$$

[Malik et al., 2018] use that definition to show that if the standard deviation of individual samples backscattering strength is 5.6 dB [Simons and Snellen, 2009] (i.e. they follow a Log-Rayleigh distribution, see equation 5.17) and if they are averaged in decibels values, then more than 30 individual samples are required to reduce the standard deviation to 1 dB (which corresponds to a small/moderate uncertainty according to the authors classification discussed in section 4.1.2). Consequently, averaging the magnitudes of time-samples as described by [Eleftherakis et al., 2018] decreases significantly the backscattering strength standard deviation. In the above case of a Log-Rayleigh distribution this averaging is made with decibels values, nevertheless it is also discussed in [Malik et al., 2018] when made on squared amplitudes of the time-samples. This way, the authors show that the standard deviation reduces to 1 dB when using 20 samples. The reduction result is therefore directly related to the type of BS data averaged (squared amplitude, decibels, etc.) and to the number of data averaged.

Finally, a non-exhaustive list of methods found in the literature to reduce the BS variability is given below:

- the mean of time-samples amplitudes [Fonseca et al., 2021]
- the mean of their squared amplitudes [Fonseca et al., 2021, Simons and Snellen, 2009, Amiri-Simkooei et al., 2009]
- the mean of their amplitudes in decibels [Fonseca et al., 2021, Simons and Snellen, 2009]
- the median of their amplitudes [Fonseca et al., 2021]
- the maximum of their amplitudes [Burckhardt, 1978]

4.3.2 Features characterizing the variability

For seabed classification, and particularly when automatic classification is performed, the variability of the seafloor response needs to be described by comparable features. Theses features can be of two sorts: 1) calculated from BS data with or without using statistical models, 2) calculated after transformations of BS data. They are then employed as inputs of classification algorithms. When using statistical models, features can be deduced theoretically or after fitting specific models to the BS data distribution.

Table 4.3 regroups some examples of features that are found in literature to classify seabed response measurements.

It is important to note that depending on the authors and on the application data used to infer the features can be different. In this PhD context they are BS values taken from seabed echo time-samples, BS values from pings, or BS values calculated for each cells of a DTM. However, in some classification algorithms [van Walree et al., 2005][Snellen et al., 2011] input parameters are not necessarily backscattering strengths but can be directly infer from raw data. As an example, [Pouliquen and Lurton, 1992] or [Ferretti et al., 2015] use as features the areas (integral) under the first and second seabed echo received by a singlebeam echosounder (echo energy). According to the system employed, the type of raw data can

Sort of features	Features	References
Calulated from data	Mean	[Preston, 2009], [Amiri-Simkooei et al., 2009], [Eleftherakis et al., 2012], [Galloway, 2008]
	Standard deviation	[Preston, 2009], [Eleftherakis et al., 2012], [Galloway, 2008]
	Skewness	[Preston, 2009], [Eleftherakis et al., 2012]
	Kurtosis	[Preston, 2009], [Eleftherakis et al., 2012]
	Quantiles	[Preston, 2009], [Eleftherakis et al., 2012], [Galloway, 2008]
	Median	[Eleftherakis et al., 2012]
	Mode	[Eleftherakis et al., 2012]
	Minimum	[Eleftherakis et al., 2012]
	Maximum	[Eleftherakis et al., 2012]
Calculated after transformations of data	Texture	[Blondel et al., 2015][Prampolini et al., 2018]
	Power spectra	[Buscombe et al., 2014, Galloway, 2008]

Table 4.3 – Examples of features found in literature as inputs of classification algorithms

differ leading to echo areas of different units. The echosounder used in [Ferretti et al., 2015] is Kongsberg EA400. We saw in section 3.1.3 that raw data provided by this echosounder are acoustic powers, consequently the resulting features created with the echo area method are not equivalent to backscattering strength.

4.4 Summary

In this chapter we saw that the measurement of the seafloor acoustic response BS is a variable and that its variability can have different origins. At first it can be due to external phenomena such as modifications of the system characteristics (sensitivities, directivities...) or modifications of the environment during measurements (sound speed, absorption...). It is also related to the characteristics of the terrain itself: variations can appear at large scale in time and space (seafloor type changes annually/daily or along survey lines), or at small scale inside the beam footprint (sediment composition, biology...). In addition to those variabilities, an intrinsic randomness of BS is due to the roughness of the seafloor. This roughness leads to random locations of seabed scatterers and ensues a randomness between seafloor echo time-samples magnitudes. When dealing with seafloor response measurements, the observed ping to ping spreading (see figure 4.1) consequently includes all variabilities from all those sources.

In order to limit the impact of environment and system variations, measurements of the sea water parameters are usually made frequently during surveys and calibrations of the echosounders are performed when possible (in tank or *in situ*). A bias, nevertheless, will

always be present when using models for insonified area compensation because of the geometry of acquisition.

For seabed classification, the BS variability is a fundamental parameter. Features calculated from echosounders recorded signals are in this case employed as inputs of classification algorithms. In other cases, the BS variability is reduced so that final results have a small standard deviation. Methods such as averaging BS pings values are used. At the end, the seafloor response measurement is then considered as a single value resuming its variability. It is characteristic of the seafloor studied for a given incidence angle and frequency. It is important to note that when reducing the variability this way, a compromise is made between the number of time-samples and pings taken into account and the spatial resolution of the resulting measurement which is directly affected.

When reducing the information, a number of seabed echo time-samples or pings are used. Different reduction method can be employed such as the average. As an example, [Malik et al., 2018] advise that 20 time-samples are necessary to reduce BS standard deviation to 1 dB using the mean of square time-samples corrected magnitudes. A question then arise: what is the link between the number of data averaged and the standard deviation of the result? In other words, can we estimate the reduced BS variance from the number of data available?

Conclusion and problem statement

The question of the definition of the acoustic response of the seafloor has been discussed in this first part of the manuscript. It has been shown that in most of the literature on the subject, it is mainly named, described, modelled, and processed as a single value. Indeed, the preamble of this part argued about the terms employed in the state of the art to describe the seafloor acoustic response. It results that most of the word used correspond to a unique value. In chapter 2 models also derived the seafloor response as a deterministic value and chapter 3 shows that in practice it is also processed as a single value. But this value was observed and proved to be dependent of the incidence angle of the signal on the interface θ_{i} and on its frequency $\mathfrak{f}$. Consequently, by definition, the acoustic response of the seafloor is a single value, specific to a type of seafloor, an angle, and a frequency. The name chosen in this manuscript to describe it is the backscattering strength which involves mono-static measurements. It is shorten as BS which can also be written $\mathrm{BS}(\theta_{\mathrm{i}}, \mathfrak{f})$ resulting in angular curves named ARC.

Theoretical backscattering strength models were presented in chapter 2. They are numerous but they all model the seafloor as an interface between two fluid media: the sea water and the sediment. This interface can have different properties depending on the application and which details the user is interested in: it can be supposed flat or of zero mean in height, rough at large- or small-scale, penetrable, etc. Employed models can be totally heuristic with a limited number of parameters, or based on physical or geoacoustic developments where the number of parameters highly increases. The number of parameter is important to take into account especially for inversion problems where the accuracy of the estimation is directly linked to the complexity of the model.
Similarly, in practice, the acoustic response of the seabed is generally derived from echosounder measurements using a sonar equation which has also to be chosen among numerous type of equations. Chapter 3 presented three kinds of sonar equations and their parameters: 1) employed to evaluate echosounders performances and written as a signal to noise ratio, 2) used to estimate a specific parameter among the equation parameters, 3) derived to design echosounders and used in real time operation. The choice of one equation is also in this case made according to the application, the precision desired, and the parameters available. With the aim to process the backscattering strength, equations such as 3.10, 3.19 and 3.23 can be used.
Consequently, either with modelling or processing the seafloor acoustic response, the precision of the result is linked to the model or the sonar equation chosen by the user.

Both theoretical models and sonar equations derived the backscattering strength in a deterministic way. However, when observing BS measurements as shown in chapter 4 a large variability appears. It can be due to two main sources: external phenomena with no relation to the seafloor (changes in echosounder characteristics, environment modifications, etc.) and specific characteristics of the seafloor (temporal changes of the seabed, geographical variations, spatial variabilities in the echosounder beam footprint linked to the terrain type, intrinsic variability of the scattering mechanism). The first source impacts are limited by frequent measurements of the environment parameters (sound speed, absorption) during surveys and by performing echosounder calibrations as often as possible. In order to limit the impacts of the second source, time and spatial spread of the survey can be reduced. However, the intrinsic randomness of the scattering process will remain. It was shown in chapter 4 that the scattering process is directly related to the backscattering strength therefore a random scattering leads to a random backscattering strength. Consequently, from this point of view the seafloor acoustic response is actually a random variable which mean and variance are specific to a seafloor type (at a given incidence angle and frequency).

The seafloor response intrinsic randomness is equally a useful information that can be of interest and a constraint that users try to reduce. Chapter 4 presented features that are derived in literature from BS measurement variability in order to feed classification algorithms (skewness, kurtosis, etc.). It also discussed methods employed by authors to reduce this variability (such as averaging data). This last point is of interest in this PhD. In this case, the variability of the measurements decreases compared to its native variability. Also the resulting BS measurement is a unique value, associated to an angle and frequency, that can then be compared to theoretical models or used to identify seabed types. According to the method of reduction employed, the standard deviation of the result therefore decreases. In [Malik et al., 2018], examples of reduction of the variability using the average of the seabed echo time-samples are given. However, the link between the resulting standard deviation and the number of time-samples to use is not proposed. In addition, when BS from successive pings are averaged in literature, the number of pings used is chosen arbitrarily and never related to the variance of the result.
Consequently, in the next part of this manuscript different methods of backscattering strength variance reduction found in literature are discussed and the resulting BS variance associated is derived theoretically according to the number of pings and time-samples. Based on these results, the best estimator of the backscattering strength is defined among the reduction methods.

Following this theoretical part, a third part apply the best estimator of the seafloor acoustic response of *in situ* data. Nevertheless, the intrinsic randomness of the backscattering strength can only be studied when other sources of variability are negligible. Therefore a specific singlebeam echosounder was manufactured during the PhD in order to control every sonar equation parameters linked to the system. In particular, the directivity functions are measured in tank so that the insonified area could be simulated according to the receiving time. The use of a model of insonified area is therefore avoided. Backscattering strength measurements are also made specifically in tank with the echosounder fixed (at the university of Bath where sediment are disposed in the bottom of the tank) or on dock in the harbour of Brest to ensure that environment parameters variations are negligible on the survey duration.

Design of the echosounder and descriptions of the surveys are presented in the third part of this manuscript.

To conclude, the main issues this PhD discusses are:

- How to estimate accurately the seafloor acoustic response? What is the theoretical formula linking the backscattering strength variance and the number of pings or seabed echo time-samples used for estimation?
- How to apply in practice the BS estimator defined in the first question on echosounder data? How are time-samples from the seabed echo chosen to be used?

Part II

How to estimate the seabed acoustic response?

Preamble

The seabed acoustic response has been defined in the first part of this PhD as a single value called backscattering strength or index which synthesising the intrinsic variability of the seabed echo due to the random location of scatterers. Indeed, from one ping to another, the seabed content is the same but scatterers are located at different places inducing variations in the backscattered signal. These variations are therefore characteristic of a seafloor type and contribute to its signature. The main objective of this second part is to understand how this intrinsic variability can be modelled as a random variable and to derive estimates of the seafloor response from this random variable.

In order to model the scattering effect, the following hypotheses are taken:

- Other variabilities impacting the seafloor response are neglected. In practice, environment and system parameters have to be perfectly measured and controlled but in this theoretical part of the PhD they are supposed perfectly known and constant.
- The seafloor is modelled as an ensemble of scatterers described by an amplitude and a phase that backscatter the incident acoustic signal with their own strengths. Their number and locations are linked to the roughness of the interface water/sediment.
- The system modelled is an echosounder (single- or multi-beam) which beam insonifies an area $\mathcal{A}$ on the seafloor.

In the first chapter of this part, a statistical model of seafloor scattering is derived and discussed. Then estimators of the backscattering strength are calculated analytically based on the bathymetric processing usually employed with single- and multi-beam echosounders. This process reduces the seafloor echo of one ping into a single value called sounding, and then merges all soundings of all pings into one cell of the digital terrain model DTM (see figure 4.4). Because seafloor response data are generally provided by echosounder with bathymetric data, an equivalent method is employed. As shown in figure 4.5 each seafloor echo magnitude of a ping is then reduced to a single value, then these values are averaged together to obtain the resulting backscattering strength measurement. Four methods of reduction are discussed and derived analytically in chapter 5. They result in backscattering estimators formulae that are given according to the number of time-samples of the seafloor echo and the number of pings.

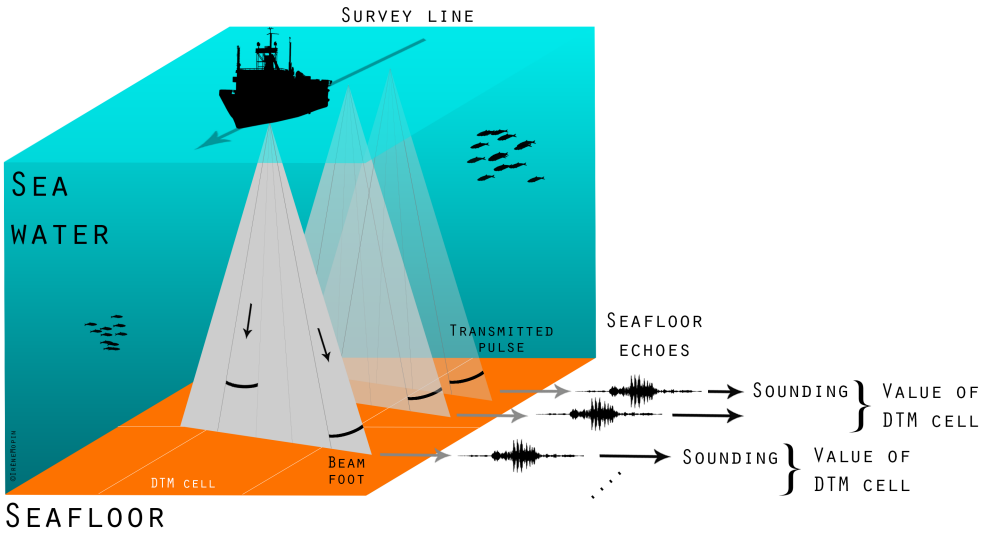

Figure 4.4 – Bathymetry methodology: sounding detection from each seabed echo and merge of soundings to get a value per DTM cell.

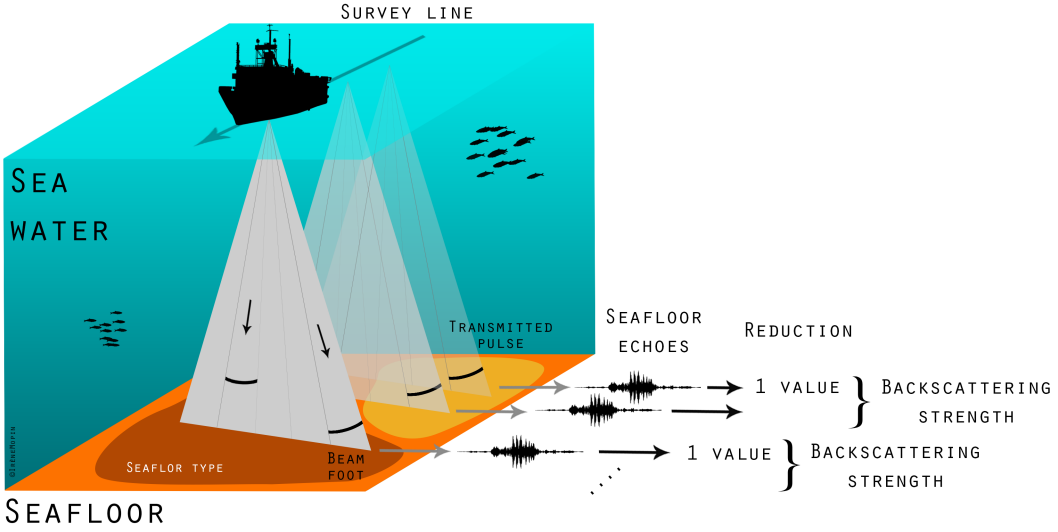

Figure 4.5 – Seafloor response methodology equivalent to the bathymetric one shown in figure 4.4: reduction of information from each seabed echo and merge to get a value of backscattering strength for a given number of ping.

As discussed in the previous part, the reduction of seafloor echoes information aims at decreasing the standard deviation of the measurement. In this part the variance is used to describe the variability. Chapter 6 compares the four backscattering strength estimators based on their expected values and variances. At the end, the uncertainty of the measurement for the best backscattering strength estimator is derived analytically according to the number of time-samples and pings. It is used to compare results of a survey in a practical point of view, where the level of variability is given in decibels. Applications of the theoretical formulation of

the uncertainty are proposed at the end on concrete singlebeam and multibeam echosounder data.

Chapter 5

Modelling and estimating the seafloor acoustic response

In order to derive an estimate of the seafloor acoustic response, a point-scattering formalism (e.g. [Alexandrou et al., 1992]) is employed in this chapter. The seafloor is supposed composed of several individual scatterers that send back to the receiver a specific amount of the incident signal with a specific phase. In the first section, the geometry of acquisition and the model are presented. Then characteristics of the scatterers are analysed based on literature. And finally, the link between the point-scattering model and rough interface statistics is discussed. In the second section, a mathematical representation of backscattering strength measurement data is presented. And estimators of the seafloor response are derived analytically from it. Four methods of reduction are derived based on literature and operational methods (echosounder manufacturers methods).

5.1 Models of the seabed response intrinsic variability

The seafloor acoustic response variability is mainly studied in the literature because of its capacity to discriminate different types of seafloor using in particular its probability density function PDF. Several point-scattering models have therefore been designed to describe backscattering strength measurements. In this PhD, one discrete scattering model is chosen that leads to a Rayleigh distribution of the backscattering strength as a random variable. The first part of this section derives this model. After that, other models leading to different PDF are presented with their background hypotheses and context of application. Finally, in the context of a Rayleigh distribution, the link between the Rayleigh PDF parameter and the seafloor roughness and response is discussed.

5.1.1 Discrete scattering model and Rayleigh distribution

The point-scattering model used is based on the assumption that the seafloor area $\mathcal{A}$ insonified by the echosounder is composed of individual scatterers that contribute to the final backscattered signal (see figure 5.1).

The analytic signal backscattered from the insonified area is written:

$$s(\vec{x}_0, t) = A_\mathrm{s}(\vec{x}_0) e^{j\omega_\mathrm{i} t} \tag{5.1}$$

where $\vec{x_0}$ is the location of the echosounder, t is the propagation time, ω_i is the pulsation of the incident signal, and $A_\mathrm{s}(\vec{x}_0)$ is the complex amplitude scattered from the instantaneous insonified area. This amplitude A_s can be written based on equations 4.13 and 4.14 as:

$$A_\mathrm{s}(\vec{x}_0) = A_\mathrm{i} C_\mathrm{eq.so} A(\vec{x}_0) \tag{5.2}$$

where $C_\mathrm{eq.so}$ is a constant including all the sonar equation parameters (systems and environment), A_i is the amplitude of the incident signal on the seafloor, and $A(\vec{x}_0)$ is the complex backscattering index amplitude. The latter can be written as:

$$A(\vec{x}_0) = |A(\vec{x}_0)| e^{j\varphi(\vec{x}_0)} \tag{5.3}$$

with $|A(\vec{x}_0)|$ the modulus of the complex amplitude and $\varphi(\vec{x}_0)$ its phase [Burckhardt, 1978].

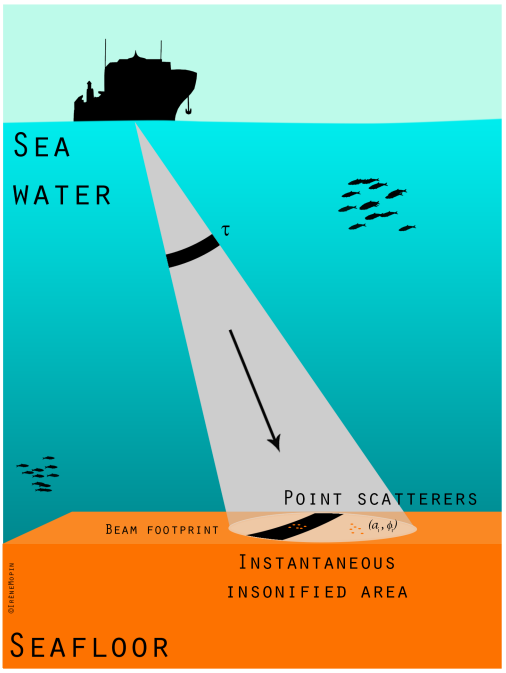

Figure 5.1 – Schematic representation of the scattering process inside the intantaneous insonified area

Considering the insonified area is composed of M scatterers, the amplitude $A(\vec{x}_0)$ received at the observation point $\vec{x}_0$ is composed of the time-shifted contributions of the different scatterers of the surface. It can therefore be defined as [Trevorrow, 2004]:

$$A(\vec{x}_0) = \sum_{i=1}^{M} \frac{1}{\sqrt{M}} a_i(\vec{x}_0) = \frac{1}{\sqrt{M}} \sum_{i=1}^{M} |a_i(\vec{x}_0)| e^{j\phi_i} \tag{5.4}$$

where $\frac{1}{\sqrt{M}} a_i(\vec{x}_0)$ is the complex contribution of the i$^{\text{th}}$ scatterer of modulus $|a_i(\vec{x}_0)|$ and phase ϕ_i . Figure 5.2 illustrates the summation of the complex scatterers contribution to the complex amplitude $A(\vec{x}_0)$. Geometrically, the accumulation can be described as a random walk [Goodman, 1975, Wagner et al., 1983].

The complex amplitude can also be defined by its real and imaginary parts that can be written as:

$$\begin{cases} A^{(r)} = \text{Re}\{A\} = \frac{1}{\sqrt{M}} \sum_{i=1}^{M} |a_i(\vec{x}_0)| \cos\phi_i \\ A^{(i)} = \text{Im}\{A\} = \frac{1}{\sqrt{M}} \sum_{i=1}^{M} |a_i(\vec{x}_0)| \sin\phi_i \end{cases} \tag{5.5}$$

Assuming that:

- the amplitude a_i and phase ϕ_i of the i$^{\text{th}}$ scatterer are statistically independent of each other and of the amplitudes and phases of all other scatterers (i.e. the scatterers are unrelated and the strength of a given scatttered component bears no relation to its phase),

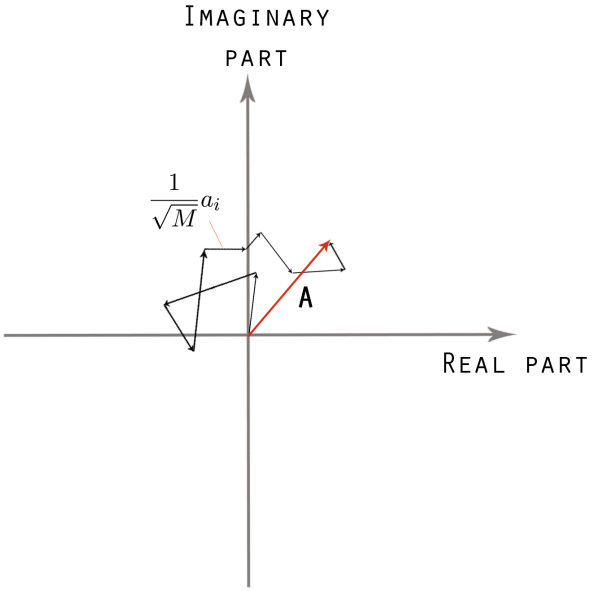

Figure 5.2 – Scheme of the random walk in the complex plane

- the phase ϕ_i are uniformly distributed on the interval $(-\pi, \pi)$ (i.e. the seabed surface is rough compared to the wavelength, with the result that phase excursions of many times 2π radians produce a uniform distribution on the interval),

lead to the fact that $|a_i|$ and ϕ_i can be averaged separately and that $\langle \cos\phi_i \rangle = 0$ and $\langle \sin\phi_i \rangle = 0$, where $\langle . \rangle$ stands for the expected value. Because the phases ϕ_i are independent and uniformly distributed, we can write:

$$\left| \begin{array}{l} \langle \cos\phi_i \cos\phi_k \rangle = \langle \sin\phi_i \sin\phi_k \rangle = \left\{ \begin{array}{l} \frac{1}{2} \text{ for } i = k \\ 0 \text{ for } i \neq k \end{array} \right. \\ \langle \cos\phi_i \sin\phi_k \rangle = 0 \end{array} \right. \tag{5.6}$$

Therefore, the expected values of the random variables $\mathbf{A}^{(r)}$ and $\mathbf{A}^{(i)}$ estimated as the means over the insonified ensemble of scatterers are:

$$\left| \begin{array}{l} \langle \mathbf{A}^{(r)} \rangle = \frac{1}{\sqrt{M}} \sum_{i=1}^{M} \langle |a_i| \cos\phi_i \rangle = \sum_{i=1}^{M} \langle |a_i| \rangle \langle \cos\phi_i \rangle = 0 \\ \langle \mathbf{A}^{(i)} \rangle = \frac{1}{\sqrt{M}} \sum_{i=1}^{M} \langle |a_i| \sin\phi_i \rangle = \sum_{i=1}^{M} \langle |a_i| \rangle \langle \sin\phi_i \rangle = 0 \\ \langle [\mathbf{A}^{(r)}]^2 \rangle = \frac{1}{M} \sum_{i=1}^{M} \sum_{k=1}^{M} \langle |a_i||a_k| \rangle \langle \cos\phi_i \cos\phi_k \rangle = \frac{1}{M} \sum_{i=1}^{M} \frac{\langle |a_i|^2 \rangle}{2} \\ \langle [\mathbf{A}^{(i)}]^2 \rangle = \frac{1}{M} \sum_{i=1}^{M} \sum_{k=1}^{M} \langle |a_i||a_k| \rangle \langle \sin\phi_i \sin\phi_k \rangle = \frac{1}{M} \sum_{i=1}^{M} \frac{\langle |a_i|^2 \rangle}{2} \\ \langle \mathbf{A}^{(r)} \mathbf{A}^{(i)} \rangle = \frac{1}{M} \sum_{i=1}^{M} \sum_{k=1}^{M} \langle |a_i||a_k| \rangle \langle \cos\phi_i \sin\phi_k \rangle = 0 \end{array} \right. \tag{5.7}$$

Consequently, the real and imaginary parts of the complex received amplitude $A(\vec{x}_0)$ have zero means, identical variances and are uncorrelated.

Supposing that the insonified area is sufficiently large that the number of scatterers M is very large, the real and imaginary parts of $A(\vec{x}_0)$ therefore correspond to the sum of a large

number of independent and identically distributed random variables. In these conditions, the central limit theorem allows to concluded that for $M \to \infty$, $\mathbf{A}^{(r)}$ and $\mathbf{A}^{(i)}$ are asymptotically Gaussian. Their probability density functions respectively $f_{\mathbf{A}^{(r)}}(A^{(r)})$ and $f_{\mathbf{A}^{(i)}}(A^{(i)})$ can then be approximated by a Gaussian distribution as:

$$\left| \begin{array}{l} f_{\mathbf{A}^{(r)}}(A^{(r)}) = \frac{1}{\sigma\sqrt{2\pi}} e^{-\frac{1}{2}\left(\frac{A^{(r)}}{\sigma}\right)^2} \\ f_{\mathbf{A}^{(i)}}(A^{(i)}) = \frac{1}{\sigma\sqrt{2\pi}} e^{-\frac{1}{2}\left(\frac{A^{(i)}}{\sigma}\right)^2} \end{array} \right. \tag{5.8}$$

where $A^{(r)}$ and $A^{(i)}$ are respectively realisations of the random variables $\mathbf{A}^{(r)}$ and $\mathbf{A}^{(i)}$. From equations 5.7, $\mathbf{A}^{(r)}$ and $\mathbf{A}^{(i)}$ have identical zero means and identical variances σ^2, i.e.:

$$\sigma^2 = \langle [\mathbf{A}^{(r)}]^2 \rangle - \langle [\mathbf{A}^{(r)}] \rangle^2 = \langle [\mathbf{A}^{(i)}]^2 \rangle - \langle [\mathbf{A}^{(i)}] \rangle^2 = \lim_{M \to \infty} \frac{1}{M} \sum_{i=1}^{M} \frac{\langle |a_i|^2 \rangle}{2} \tag{5.9}$$

Their joint probability $f_{\mathbf{A}^{(r)},\mathbf{A}^{(i)}}(A^{(r)}, A^{(i)})$ is consequently given by [Wagner et al., 1983, Goodman, 1975, Narayanan et al., 1994]:

$$f_{\mathbf{A}^{(r)},\mathbf{A}^{(i)}}(A^{(r)}, A^{(i)}) = \frac{1}{2\pi\sigma^2} e^{-\frac{[A^{(r)}]^2 + [A^{(r)}]^2}{2\sigma^2}} \tag{5.10}$$

In practice, the measured signal received by an echosounder is the real part of the complex signal $s(\vec{x}_0, t)$. From equation 5.3, the real and imaginary parts of $s(\vec{x}_0, t)$ correspond to those of $A(\vec{x}_0)$ and are defined as:

$$\left| \begin{array}{l} A^{(r)} = |A(\vec{x}_0)| \cos\varphi(\vec{x}_0) \\ A^{(i)} = |A(\vec{x}_0)| \sin\varphi(\vec{x}_0) \end{array} \right. \tag{5.11}$$

In following, $|A(\vec{x}_0)|$ and $\varphi(\vec{x}_0)$ are still dependent on the location of the echosounder $\vec{x}_0$ but for clarity of reading the $\vec{x}_0$ component is omitted.

Using the change of variable of equation 5.11, the Jacobian transformation allows to derive the joint PDF of $|\mathbf{A}|$ and $\boldsymbol{\varphi}$ from the joint probability of $\mathbf{A}^{(r)}$ and $\mathbf{A}^{(i)}$ by:

$$f_{|\mathbf{A}|,\boldsymbol{\varphi}}(|A|, \varphi) = \left| \begin{array}{cc} \frac{\partial A^{(r)}}{\partial |A|} & \frac{\partial A^{(r)}}{\partial \varphi} \\ \frac{\partial A^{(i)}}{\partial |A|} & \frac{\partial A^{(i)}}{\partial \varphi} \end{array} \right| f_{\mathbf{A}^{(r)},\mathbf{A}^{(i)}}(A^{(r)}, A^{(i)}) \tag{5.12}$$

which leads to:

$$\begin{aligned} f_{|\mathbf{A}|,\boldsymbol{\varphi}}(|A|, \varphi) &= |A| f_{\mathbf{A}^{(r)},\mathbf{A}^{(i)}}(A^{(r)}, A^{(i)}) \\ &= \frac{|A|}{2\pi\sigma^2} e^{-\frac{|A|^2}{2\sigma^2}} \end{aligned} \tag{5.13}$$

The marginal PDF of the modulus of the received signal and its phase can finally be derived as :

$$\left| \begin{array}{l} f_{|\mathbf{A}|}(|A|) = \int_{-\pi}^{\pi} f_{|\mathbf{A}|,\boldsymbol{\varphi}}(|A|, \varphi) d\varphi = \left\{ \begin{array}{l} \frac{|A|}{\sigma^2} e^{-\frac{|A|^2}{2\sigma^2}} \text{ for } |A| \in [0, +\infty[\\ 0 \text{ otherwise} \end{array} \right. \\ f_{\boldsymbol{\varphi}}(\varphi) = \int_0^{\infty} f_{|\mathbf{A}|,\boldsymbol{\varphi}}(|A|, \varphi) d|A| = \left\{ \begin{array}{l} \frac{1}{2\pi} \text{ for } \varphi \in [-\pi, \pi[\\ 0 \text{ otherwise} \end{array} \right. \end{array} \right. \tag{5.14}$$

The measured real amplitude of the signal is consequently following a Rayleigh law of parameter σ^2 on $[0, +\infty[$ [Rivet et al., 2007] and the phase of the corresponding complex signal is, as supposed above, uniformly distributed on $[-\pi, \pi[$.

To conclude, the amplitude of the backscattered signal from the seabed is a random variable following a Rayleigh law under the hypotheses of an insonified area large enough to ensure a sufficient number of scatterers and that these scatterers are independent and their phases uniformly distributed. Characteristics of the Rayleigh distribution give:

- the mean of the random variable $|\mathbf{A}|$: $\mu(|\mathbf{A}|) = \sigma\sqrt{\frac{\pi}{2}}$
- its median: $q(|\mathbf{A}|) = \sigma\sqrt{2\ln 2}$
- its mode: $\varsigma(|\mathbf{A}|) = \sigma$
- its variance: $\mathrm{var}(|\mathbf{A}|) = \frac{4-\pi}{2}\sigma^2$

In order to derive the probability density function of the amplitude in decibels A_{dB} we use the change of variable:

$$A_{\mathrm{dB}} = 20\log_{10}(|A|) = \frac{20}{\log(10)}\log\left(|A|\right) \tag{5.15}$$

where $|A| = e^{A_{\mathrm{dB}}\log(10)/20}$ which leads to the distribution of $\mathbf{A}_{\mathrm{dB}}$ as:

$$\begin{aligned} f_{\mathbf{A}_{\mathrm{dB}}}(A_{\mathrm{dB}}) &= \left|\frac{\partial|A|}{\partial A_{\mathrm{dB}}}\right| f_{|\mathbf{A}|}(|A|) \\ &= \left|\frac{\log(10)}{20}\right| \frac{|A|}{\sigma^2} e^{-\frac{|A|^2}{2\sigma^2}} \\ f_{\mathbf{A}_{\mathrm{dB}}}(A_{\mathrm{dB}}) &= \frac{\log(10)}{20\sigma^2}\exp\left[\frac{\log(10)}{10}A_{\mathrm{dB}} - \frac{1}{2\sigma^2}e^{\frac{\log(10)}{10}A_{\mathrm{dB}}}\right] \end{aligned} \tag{5.16}$$

The PDF $f_{\mathbf{A}_{\mathrm{dB}}}(A_{\mathrm{dB}})$ is usually called the log-Rayleigh distribution and, unlike the Rayleigh distribution, its variance is constant and equal to [Shepherd and Milnarich, 1973, Duncan et al., 2013]:

$$\mathrm{var}(\mathbf{A}_{\mathrm{dB}}) = 1.6 \cdot \left(\frac{10}{\log(10)}\right)^2 = 31\mathrm{dB} \tag{5.17}$$

Which gives a standard deviation of 5.6dB.

5.1.2 Other distributions

In the literature, some cases have been studied where the conditions leading to a Rayleigh distribution are not satisfied which results in non-Rayleigh statistics. In practice, some authors also use other distributions than Rayleigh in order to better fit measurements of different types of seafloor. In the following some examples of Rayleigh statistics departure and their reasons are discussed.

Equation 5.4 describes the relation between the complex amplitude of the received signal and the amplitude $|a_i|$ and phase ϕ_i of the i$^{\mathrm{th}}$ scatterers as the sum $A \sim \sum_{i=1}^{M} |a_i| e^{j\phi_i}$ with M the number of scatterers. Fluctuations of A from one realization to another is therefore strongly dependent on the statistical properties of $|a_i|$ and ϕ_i.

In the case where $|a_i|$ is constant, i.e. $|a_i| = a$ and ϕ_i is randomly and uniformly distributed in $[0, 2\pi[$, the sum becomes $A \sim a \sum_{i=1}^{M} e^{j\phi_i}$ and fluctuates greatly from realization to realization due to the variability in constructive and destructive interference effects associated with phase variability alone [Stanton et al., 2018]. For examples, there may be complete constructive interference such as A is maximum in one realization, but complete destructive interference in another realization where A is minimum. The statistics of the fluctuation is then depending mostly on the number of scatterers M. If $M = \infty$, equation 5.8 is valid and the PDF of $|A|$ is the Rayleigh distribution. For smaller M equation 5.8 is not valid, however an expression of the pdf of $|A|^2$ is given in [Pusey et al., 1974] where it is derived from [Kluyver, 1905]'s work on the two-dimensional random walk [Jakeman and Pusey, 1976, Pearson, 1906]:

$$f_{M<\infty}(|A|^2) = \frac{1}{2}\int_0^\infty u J_0\left(u\sqrt{|A|^2}\right)[J_0(u\beta)]^M du \tag{5.18}$$

where $J_0(.)$ is the zero-order Bessel function of the first kind and $\beta^2 = \frac{1}{M}\langle|A|^2\rangle$ the mean intensity backscattered by one scatterer.
If $M = 1$ the signal is composed of one single value, the PDF of the signal amplitude $|A|$ is the delta function and $\beta^2 = |A|^2$. If $M = 2$ [Pusey et al., 1974, Pearson, 1906]:

$$f_{M=2}(|A|^2) = \frac{1}{\pi\sqrt{|A|^2(2\langle|A|^2\rangle - |A|^2)}} \tag{5.19}$$

with $\langle|A|^2\rangle = 2\beta^2$. [Pearson, 1906] derived also an expression for $M = 3$ (elliptic integrals) and graphical solutions for $3 < M < 7$. Figure 5.3 shows PDFs of $|A|$ for $M = [2, 3, 4, 100]$ (same figures are shown in [Pusey et al., 1974] but for $|A|^2$). The resulting PDF for $M = 100$ is considered by the authors a Rayleigh distribution.

In the case where $|a_i|$ is a random variable i.e. heterogeneity of the seafloor induces random fluctuations of the scatterers amplitudes, the number of scatterers can be replaced by an effective number of scatterers M_{eff} [Narayanan et al., 1994]. The more $|a_i|$ are random (i.e. variance of $|a_i|$ increases), the smaller is M_{eff}. The effective number can therefore reach a value where the central limit theorem is not applicable and the resultant PDF is consequently not the Rayleigh distribution. [Jakeman and Pusey, 1976] and [Narayanan et al., 1994] show that the PDF of $|\mathbf{A}|$ in this case is the K-distribution of the form:

$$f_{K_{\text{eff}}}(|A|) = \frac{2b}{\Gamma(M_{\text{eff}})}\left(\frac{b|A|}{2}\right)^{M_{\text{eff}}} J_{M_{\text{eff}}-1}(b|A|) \tag{5.20}$$

where $\Gamma(.)$ is the gamma function, $J_{M_{\text{eff}}-1}$ is the modified Bessel function of order $M_{\text{eff}} - 1$, and b is a scaling factor related to the scale parameter of the K-distribution λ_K (see equation 5.24) by $b = 2/\sqrt{\lambda_K}$. The effective number of scatterers can be expressed from the actual number of scatterers M by [Narayanan et al., 1994]:

$$M_{\text{eff}} = M(\gamma + 1) \text{ with } -1 < \gamma < 0 \tag{5.21}$$

where the parameter γ describes the variation of uniformity of the scatterers amplitudes $|a_i|$ in the instantaneous insonified area. When $\gamma \to -1$, the amplitudes $|a_i|$ are highly fluctuating and the PDF of $|\mathbf{A}|$ tends towards the log-normal distribution. On the contrary, when $\gamma \to 0$ and M is larger than 10, the amplitudes $|A|$ are Rayleigh distributed [Narayanan et al., 1994].

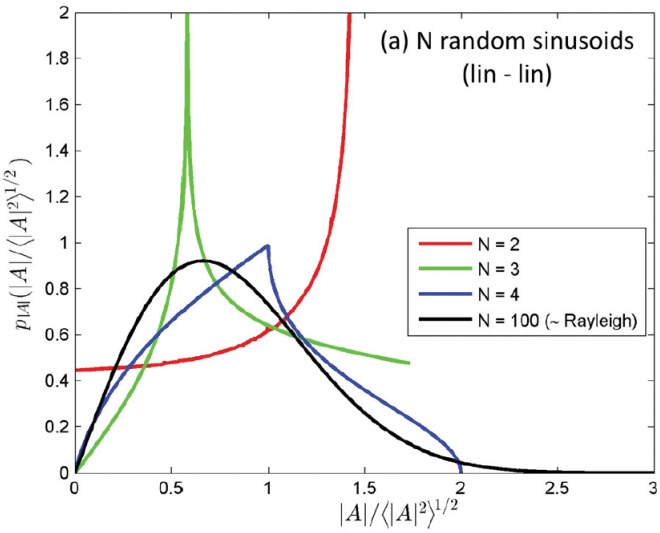

Figure 5.3 – PDFs of magnitudes of sums of M random phase sinusoids of identical amplitude, from [Stanton et al., 2018]. The scatterers addition given in equation 5.4 is evaluated using Monte Carlo simulations (107 realizations) in which $|a_i| = a$ are constant and ϕ_i are randomly and uniformly distributed over $[0, 2\pi[$. The curves are shown to vary significantly for small M and approach the Rayleigh PDF for high M. The curves for $M = 2$ and 3 in this figure are also presented in [Jao and Elbaum, 1978] using an analytical approach involving characteristic functions.

Sometimes the instantaneous insonified area can contain a scatterer of permanent amplitude together with a lot of other scatterers with random amplitudes, e.g. a rock on a sandy terrain [Trevorrow, 2004], a sphere near a rough interface, or a structure of periodic scatterers [Tuthill et al., 1988]. The model of equation 5.4 is therefore modified by extracting one scatterer with a constant amplitude $|a|$ and phase ϕ from the rest of the scattered sum [Stanton et al., 2018] as:

$$A \sim |a|e^{j\phi} + \sum_{i=1}^{M} |a_i|e^{j\phi_i} \tag{5.22}$$

The PDF of the permanent amplitudes $|\mathbf{a}|$ is the delta function, and M is supposed sufficiently large so that the PDF of the sum is Rayleigh distributed. In those conditions, the amplitude random variable $|\mathbf{A}|$ is following a Rice distribution [Stanton et al., 2018] i.e.:

$$f_{\text{Rice}}(|A|) = 2|A|\frac{1+\gamma}{\langle|A|^2\rangle}\exp\left[\frac{(1+\gamma)|A|^2 + \gamma\langle|A|^2\rangle}{\langle|A|^2\rangle}\right] I_0\left(2|A|\sqrt{\frac{\gamma(1+\gamma)}{\langle|A|^2\rangle}}\right) \tag{5.23}$$

where the term γ is the ratio of the mean squared permanent amplitude over the other scatterers amplitudes (i.e. the signal to noise ratio of the most reflecting scatterer above the others), and $I_0(.)$ is the zero-order modified Bessel function of the first kind.
The shape of the Rice PDF depends strongly on γ (see figure 5.4). If $\gamma \to \infty$ the PDF will tends to a Gaussian distribution. It corresponds to the case where the strong scatterer is predominant. Inversely, if $\gamma \to 0$ the PDF tends to the Rayleigh distribution of all the other scatterers. Those two cases are considered in [Middleton et al., 1960] and [Wagner

et al., 1983] as, respectively, the strong distributed specular with weak diffuse component leading to a Gaussian distribution and, on the contrary, the pure diffuse scattering leading to a Rayleigh distribution (also called fully developed speckle). The Rayleigh PDF is therefore a special case of the Rice distribution.

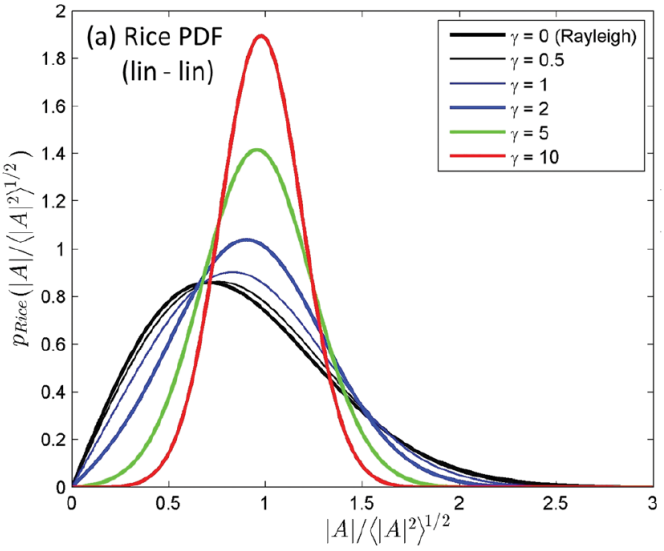

Figure 5.4 – Rice PDF for various values of its shape parameter γ, from [Stanton et al., 2018].

In literature, the considered random variable is not always the amplitude or phase of the scatterers but can also be the number of scatterers M. If the phases are randomly and uniformly distributed in $[0, 2\pi[$ and M follows a negative binomial PDF where its average value tends to infinity, then $|A|$ from equation 5.4 is following a K-distribution [Stanton et al., 2018]:

$$f_K(|A|) = \frac{4}{\sqrt{\lambda_K}\Gamma(\alpha_K)} \left(\frac{|A|}{\sqrt{\lambda_K}}\right)^{\alpha_K} K_{\alpha_K - 1}\left(\frac{2|A|}{\sqrt{\lambda_K}}\right) \tag{5.24}$$

where $K(.)$ is the modified Bessel function of the second kind, Γ is the gamma function, and α_K and λ_K respectively the shape and scale parameter of the K-distribution. When $\alpha_K \to \infty$, the distribution tends to Rayleigh (see figure 5.5).

The amplitude random variable $|\mathbf{A}|$ follows a K-distribution in some other cases with different hypotheses such as:

- $|A|$ is composed of a finite number M of scatterers with their amplitudes $|a_i|$ following an exponential distribution [Abraham and Lyons, 2002].
- $|A|$ is the product of two independent random variables that are Rayleigh distributed and χ-distributed. [Ward, 1981] attributes the Rayleigh term as being due to quickly varying interference between scatterers and the χ term being due to slowly varying changes in the echo from larger-scale in the bunching or patchiness of scatterers.
- $|A|$ follows a Rayleigh distribution whose mean-square value is Gamma distributed [Jakeman and Tough, 1987]

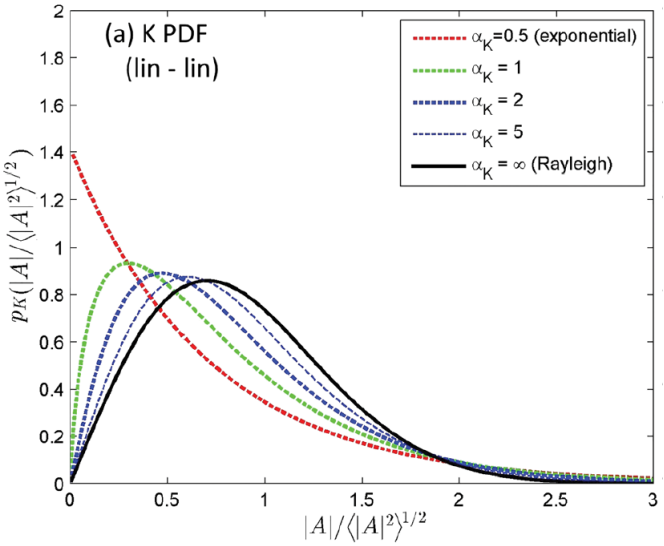

Figure 5.5 – K PDF for various values of shape parameter α_K, from [Stanton et al., 2018].

In the case where M follows a negative binomial distribution where its average value tends to infinity but the distribution of the phases ϕ_i is non-uniform, $|A|$ from equation 5.4 follows a generalized K-distribution [Jakeman and Tough, 1987]. The latter is described by three parameters: α_K and λ_K respectively the shape and scale parameter and the third parameter that describes the non-uniform phase distribution. The generalized K-distribution can also be represented by a Rice distribution with the two components of the signal to noise ratio being Gamma distributed in a correlated way. It can therefore be applicable to the case in which one or several scatterers dominate the scattering from a field of many scatterers [Ferrara et al., 2011].

To sum up, if scatterers are randomly distributed over the instantaneous insonified area and if they all have comparable scattering strength, the PDF of the amplitudes $|A|$ of the received backscattered signal is a Rayleigh distribution [Stanic and Kennedy, 1992]. In other cases, the PDF deviates to other distributions as shown in table 5.1. The second column of the table shows the hypotheses on the parameters of the point-scattering model (see equation 5.4) that lead to the associated distributions.

When modelling the randomness of the seafloor response i.e. of the received signal corrected from sonar equation parameters, a choice is generally made to use fluctuations of the number of scatterers M or their amplitudes $|a_i|$ or phases ϕ_i. Physically, fluctuations of these three parameters can originate from different effects. Some of them are cited in the literature and listed below:

- The phase ϕ_i of the scatterers can be randomized by either scintillation effects, whereby the incident wave number varies due to refractive index variability, and/or micro-multipaths, whereby the scatterer range varies due to small fluctuations in water stratification. Theses effects are especially observed with a fixed echosounder in [Trevorrow, 2004] and [Stanic and Kennedy, 1992].

Distributions of $\|\mathbf{A}\|$	Hypotheses	References
Rayleigh	Large number of scatterers, i.e. $M = \infty$ ($M > 10$)	[Goodman, 1975][Wagner et al., 1983][Narayanan et al., 1994]
Delta function	One scatterer only, i.e. $M = 1$	[Pusey et al., 1974][Stanton et al., 2018]
Rice	Scatterer(s) of constant amplitude together with diffuse scattering, i.e. delta function + Rayleigh scattering	[Stanton et al., 2018][Wagner et al., 1983]
Gaussian	Strong predominant scatterers of constant amplitude (coherent scattering) over diffuse (incoherent) scattering	[Stanic and Kennedy, 1992][Stanton et al., 2018]
K	• M is a random variable whose pdf is a negative binomial distribution and its average $\to \infty$ • M is a finite number of scatterers with their amplitudes $\|a_i\|$ following an exponential law • Scatterers amplitudes $\|a_i\|$ are so random that the effective number of scatterers M_{eff} is too low for the central limit theorem to be applicable	[Stanton et al., 2018] [Abraham and Lyons, 2002] [Narayanan et al., 1994][Jakeman and Pusey, 1976]
Log-normal	• Scatterers amplitudes $\|a_i\|$ are random and $M_{\text{eff}} \to 0$ • Variance of ϕ_i decreases • Diversity of the scatterers amplitudes a_i increases i.e. M_{eff} decreases	[Narayanan et al., 1994] [Trevorrow, 2004] [Trevorrow, 2004]
Generalized K	M follows a negative binomial pdf where its average value tends to infinity, and the distribution of the phases ϕ_i is non-uniform	[Jakeman and Tough, 1987]

Table 5.1 – Received signal magnitude $|A|$ distributions, hypotheses that can lead to them and reference publications.

- An increasing number of scatterers M is observed when the insonified area increases with range [Trevorrow, 2004] or when the beamwidth increases [Stanic and Kennedy, 1992], leading to an increase of the Rayleighness of the received amplitude distribution .
- When the level of phase ϕ_i variation decreases, it was shown by [Trevorrow, 2004] that the distribution of $|\mathbf{A}|$ transforms from Rayleigh distribution to Log-normal distribu-

tion. This effect could explain the transition to more Rayleigh-like behaviour with increasing range where the phase variations increase because of greater path lengths through the water (along-path turbulences).

- Changing from Rayleigh to Log-normal is also observed when the diversity of the scatterers amplitudes $|a_i|$ increases (non-homogeneity of the seabed) which is also accompanied by the diminution of the effective number of scattererss M_{eff} [Trevorrow, 2004].
- Incoherent scattering leading to a Log-normal distribution are generally observed for high ground clutter seabed [Stanic and Kennedy, 1992]. Scatterers have in that case no comparable scattering strength.
- Deviation from the Rayleigh scattering appears strongly when some scatterers in the insonified area are oriented so as to have facets that have just the right arrangement to cause strong Bragg scattering reinforcement in the backscattering direction [Stanic and Kennedy, 1992]. Small insonified area with large directional facets will tend to have a Gaussian distribution (specular effect).

In practice, some authors use the Weibull distribution because of its versatility, even if it is hard to link it to physical seabed properties, [Marandino, 1987, Fonseca et al., 2021, Billon et al., 1981]. Indeed, according to its parameters it can be related to Rayleigh, Exponential or Log-normal distributions. The χ^2-distribution is also used for the same reasons [Gensane, 1989].

5.1.3 Relation between seafloor response, point-scattering model and rough interface characteristics

To begin, we choose in this PhD to follow the hypotheses of section 5.1.1. Thus, the backscattering index amplitude $|\mathbf{A}|$ is a random variable that follows a Rayleigh distribution of parameter σ^2 and its phase $\boldsymbol{\varphi}$ is also a random variable uniformly distributed (see equations 5.14). Equations 5.8 to 5.14 demonstrate that in the case of a large number of scatterers in the instantaneous insonified area, the Rayleigh parameter σ^2 is originally the variance of the Gaussian distribution modelling the real and imaginary parts of the complex backscattering index amplitude, respectively $\mathbf{A}^{(r)}$ and $\mathbf{A}^{(i)}$ [Narayanan et al., 1994]. These hypotheses can be written as :

$$\left.\begin{array}{ll} \text{var}\left[\mathbf{A}^{(r)}\right] & = \sigma^2 \\ \text{var}\left[\mathbf{A}^{(i)}\right] & = \sigma^2 \end{array}\right\} \Leftrightarrow |\mathbf{A}| \sim \mathcal{R}\text{ayl}(\sigma^2) \tag{5.25}$$

In the first part of the manuscript, the seafloor acoustic response was defined as a deterministic parameter BS in decibels. Its non-decibels equivalent bs then corresponds to the ratio of the acoustic intensity scattered by the rough interface I_{s} on the incident signal intensity I_{i} (see equations 2.7 and 2.8) for a unit area of 1m^2. Thus it goes in that deterministic context that:

$$\text{BS} = 10\log_{10}(\text{bs}) = 10\log_{10}\left(\frac{\underline{I_{\text{s}}}}{\underline{I_{\text{i}}}}\right) = 10\log_{10}\left(\frac{|A_{\text{s}}|^2}{|A_{\text{i}}|^2}\right) = 10\log_{10}\left(|A|^2\right) \tag{5.26}$$

where A_{s} is the complex amplitude of the scattered signal from the insonified area, A_{i} the incident signal amplitude, and A is the corrected complex backscattering index amplitude. In the equation, intensities are underlined. This is because we demonstrate in the first part

of the PhD that the sonar equation is written with RMS values (see in particular in equations 3.8, 4.13 and 4.14). Therefore, in equation 5.26 $\underline{I_{\mathrm{s}}}$ and $\underline{I_{\mathrm{i}}}$ are RMS values of the intensities.

In the stochastic context introduced in this chapter the backscattered amplitude $|A_{\mathrm{s}}|$ is a random variable, then the backscattering index amplitude $|\mathbf{A}|$ is also a random variable from equation 5.26. Consequently the backscattering strength **bs** is also a random variable and can be derived as:

$$10\log_{10}(\mathbf{bs}) = 10\log_{10}\left(\frac{|\mathbf{A}_{\mathrm{s}}|^2}{|A_{\mathrm{i}}|^2}\right) = 10\log_{10}\left(|\mathbf{A}|^2\right) \tag{5.27}$$

The random variable **bs** is therefore the square of $|\mathbf{A}|$ which was demonstrated in section 5.1.1 to follow the Rayleigh distribution of equation 5.14 of parameter σ^2, i.e.:

$$f_{\underline{|\mathbf{A}|}}(\underline{|A|}) = \begin{cases} \frac{\underline{|A|}}{\sigma^2} e^{-\frac{\underline{|A|}^2}{2\sigma^2}} \text{ for } \underline{|A|} \in [0, +\infty[\\ 0 \text{ otherwise} \end{cases} \tag{5.28}$$

Consequently, we can write the backscattering strength as:

$$\mathbf{bs} = \underline{|\mathbf{A}|}^2 \tag{5.29}$$

And its distribution is then the exponential distribution of parameter two times the parameter of the Rayleigh distribution of equation 5.28 i.e. $2\sigma^2$, i.e.:

$$f_{\mathbf{bs}}(\mathrm{bs}) = \frac{1}{2\sigma^2} e^{-\frac{\mathrm{bs}}{2\sigma^2}} \tag{5.30}$$

In the deterministic context, the seafloor response BS is directly linked to bs by equation 5.26. However, in the stochastic context, we saw in section 4.3.1 that in literature the variable component of the backscattering strength bs is reduced to obtain the seabed response. Consequently the seabed response is a single value derived from a stochastic variable. In order to respect this hypothesis, BS is defined as the expected value of the random variable **bs**, i.e.:

$$\mathrm{BS} = 10\log_{10}(\mathrm{E}[\mathbf{bs}]) \tag{5.31}$$

The expected value of the exponential distribution is equal to its parameter, therefore the expected value of **bs** is the parameter of the distribution of equation 5.30, i.e.:

$$\mathrm{E}[\mathbf{bs}] = 2\sigma^2 \tag{5.32}$$

Therefore:

$$\mathrm{BS} = 10\log_{10}\left(2\sigma^2\right) = 10\log_{10}\left(\sigma^2\right) + 3 \tag{5.33}$$

The seabed acoustic response, or backscattering strength, is consequently directly linked to the Rayleigh distribution parameter σ^2. This parameter is also the variance of the real and imaginary parts of the complex backscattering index amplitude which is linked to the number of scatterers M in the instantaneous insonified area and their magnitudes $|a_i|$ distributions. The seabed acoustics response corresponds therefore to the stochastic scattering ability of the scatterers composing the interface to reflect the incident intensity.

On the other side, the seabed acoustic response is defined as the response of a rough interface to an incoming signal. The interface is modelled as a random process $\mathbf{Z}$ where the roughness is described by deviations in height ζ as function of space $\vec{x}$ compared to a reference planar surface (its mean in figure 2.5). It gives [Becker, 2004, Ogilvy, 1988]:

$$z = \zeta(\vec{x}) \tag{5.34}$$

The rough surface is supposed to have a null expected value $\langle \mathbf{Z} \rangle = 0$ and is represented as a set of points z_i corresponding to height ζ at the spatial point $\vec{x}_i$, i.e.:

$$z_i = \zeta(\vec{x}_i) \tag{5.35}$$

All $\mathbf{Z} = [z_1, \cdots, z_i]$ are correlated random variables which are generally modelled by a normal distribution $f_{\mathbf{Z}}(z_i)$ of variance σ_ζ^2 and zero mean [Becker, 2004, Ogilvy, 1988] i.e.:

$$f_{\mathbf{Z}}(z_i) = \frac{1}{\sigma_\zeta \sqrt{2\pi}} \exp\left[-\frac{z_i^2}{2\sigma_\zeta^2}\right] \tag{5.36}$$

In these conditions, the variability of the seafloor can be described by:

- its mean square value, or variance of its irregularities, given by:

$$\sigma_\zeta^2 = \langle z_i^2 \rangle \tag{5.37}$$

- its height correlation function $\rho_\zeta(x)$

$$\rho_\zeta(\vec{x}) = \frac{\langle \zeta(\vec{x}_0)\zeta(\vec{x}_0 + \vec{x}) \rangle}{\langle \zeta^2 \rangle} \tag{5.38}$$

- its gradient correlation function $\rho_g(x)$ which is related to the height correlation function $\rho_\zeta(x)$ by [Ogilvy, 1988]:

$$\rho_g(x) = -\sigma_\zeta^2 \frac{\mathrm{d}\rho_\zeta(\vec{x})}{\mathrm{d}\vec{x}} \tag{5.39}$$

In order to fully describe the variability of the random process $\mathbf{Z}$ the correlations can be employed, however they need to be derived for all different lags corresponding to the different spatial frequencies present in the relief. A more concise method to describe it is therefore to take the Fourier transform of the correlation functions which gives the power spectral density function $W(\vec{k})$, also called variance spectrum or roughness spectrum (see section 2.3.2 and 2.3.3). A definition of the spectrum is given equation 2.76 using the Fourier transform of the covariance function of $\mathbf{Z}$. The spectrum is also directly related to the RMS relief or variance of the roughness σ_ζ^2 by equation 2.57 or 2.77.

The backscattering strength of a rough interface is derived by [Novarini and Caruther, 1998], [Essen, 1994] and [Jackson et al., 1986] using an equivalent of the reflection coefficient to control the strength of the index and the roughness spectrum (see sections 2.3.2 and 2.3.3). The spectrum $W(\vec{k})$ is divided in two parts corresponding to two regimes of spatial frequencies present in the seafloor relief (see figure 5.6):

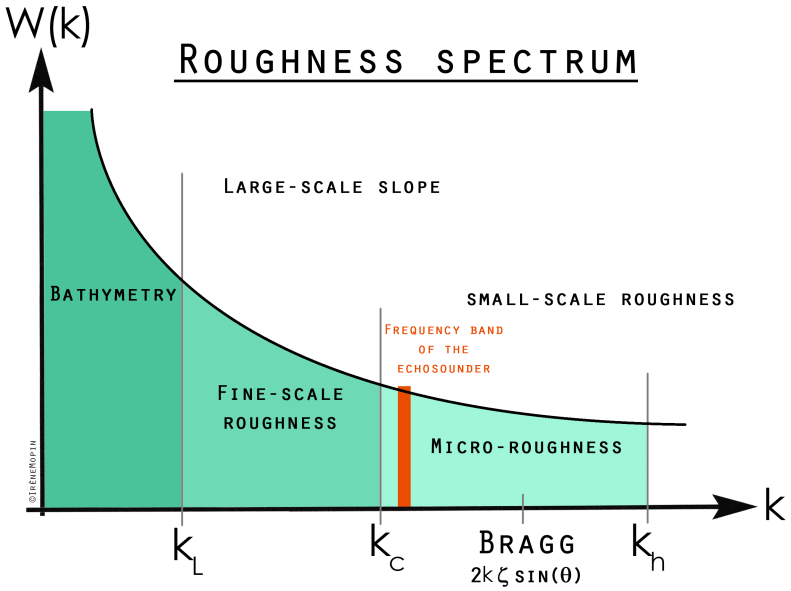

Figure 5.6 – Illustration of the roughness spectrum $W(\vec{k})$ of the seafloor, inspired from [Novarini and Caruther, 1998], [Essen, 1994] and [Jackson et al., 1986]. k is the spatial frequency. Names of the two regimes of roughness are given by the authors. The cut-off frequency k_c is used by all authors. Boundaries k_L and k_h are defined by [Novarini and Caruther, 1998] (see section 2.1.4). Because the beam footprint of the echosounder is always limited k_L cannot go to zero.

- low spatial frequencies: the large-scale slopes which correspond to the second moment of the interface random process
- high spatial frequencies: the small-scale roughness which corresponds to the zero moment of the interface random process

These two regimes are illustrated in figure 5.6 with their definitions from [Novarini and Caruther, 1998] and [Jackson et al., 1986]. They are separated by the cut-off frequency k_c. Consequently, the backscattering strength depends on the material of the seafloor (more precisely its impedance difference with water) and the distribution of the spatial frequencies of the rough interface i.e. the seafloor acoustic response is directly linked to the sediment type and the random characteristics of the interface.

To conclude, the seafloor acoustic response (or backscattering strength BS) has been defined in this section as:

— twice the Rayleigh distribution parameter σ^2 i.e. $\mathrm{BS} = 10\log_{10}(2\sigma^2)$

— the sum of the variances of the real and imaginary parts of the complex received signal amplitude in the case of a large number of scatterers M in the instantaneous insonified area and their equal distributed magnitudes $|a_i|$.

It was also shown to be related to the stochastic scattering ability of the rough interface to reflect the incident intensity, or equivalently the sediment type and the random characteristics of the interface.

5.2 Estimators of seafloor backscattering strength

It has been shown previously that the seabed acoustic response is directly related to the backscattering index amplitude $|\mathbf{A}|$ as a random variable by the parameter of its distribution (Rayleigh) σ^2. They are linked by the formula of equation 5.33. This result is valid in the case of a perfectly homogeneous seafloor (i.e. scatterers are independent, their amplitudes are identically distributed and their phases are uniformly distributed) and a large insonified area so that the number of scatterers is sufficient to apply the central limit theorem (see equation 5.8). All calculus in the following are based on these assumptions i.e. $\mathrm{BS} = 10\log_{10}(\sigma^2) + 3$.

The aim of this section is to define estimators of the backscattering strength BS that could be used on echosounders data. The method is based on the bathymetric measurement method mostly use nowadays by multi- and single-beam echosounders (see figures 4.4 and 4.5). At first, a mathematical representation of the echosounder data is introduced assuming the necessary hypotheses (perfect compensation of sonar equation parameters, independence, etc.). Then the choice of reduction methods is discussed based on literature. And finally, estimators of the seafloor response are derived analytically.

5.2.1 Mathematical representation of echosounder measurements

During survey at sea, vessels are following parallel lines in order to map efficiently an area. Along theses survey lines, single- or multi-beam echosounders transmit acoustics signals at a given frequency and with a chosen pulse length as shown in figure 4.5. In this manuscript signals used are pure sinusoids of duration τ called continuous wave (CW). The recorded signal between one transmission to another is called a ping. Backscattered signal from the seabed is then recorded by the echosounder inside this ping. In practice, the vessel never stops during survey each seabed echoes are recorded from different parts of the seafloor that can be of different types (see figure 4.5). However, in order to derive the mathematical model below, pings are supposed recorded on the same type of seafloor but independent of each other. This can correspond to a survey following lines that stay on the same seafloor type for all pings with no overlapping beam footprints, or to a stationary survey where the vessel is drifting so that pings are recorded on the same seafloor type but not on the exact same beam footprint [Mopin et al., 2022].

As shown of figure 4.5 and 5.7 the seafloor echo is spread over a time longer than the transmitted pulse length. This is due to the backscattering process illustrated figure 5.1: the transmitted signal intersects the seafloor on one side of the beam footprint and then continues to propagate. It results in consecutive areas insonified by the projection of the transmitted pulse on the seafloor. Each of these areas (also called instantaneous insonified areas) backscattered the signal at a different time which leads to the recorded seafloor echo. It comes naturally that the greater in the incident angle of the transmitted pulse on the seafloor, the more pronounced is the spread of the seafloor echo. In the bathymetric process, the sounding is mostly detected as the time-sample (or range) corresponding the center of the beam footprint i.e. to the beam axis.

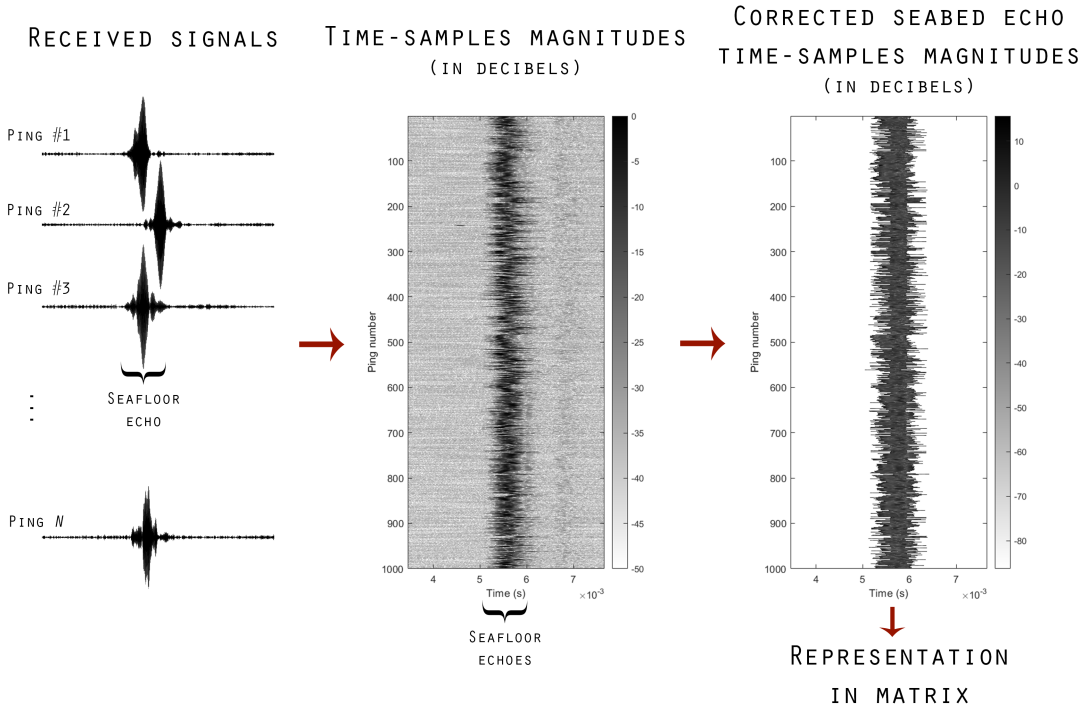

Figure 5.7 – Illustration of echosounder data gathered as a waterfall. The list of received signal amplitudes are plotted in decibels then seafloor echoes are extracted and their magnitudes corrected from sonar equation parameters. The final list of corrected time-samples magnitudes corresponds to the matrix of equation 5.2.1. Data in this illustration come from measurement at sea with the echosounder developed during this PhD (see the third part of manuscript). The echosounder is tilted at 25°.

The result of the survey is consequently a list of recorded seabed echoes such as shown in figure 4.5. Each echo is itself a list of time-samples with their own magnitudes. These magnitudes are supposed in this part of the PhD perfectly corrected from all sonar equation parameters. The list of time-samples corrected magnitudes of a seafloor echo from one ping can therefore be written as $[x_1, \cdots, x_n]$ with n the number of time-samples in the echo. Statistically they correspond to realizations of the backscattering index amplitude $|\mathbf{A}|$ which follows a Rayleigh distribution $\mathcal{R}(\sigma^2)$. This can be represented as:

$$\begin{array}{lcccccc} & & \text{Time-sample 1} & & \cdots & & \text{Time-sample n} \\ \text{One ping: } |\mathbf{A}| \sim \mathcal{R}(\sigma^2) & (& x_1, & & \cdots & & , x_n \quad) \end{array}$$

Because every pings are supposed recorded on the same seafloor type, the corrected seafloor echo magnitudes $|\mathbf{A}|$ of each ping are following the same Rayleigh distribution. A list of N

pings of corrected seafloor echo magnitudes can then be represented as:

$$\begin{array}{r} \\ \text{Ping 1: } |\mathbf{A}|_1 \sim \mathcal{R}(\sigma^2) \\ \vdots \\ \text{Ping } j\text{: } |\mathbf{A}|_j \sim \mathcal{R}(\sigma^2) \\ \vdots \\ \text{Ping } N\text{: } |\mathbf{A}|_N \sim \mathcal{R}(\sigma^2) \end{array} \begin{array}{c} \begin{array}{ccc} \text{Time-sample 1} & \cdots & \text{Time-sample n} \end{array} \\ \begin{pmatrix} x_{11} & \cdots & x_{n1} \\ \cdots & \cdots & \cdots \\ x_{1j} & x_{ij} & x_{nj} \\ \cdots & \cdots & \cdots \\ x_{1N} & \cdots & x_{nN} \end{pmatrix} \end{array}$$

where lines $j = 1, \cdots, N$ of the matrix correspond to the pings recorded, and columns $i = 1, \cdots, n$ of the matrix correspond to the time-samples of the seafloor echoes recorded.

The matrix of equation 5.2.1 corresponds in practice to what is called the waterfall representation of seafloor echo data. As shown in figure 5.7, seafloor echoes are listed and their magnitudes are corrected from sonar equation parameters. Then they are plotted as an image, generally with color corresponding to magnitude level in decibels i.e. $10\log_{10}(x_{ij}^2)$. For example, using singlebeam echosounder lines of the matrix correspond to successive recorded pings. Using multibeam echosounders data, they correspond to successive pings recorded from the same beam.

5.2.2 Estimation method

In bathymetric data processing, ping information received by a beam of the echosounder is reduced to a single time value (or range value) called the sounding. Then all soundings are gathered to provided the depth value of a cell of the numerical terrain model (DTM). This process in illustrated in figure 4.4. The seabed response estimation method developed in this PhD preserves this technique of reduction of the seabed echo in one value per ping which are then combined to provided one value, such as illustrated in figure 4.5. The equivalent of the bathymetric sounding but for the backscattering index magnitudes x_{ij} is called in this manuscript a descriptor. It is a single scalar value derived from a line (i.e. a ping) of the list of corrected time-samples magnitudes of the seabed echo (i.e. the matrix representation of equation 5.2.1). It is noted d in the mathematical representation below [Mopin et al., 2021]:

$$\begin{array}{r} \\ \text{Ping 1: } |\mathbf{A}|_1 \sim \mathcal{R}(\sigma^2) \\ \vdots \\ \text{Ping } j\text{: } |\mathbf{A}|_j \sim \mathcal{R}(\sigma^2) \\ \vdots \\ \text{Ping } N\text{: } |\mathbf{A}|_N \sim \mathcal{R}(\sigma^2) \end{array} \begin{array}{c} \begin{array}{ccc} \text{Time-sample 1} & \cdots & \text{Time-sample n} \end{array} \\ \begin{pmatrix} x_{11} & \cdots & x_{n1} \\ \cdots & \cdots & \cdots \\ x_{1j} & x_{ij} & x_{nj} \\ \cdots & \cdots & \cdots \\ x_{1N} & \cdots & x_{nN} \end{pmatrix} \end{array} \begin{array}{c} \\ \longrightarrow \\ \vdots \\ \longrightarrow \\ \vdots \\ \longrightarrow \end{array} \begin{array}{c} \text{Descriptor} \\ d_1 \\ \vdots \\ d_j \\ \vdots \\ d_N \end{array}$$

In literature, several descriptors can be found to reduce the echo information to one value. Four of them are predominantly used, therefore they are studied in this manuscript [Mopin et al., 2021]:

- **the maximum** value m of the n corrected time-samples magnitudes x of a seafloor echo i.e.:

$$m = \max(x_i) \tag{5.40}$$

  This descriptor is used and theoretically studied by [Penrose et al., 2008] to process the backscatter echoes of multibeam echosounders (Reson SeaBat 81 and 71 series models). They called it the peak amplitude. In [Le Chenadec, 2004], the maximum value is processed although unplanned on side scan sonar data (Edgetech DF1000). In another field of ultrasound imaging (health ultrasound scan), the maximum descriptor is also employed, mainly for practicality reasons, as shown in [Burckhardt, 1978].

- **the median** q of the n corrected time-samples magnitudes x of a seafloor echo.

$$q = \text{median}(x_i) \tag{5.41}$$

  This descriptor is proposed in [Fonseca et al., 2021] for backscattering strength processing of multibeam echosounder (Kongsberg EM2040C). It is known to be most robust to outliers in the data than the other descriptors [Zhang et al., 2020][Canepa and Pace, 2000].

- **the sample mean** μ of the n corrected time-samples magnitudes x of a seafloor echo i.e.:

$$\mu = \frac{1}{n}\sum_{i}^{n} x_i \tag{5.42}$$

  This descriptor is also proposed in [Fonseca et al., 2021], and sometimes called *mean in amplitude* in technical jargon.

- **the square sample mean** r of the n corrected time-samples magnitudes x of a seafloor echo i.e.:

$$r = \frac{1}{n}\sum_{i}^{n} x_i^2 \tag{5.43}$$

  This descriptor is the most employed with multi- or single-beam echosounders backscattering strength data. It is used by several authors [Gensane, 1989, Fonseca et al., 2021, Eleftherakis et al., 2018], and called sometimes *mean in intensity* in technical jargon because of the squared value x^2.

In practice, the list of time-samples of the seabed echo used in a ping is generally called snippet by echosounder manufacturers [Malik et al., 2019] referring to a part of the seabed echo. Indeed, the samples retained generally do not correspond to the entire seabed echo but are chosen using empirical boundaries around the bathymetric sounding. Several boundaries can therefore be employed by different echosounder processors in real time or by different users in post-processing. As an example, [Eleftherakis et al., 2018] retains seabed echo time-samples which angles are inside $\pm 1°$ around the sounding inside the beam.

The acoustic seabed response was defined previously as twice the parameter σ^2 of the Rayleigh distribution. Corrected time-samples magnitude x_{ij} are realizations of this distribution. To estimate the seafloor response BS, σ^2 has to be estimated and then doubled. In the representation chosen in this PhD, estimates $2\hat{\sigma}^2$ are derived from descriptor values. This

can be done deriving the descriptor distribution and using an estimation method to estimate the parameter of the distribution. Each descriptor is a combination of Rayleigh distributed samples x_{ij} thus its distribution f is a function of the descriptor d and the Rayleigh parameter σ^2, i.e.:

$$f_{\text{name of descriptor}} = f(d, \sigma^2) \tag{5.44}$$

In these works, the maximum likelihood estimation (MLE) method [Millar, 2011][Saporta, 2006] is used to estimate σ^2 from the distribution f of the descriptor. The final estimate of $2\sigma^2$ is noted $2\hat{\sigma}^2$ in the mathematical representation below

$$\begin{array}{rcccccc} & & & & \text{Descriptor} & & 2\sigma^2 \text{ estimates} \\ \text{Ping 1: } |\mathbf{A}|_1 \sim \mathcal{R}(\sigma^2) & \begin{pmatrix} x_{11} & \cdots & x_{n1} \end{pmatrix} & \longrightarrow & d_1 & \xrightarrow{\text{MLE}} & 2\hat{\sigma}_1^2 \\ \vdots & \begin{pmatrix} \cdots & \cdots & \cdots \end{pmatrix} & & \vdots & & \vdots \\ \text{Ping } j\text{: } |\mathbf{A}|_j \sim \mathcal{R}(\sigma^2) & \begin{pmatrix} x_{1j} & x_{ij} & x_{nj} \end{pmatrix} & \longrightarrow & d_j & \xrightarrow{\text{MLE}} & 2\hat{\sigma}_j^2 \\ \vdots & \begin{pmatrix} \cdots & \cdots & \cdots \end{pmatrix} & & \vdots & & \vdots \\ \text{Ping } N\text{: } |\mathbf{A}|_N \sim \mathcal{R}(\sigma^2) & \begin{pmatrix} x_{1N} & \cdots & x_{nN} \end{pmatrix} & \longrightarrow & d_N & \xrightarrow{\text{MLE}} & 2\hat{\sigma}_N^2 \end{array}$$

Note that estimations of $2\sigma^2$ are made as estimation of the square of the Rayleigh parameters and then doubled. They correspond directly to the distribution parameter of the random variable $\underline{|\mathbf{A}|}^2$ (see equations 5.30 and 5.29) i.e. they are estimates of the backscattering strength as a random variable bs.

An estimate of bs (i.e. $2\hat{\sigma}^2$) is consequently obtained for each ping. As derived in equation 5.31, the seafloor response BS is defined as the expected value of all theses estimates. This expected value is estimated by the sample mean giving an estimate $\widehat{\text{BS}}$ of the backscattering strength as:

$$\widehat{\text{BS}} = 10\log_{10}\left(\frac{1}{N}\sum_{j=1}^{N}\hat{\text{bs}}_j\right) = 10\log_{10}\left(\frac{1}{N}\sum_{j=1}^{N}2\hat{\sigma}_j^2\right) \tag{5.45}$$

The mean in equation 5.45 can be seen as the equivalent of the backscattering strength average along the survey track (usually called ping average) described by many authors especially when dealing with multibeam echosounders data [Eleftherakis et al., 2018, Fezzani et al., 2021, Lucieer et al., 2018, Lurton et al., 2015, Clarke et al., 2012, Malik et al., 2019].

The acoustic seabed response estimation $\widehat{\text{BS}}$ consequently depends on:

- the number of time-samples n of the seabed echo available to evaluate the descriptor d
- the descriptor used (maximum, median, sample mean, square sample mean)
- the number of pings N available on the same seafloor type

In addition, the dependence of the seafloor response with frequency and incidence angle discussed in the first part of this manuscript is still valid. Consequently, the backscattering strength estimate can be written:

$$\widehat{\text{BS}} = \widehat{\text{BS}}_d(\mathfrak{f}, \theta_\text{i}, n, N) \tag{5.46}$$

with d the descriptor employed to reduce the corrected time-samples magnitudes to one value, ƒ the acoustic frequency of the transmitted signal, θ_{i} the incidence angle of the transmitted signal on the seafloor, n the number of time-samples of the seabed echo used to evaluate $\widehat{\mathrm{BS}}$, and N the number of pings averaged to evaluate $\widehat{\mathrm{BS}}$. This result is in accordance with the discussion of [Fezzani et al., 2021] where the authors notice that the backscattering strength level may vary significantly depending on the acoustic frequency, the incidence angle, the number of averaged samples and the way the samples are averaged.

5.2.3 Estimators computation

The aim of this section is to derive the different estimators of σ^2 from the different descriptors described in section 5.2.2. The backscattering index amplitude $|\mathbf{A}|$ of the seabeed is a random variable following a Rayleigh distribution $f_{|\mathbf{A}|}$ of parameter σ^2, i.e.:

$$f_{|\mathbf{A}|}(x;\sigma^2) = \frac{x}{\sigma^2}\exp\left(\frac{-x^2}{2\sigma^2}\right) \text{ for x} \in [0, +\infty[\tag{5.47}$$

Its cumulative distribution function is:

$$F_{|\mathbf{A}|}(x;\sigma^2) = P(|\mathbf{A}| \leq x) = \int_{-\infty}^{x} f_{|\mathbf{A}|}(u)du = 1 - \exp\left(\frac{-x^2}{2\sigma^2}\right) \tag{5.48}$$

In the following, the probability density functions PDF of each descriptor is derived, the estimators of σ^2 are computed from them and then doubled to obtained estimators of $2\sigma^2$.

5.2.3.1 Descriptor: maximum

The first descriptor studied is the maximum of the corrected time-samples magnitudes x_{ij}. We define the random variable $\mathbf{M}_n$ as the maximum of $|\mathbf{A}| = (|A|_1, ..., |A|_n)$ which follow the Rayleigh distribution of parameter σ^2, i.e.:

$$\mathbf{M}_n = \max(|\mathbf{A}|) \tag{5.49}$$

All $|A|_i$ are independent. The cumulative distribution of $\mathbf{M}_n$ is therefore:

$$\begin{aligned} F_{\mathbf{M}_n}(m;\sigma^2) &= P(\mathbf{M}_n \leq m) \\ &= P(|A|_1 \leq m).P(|A|_2 \leq m)...P(|A|_n \leq m) \\ &= \prod_{i=1}^{n} P(|A|_i \leq m) \\ &= \prod_{i=1}^{n} F_{|A|_i}(m;\sigma) \\ F_{\mathbf{M}_n}(m;\sigma^2) &= \Big[F_{|\mathbf{A}|}(m;\sigma)\Big]^n \end{aligned} \tag{5.50}$$

where m is the maximum of a realization of $|\mathbf{A}|$ i.e. the maximum of a line of the matrix of equation 5.2.1 (see equation 5.40). The probability density function (PDF) of $\mathbf{M}_n$ is therefore:

$$\begin{aligned} f_{\mathbf{M}_n}(m;\sigma^2) &= \frac{\partial F_{M_n}(m;\sigma^2)}{\partial m} \\ &= n.f_{|A|}(m;\sigma^2).\left[F_{|A|}(m;\sigma^2)\right]^{n-1} \\ f_{\mathbf{M}_n}(m;\sigma^2) &= n\frac{m}{\sigma^2}e^{\frac{-m^2}{2\sigma^2}}\left[1-e^{\frac{-m^2}{2\sigma^2}}\right]^{n-1} \end{aligned} \tag{5.51}$$

This result is coherent with the PDF derived in [Burckhardt, 1978] and [Le Chenadec, 2004] for the maximum descriptor.

Another way to derive the PDF of the maximum of a random variable is to use the order statistic density function [Siddiqui, 1964]. For a random variable $\mathbf{X}$ with a cumulative distribution $F_{\mathbf{X}}(x)$, the order statistics of rank k have the following probability density function:

$$f_{\mathbf{X}_{(k)}}(x) = \frac{n!}{(k-1)!(n-k)!}f_{\mathbf{X}}(x)F_{\mathbf{X}}(x)^{k-1}\left[1-F_{\mathbf{X}}(x)\right]^{n-k} \tag{5.52}$$

The PDF of the maximum m corresponds to the order $k=n$ where n is the total number of time-samples available. This leads to:

$$f_{\mathbf{X}_{(n)}}(m) = nF_{\mathbf{X}}(m)^{n-1}f_{\mathbf{X}}(m) \tag{5.53}$$

This gives exactly the same result found in equation 5.51.

In the following we derive the likelihood function $L(\sigma^2;m)$ and find the estimator $\hat{\sigma}^2_{\max}$ that maximise its derivative:

$$\begin{aligned} L(\sigma^2;m) &= \prod_{i=1}^{1} f_{\mathbf{M}_n}(m;\sigma^2) \\ &= f_{\mathbf{M}_n}(m;\sigma^2) \\ &= n.f_{|\mathbf{A}|}(m).\left[F_{|\mathbf{A}|}(m)\right]^{n-1} \\ L(\sigma^2;m) &= n\frac{m}{\sigma^2}e^{\frac{-m^2}{2\sigma^2}}(1-e^{\frac{-m^2}{2\sigma^2}})^{n-1} \end{aligned} \tag{5.54}$$

The logarithm of the likelihood is:

$$\begin{aligned} \log\left(L(\sigma^2;m)\right) &= \log\left(n\frac{m}{\sigma^2}e^{\frac{-m^2}{2\sigma^2}}(1-e^{\frac{-m^2}{2\sigma^2}})^{n-1}\right) \\ &= \log(nm) - \log(\sigma^2) - \frac{m^2}{2\sigma^2} + (n-1)\log\left(1-e^{\frac{-m^2}{2\sigma^2}}\right) \end{aligned} \tag{5.55}$$

And its derivative according to σ^2 is:

$$\begin{aligned} \frac{\partial \log\left(L(\sigma^2;m)\right)}{\partial\sigma^2} &= \frac{\partial}{\partial\sigma^2}\left[\log(nm) - \log(\sigma^2) - \frac{m^2}{2\sigma^2} + (n-1)\log\left(1-e^{\frac{-m^2}{2\sigma^2}}\right)\right] \\ &= -\frac{1}{\sigma^2} + \frac{m^2}{2\sigma^4} - (n-1)\left(\frac{m^2}{2\sigma^4}e^{\frac{-m^2}{2\sigma^2}}\right)\frac{1}{1-e^{\frac{-m^2}{2\sigma^2}}} \\ &= -\frac{1}{\sigma^2} + \frac{m^2}{2\sigma^4} - (n-1)\frac{m^2}{2\sigma^4}\frac{1}{e^{\frac{m^2}{2\sigma^2}}-1} \end{aligned} \tag{5.56}$$

To find the best estimator $\hat{\sigma}^2_{\max}$ of σ^2 we look for the value of $\hat{\sigma}^2_{\max}$ that minimize the function $\mathcal{L}(\sigma^2) = \frac{\partial L(\sigma^2;m)}{\partial \sigma^2}$ with:

$$\mathcal{L}(\hat{\sigma}^2_{\max}) = \frac{1}{\hat{\sigma}^2_{\max}} \left[-1 + \frac{m^2}{2\hat{\sigma}^2_{\max}} \left(1 - \frac{n-1}{e^{\frac{m^2}{2\hat{\sigma}^2_{\max}}} - 1} \right) \right] \tag{5.57}$$

which results in [Mopin et al., 2021]:

$$\boxed{2\hat{\sigma}^2_{\max} = m^2 \left(1 - \frac{n-1}{e^{\frac{m^2}{2\hat{\sigma}^2_{\max}}} - 1} \right)} \tag{5.58}$$

The estimator of twice the Rayleigh parameter (i.e. of the backscattering strength) based of the maximum descriptor $2\hat{\sigma}^2_{\max}$ therefore cannot be derived analytically. However, a simulation of equation 5.58 can be processed to estimate the result.

5.2.3.2 Descriptor: median

In this section we define the median $\mathbf{Q}_n$ of $|\mathbf{A}| = (|A|_1, ..., |A|_n)$ which follow the Rayleigh distribution of parameter σ^2 as:

$$\mathbf{Q}_n = \text{median}(|\mathbf{A}|) \tag{5.59}$$

The probability density function of $\mathbf{Q}_n$ can be found from the order statistics formula 5.52 for k equal to the position of the center of $[1, ..., n]$ i.e. for $k = \frac{n}{2}$ which gives:

$$\begin{aligned} f_{\mathbf{Q}_n}(q;\sigma^2) &= \frac{n!}{(\frac{n}{2}-1)!(n-\frac{n}{2})} f_{|\mathbf{A}|}(q;\sigma^2). \left[F_{|\mathbf{A}|}(q;\sigma^2) \right]^{\frac{n}{2}-1} \left[1 - F_{|\mathbf{A}|}(q;\sigma^2) \right]^{n-\frac{n}{2}} \\ &= \frac{n!}{(\frac{n}{2}-1)!\,(\frac{n}{2})!} \frac{q}{\sigma^2} e^{-\left(\frac{n}{2}+1\right)\frac{q^2}{2\sigma^2}} \left[1 - e^{-\frac{q^2}{2\sigma^2}} \right]^{\frac{n}{2}-1} \end{aligned} \tag{5.60}$$

where q is the median of a realization of $|\mathbf{A}|$ i.e. the median of a line of the matrix of equation 5.2.1 (see equation 5.41).

Because the median is unique for each realization of $|\mathbf{A}|$, its likelihood is:

$$\begin{aligned} L(\sigma^2; q) &= f_{\mathbf{Q}_n}(q;\sigma^2) \\ &= \frac{n!}{(\frac{n}{2}-1)!\,(\frac{n}{2})!} \frac{q}{\sigma^2} e^{-\left(\frac{n}{2}+1\right)\frac{q^2}{2\sigma^2}} \left[1 - e^{-\frac{q^2}{2\sigma^2}} \right]^{\frac{n}{2}-1} \end{aligned} \tag{5.61}$$

The logarithm of the likelihood is then:

$$\log\Big(L(\sigma^2; q)\Big) = \log\left(\frac{n!}{(\frac{n}{2}-1)!\,(\frac{n}{2})!} q \right) - \log(\sigma^2) - \frac{q^2}{2\sigma^2} - \frac{n}{2}\frac{q^2}{2\sigma^2} + \left(\frac{n}{2} - 1\right) \log\left(1 - e^{\frac{-q^2}{2\sigma^2}} \right) \tag{5.62}$$

And its derivative:

$$\begin{aligned}\frac{\partial \log\left(L(\sigma^2;q)\right)}{\partial\sigma^2} &= -\frac{1}{\sigma^2}+\frac{q^2}{2\sigma^4}+\frac{n}{2}\frac{q^2}{2\sigma^4}+\left(\frac{n}{2}-1\right)\frac{\partial}{\partial\sigma^2}\left(\log\left[1-e^{\frac{-q^2}{2\sigma^2}}\right]\right)\\ &= -\frac{1}{\sigma^2}+\frac{q^2}{2\sigma^4}+\frac{n}{2}\frac{q^2}{2\sigma^4}-\left(\frac{n}{2}-1\right)\frac{\frac{q^2}{2\sigma^4}e^{-\frac{q^2}{2\sigma^2}}}{1-e^{-\frac{q^2}{2\sigma^2}}}\\ &= -\frac{1}{\sigma^2}+\frac{q^2}{2\sigma^4}+\frac{n}{2}\frac{q^2}{2\sigma^4}-\left(\frac{n}{2}-1\right)\frac{q^2}{2\sigma^4}\frac{1}{e^{\frac{q^2}{2\sigma^2}}-1}\end{aligned} \tag{5.63}$$

Consequently, the estimator of σ^2 based on the median descriptor and noted $\hat{\sigma}^2_{\text{med}}$ can be found by minimizing the function $\mathcal{L}(\hat{\sigma}^2_{\text{med}})$ as:

$$\mathcal{L}(\hat{\sigma}^2_{\text{med}}) = -\frac{1}{\hat{\sigma}^2_{\text{med}}}+\frac{q^2}{2\hat{\sigma}^4_{\text{med}}}\left[1+\frac{n}{2}-\frac{n}{2}\frac{1}{e^{\frac{q^2}{2\sigma^2}}-1}+\frac{1}{e^{\frac{q^2}{2\sigma^2}}-1}\right] \tag{5.64}$$

which results in [Mopin et al., 2021]:

$$\boxed{2\hat{\sigma}^2_{\text{med}} = q^2\left[1+\frac{n}{2}-\frac{n}{2}\frac{1}{e^{\frac{q^2}{2\hat{\sigma}^2_{\text{med}}}}-1}+\frac{1}{e^{\frac{q^2}{2\hat{\sigma}^2_{\text{med}}}}-1}\right]} \tag{5.65}$$

Again, the estimator of twice the Rayleigh parameter (i.e. of the backscattering strength) based of the median descriptor $2\hat{\sigma}^2_{\text{med}}$ cannot be derived analytically. However, a simulation of equation 5.65 can be processed to estimate the result.

5.2.3.3 Descriptor: sample mean

In this section we define as the sample mean S_n of $|\mathbf{A}| = (|A|_1, ..., |A|_n)$ which are independent and follow a Rayleigh distribution of parameter σ^2, i.e.:

$$\mathbf{S}_n = \frac{1}{n}\sum_{i=1}^{n}|A|_i \tag{5.66}$$

The probability density function of $\mathbf{S}_n$ cannot be derived analytically, however [Beaulieu, 1990] demonstrates that it can be approximated by:

$$f_{\mathbf{S}_n}(\mu;\sigma^2) \approx \mu^{2n-1}\frac{n^n}{2^{n-1}b^n\Gamma(n)}e^{\frac{-\mu^2 n}{2b}} \tag{5.67}$$

with

$$b = \frac{\sigma^2}{n}\left[(2n-1)!!\right]^{\frac{1}{n}} \tag{5.68}$$

and where μ is the sample mean of a realization of $|\mathbf{A}|$ i.e. the sample mean of a line of the matrix of equation 5.2.1 (see equation 5.42).

This approximation is also used by [Aja-Fernandez et al., 2008] and [Aja-Fernández and Vegas-Sánchez-Ferrero, 2016] where they derive the double factorial from [Abramowitz and Stegun, 1964] as:

$$[(2n-1)!!]^{\frac{1}{n}} = \left[\frac{2^{1-n}\Gamma(2n)}{\Gamma(n)}\right]^{\frac{1}{n}} \tag{5.69}$$

The PDF approximation of equation 5.67 is demonstrated by [Beaulieu, 1990] to be best for small values of n and for numerical reasons, for large n, one should be forced to use the approximation $[(2n-1)!!]^{\frac{1}{n}} \approx \frac{2n}{e}$ proposed by [Aja-Fernandez et al., 2008].

Because the mean is unique for each realization of $|\mathbf{A}|$, its likelihood is:

$$\begin{aligned} L(\sigma^2;\mu) &= f_{\mathbf{S}_n}(\mu;\sigma^2) \\ &= \mu^{2n-1}\frac{n^n}{2^{n-1}b^n\Gamma(n)}e^{\frac{-\mu^2 n}{2b}} \end{aligned} \tag{5.70}$$

The maximum of $L(\sigma^2;\mu)$ will give us the estimation $\hat{\sigma}^2_{\text{mean}}$ of σ^2. The logarithm of the likelihood is:

$$\begin{aligned} \log\Big(L(\sigma^2;\mu)\Big) &= \log(\mu^{2n-1}) + \log(n^n) - \log(2^{n-1}\Gamma(n)) - \log(b^n) - \frac{\mu^2 n}{2b} \\ &= \log(\mu^{2n-1}) + \log(n^n) - \log(2^{n-1}\Gamma(n)) \cdots \\ &- \log(\sigma^{2n}) - \log\left[(2n-1)!!\right] + \log(n^n) - \frac{\mu^2 n}{2\frac{\sigma^2}{n}\left[(2n-1)!!\right]^{\frac{1}{n}}} \end{aligned} \tag{5.71}$$

And its derivative:

$$\begin{aligned} \frac{\partial \log\left(L(\sigma^2;\mu)\right)}{\partial\sigma^2} &= -\frac{\partial}{\partial\sigma^2}\Big(\log(\sigma^{2n})\Big) - \frac{\partial}{\partial\sigma^2}\left(\frac{1}{\sigma^2}\frac{\mu^2 n}{\frac{2}{n}\left[(2n-1)!!\right]^{\frac{1}{n}}}\right) \\ &= -\frac{n}{\sigma^2} + \frac{1}{\sigma^4}\left(\frac{\mu^2 n}{\frac{2}{n}\left[(2n-1)!!\right]^{\frac{1}{n}}}\right) \end{aligned} \tag{5.72}$$

Consequently, the estimator of σ^2 based the sample mean descriptor and noted $\hat{\sigma}^2_{\text{mean}}$ can be found by minimizing the function $\mathcal{L}(\hat{\sigma}^2_{\text{mean}})$ as:

$$\mathcal{L}(\hat{\sigma}^2_{\text{mean}}) = -\frac{n}{\hat{\sigma}^2} + \frac{1}{\hat{\sigma}^4}\left(\frac{\mu^2 n^2}{2\left[(2n-1)!!\right]^{\frac{1}{n}}}\right) \tag{5.73}$$

Which gives:

$$\boxed{2\hat{\sigma}^2_{\text{mean}} = \mu^2 n\left[(2n-1)!!\right]^{-\frac{1}{n}} = \mu^2 n\left[\frac{2^{1-n}\Gamma(2n)}{\Gamma(n)}\right]^{-\frac{1}{n}}} \tag{5.74}$$

Numerically, using the approximation $[(2n-1)!!]^{\frac{1}{n}} \approx \frac{2n}{e}$ it gives [Mopin et al., 2021]:

$$\boxed{2\hat{\sigma}^2_{\text{mean}} \approx \frac{\mu^2 e}{2}} \tag{5.75}$$

Consequently, the estimator of twice the Rayleigh parameter (i.e. of the backscattering strength) based of the sample mean descriptor $2\hat{\sigma}^2_{\text{mean}}$ can be derived analytically when the approximation of equation 5.75 is used.

5.2.3.4 Descriptor: square sample mean

In this section we define the square sample mean $\mathbf{R}_n$ of $|\mathbf{A}|^2 = (|A|_1^2, ..., |A|_n^2)$ which are independent and follow a Rayleigh distribution of parameter σ^2, i.e.

$$\mathbf{R}_n = \frac{1}{n}\sum_{i=1}^{n} |A|_i^2 \tag{5.76}$$

The probability density function of $\mathbf{R}_n$ is given in [Aja-Fernandez et al., 2008][Aja-Fernández and Vegas-Sánchez-Ferrero, 2016] from [Papoulis and Pillai, 2002] as the gamma distribution $\gamma\left(n, \frac{2\sigma^2}{n}\right)$, i.e.:

$$f_{\mathbf{R}_n}(r;\sigma^2) = r^{n-1}\frac{n^n}{(2\sigma^2)^n\Gamma(n)}e^{\frac{-rn}{2\sigma^2}} \tag{5.77}$$

where r is the square sample mean of a realization of $|\mathbf{A}|$ i.e. the square sample mean of a line of the matrix of equation 5.2.1 (see equation 5.43).

Because the square sample mean is unique for each realization of $|\mathbf{A}|$, the likelihood of $\mathbf{R}_n$ is:

$$\begin{aligned} L(\sigma^2;r) &= f_{\mathbf{R}_n}(r;\sigma^2) \\ &= r^{n-1}\frac{n^n}{(2\sigma^2)^n\Gamma(n)}e^{\frac{-rn}{2\sigma^2}} \end{aligned} \tag{5.78}$$

The maximum of $L(\sigma^2;r)$ will give us the estimation $\hat{\sigma}^2_{\text{MS}}$ of σ^2. The logarithm of the likelihood is:

$$\log\Big(L(\sigma^2;r)\Big) = \log(r^{n-1}) + \log(n^n) - \log(2^n\Gamma(n)) - \log(\sigma^{2n}) - \frac{rn}{2\sigma^2} \tag{5.79}$$

And its derivative:

$$\frac{\partial \log\left(L(\sigma^2;r)\right)}{\partial\sigma^2} = -\frac{n}{\sigma^2} + \frac{rn}{2\sigma^4} \tag{5.80}$$

Consequently, the estimator of σ^2 from the sample mean of the square Rayleigh distribution, noted $\hat{\sigma}^2_{\text{SSM}}$, can be found by minimizing the function $\mathcal{L}(\hat{\sigma}^2_{\text{SSM}})$ as:

$$\mathcal{L}(\hat{\sigma}^2_{\text{SSM}}) = -\frac{n}{\sigma^2} + \frac{rn}{2\sigma^4} \tag{5.81}$$

Which gives [Mopin et al., 2021]:

$$\boxed{2\hat{\sigma}^2_{\text{SSM}} = r} \tag{5.82}$$

Consequently, the estimator of twice the Rayleigh parameter (i.e. of the backscattering strength) based of the sample mean descriptor $2\hat{\sigma}^2_{\text{SSM}}$ can be perfectly derived analytically.

5.3 Summary

In this chapter we developed a point-scattering model in order to describe the intrinsic variability of the seafloor acoustic response. The model supposed the instantaneous insonified area composed of several scatterers. The backscattered signal recorded by the echosounder therefore contains the contributions of all the scatterers. In this stochastic context, a definition of the backscattering strength BS was derived. It was demonstrated that BS is the expected value of the random variable **bs** see section 5.1.3). This random variable appears in the sonar equation, it is then of the order of magnitude of the acoustic intensity. It corresponds to the square backscattering index amplitude in RMS values $\underline{|\mathbf{A}|}^2$ corrected from all sonar equation parameters (see equation 5.29). The index amplitude $\underline{\mathbf{A}}$ is a complex random variable defined by the point scattering model. This definition of the seafloor response is only valid under the following conditions:

- all the sonar equation parameters are perfectly known and corrected;
- the instantaneous insonified area is large enough to ensure the central limit theorem is valid (i.e. large beam aperture and long pulse length);
- the amplitudes of the point scatterers are identically distributed and their phases are uniformly distributed. This condition can be considered as the local definition of an homogeneous seafloor.

In the second part of this chapter, a mathematical representation of echosounder data was derived in order to estimate the seafloor response. The model is based on the bathymetric method of reduction of the information from the seafloor echoes to one single value (see figures 4.4 and 4.5). In the case of the backscattering strength, the reduction is made in literature using several descriptors. Four of them are studied in this chapter: the maximum, the median, the sample mean, and the square sample mean. In section 5.2.3 we derived analytically the backscattering strength estimators based on these four descriptors. The results are summed up in table 5.2. Note that some estimators cannot be calculated analytically but can be estimate by numerical processing.

Finally, the estimator of the seafloor acoustic response is defined as the estimator of the backscattering strength which depends on the acoustic frequency of the transmitted signal, the incidence angle of the transmitted signal on the seafloor, the descriptor employed to reduce the corrected time-samples magnitudes to one value, the number of time-samples of the seabed echo used, and the number of pings averaged (see equation 5.46).

		Formulae of the raw descriptor	Estimators of σ^2	Estimators of BS
Maximum	m	$m = \max(x_i)$	Solution of $2\hat{\sigma}^2_{\max} = m^2 \left(1 - \frac{n-1}{e^{\frac{m^2}{2\hat{\sigma}^2_{\max}}} - 1}\right)$	$\widehat{\mathrm{BS}}_{\max} = 10\log_{10}\left(\frac{1}{N}\sum_{j=1}^{N} 2\hat{\sigma}^2_{\max,j}\right)$
Median	q	$q = \mathrm{median}(x_i)$	Solution of $2\hat{\sigma}^2_{\mathrm{med}} = q^2\left[1 + \frac{n}{2} - \frac{n}{2}\frac{1}{e^{\frac{q^2}{2\hat{\sigma}^2_{\mathrm{med}}}} - 1} + \frac{1}{e^{\frac{q^2}{2\hat{\sigma}^2_{\mathrm{med}}}} - 1}\right]$	$\widehat{\mathrm{BS}}_{\mathrm{med}} = 10\log_{10}\left(\frac{1}{N}\sum_{j=1}^{N} 2\hat{\sigma}^2_{\mathrm{med},j}\right)$
Sample mean	μ	$\mu = \frac{1}{n}\sum_{i=1}^{n} x_i$	$2\hat{\sigma}^2_{\mathrm{mean}} = \mu^2\left[\frac{2^{1-n}\Gamma(2n)}{\Gamma(n)}\right]^{-\frac{1}{n}}$	$\widehat{\mathrm{BS}}_{\mathrm{mean}} = 10\log_{10}\left(\frac{1}{N}\sum_{j=1}^{N} 2\hat{\sigma}^2_{\mathrm{mean},j}\right)$
Square sample mean	r	$r = \frac{1}{n}\sum_{i=1}^{n} x_i^2$	$2\hat{\sigma}^2_{\mathrm{SSM}} = r$	$\widehat{\mathrm{BS}}_{\mathrm{SSM}} = 10\log_{10}\left(\frac{1}{N}\sum_{j=1}^{N} 2\hat{\sigma}^2_{\mathrm{SSM},j}\right)$

Table 5.2 – Descriptors used to reduce the corrected seabed echo time-samples magnitudes to a single value, and corresponding estimators of twice the Rayleigh parameter $2\sigma^2$ and of the backscattering strength BS. n is the total number of time-samples inside the seabed echo, N is the total number of ping.

Chapter 6

Analysis of seafloor acoustic response estimators

Using a point scattering model, the seafloor acoustic response was defined in the previous chapter as twice the Rayleigh distribution parameter describing the backscattering index amplitudes as a random variable. It is noted in decibels BS for backscattering strength. Based on the bathymetric process method described in the preamble of this manuscript part (see figures 4.4 and 4.5), BS was derived as the expected value in decibels of the random variable **bs**. Each realization of this random variable is an estimate of twice the Rayleigh distribution parameter for a ping. The latter is calculated from a reduction of the information contained inside a seafloor echo also called a descriptor d. Four reduction methods were discussed in chapter 5. They led to four estimators of BS derived analytically from each descriptor (see section 5.2.3).

The aim of this chapter is to identify the best estimator of the seafloor acoustic response. In the first section, several estimators of two times the Rayleigh parameter are compared. They are issued from the previous chapter calculations or from literature and real-time processes of echosounders data (using the descriptors). At the end, one best estimator is retained for each reduction method. In the second section, the four backscattering strength estimators based on these four reduction methods are compared using their expected values, variances and uncertainties. Finally, the best estimator is identified.

In this PhD, the comparison of estimators is based on three parameters that impact the backscattering strength: the reduction method or descriptor d, the number of time-samples magnitudes n, and the number of pings N. The general definition of equation 5.46 then becomes:

$$\widehat{\mathrm{BS}} = \widehat{\mathrm{BS}}_d(n, N) \tag{6.1}$$

The two other parameters (frequency and incident angle) are supposed constant in this part of the manuscript.

Most of the results of this chapter are based on Monte-Carlo simulations, in particular for estimators that cannot be calculated analytically (e.g. equations 5.58 and 5.65). However, results for the identified best estimator are derived analytically in sections 6.1.4.2 and 6.2.2. Based on these results, a model of the backscattering strength uncertainty is developed. It gives *a priori* information on the quality of the seafloor response measurement.

6.1 Comparison of seafloor echo information reduction methods

In chapter 5, the backscattering strength was demonstrated to be directly related to the Rayleigh distribution parameter σ^2 as $\mathrm{BS} = 10\log_{10}(2\sigma^2)$. Thus, estimating the seafloor response is equivalent to estimate $2\sigma^2$. Four estimators of two times the Rayleigh distribution parameter were then derived analytically in section 5.2.3. They were calculated from four descriptors discussed in section 5.2.2 as the maximum likelihood estimates (MLE) of the descriptors distributions. Table 5.2 shows the descriptors formulae and the associate twice Rayleigh parameter estimators based on the maximum likelihood function of the descriptors. In the first part of this section, results of these estimators are compared. They are noted $2\hat{\sigma}_d^2$ where d is replaced by the name of the descriptor used. Synthetic corrected time-samples

magnitudes x_i following a Rayleigh distribution are generated randomly to give an equivalent of a one ping seabed echo as illustrated below:

$$\text{One synthetic ping: } |\mathbf{A}| \sim \mathcal{R}(\sigma^2_{\text{th}}) \ \begin{pmatrix} x_1 & \cdots & x_n \end{pmatrix} \longrightarrow \underset{d}{\text{Descriptor}} \xrightarrow{\text{MLE}} \underset{2\hat{\sigma}^2_d}{2\sigma^2 \text{ estimate}}$$

The magnitudes x_i are generated as independent realizations of the Rayleigh distribution of parameter σ^2_{th} chosen arbitrarily as:

$$\text{BS}_{\text{th}} = 10 \log_{10} \left(2\sigma^2_{\text{th}} \right) = -10\text{dB} \tag{6.2}$$

where the synthetic seafloor acoustic response is chosen to be $\text{BS}_{\text{th}} = -10$dB.

In practice, and mostly for real-time processing reasons during surveys, the seafloor response is estimated in literature directly as the descriptor value d (see discussion on the estimators section 5.2.2). Thus, in the formalism of this PhD, estimates of twice the Rayleigh distribution parameter can be written as the descriptor value i.e. :

$$\text{One synthetic ping: } |\mathbf{A}| \sim \mathcal{R}(\sigma^2_{\text{th}}) \ \begin{pmatrix} x_1 & \cdots & x_n \end{pmatrix} \longrightarrow \underset{d}{\text{Descriptor}} \xrightarrow{=} \underset{\hat{d}^2}{2\sigma^2 \text{ estimate}}$$

where $\hat{d}^2$ is the square of the descriptor value directly i.e. $\hat{d}^2 = d^2$. Four estimators of twice the Rayleigh distribution parameter are then derived and their results compared in the second part of this section.

Because these practical estimators of the seafloor response are mostly biased, unbiased versions of them are proposed in the third part of this section. They are noted $\hat{d}^2_{\text{ub}}$ such as:

$$\text{One synthetic ping: } |\mathbf{A}| \sim \mathcal{R}(\sigma^2_{\text{th}}) \ \begin{pmatrix} x_1 & \cdots & x_n \end{pmatrix} \longrightarrow \underset{d}{\text{Descriptor}} \xrightarrow{\text{unbiased}} \underset{\hat{d}^2_{\text{ub}}}{2\sigma^2 \text{ estimate}}$$

where $\hat{d}^2_{\text{ub}}$ is the square of the descriptor value compensated from its bias C_{ub} which is a constant value (see section 6.1.3) i.e.:

$$\hat{d}^2_{\text{ub}} = C_{\text{ub}} \hat{d}^2 \text{ where } \hat{d}^2 = d^2 \tag{6.3}$$

Four estimators of twice the Rayleigh distribution parameter are derived using this method based on unbiased descriptors. Their results are compared in the third part of this section.

In the last part of this section, results of all $2\sigma^2$ estimators are discussed and the best estimator for each reduction method is identified. Analytical results are given for the latter.

6.1.1 Maximum likelihood estimates of descriptors distributions used as estimates

Four estimators of twice the Rayleigh parameter σ^2 are processed as the maximum likelihood of the descriptors distributions. They are noted $2\hat{\sigma}^2_{\text{max}}$, $2\hat{\sigma}^2_{\text{med}}$, $2\hat{\sigma}^2_{\text{mean}}$, and $2\hat{\sigma}^2_{\text{SSM}}$ corresponding respectively to the descriptor maximum, median, mean, and square sample mean of the corrected backscattering index magnitudes of the synthetic seafloor echoes.

For one realization of a ping, the resulting estimates $2\hat{\sigma}_d^2$ in decibels are shown figure 6.1. They are plotted according to the number of time-samples n taken into account to compute the descriptor d. They can be seen as the seafloor response estimates $\widehat{\mathrm{BS}}_d(n, N{=}1)$ for a single ping. At first we observe that the trend for each estimates is to converge toward an certain value for when a large number of time-samples is used. This trend is easily observed for $2\hat{\sigma}^2_{\mathrm{med}}$, $2\hat{\sigma}^2_{\mathrm{mean}}$, and $2\hat{\sigma}^2_{\mathrm{SSM}}$. It is less obvious for $2\hat{\sigma}^2_{\mathrm{max}}$ using only one ping because of the large variations happening when a new maximum is found in the time-samples magnitudes. However, the asymptotic trend is also present (and confirmed by the following analysis). Figure 6.1 shows also large variations of the estimates values when a small number of time-samples are used. These variations seem to be stronger for $2\hat{\sigma}^2_{\mathrm{med}}$. Then variations for large number of time-samples are higher for $2\hat{\sigma}^2_{\mathrm{max}}$.

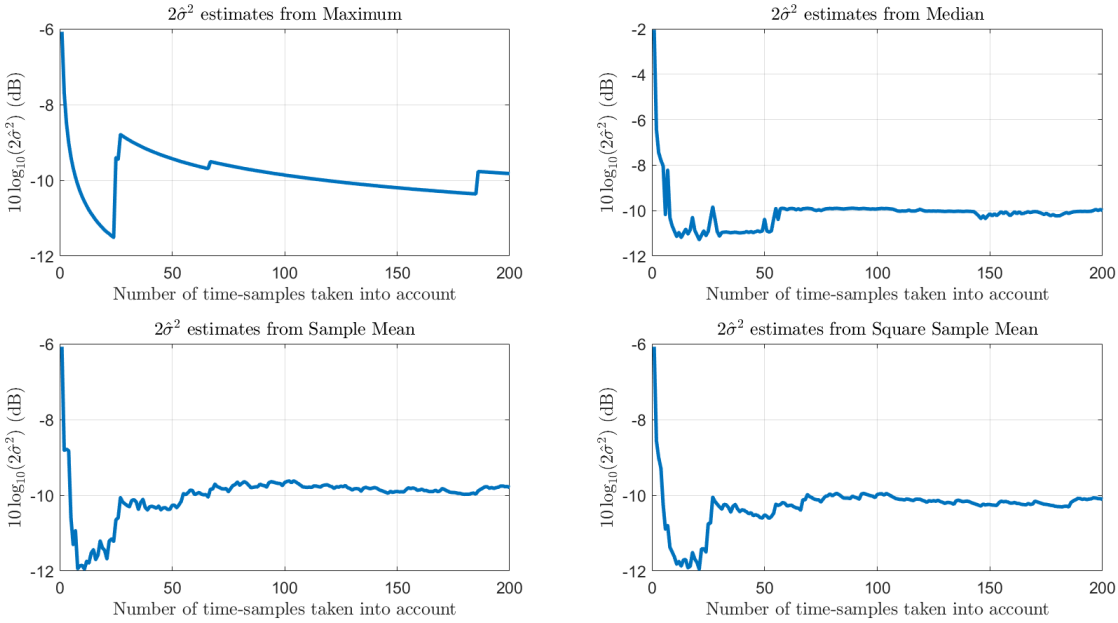

Figure 6.1 – $2\sigma^2$ estimates ($2\hat{\sigma}^2_{\mathrm{max}}$, $2\hat{\sigma}^2_{\mathrm{med}}$, $2\hat{\sigma}^2_{\mathrm{mean}}$, and $2\hat{\sigma}^2_{\mathrm{SSM}}$) according to the number of time-samples n taken into account and for one realization of a ping. In other words, $\widehat{\mathrm{BS}}_d(n, N{=}1)$ estimated by the MLE of the descriptors distributions for $N{=}1$ ping. Theoretical backscattering strength is $\mathrm{BS}_{\mathrm{th}} = 10\log_{10}(2\sigma^2_{\mathrm{th}}) = -10\mathrm{dB}$.

In order to study the asymptotic limit and the variability of each estimator, their expected values and variances are computed using the simulation as respectively their sample means and sample variance for a large number of realizations (400 realizations of one ping are generated). The results, called computed expected values and computed variances, are shown figure 6.2. They are plotted according to the number of time-samples n taken into account to calculate the descriptor. The computed expected values can be seen as the average on values that can be reached by the estimates of $2\sigma^2$ using n time-samples. The computed variances can be seen as the variability of these estimates. In other words, they correspond to the seafloor response estimates $\widehat{\mathrm{BS}}_d(n, N{=}400)$ and their variability for a number of ping

equal to the number of realization i.e. for $N = 400$ pings.

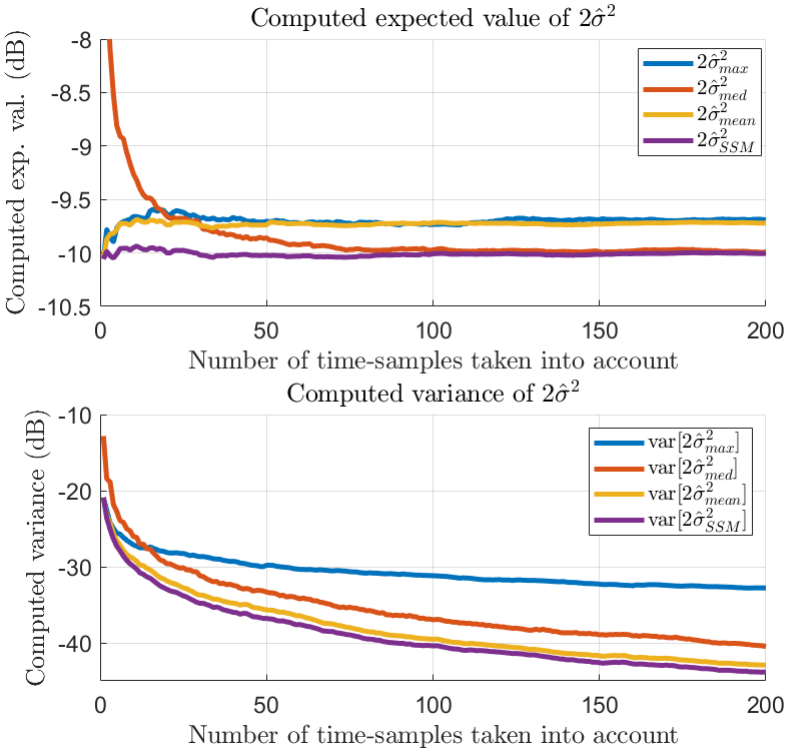

Figure 6.2 – Computed expected values and variances of $2\sigma^2$ estimates ($2\hat{\sigma}^2_{\text{max}}$, $2\hat{\sigma}^2_{\text{med}}$, $2\hat{\sigma}^2_{\text{mean}}$, and $2\hat{\sigma}^2_{\text{SSM}}$) in decibels according to the number of time-samples n taken into account and estimated using 400 realizations of a ping. In other words, they correspond to $\widehat{\text{BS}}_d(n, N{=}400)$ estimated by the MLE of the descriptors distributions for $N{=}400$ pings. Theoretical backscattering strength is $BS_{\text{th}} = 10\log_{10}(2\sigma^2_{\text{th}}) = -10\text{dB}$.

On the upper graph of figure 6.2, it can be observed that when the number of time-samples magnitudes x_i used is large the computed expected values reach different asymptotes. This means that after a certain number of time-samples used the value of the estimate is most unlikely to change. It is therefore not necessary to add more time-samples information. This asymptotic behaviour is observed for all estimates, even if it is counter-intuitive for the estimate $2\hat{\sigma}^2_{\text{max}}$ based on the maximum of the x_i values (see in figure 6.3 of the next section the non-convergent behaviour of the raw maximum descriptor). The method of using the MLE from the descriptors distribution allows therefore to compute convergent estimators of two times the Rayleigh parameter regardless the descriptor.

It can also be observed in figure 6.2 that the estimator which reaches its asymptote of computed expected values the faster is $2\hat{\sigma}^2_{\text{SSM}}$ and the slower is $2\hat{\sigma}^2_{\text{med}}$. The two others ($2\hat{\sigma}^2_{\text{max}}$ and $2\hat{\sigma}^2_{\text{mean}}$) reach their asymptotes almost together using more time-samples than $2\hat{\sigma}^2_{\text{SSM}}$ but less than $2\hat{\sigma}^2_{\text{med}}$. Therefore, a smallest number of time-samples is necessary to

reach the computed expected value of $2\hat{\sigma}^2_{\text{SSM}}$.

The theoretical backscattering strength being $-10\,\text{dB}$, it is possible to computed the difference between the asymptotic value reached by the computed expected values of the estimators and the theoretical value. This difference is called bias and derived for n=200 as:

$$\text{Bias} = 10\log_{10}\left(\text{E}\left[2\hat{\sigma}^2_d\right]\right) - \text{BS}_{\text{th}} \tag{6.4}$$

Resulting values of the bias of the four estimators are given table 6.1. The estimators $2\hat{\sigma}^2_{\text{SSM}}$ and $2\hat{\sigma}^2_{\text{med}}$ are considered not biased when a sufficient number of time-samples is used because the bias is smaller than 0.0 dB. The two other estimators are however biased but with bias smaller than 0.5 dB.

Name of the descriptors d	$2\hat{\sigma}^2_d$	Bias estimated in decibels $10\log_{10}\left(\text{E}\left[2\hat{\sigma}^2_d\right]\right) - \text{BS}_{\text{th}}$
Maximum m	$2\hat{\sigma}^2_{\text{max}}$	0.4 dB
Median q	$2\hat{\sigma}^2_{\text{med}}$	0.0 dB
Sample mean μ	$2\hat{\sigma}^2_{\text{mean}}$	0.3 dB
Square sample mean r	$2\hat{\sigma}^2_{\text{SSM}}$	0.0 dB

Table 6.1 – Bias of $2\sigma^2$ estimators computed as the MLE of the descriptors distributions. The bias are estimated by comparing the expected value of $2\hat{\sigma}^2_d$ for a large number of time-samples ($n = 200$) to the theoretical backscattering strength.

In addition, figure 6.2 also shows the computed variances of the estimators, i.e.:

$$\text{Variance} = 10\log_{10}\left(\text{E}\left[\left|2\hat{\sigma}^2_d - \text{E}\left[2\hat{\sigma}^2_d\right]\right|^2\right]\right) \tag{6.5}$$

It can be observed that $2\hat{\sigma}^2_{\text{max}}$ has the higher computed variance excepted for small amount of time-samples used where $2\hat{\sigma}^2_{\text{med}}$ has the higher computed variance. The latter is therefore not recommended to use for smaller numbers of time-samples. On the contrary $2\hat{\sigma}^2_{\text{SSM}}$ has the smallest computed variance whatever the number of time-samples .

Consequently, from these result we can identify the $2\hat{\sigma}^2_{\text{SSM}}$ as the best estimators between the four maximum likelihood estimates based on the descriptors distribution. It is unbiased, a small amount of time-samples is necessary for it to reach its asymptotic computed expected value, and its variance is the lowest whatever the number of time-samples used.

6.1.2 Raw descriptors values used as estimates

In this section, the descriptors values d are used directly as estimates of the Rayleigh parameter. The four estimates are then noted: $\hat{m}^2$ for the maximum descriptor, $\hat{q}^2$ for the median, $\hat{\mu}^2$ for the mean, and $\hat{r}$ for the square sample mean. They are computed from the corrected time-samples magnitudes x_i as the descriptors values described in table 5.2 i.e.:

$$\hat{m}^2 = m^2 = [\max(x_i)]^2 \tag{6.6}$$

$$\hat{q}^2 = q^2 = [\text{median}(x_i)]^2 \tag{6.7}$$

$$\hat{\mu}^2 = \mu^2 = \left[\frac{1}{n}\sum_{i=1}^{n} x_i\right]^2 \tag{6.8}$$

$$\hat{r} = r = \frac{1}{n}\sum_{i=1}^{n} x_i^2 \tag{6.9}$$

To analyse them, their expected values and variances are estimated using a simulation as respectively their sample mean and sample variance for a large number of realizations (400 realizations of one ping are generated). The results are plotted in figure 6.3 according to the number of time-samples n taken into account. They can be seen as the seafloor response estimates $\widehat{\text{BS}}_d(n, N{=}400)$ and their variability for a number of ping equal to the number of realization i.e. $N{=}400$ pings.

It first can be observed in figure 6.3 that the computed expected value of $\hat{m}^2$ is always increasing with new time-samples added. Therefore, this estimator is not convergent. It cannot be used as an accurate estimator. The other estimators are convergent but two of them are biased. Indeed, the theoretical BS is equal to $-10\,\text{dB}$ and $\hat{q}^2$ and $\hat{\mu}^2$ never reach this value. The more biased estimator (apart from $\hat{m}^2$) is $\hat{q}^2$. Bias values are estimated by simulating the computed expected values for $n = 200$. Results are given in table 6.2. It was also observed in figure 6.3 that $\hat{r}$ is unbiased and reach rapidly the theoretical value of $-10\,\text{dB}$. Analytically, this estimator can be derived by using the maximum likelihood estimate of the Rayleigh distribution parameter $\hat{\sigma}^2_{\text{MLE}}$ which can be calculated as [Siddiqui, 1962]:

$$\hat{\sigma}^2_{\text{MLE}} = \frac{1}{2n}\sum_{i=1}^{n} x_i^2 \tag{6.10}$$

with x_i realization of the Rayleigh distribution. It can be written in function of the square sample mean descriptor $\hat{r} = \frac{1}{n}\sum_{i=1}^{n} x_i^2$ as:

$$\hat{\sigma}^2_{\text{MLE}} = \frac{1}{2}\hat{r} \tag{6.11}$$

It then gives:

$$2\hat{\sigma}^2_{\text{MLE}} = \hat{r} = 2\hat{\sigma}^2_{\text{SSM}} \tag{6.12}$$

The estimator $\hat{r}$ is therefore equal to $2\hat{\sigma}^2_{\text{MLE}}$ and also equal to $2\hat{\sigma}^2_{\text{SSM}}$ as demonstrated in equation 5.82. The expected value of $\hat{\sigma}^2_{\text{MLE}}$ can be calculated knowing that the distribution of the square sample mean of realisations of a Rayleigh distributed random variable (i.e. x_i) is $\gamma\left(n, \frac{2\sigma^2}{n}\right)$ (see equation 5.77). It gives:

$$\begin{aligned} \text{E}\left[\hat{\sigma}^2_{\text{MLE}}\right] &= \frac{1}{2}\text{E}\left[\frac{1}{n}\sum_{i=1}^{n} x_i^2\right] \\ &= \frac{1}{2}\text{E}\left[\gamma\left(n, \frac{2\sigma^2}{n}\right)\right] \\ &= \sigma^2 \end{aligned} \tag{6.13}$$

Consequently, the estimator $\hat{\sigma}^2_{\text{MLE}}$ is unbiased and so is $\hat{r}$.

Results of figure 6.3 also shows that the computed variance of $\hat{m}^2$ is constant whatever the number of time-sample used contrary to all the other estimators which computed variances are decreasing with the number of time-samples. $\hat{q}^2$ and $\hat{r}$ has almost the same trend, and $\hat{\mu}^2$ has the lowest computed variances whatever the number of time-samples.

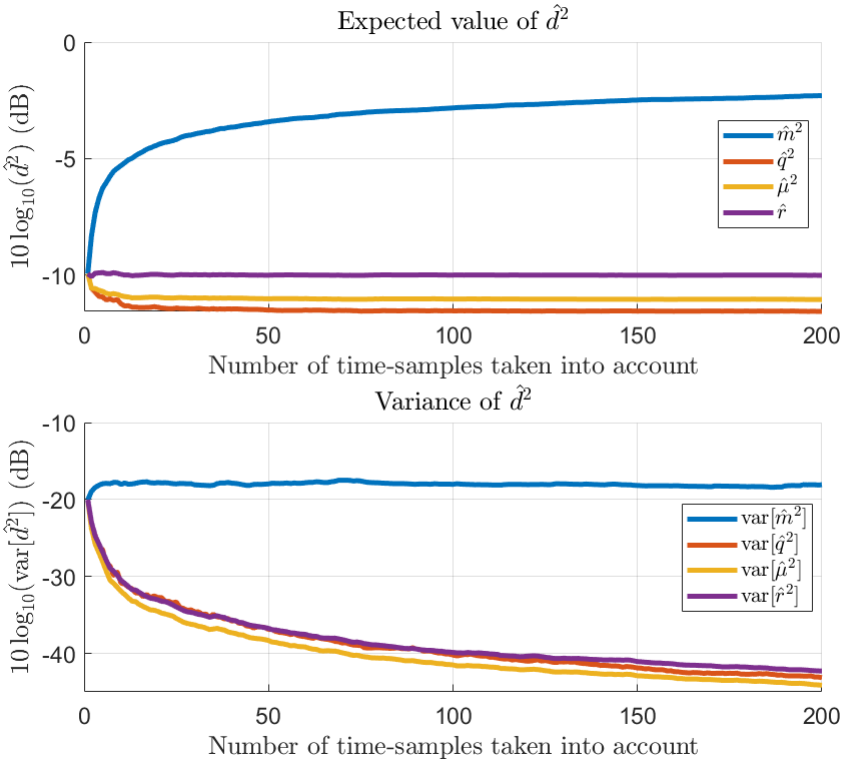

Figure 6.3 – Computed expected values and variances of $2\sigma^2$ estimates as raw values of descriptors ($\hat{m}^2$, $\hat{q}^2$, $\hat{\mu}^2$, and $\hat{r}$) according to the number of time-samples n taken into account and estimated using 400 realizations of a ping. In other words, they correspond to $\widehat{\text{BS}}_d(n, N{=}400)$ estimated directly as the descriptors values for $N{=}400$ pings. Theoretical backscattering strength is $BS_{\text{th}} = 10\log_{10}(2\sigma^2_{\text{th}}) = -10\text{dB}$.

From these results, the best estimators among the four described in this section can be identified as $\hat{r}$ because it is unbiased or $\hat{\mu}^2$ because it has the lower variability and the smaller bias.

We saw above that two estimators defined as the raw value of descriptors are biased. These bias of -1.6 dB and -1.0 dB respectively for the median descriptor and the sample mean are also found in [Fonseca et al., 2021] where a method to compensate them is proposed. In this paper, the reference measurement is the average of square amplitudes, i.e. the estimator we noted $\hat{r}$ and that we found unbiased.

Name of the descriptors d	$2\sigma^2$ estimators	Bias estimated in decibels $10\log_{10}\left(\mathrm{E}\left[\hat{d}^2\right]\right) - \mathrm{BS}_{\mathrm{th}}$
Maximum m	$\hat{m}^2$	Not convergent
Median q	$\hat{q}^2$	-1.6 dB
Sample mean μ	$\hat{\mu}^2$	-1.0 dB
Square sample mean r	$\hat{r}$	0.0 dB

Table 6.2 – Bias of $2\sigma^2$ estimators computed as raw values of descriptors. The bias are estimated by comparing the computed expected value of $\hat{d}^2$ for a large number of time-samples ($n = 200$) to the theoretical backscattering strength $\mathrm{BS}_{\mathrm{th}}$.

6.1.3 Unbiased descriptors values used as estimates

It was demonstrated in the previous section that using the raw descriptors values d in order to estimate $2\sigma^2$ is not always accurate because some of the estimators are biased. In this section, unbiased versions of the two biased estimators are derived analytically and analysed.

6.1.3.1 Unbiased descriptor based on the median

The unbiased estimator based on the median $\hat{q}_{\mathrm{ub}}$ can be derived from the quantile function of the distribution of x_i. The quantile function of a PDF is the inverse of its Cumulative Density Function (CDF) [Aktaş, 2011, Wackerly et al., 2014]. In the case of the Rayleigh distribution, its PDF is given by equation 5.48, therefore its quantile function F_{q} is (inspired from [Aktaş, 2011] and [Siddiqui, 1964]):

$$F_{\mathrm{q}}(p;\sigma^2) = \sigma\sqrt{-2\log(1-p)} \tag{6.14}$$

The median is the first 2-quantile then it can be derived for $p = 1/2$. Its value q can be written for the Rayleigh distribution as:

$$q = \sigma\sqrt{2\log(2)} \tag{6.15}$$

An estimator of $2\sigma^2$ can then be derived from the biased estimator $\hat{q}$=q as:

$$\hat{q}^2_{\mathrm{ub}} = \frac{1}{\log(2)}\hat{q}^2 \tag{6.16}$$

where $\hat{q}_{\mathrm{ub}}$ is the unbiased median estimator. In decibels this corresponds to:

$$10\log_{10}\left(\hat{q}^2_{\mathrm{ub}}\right) = 10\log_{10}\left(\hat{q}^2\right) + 1.6 \tag{6.17}$$

where 1.6 dB is also exactly the bias found in table 6.2. The estimator $\hat{q}^2_{\mathrm{ub}}$ should therefore be an unbiased estimator.

6.1.3.2 Unbiased descriptor based on the sample mean

A second unbiased estimator based on the sample mean $\hat{\mu}_{\text{ub}}$ can also be derived. The sample mean is a good estimator of the first moment of a distribution. In the case of a Rayleigh distribution, the moments M of order k are derived as [Siddiqui, 1962]:

$$M_k = \sigma^k 2^{\frac{k}{2}} \Gamma\left(1 + \frac{k}{2}\right) \tag{6.18}$$

Then the first moment, corresponding to the sample mean μ, can be written as [Aktaş, 2011, Siddiqui, 1962]:

$$\mu = M_1 = \sigma 2^{\frac{1}{2}} \Gamma\left(\frac{3}{2}\right) = \sigma \frac{\sqrt{2\pi}}{2} = \sigma \sqrt{\frac{\pi}{2}} \tag{6.19}$$

Consequently, an unbiased estimator of $2\sigma^2$ can be derived from the biased sample mean estimator $\hat{\mu}$ as:

$$\hat{\mu}^2_{\text{ub}} = \frac{4}{\pi} \hat{\mu}^2 \tag{6.20}$$

In decibels, this corresponds to:

$$10 \log_{10}\left(\hat{\mu}^2_{\text{ub}}\right) = 10 \log_{10}\left(\hat{\mu}^2\right) + 1.0 \tag{6.21}$$

where 1.0 dB is also exactly the bias found in table 6.2. The estimator $\hat{\mu}^2_{\text{ub}}$ should therefore be an unbiased estimator.

6.1.3.3 Comparison of unbiased estimators

As is the previous section, a comparison of the two unbiased estimators ($\hat{q}^2_{\text{ub}}$ and $\hat{\mu}^2_{\text{ub}}$) derived above is made based on their computed expected values and variances. The latter are estimated using a simulation as respectively their sample means and sample variance for a large number of realizations (400 realizations of one ping are generated). The results are plotted in figure 6.4 according to the number of time-samples n taken into account. They can be seen as the seafloor response estimates $\widehat{\text{BS}}_d(n, N{=}400)$ and their variability for a number of ping equal to the number of realization i.e. $N{=}400$ pings.

As observed in figure 6.4, the computed expected values of the two estimators tend toward the theoretical backscattering strength with no bias (i.e. a bias $<$0.1 dB) when the number of time-samples is large ($>$50). However, bias still remain for small amount of time-samples. In addition, the computed variance of $\hat{q}^2_{\text{ub}}$ is the highest.

From these results, the unbiased estimator derived from the sample mean of corrected time-samples magnitudes $\hat{\mu}^2_{\text{ub}}$ can be identified as the best of the two estimators analysed in this section.

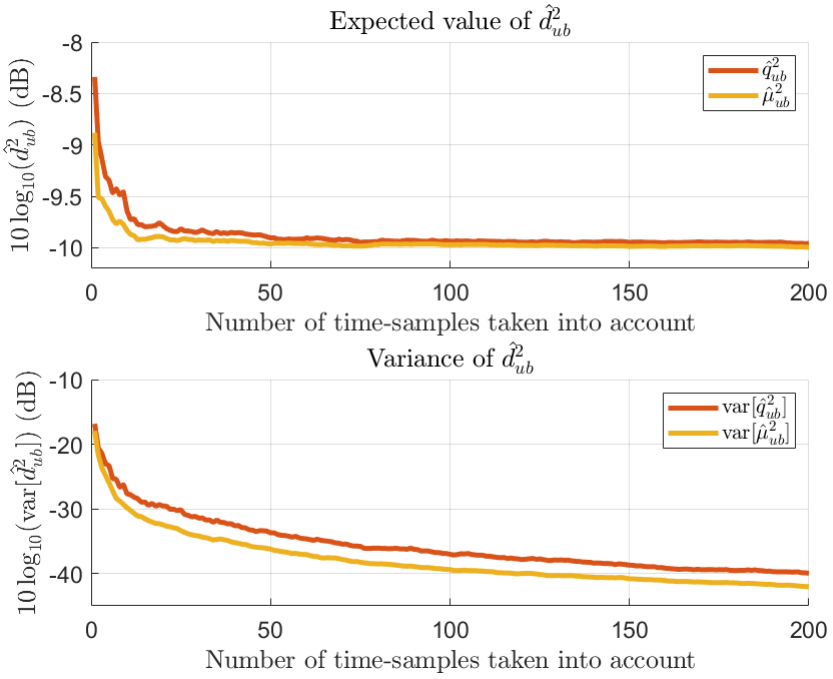

Figure 6.4 – Computed expected values and variances of $2\sigma^2$ estimates as unbiased values of descriptors ($\hat{q}^2_{\mathrm{ub}}$ and $\hat{\mu}^2_{\mathrm{ub}}$) according to the number of time-samples n taken into account and estimated using 400 realizations of a ping. In other words, they correspond to $\widehat{\mathrm{BS}}_d(n, N{=}400)$ estimated as the unbiased descriptors values for $N{=}400$ pings. Theoretical backscattering strength is $BS_{\mathrm{th}} = 10\log_{10}\left(2\sigma^2_{\mathrm{th}}\right) = -10\mathrm{dB}$.

6.1.4 Identification of the best estimator for a given number of pings

Ten estimators of the backscattering strength were derived in the previous sections. They are based on four reduction methods of the information contained in a seafloor echo otherwise called descriptors. In the following, a sum up of the analyses made in the previous sections is presented, and the four best estimators corresponding to each descriptor are identified. At the end only one estimator is retained as the best estimator of the backscattering strength.

These results are valid for a constant number of ping $N{=}400$ which corresponds to the number of realizations of one ping generated during the simulation. Results are given according to the number of pings in section 6.2.

6.1.4.1 Setting the best estimators for each reduction method

Three methods of estimating the backscattering strength (i.e. twice the Rayleigh parameter $2\sigma^2$) from four descriptors has been discussed in the last sections. In summary, we saw that:

— when using the maximum descriptor (i.e. when d is the maximum of the corrected time-samples magnitudes x_i) only the MLE method is valid because an unbiased estimator is not available and the raw descriptor estimator is not valid (it does not converge).

— When using the median descriptor the method using the raw descriptor values as estimates is to proscribe because of its bias. The two other methods give identical variances and are unbiased, but the unbiased descriptor used as an estimator converge faster to the computed expected value.

— When using the sample mean descriptor the MLE method and the raw descriptor method are biased. In this case, only the unbiased descriptor method is valid. The bias in the MLE method is probably due to the approximation of the probability density function (see equations 5.67 and 5.75).

— When using the square sample mean descriptor, the MLE method and the raw descriptor method give exactly the same results. They are both unbiased.

Detailed results of the analyses of all the different estimators are summed up in table 6.3. In order to compare them, they are sorted by descriptor. Computed bias and variances are given for two different numbers of time-samples used to calculate the descriptor: n=5 representing a small amount of time-samples and n=200 representing a large amount of time-samples. Results are based on the computed expected values and variance of the estimators generated using 400 realizations of a ping. They therefore can be considered as estimates of the backscattering strength $\widehat{\mathrm{BS}}_d(n, N{=}400)$ for N=400 pings.

Name of the descriptors d estimators are based on	Est.	Bias estimation (dB) $10\log_{10}\left(\mathrm{E}\left[2\hat{\sigma}^2\right]\right) - \mathrm{BS_{th}}$		Variance estimation (dB)	
		n=5	n=200	n=5	n=200
Maximum m	$2\hat{\sigma}^2_{\max}$	0.4 dB	0.4 dB	-24.5 dB	-32.8 dB
	$\hat{m}^2$	Not convergent		-17.9 dB	-18.0 dB
Median q	$2\hat{\sigma}^2_{\mathrm{med}}$	1.3 dB	0.0 dB*	-22.0 dB	-39.9 dB
	$\hat{q}^2$	-1.0 dB	-1.6 dB	-26.5 dB	-43.1 dB
	$\hat{q}^2_{\mathrm{ub}}$	0.7 dB	0.0 dB*	-23.3 dB	-39.9 dB
Sample mean μ	$2\hat{\sigma}^2_{\mathrm{mean}}$	0.3 dB	0.3 dB	-25.9 dB	-41.5 dB
	$\hat{\mu}^2$	-0.7 dB	-1.0 dB	-28.0 dB	-44.1 dB
	$\hat{\mu}^2_{\mathrm{ub}}$	0.4 dB	0.0 dB*	-25.9 dB	-42.0 dB
Square sample mean r	$2\hat{\sigma}^2_{\mathrm{SSM}}$	0.0 dB*	0.0 dB*	-26.8 dB	-42.3 dB
	$\hat{r}$	0.0 dB*	0.0 dB*	-26.8 dB	-42.3 dB

Table 6.3 – Summary of the estimators of $2\sigma^2$ analysed in section 6.1. Bias are estimated comparing the computed expected value of estimators for a small ($n = 5$) and a large ($n = 200$) number of time-samples to the theoretical backscattering strength $\mathrm{BS_{th}}$. Computed variances are estimated for same arbitrary numbers of time-samples. All estimations are made by generating 400 realizations of a ping. (*: bias are not perfectly equal to zero in simulations but are less than the tenth of decibels which is rounded to 0.0 dB.)

From the results of table 6.3 the best estimators for each descriptor are identified in the following:

- Estimators based on the maximum of the corrected time-samples magnitudes: the best estimator is identified as $2\hat{\sigma}^2_{\max}$ with a bias of 0.4 dB and a computed variance of -

32.8 dB for $n = 200$. The other estimator is not convergent so it cannot be used as an accurate estimator.

- Estimators based on the median of the corrected time-samples magnitudes: two estimators ($2\hat{\sigma}^2_{\text{med}}$ and $\hat{q}^2_{\text{ub}}$) are equivalently the best estimators according to table 6.3 if only the results for $n = 200$ are taken into account, with a bias null and a computed variance of -39.9 dB. However, results for $n = 5$ inform us that $\hat{q}^2_{\text{ub}}$ converge faster with a bias of 0.7 dB against 1.3 dB for $2\hat{\sigma}^2_{\text{med}}$. Figures 6.2 and 6.4 also describe these behaviours for small n. The best estimator is therefore identified as $\hat{q}^2_{\text{ub}}$.
- Estimators based on the sample mean of the corrected time-samples magnitudes: the best estimator is identified as $\hat{\mu}^2_{\text{ub}}$ with a bias null and a computed variance of -42.0 dB for $n = 200$.
- Estimators based on the square sample mean of the corrected time-samples magnitudes: the best estimators are equivalently identified as $2\hat{\sigma}^2_{\text{SSM}}$ and $\hat{r}$. They have been demonstrated to be equal and also equal to twice the MLE of the Rayleigh distribution parameter $2\hat{\sigma}^2_{\text{MLE}}$ (see equation 6.11). They have a bias null and a computed variance of -42.3 dB for $n = 200$.

6.1.4.2 Analytical results

Between the best estimators identified above for each reduction method, the best estimator of the backscattering strength (for a given number of pings equal to N=400) can be identified as $2\hat{\sigma}^2_{\text{SSM}}$, or equivalently $\hat{r}$ or $\hat{\sigma}^2_{\text{MLE}}$. This result is based on their ability to converge toward the theoretical backscattering strength (bias null), their speed of convergence (with n=5 their bias are already null), and their low variance (they have the lower variance for n=5 and n=200). In the following, we analyse analytically this best estimator. The name of the estimator is chosen to be $2\hat{\sigma}^2_{\text{SSM}}$.

In short, we can write the best estimator of the backscattering strength from equations 5.82, 6.9 and 6.11 as:

$$2\hat{\sigma}^2_{\text{SSM}} = \hat{r} = 2\hat{\sigma}^2_{\text{MLE}} = r = \frac{1}{n}\sum_{i=1}^{n} x_i^2 \tag{6.22}$$

where r is the square sample mean of the corrected time-samples magnitudes x_i and n the number of time-samples.

Based on equation 6.22 we can derive the variance and the expected value of $2\hat{\sigma}^2_{\text{SSM}}$ as a random variable analytically. We saw previously that, if x_i are realizations of a Rayleigh distribution then their square sample means $\frac{1}{n}\sum_{i=1}^{n} x_i^2$ are realizations of the gamma distribution $\gamma\left(n, \frac{2\sigma^2}{n}\right)$ (see equation 5.77). Consequently, the estimate as a random variable noted $2\hat{\boldsymbol{\sigma}}^2_{\text{SSM}}$ follows also a gamma distribution, as:

$$2\hat{\boldsymbol{\sigma}}^2_{\text{SSM}} \sim \gamma\left(n, \frac{2\sigma^2}{n}\right) \tag{6.23}$$

The expected value of a gamma distribution is given by the product of its two parameters, therefore:

$$\mathrm{E}\left[2\hat{\boldsymbol{\sigma}}^2_{\mathrm{SSM}}\right] = \mathrm{E}\left[\gamma\left(n, \frac{2\sigma^2}{n}\right)\right] = 2\sigma^2 \tag{6.24}$$

The variance of a gamma distribution is given by $\mathrm{var}\left[\gamma(k,\theta)\right] = k\theta^2$, therefore the variance of the random variable $2\hat{\boldsymbol{\sigma}}^2_{\mathrm{SSM}}$ is:

$$\mathrm{var}\left[2\hat{\boldsymbol{\sigma}}^2_{\mathrm{SSM}}\right] = \mathrm{var}\left[\gamma\left(n, \frac{2\sigma^2}{n}\right)\right] = \frac{(2\sigma^2)^2}{n} \tag{6.25}$$

These two results validate the simulation results described previously (see figure 6.2): the expected value of $2\hat{\boldsymbol{\sigma}}^2_{\mathrm{SSM}}$ is equal to two times the Rayleigh parameter $2\sigma^2$ therefore the estimator $2\hat{\sigma}^2_{\mathrm{SSM}}$ is unbiased; its variance depends on the number of time-samples taken into account. Using the theoretical result of equation 6.25, the analytical behaviour of the variance of $2\hat{\boldsymbol{\sigma}}^2_{\mathrm{SSM}}$ can be compared to the computed variance derived in section 6.1.1. Results are given in figure 6.5. A perfect match between the analytical result and the simulation results is observed, validating the simulation. This result can also be found in literature (e.g. [Gabella, 2014] and [Zrnic, 1975]).

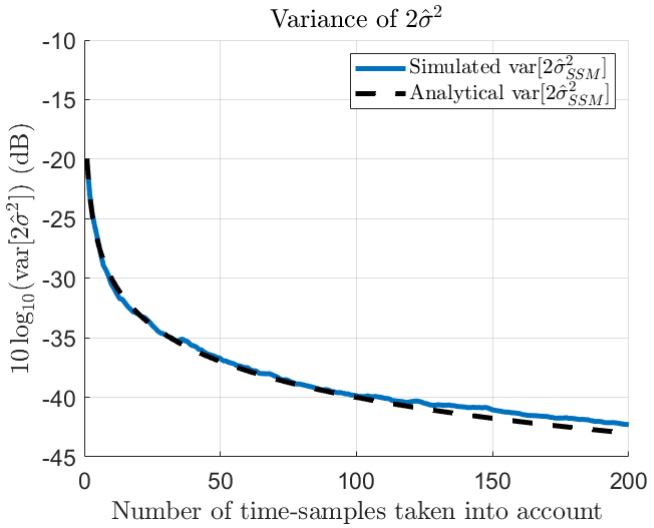

Figure 6.5 – Simulated and analytical variances of $2\hat{\boldsymbol{\sigma}}^2_{\mathrm{SSM}}$ according to the number of time-samples n taken into account. Estimations are made on 400 realizations of a ping.

The results of table 6.3 can also be retrieved using equation 6.25. In the simulation the theoretical backscattering was chosen as $\mathrm{BS_{th}} = 10\log_{10}\left(2\sigma^2_{\mathrm{th}}\right) = -10\mathrm{dB}$, therefore we can write:

$$\begin{aligned} 10\log_{10}\left(\mathrm{var}\left[2\hat{\boldsymbol{\sigma}}^2_{\mathrm{SSM}}\left(2\sigma^2_{\mathrm{th}}, n\right)\right]\right) &= 10\log_{10}\left(\frac{(2\sigma^2_{\mathrm{th}})^2}{n}\right) \\ &= 2 \cdot 10\log_{10}\left(2\sigma^2_{\mathrm{th}}\right) - 10\log_{10}(n) \\ &= -20 - 10\log_{10}(n) \end{aligned} \tag{6.26}$$

For n=5, the variance is therefore equal to -27.0 dB, or n=200, the variance is equal to -43.0 dB. These two results correspond to the results of the simulation given in table 6.3.

In conclusion, the best of the ten estimators analysed in this section is, in term of expected value and variance, the square sample mean or $2\hat{\sigma}^2_{\text{SSM}}$. We saw that this estimator is also the double of the maximum likelihood estimate of the Rayleigh distribution parameter (see equation 6.22). This result was predictable as soon as we demonstrate that the backscattering strength was two times the Rayleigh distribution parameter (see equation 5.33), the maximum likelihood estimation being one of the renowned method to estimate a distribution parameter. In term of variability, the variance of this estimator was demonstrated to be equal to $(2\sigma^2)^2/n$ (see equation 6.25) with n the number of time-samples taken into account. This result also corresponds to the Cramer-Rao bound of twice the Rayleigh distribution parameter variance i.e. the variance found is the lowest variance that can be reached with this unbiased estimator. Indeed, taking the Rayleigh distribution as described in equation 5.47, its likelihood can be written as:

$$L(\sigma^2; x) = \prod_{i=1}^{n} f_{|\mathbf{A}|}(x_i; \sigma^2) \tag{6.27}$$

where x_i are realization of the Rayleigh distribution of parameter σ^2 i.e. corrected time-samples magnitudes of the seabed echo, and n is their total number. The likelihood logarithm is then:

$$\begin{aligned}
\log\Big(L(\sigma^2; m)\Big) &= \log\left[\prod_{i=1}^{n} f_{|\mathbf{A}|}(x; \sigma^2)\right] \\
&= \sum_{i=1}^{n} \log\Big[f_{|\mathbf{A}|}(x_i; \sigma^2)\Big] \\
&= \sum_{i=1}^{n} \log\left[\frac{x_i}{\sigma^2}\exp\left(\frac{-x_i^2}{2\sigma^2}\right)\right] \\
&= \sum_{i=1}^{n} \log(x_i) - n\log(\sigma^2) - \frac{1}{2\sigma^2}\sum_{i=1}^{n} x_i^2
\end{aligned} \tag{6.28}$$

And its derivative:

$$\begin{aligned}
\frac{\partial \log\left(L(\sigma^2; m)\right)}{\partial \sigma^2} &= \frac{\partial}{\partial \sigma^2}\left[\sum_{i=1}^{n} \log(x_i) - n\log(\sigma^2) - \frac{1}{2\sigma^2}\sum_{i=1}^{n} x_i^2\right] \\
&= -\frac{n}{\sigma^2} + \frac{1}{2\sigma^4}\sum_{i=1}^{n} x_i^2
\end{aligned} \tag{6.29}$$

The Fisher information of a parameter θ noted $\mathcal{I}(\theta)$ is by definition the expected value of this square derivative, i.e.:

$$\mathcal{I}(\theta) = \mathrm{E}\left[\left(\frac{\partial \log\left(L(\theta, x_i)\right)}{\partial \sigma^2}\right)^2\right] \tag{6.30}$$

Therefore, for the Rayleigh distribution:

$$\begin{aligned}\mathcal{I}(\sigma^2) &= \mathrm{E}\left[\left(-\frac{n}{\sigma^2}+\frac{1}{2\sigma^4}\sum_{i=1}^{n}x_i^2\right)^2\right]\\ &= \mathrm{E}\left[\left(\frac{1}{2\sigma^4}\sum_{i=1}^{n}x_i^2\right)^2-\frac{n}{2\sigma^6}\sum_{i=1}^{n}x_i^2+\frac{n^2}{\sigma^4}\right]\\ &= \mathrm{E}\left[\frac{1}{4\sigma^8}\left(\sum_{i=1}^{n}x_i^2\right)^2\right]-\frac{n}{2\sigma^6}E\left[\sum_{i=1}^{n}x_i^2\right]+\frac{n^2}{\sigma^4}\\ &= \frac{1}{4\sigma^8}\sum_{i=1}^{n}E\left[x_i^4\right]+\frac{1}{4\sigma^8}\sum_{i\neq j}E\left[x_i^2x_j^2\right]-\frac{n}{2\sigma^6}\sum_{i=1}^{n}E\left[x_i^2\right]+\frac{n^2}{\sigma^4}\end{aligned} \tag{6.31}$$

Because all x_i are independent, we can writte $\mathrm{E}\left[x_i^2x_j^2\right] = \mathrm{E}\left[x_i^2\right]\mathrm{E}\left[x_j^2\right]$. In equation 6.31, all $\mathrm{E}\left[x_i^k\right]$ correspond to the moment M of order k of the Rayleigh distribution that can be derived from equation 6.18. Therefore:

$$\mathrm{E}\left[x_i^2\right] = M_2 = \sigma^2 2^{\frac{2}{2}}\Gamma\left(1+\frac{2}{2}\right) = 2\sigma^2 \tag{6.32}$$

and

$$\mathrm{E}\left[x_i^4\right] = M_4 = \sigma^4 2^{\frac{4}{2}}\Gamma\left(1+\frac{4}{2}\right) = 8\sigma^4 \tag{6.33}$$

Consequently, the Fisher information becomes:

$$\begin{aligned}\mathcal{I}(\sigma^2) &= \frac{1}{4\sigma^8}n8\sigma^4+\frac{1}{4\sigma^8}n(2\sigma^2)^2-\frac{n}{2\sigma^6}n2\sigma^2+\frac{n^2}{\sigma^4}\\ &= \frac{n}{\sigma^4}\end{aligned} \tag{6.34}$$

The Fisher information corresponding to the estimator of $2\sigma^2$ can finally be linked to $\mathcal{I}(\sigma^2)$ as [Lehmann and Casella, 2006]:

$$\mathcal{I}(\sigma^2) = \mathcal{I}(2\sigma^2)\left(\frac{d2\sigma^2}{d\sigma^2}\right) = 4\cdot\mathcal{I}(2\sigma^2) \tag{6.35}$$

Then:

$$\mathcal{I}(2\sigma^2) = \frac{1}{4}\mathcal{I}(\sigma^2) = \frac{n}{(2\sigma^2)^2} \tag{6.36}$$

The Cramer-Rao bound being the inverse of Fisher information, i.e. $\left[\mathcal{I}(2\sigma^2)\right]^{-1}$, then it is equal to $\frac{(2\sigma^2)^2}{n}$. The variance of the best estimator of the backscattering strength identified in this section is therefore equal to the Cramer-Rao bound. It is then the smallest variance that can be reached. This made the best estimator of the backscattering strength also an efficient estimate [Saporta, 2006].

6.2 Identification of the best backscattering strength estimator

In this section, the four best estimators ($2\hat{\sigma}^2_{\max}$, $\hat{q}^2_{\text{ub}}$, $\hat{\mu}^2_{\text{ub}}$, and $2\hat{\sigma}^2_{\text{SSM}}$) are compared according to the number of time-samples n but also according to the number of pings N. The results will therefore lead directly to the best estimator of the backscattering strength as defined in equation 6.1: $\widehat{\text{BS}}_d(n, N)$.

It was demonstrated in chapter 5 that the backscattering strength BS can be estimated as the mean of $2\sigma^2$ estimates over a certain number of pings N (see equation 5.45). The corresponding four BS estimators based on the estimators selected in the previous section (one for each descriptor) are then:

$$\widehat{\text{BS}}_{\max} = 10\log_{10}\left(\langle\widehat{\text{bs}}\rangle_{\max}\right) = 10\log_{10}\left(\frac{1}{N}\sum_{j=1}^{N} 2\hat{\sigma}^2_{j,\max}\right) \tag{6.37}$$

$$\widehat{\text{BS}}_{\text{med}} = 10\log_{10}\left(\langle\widehat{\text{bs}}\rangle_{\text{med}}\right) = 10\log_{10}\left(\frac{1}{N}\sum_{j=1}^{N} \hat{q}^2_{j,\text{ub}}\right) \tag{6.38}$$

$$\widehat{\text{BS}}_{\text{mean}} = 10\log_{10}\left(\langle\widehat{\text{bs}}\rangle_{\text{mean}}\right) = 10\log_{10}\left(\frac{1}{N}\sum_{j=1}^{N} \hat{\mu}^2_{j,\text{ub}}\right) \tag{6.39}$$

$$\widehat{\text{BS}}_{\text{SSM}} = 10\log_{10}\left(\langle\widehat{\text{bs}}\rangle_{\text{SSM}}\right) = 10\log_{10}\left(\frac{1}{N}\sum_{j=1}^{N} 2\hat{\sigma}^2_{j,\text{SSM}}\right) \tag{6.40}$$

where $\langle\widehat{\text{bs}}\rangle_d$ is the expected value of $\widehat{\text{bs}}_d$ (see equation 5.31) estimated as the mean of the estimators of twice the Rayleigh parameter $2\hat{\sigma}^2_{j,d}$ over the number of pings N. In the following the backscattering strengths $\widehat{\text{BS}}_d$ are discussed in decibels but all analyses are made on $\langle\widehat{\text{bs}}\rangle_d$.

The comparison of these estimators is also based on a Monte-Carlo simulation. Corrected time-samples magnitudes x_i are generated as realizations of a Rayleigh distribution of parameter σ^2. Then N random lists of these x_i are generated to simulate pings over the same seafloor type. For each list (i.e. ping), one of the four estimates ($2\hat{\sigma}^2_{\max}$, $\hat{q}^2_{\text{ub}}$, $\hat{\mu}^2_{\text{ub}}$, and $2\hat{\sigma}^2_{\text{SSM}}$) is calculated which leads to a list of estimates $2\hat{\sigma}^2_j$ with $j \in [1, N]$ the ping index. Finally, the backscattering strengths based on each descriptors d are estimated by averaging the estimates $2\hat{\sigma}^2_j$ over the ping as, respectively, in equations 6.37, 6.38, 6.39, and 6.40. This can be summed up as [Mopin et al., 2021]:

$$\begin{array}{r} \text{Ping 1: } |\mathbf{A}|_1 \sim \mathcal{R}(\sigma^2) \\ \vdots \\ \text{Ping } j\text{: } |\mathbf{A}|_j \sim \mathcal{R}(\sigma^2) \\ \vdots \\ \text{Ping } N\text{: } |\mathbf{A}|_N \sim \mathcal{R}(\sigma^2) \end{array} \left.\begin{array}{c} \begin{pmatrix} x_{11} & \cdots & x_{n1} \\ \cdots & \cdots & \cdots \\ x_{1j} & x_{ij} & x_{nj} \\ \cdots & \cdots & \cdots \\ x_{1N} & \cdots & x_{nN} \end{pmatrix} \\ \end{array}\right. \begin{array}{c} \longrightarrow \\ \longrightarrow \\ \longrightarrow \\ \longrightarrow \\ \longrightarrow \end{array} \left.\begin{array}{c} 2\hat{\sigma}^2_1 \\ \vdots \\ \vdots \\ \vdots \\ 2\hat{\sigma}^2_N \end{array}\right\} \rightarrow \langle\widehat{\text{bs}}\rangle_d = \frac{1}{N}\sum_{j=1}^{N} 2\hat{\sigma}^2_{j,d}$$

This scheme only illustrates the backscattering estimation for a given number of time-samples n taken into account. As an example, figure 6.6 shows the four resulting $\widehat{\mathrm{BS}}_d = 10\log_{10}\left(\langle\widehat{\mathrm{bs}}\rangle_d\right)$ in function of the number of pings for $n = 200$. We can observe at first that the BS estimator based on the maximum descriptor is biased, as expected from the results on the previous section. The three others are unbiased. In addition, we can observe that whatever the descriptor used, $\widehat{\mathrm{BS}}$ is variable for a small number of pings taken into account. However, they finally converge to an asymptotic value for large N.

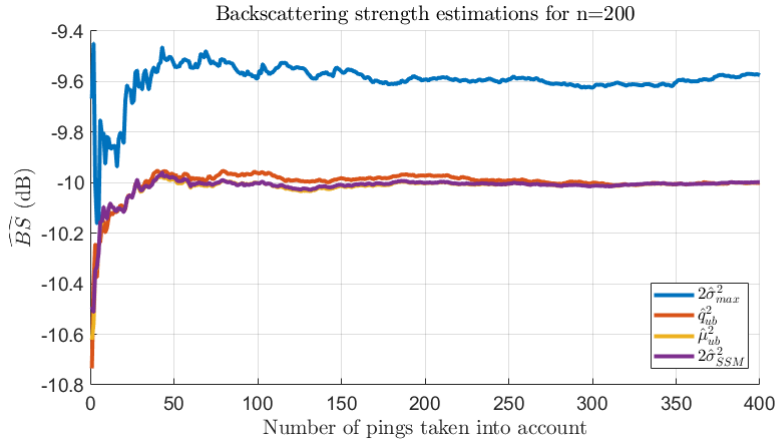

Figure 6.6 – Backscattering strength estimates $\widehat{\mathrm{BS}}_d$ based on each descriptor d in function of the number of pings taken into account: $\widehat{\mathrm{BS}}_{\max}$, $\widehat{\mathrm{BS}}_{\mathrm{med}}$, $\widehat{\mathrm{BS}}_{\mathrm{mean}}$, and $\widehat{\mathrm{BS}}_{\mathrm{SSM}}$. The number of time-samples taken into account is fixed at $n = 200$. Theoretical backscattering strength is $\mathrm{BS}_{\mathrm{th}} = 10\log_{10}\left(2\sigma^2_{\mathrm{th}}\right) = -10\mathrm{dB}$.

In order to analyse the estimators according to the number of pings and also the number of time-samples taken into account, $\langle\widehat{\mathrm{bs}}\rangle_d$ are derived in function of these two parameters. The results are therefore matrix of estimates $\langle\widehat{\mathrm{bs}}\rangle_{ij,d}$ for each descriptor d. It can be represented as:

$$\begin{array}{l} \text{Ping 1: } |\mathbf{A}|_1 \sim \mathcal{R}(\sigma^2) \\ \vdots \\ \text{Ping } j\text{: } |\mathbf{A}|_j \sim \mathcal{R}(\sigma^2) \\ \vdots \\ \text{Ping } N\text{: } |\mathbf{A}|_N \sim \mathcal{R}(\sigma^2) \end{array} \begin{pmatrix} x_{11} & \cdots & x_{n1} \\ \cdots & \cdots & \cdots \\ x_{1j} & x_{ij} & x_{nj} \\ \cdots & \cdots & \cdots \\ x_{1N} & \cdots & x_{nN} \end{pmatrix} \begin{array}{c} \longrightarrow \\ \longrightarrow \\ \longrightarrow \\ \longrightarrow \\ \longrightarrow \end{array} \begin{array}{c} 2\hat{\sigma}^2_1 \\ \vdots \\ \vdots \\ \vdots \\ 2\hat{\sigma}^2_N \end{array} \Bigg\} \rightarrow \begin{pmatrix} \langle\widehat{\mathrm{bs}}\rangle_{11,d} & \cdots & \langle\widehat{\mathrm{bs}}\rangle_{n1,d} \\ \cdots & \cdots & \cdots \\ \langle\widehat{\mathrm{bs}}\rangle_{1j,d} & \langle\widehat{\mathrm{bs}}\rangle_{ij,d} & \langle\widehat{\mathrm{bs}}\rangle_{nj,d} \\ \cdots & \cdots & \cdots \\ \langle\widehat{\mathrm{bs}}\rangle_{1N,d} & \cdots & \langle\widehat{\mathrm{bs}}\rangle_{nN,d} \end{pmatrix}$$

In the first part of this section, the four estimators $\widehat{\mathrm{BS}}_d$ are compared based on the behaviour according to n and N of their expected values and variances. The latter are estimated as the sample mean and the sample variance and called computed expected value and computed variance. From the results of this part, the best backscattering strength estimator is identified and analytical results are derived for it in the second part.

6.2.1 Comparison of the estimators based on their computed expected values and variances

In order to process the computed expected value and variance of the four backscattering strength estimators, the generation of the matrix $\langle\widehat{\mathrm{bs}}\rangle_{ij,d}$ is made 300 times. A matrix of computed expected values is then calculated as the sample mean of $\langle\widehat{\mathrm{bs}}\rangle_{ij,d}$ over 300 realizations. The same way, a matrix of the computed variances is calculated as the sample variance of $\langle\widehat{\mathrm{bs}}\rangle_{ij,d}$ over its 300 realizations. The resulting matrix are plotted as images according to the number of time-samples n and pings N taken into account with in color the $\widehat{\mathrm{BS}}_{ij,d}$ level in decibels (see figures 6.7 and 6.8).

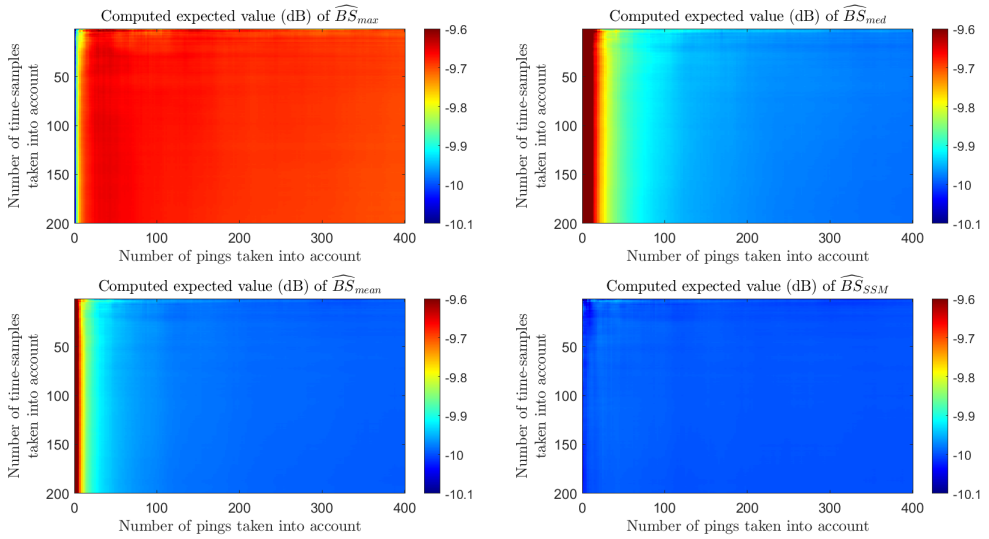

Figure 6.7 – Computed expected values of backscattering strength estimators $\widehat{\mathrm{BS}}_d = 10\log_{10}\left(\langle\widehat{\mathrm{bs}}\rangle_d\right)$ according to the number of time-samples and pings taken into account for each descriptor d: $\widehat{\mathrm{BS}}_{\mathrm{max}}$, $\widehat{\mathrm{BS}}_{\mathrm{med}}$, $\widehat{\mathrm{BS}}_{\mathrm{mean}}$, $\widehat{\mathrm{BS}}_{\mathrm{SSM}}$. Theoretical backscattering strength is $\mathrm{BS}_{\mathrm{th}} = 10\log_{10}\left(2\sigma_{\mathrm{th}}^2\right) = -10\mathrm{dB}$. Simulations of 300 realizations of $\widehat{\mathrm{BS}}_d$ are generated.

Results of the computed expected values of the four estimators are given figure 6.7. We can observe that, as expected from the previous results, $\widehat{\mathrm{BS}}_{\mathrm{max}}$ is biased when it reaches its asymptote. In this case, the computed expected value of $\widehat{\mathrm{BS}}_{\mathrm{SSM}}$ is the closest to the theoretical value $\mathrm{BS}_{\mathrm{th}} = -10\mathrm{dB}$. For three of the estimators ($\widehat{\mathrm{BS}}_{\mathrm{max}}$, $\widehat{\mathrm{BS}}_{\mathrm{med}}$, $\widehat{\mathrm{BS}}_{\mathrm{mean}}$), the computed expected values have observable variabilities for small number of time-samples and small numbers of pings. However, the number of ping (x-axis) has a higher impact on them than the number of time-samples, especially for the two estimators $\widehat{\mathrm{BS}}_{\mathrm{med}}$ and $\widehat{\mathrm{BS}}_{\mathrm{mean}}$. The number of ping used to estimate the $\widehat{\mathrm{BS}}_{\mathrm{max}}$, $\widehat{\mathrm{BS}}_{\mathrm{med}}$, and $\widehat{\mathrm{BS}}_{\mathrm{mean}}$ can therefore be interpreted as a main parameter in their process. In particular it affect their estimation values, especially when this number is small. On the contrary, the estimator $\widehat{\mathrm{BS}}_{\mathrm{SSM}}$ seems to have a computed expected value nearly constant and close to the theoretical value whatever the number of time-samples or pings.

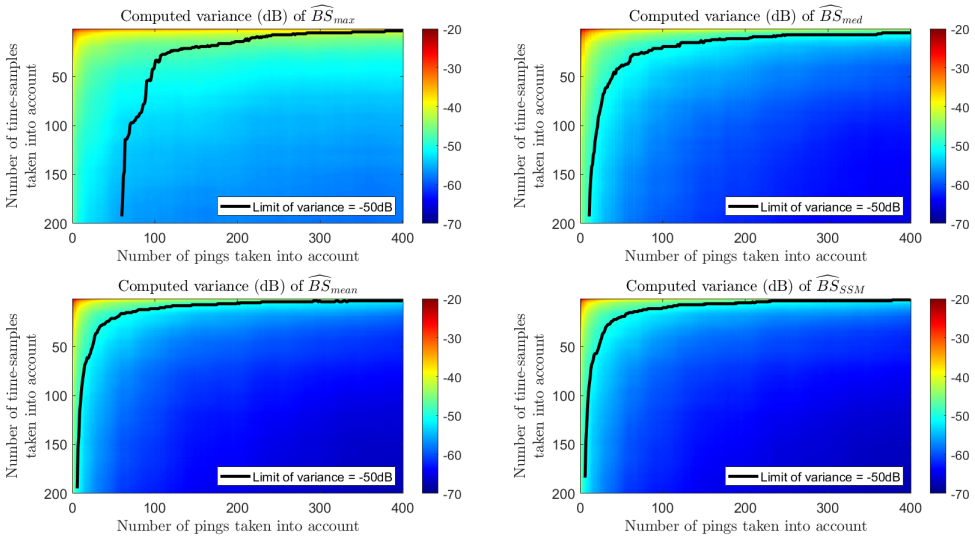

Figure 6.8 – Computed variances of backscattering strength estimators $\widehat{\mathrm{BS}}_d = 10\log_{10}\left(\langle\widehat{\mathrm{bs}}\rangle_d\right)$ according to the number of time-samples and pings taken into account for each descriptor d: $\widehat{\mathrm{BS}}_{\mathrm{max}}$, $\widehat{\mathrm{BS}}_{\mathrm{med}}$, $\widehat{\mathrm{BS}}_{\mathrm{mean}}$, $\widehat{\mathrm{BS}}_{\mathrm{SSM}}$. The black curve corresponds to the limit where the computed variance is equal to $-50\,\mathrm{dB}$. Simulations of 300 realizations of $\widehat{\mathrm{BS}}_d$ a generated.

Computed variances of the four estimators are given figure 6.8 according to the number of time-samples n and pings N taken into account. Even if their levels are not exactly the same, their variations are similar according to n and N. This variations seem also symmetrical as a function of n or N. We can also observe that computed variances are higher for small n or N which means that the number of time-samples and pings used to estimate the backscattering as an impact on its variability.

In order to compare the speed of convergence of the estimators, in figure 6.8 are added black curves corresponding to the limit where the computed variances are equal to the arbitrary values of $-50\,\mathrm{dB}$. Under these curves (i.e. on the bottom right of the images), computed variances are guaranteed to be less than $-50\,\mathrm{dB}$. On this figure we can observe that for the estimator $\widehat{\mathrm{BS}}_{\mathrm{max}}$, more time-samples and pings are necessary to use in order for its computed variance to reach the value of $-50\,\mathrm{dB}$ than for the other estimators. The comparison is specified by plotting the four curves on a single graph. Results are given figure 6.9. It shows that the fastest BS estimator to reach a computed variance of $-50\,\mathrm{dB}$ are $\widehat{\mathrm{BS}}_{\mathrm{mean}}$ and $\widehat{\mathrm{BS}}_{\mathrm{SSM}}$ with identical curves. They need less time-samples or pings to reach this variance. On the contrary, the estimator $\widehat{\mathrm{BS}}_{\mathrm{max}}$ is, as expected, the slower to converge. In other words, these curves can be interpreted as limits of the number of time-samples and pings necessary to use in order to obtain a backscattering strength estimate with a chosen variability of $-50\,\mathrm{dB}$.

Some key values of the results of figure 6.7 and 6.8 are given in table 6.4. In this table, results of the computed expected values are presented as bias of the estimate i.e. as the difference between the computed value and the theoretical backscattering strength $\mathrm{BS}_{\mathrm{th}} = -10\,\mathrm{dB}$ used for the simulation. From this table we can retrieve previous results such as that

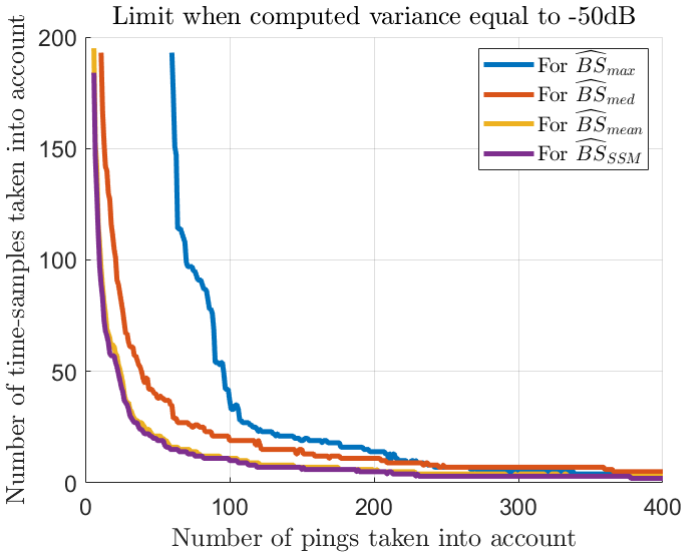

Figure 6.9 – Limits at $-50\,\mathrm{dB}$ of computed variances of backscattering strength estimates $\widehat{\mathrm{BS}}_d = 10\log_{10}\left(\langle\widehat{\mathrm{bs}}\rangle_d\right)$ according to the number of time-samples and number of pings taken into account for each descriptor d: $\widehat{\mathrm{BS}}_{\mathrm{max}}$, $\widehat{\mathrm{BS}}_{\mathrm{med}}$, $\widehat{\mathrm{BS}}_{\mathrm{mean}}$, $\widehat{\mathrm{BS}}_{\mathrm{SSM}}$. Simulation of 300 realizations of $\widehat{\mathrm{BS}}$ are generated.

Name of the descriptors d estimators are based on	Estimators	Bias estimation (dB) $\widehat{\mathrm{BS}}_d(n,N) - \mathrm{BS}_{\mathrm{th}}$		Variance estimation (dB)	
		n=5	n=200	n=5	n=200
		N=5	N=400	n=5	N=400
Maximum m	$\widehat{\mathrm{BS}}_{\mathrm{max}}$	0.1 dB	0.3 dB	-33.7 dB	-58.4 dB
Median q	$\widehat{\mathrm{BS}}_{\mathrm{med}}$	0.7 dB	0.0 dB*	-30.8 dB	-65.2 dB
Sample mean μ	$\widehat{\mathrm{BS}}_{\mathrm{mean}}$	0.3 dB	0.0 dB*	-33.6 dB	-67.8 dB
Square sample mean r	$\widehat{\mathrm{BS}}_{\mathrm{SSM}}$	0.0 dB*	0.0 dB*	-34.8 dB	-68.1 dB

Table 6.4 – Summary of the estimators of BS analysed in section 6.2.1. Bias are estimated comparing the computed expected value of estimates for small ($n = 5$, $N = 5$) and a large ($n = 200$, $N = 400$) number of time-samples and pings to the theoretical backscattering strength $\mathrm{BS}_{\mathrm{th}}$. Computed variances are estimated for same arbitrary numbers of time-samples. All estimations are made by generating 300 realizations of the group of N pings. (*: bias are not perfectly equal to zero in simulations but are less than the tenth of decibels which is rounded to 0.0 dB.)

$\widehat{\mathrm{BS}}_{\mathrm{max}}$ is in effect a biased estimator, and that for small number of time-samples and pings $\widehat{\mathrm{BS}}_{\mathrm{med}}$ has the higher computed variance. We can also identify the best estimator as $\widehat{\mathrm{BS}}_{\mathrm{SSM}}$ as it has the lower computed variances for small and high number of time-samples and pings, and a high speed of convergence (for $n, N = 5$ its computed bias is already close to null), and it is unbiased.

6.2.2 Analytical results

Four backscattering strength estimators $\widehat{\mathrm{BS}}_d$ have been compared in this section based on their computed expected values and computed variances. It was shown that in term of computed variance and computed uncertainties two estimators are equally identified as the best: $\widehat{\mathrm{BS}}_{\mathrm{mean}}$ and $\widehat{\mathrm{BS}}_{\mathrm{SSM}}$. Results of the comparison of their computed expected values makes possible to separate the two. Indeed, $\widehat{\mathrm{BS}}_{\mathrm{mean}}$ is not accurate for small numbers of pings of time-samples therefore it is set aside. Consequently, the best estimator is therefore identified as $\widehat{\mathrm{BS}}_{\mathrm{SSM}}$. In this section, an analytical analysis of this best estimator is made. Its variance is demonstrated to be a function of the number of time-samples n and pings N taken into account.

We demonstrated in section 6.1.1 that the random variable $\widehat{\mathbf{bs}}_{\mathrm{SSM}} = 2\hat{\boldsymbol{\sigma}}^2_{\mathrm{SSM}}$ follows a gamma distribution of parameter n and $\frac{2\sigma^2}{n}$ (see equation 6.23). Consequently, the backscattering strength $\langle\widehat{\mathbf{bs}}\rangle_{\mathrm{SSM}}$ which is processed in practice as the sample mean of N realisations of $2\hat{\boldsymbol{\sigma}}^2_{\mathrm{SSM}}$ is also following a gamma distribution as:

$$\langle\widehat{\mathbf{bs}}\rangle_{\mathrm{SSM}} \sim \frac{1}{N}\gamma\left(nN, \frac{2\sigma^2}{n}\right) \sim \gamma\left(nN, \frac{2\sigma^2}{nN}\right) \tag{6.41}$$

The expected value of $\langle\widehat{\mathbf{bs}}\rangle_{\mathrm{SSM}}$ is then:

$$\mathrm{E}\left[\langle\widehat{\mathbf{bs}}\rangle_{\mathrm{SSM}}\right] = \mathrm{E}\left[\gamma\left(nN, \frac{2\sigma^2}{nN}\right)\right] = 2\sigma^2 \tag{6.42}$$

The expected value of $\langle\widehat{\mathbf{bs}}\rangle_{\mathrm{SSM}}$ is therefore two times the Rayleigh parameter $2\sigma^2$ which is the parameter of interest. This estimator is consequently unbiased, as expected from the previous results.

The variance of $\langle\widehat{\mathbf{bs}}\rangle_{\mathrm{SSM}}$ can also be derived from equation 6.41 as:

$$\mathrm{var}\left[\langle\widehat{\mathbf{bs}}\rangle_{\mathrm{SSM}}\right] = \mathrm{var}\left[\gamma\left(nN, \frac{2\sigma^2}{nN}\right)\right] = \frac{(2\sigma^2)^2}{nN} \tag{6.43}$$

From this result we can see that the variance of the backscattering estimator depends on the number of time-samples n and pings N in the same manner. The behaviour of the variance is therefore symmetrical in n and N as observed in section 6.2.1. This analytical result is compared to the simulation result of figure 6.8 by plotting n as a function of N and the variance for an arbitrary value of $-50\,\mathrm{dB}$ and a theoretical backscattering strength of -10 dB in figure 6.10 with the computed variance curve for this same values. We can observe that the two curves match perfectly, which allows to validate the simulation and analytical results.

6.3 Backscattering strength uncertainty

In practice, a useful criterion describing the accuracy of the seafloor acoustic response measurement is its uncertainty. It includes the uncertainties of all the parameters appearing

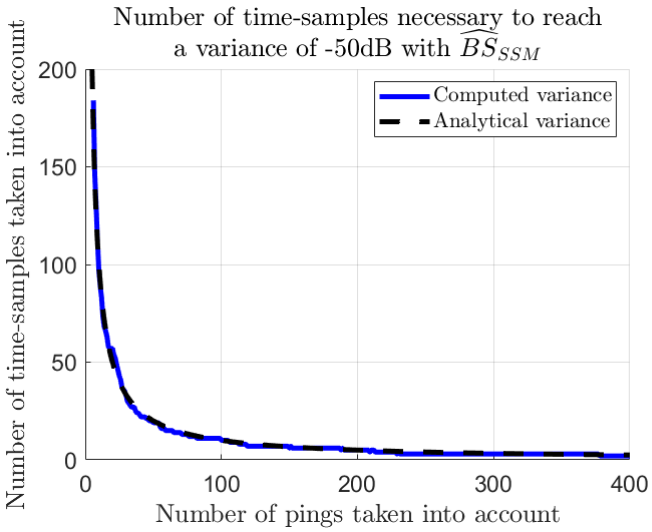

Figure 6.10 – Analytical and computed limits at $-50\,\mathrm{dB}$ of the variance of the best backscattering strength estimator $\widehat{\mathrm{BS}}_{\mathrm{SSM}}]$ according to the number of time-samples and pings taken into account. From simulations of 300 realizations of $\langle\widehat{\mathbf{bs}}\rangle_{\mathrm{SSM}}$.

in the sonar equation as described in [Malik et al., 2018] in addition to the intrinsic uncertainty of the backscattering strength. In this part of the PhD, sonar equation parameters are supposed constant and perfectly known so that we can study the intrinsic uncertainty of the backscattering strength estimation. In this section, only this uncertainty is discussed and an analytical model is derived to calculate its values for the best backscattering strength estimator.

In the following, the uncertainty of the backscattering strength estimate $\langle\widehat{\mathbf{bs}}\rangle$ is given in decibels and noted $T[\langle\widehat{\mathbf{bs}}\rangle]$ where $\langle\widehat{\mathbf{bs}}\rangle$ is processed as the sample mean of N realizations of the random variable $\widehat{\mathbf{bs}}$ i.e. the sample mean of N backscattering strengths estimated from N different pings. The uncertainty can be calculated as shown in [Taraldsen et al., 2015] and [Malik et al., 2018] from the expected value and the variance of $\langle\widehat{\mathbf{bs}}\rangle$ as:

$$T[\langle\widehat{\mathbf{bs}}\rangle] = 10\log_{10}\left(1+\frac{\sqrt{\mathrm{var}\left[\langle\widehat{\mathbf{bs}}\rangle\right]}}{\mathrm{E}\left[\langle\widehat{\mathbf{bs}}\rangle\right]}\right) \tag{6.44}$$

This definition corresponds to the variation (taken as the standard deviation) from the expected value in the positive side i.e.:

$$T[\langle\widehat{\mathbf{bs}}\rangle] = 10\log_{10}\left(\mathrm{E}\left[\langle\widehat{\mathbf{bs}}\rangle\right]+\sqrt{\mathrm{var}\left[\langle\widehat{\mathbf{bs}}\rangle\right]}\right) - 10\log_{10}\left(\mathrm{E}\left[\langle\widehat{\mathbf{bs}}\rangle\right]\right) \tag{6.45}$$

On the other side of the expected value, the uncertainty can therefore be defined as:

$$T_{-}[\langle\widehat{\mathbf{bs}}\rangle] = 10\log_{10}\left(1-\frac{\sqrt{\mathrm{var}\left[\langle\widehat{\mathbf{bs}}\rangle\right]}}{\mathrm{E}\left[\langle\widehat{\mathbf{bs}}\rangle\right]}\right) \tag{6.46}$$

In the following, only $T[\langle\widehat{\mathbf{bs}}\rangle]$ is discussed, but the same calculations can be applied to $T_{-}[\langle\widehat{\mathbf{bs}}\rangle]$ [1].

6.3.1 Uncertainty analytical model for the best backscattering strength estimator

From equation 6.44, computed uncertainties can be simulated using the computed expected values and variances of section 6.2.1 according to the number of time-samples n and pings N. Results are given in figure 6.11 for 300 realizations generated. On the figure, a black curve is also plotted, representing the limit where the computed uncertainty is equal to 0.1 dB. We can observe from these results that the computed uncertainty seems to vary symmetrically in n and N.

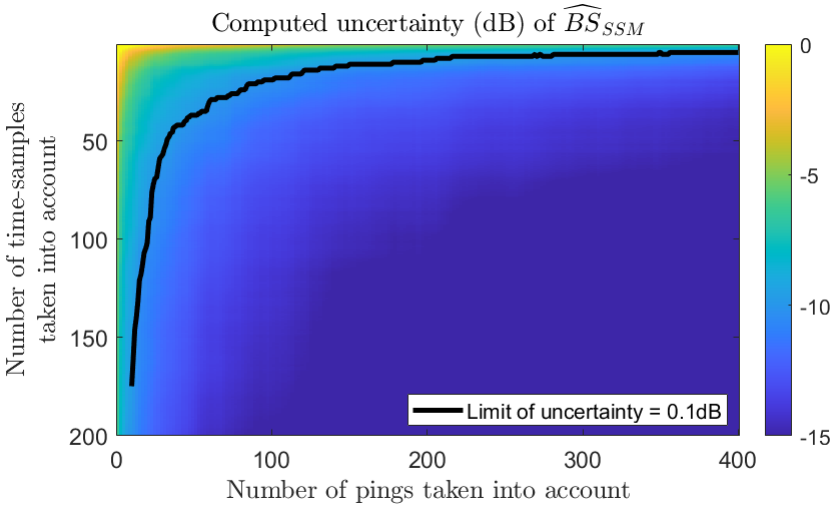

Figure 6.11 – Computed uncertainties of backscattering strength estimates $\widehat{\mathrm{BS}}_{\mathrm{SSM}} = 10\log_{10}\left(\langle\widehat{\mathrm{bs}}\rangle_{\mathrm{SSM}}\right)$ according to the number of time-samples and pings taken into account. The black curves correspond to the limit where the computed uncertainties are equal to 0.1 dB. Simulations of 300 realizations of $\widehat{\mathrm{BS}}_{\mathrm{SSM}}$ are generated.

In addition, the uncertainty of the best estimate $\widehat{BS}_{\mathrm{SSM}}$ can also be derived analytically from equation 6.44 and the previous analytical results (see equations 6.42 and 6.43) as [Mopin

1. Note that the standard deviation is a symmetrical tool that is used here on an asymmetrical distribution (see equation 6.41). The question of a different tool to describe the variability in such distributions can consequently be of interest in future works.

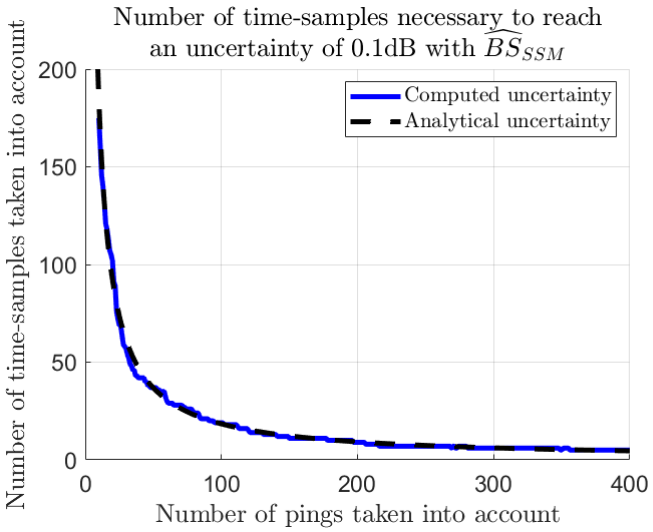

Figure 6.12 – Analytical and simulated limits at 0.1 dB of backscattering strength estimate uncertainty $T[\langle\widehat{\mathbf{bs}}\rangle_{\mathrm{SSM}}]$ according to the number of time-samples and pings taken into account. From simulation of 300 realizations of $\langle\widehat{\mathbf{bs}}\rangle_{\mathrm{SSM}}$.

et al., 2021]:

$$\begin{aligned} T[\langle\widehat{\mathbf{bs}}\rangle_{\mathrm{SSM}}] &= 10\log_{10}\left(1+\frac{\sqrt{\mathrm{var}\left[\langle\widehat{\mathbf{bs}}\rangle_{\mathrm{SSM}}\right]}}{\mathrm{E}\left[\langle\widehat{\mathbf{bs}}\rangle_{\mathrm{SSM}}\right]}\right) \\ &= 10\log_{10}\left(1+\sqrt{\frac{(\sigma^2)^2}{nN}}\frac{1}{\sigma^2}\right) \\ T[\langle\widehat{\mathbf{bs}}\rangle_{\mathrm{SSM}}] &= 10\log_{10}\left(1+\frac{1}{\sqrt{nN}}\right) \end{aligned} \tag{6.47}$$

The uncertainty of the estimate $\widehat{BS}_{\mathrm{SSM}}$ consequently depends only on the number of time-samples and pings taken into account. Equation 6.47 also validate that the impact of these numbers on the resulting uncertainty is symmetrical. This analytical result can be also compared to the simulation results of figure 6.11 by plotting n as a function of N and the uncertainty for an arbitrary value of 0.1 dB and for a theoretical backscattering strength of -10dB with the computed uncertainty curve for this same values. Results are given figure 6.12. The two curves appear to match perfectly, so the calculation of the uncertainty is validated.

6.3.2 Look-up tables of backscattering strength uncertainty

Equation 6.47 can be seen as an analytical formulation of the uncertainty of the best backscattering strength estimate $\widehat{\mathrm{BS}}_{\mathrm{SSM}}$. This formulation can be useful, for example, to calculate uncertainties obtained when using a certain number of time-samples n or pings N to estimate the backscattering strength of an homogeneous seafloor. In practice, this corresponds

to an *a priori* uncertainty of the measurement. As examples, some theoretical uncertainty values are calculated and shown figure 6.13 according to N and for $n = [1, 5, 10, 100]$.

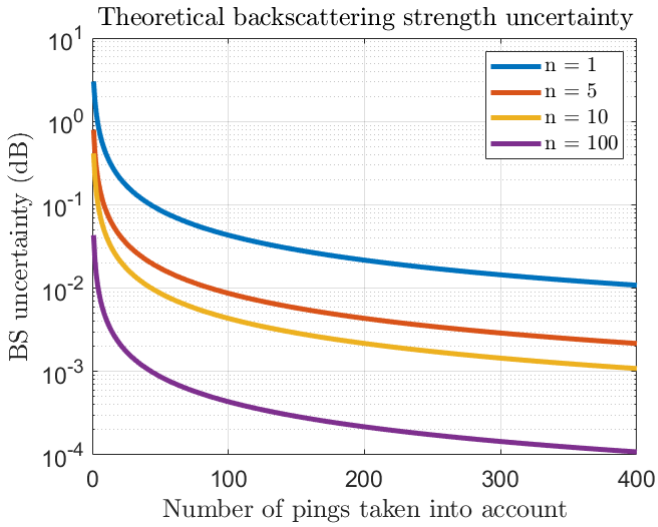

Figure 6.13 – Theoretical uncertainty of the best backscattering strength estimate $T[\langle\widehat{\mathbf{bs}}\rangle_{\mathrm{SSM}}]$ according to the number of time-samples and pings taken into account. From analytical formula 6.47.

Instead of calculating uncertainty values from given number of time-samples and pings, the formulation of equation 6.47 can be used to calculate the minimum number of time-samples or pings necessary to reach a certain value of uncertainty. In other words, it does not need more than the recommended couple of values (n, N) to reach a desired value of uncertainty. Once a level of uncertainty is identified by the user, the design of the survey can therefore be corrected in order to full-fill the recommendation of n and N values.

In this context, a look up table of resulting uncertainty values for the best backscattering estimate $T[\langle\widehat{\mathbf{bs}}\rangle_{\mathrm{SSM}}]$ is generated and shown figure 6.14 [Mopin et al., 2021]. On the one hand, it can be used to estimate the uncertainty level that can be obtain with the number of available time-samples and pings. In the other hand, the look-up table can be used to define the number of time-samples and pings necessary to reach a certain level of uncertainty. As examples, some values are presented in figure 6.14 e.g. when $n = 4$ and $N = 4$ the uncertainty level is $T = 1\,\mathrm{dB}$, and if an uncertainty level of $0.1\,\mathrm{dB}$ is required then $(n = 43, N = 43)$ is an example of couple of time-samples and pings that can be used. If the number of time-samples is not available, the number of pings can be increased and inversely.

On the look-up table of figure 6.14, particular values of the backscattering strength uncertainty are plotted: $T = [0.1, 0.2, 0.3, 0.4, 0.5, 1, 2]\,\mathrm{dB}$. An uncertainty level of $1\,\mathrm{dB}$ is considered by [Lucieer et al., 2018] to be the necessary order of magnitude for a measurement of the backscattering strength in the context of sediment discrimination with multibeam echosounders. The smaller value $0.1\,\mathrm{dB}$ corresponds to the level of uncertainty classified by [Malik et al., 2018] as negligible in the context of backscattering strength measurements with

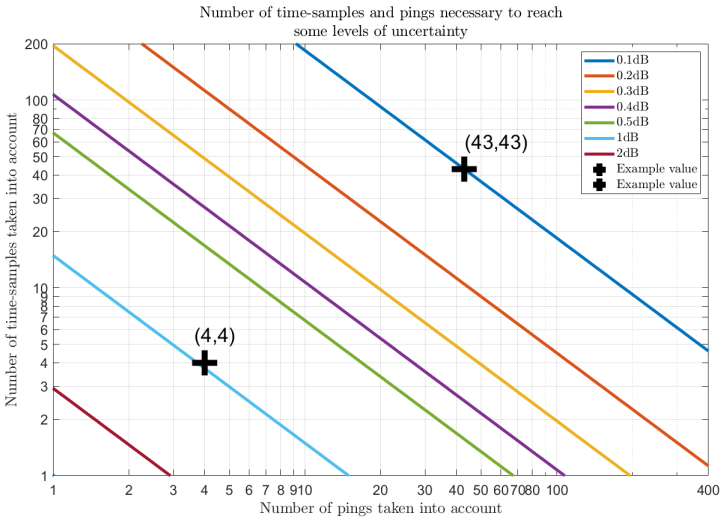

Figure 6.14 – Look-up table of particular values of uncertainty of the best backscattering strength estimate $T[\langle\widehat{\mathbf{bs}}\rangle_{\mathrm{SSM}}]$ according to the number of time-samples and pings taken into account. Calculated from the analytical formula of equation 6.47.

multibeam echosounder. In this paper, a level of uncertainty of 1 dB is considered by the authors as small, and 2 dB as moderate. The maximum uncertainty level that can be obtained theoretically is when only one ping and one time-samples are available i.e. $n = 1$ and $N = 1$ so that $T = 3.0\,\mathrm{dB}$.

We remind that the uncertainty levels discussed in this section are only valid when the formulation of equation 6.47 is valid i.e. for the best estimator of the backscattering strength $\widehat{\mathrm{BS}}_{\mathrm{SSM}}$ in the ideal case where the sonar equation parameters are perfectly known and the corrected time-samples magnitudes are realizations of a Rayleigh distribution.

6.3.3 Application to echosounders survey

As discussed in the previous section, the uncertainty theoretical formulation of equation 6.47 can be used to calculate the *a priori* uncertainty of a backscattering measurement knowing the number of time-samples and pings that are used to estimate the backscattering strength (in the case of the best estimator). Inversely, it can also be used to design the survey in order to maintain a given level of uncertainty by anticipating the number of time-samples and pings that will be used to estimate the backscattering strength. In this section, these two methods are discussed in the context of echosounders surveys as examples of applications of the uncertainty formulation.

In order to use the uncertainty formulation, the conditions of the backscattering measurement should respect the hypotheses under which it is valid i.e. [Mopin et al., 2021]:

- **Random nature of the seafloor**: the seafloor have to be rough to ensure that a signal is backscattered to the echosounder, and also in a stochastic point of view that the received signal magnitudes are realizations of a random variable.

- **Sonar equation perfectly corrected**: sonar equations parameters have to be perfectly known in order to correct the recorded time-samples magnitudes.
- **Rayleigh distribution**: the number of scatterers inside the instantaneous insonified area $\mathcal{A}$ have to be enough for the central limit theorem to be valid (see section 5.1.1). This ensures the corrected time-samples magnitudes to be realizations of a Rayleigh distribution. The number of scatterer can be controlled by the size of the echosounder beam footprint using the pulse length and the beam aperture.
- **Independent time-samples magnitudes**: the corrected time-samples magnitudes have to be independent realizations of the Rayleigh distributions.
- **Identically distributed time-samples magnitudes**: the corrected time-samples magnitudes have to be realizations of the same Rayleigh distributions.
- **Homogeneous seafloor**: recorded data of all pings have to be measured on the same type i.e. the corrected time-samples magnitudes have to be realizations of the same Rayleigh distribution.
- **Using the best** BS **estimator**: the uncertainty formation of equation 6.47 is only valid for the best estimator of the backscattering strength i.e. the square sample mean of the corrected times-samples magnitudes.

6.3.3.1 Singlebeam echosounder

In this section two manufactured singlebeam echosounders are chosen as an example to apply the theoretical formulation of the uncertainty: Kongsberg EA400 mainly used for bathymetry, and Simrad EK60 mainly used for fishery. These echosounders were also discussed in section 3.1.3.

The echosounder Kongsberg EA400 is generally mounted under the survey vessel toward the nadir i.e. the incident angle of the transmitted signal on a supposed flat seafloor is 0°. The echosounder detects the seafloor echo on the maximum of the received magnitudes. From this detection, the sounding is processed and associated to a received power value. The backscattering strength level $\mathrm{BS}_{\mathrm{EA400}}$ is calculated from this value using the sonar equation of equation 3.19. One value is provided for each ping and is computed using only one time-sample of the seafloor echo which corresponds to the maximum of the received power P_{Rx}. Consequently, in these conditions, whatever the depth or the slope of the seafloor, the number of time-sample used to derive the backscattering strength is $n = 1$ and the number of ping is $N = 1$. It leads to a theoretical uncertainty of $T_{\mathrm{EA400}} = 3.0\,\mathrm{dB}$. Consequently, without further processing of the data provided by Kongsberg EA400, the resulting backscattering strength (theoretical) uncertainty level is therefore a constant of 3.0 dB. This result can be enhance by averaging several pings values. However, the strong hypothesis of homogeneous seafloor should be respected i.e. every pings averaged should be supposed recorded on the same seafloor type.

The same result is obtained using Simrad EK60 if only the backscattering strength of the sounding is of interest. However, this echosounder provides the entire list of time-samples of each pings (from transmission at $t = 0$ to the range adjusted by the user) and also the list of target positions inside the beam corresponding to every time-samples. All time-samples

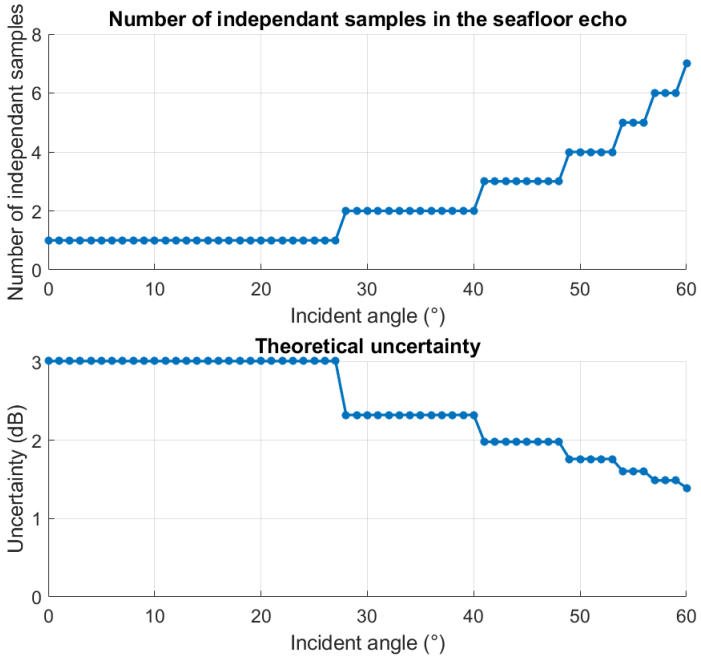

Figure 6.15 – Simulation of Simrad EK60 beam footprint geometry at 200 kHz with a pulse length of 256μs and for a depth of 20 m. The number of ping is $N = 1$. Up: Number of time-samples independent inside $\pm 1°$ in the beam according to the incident angle on the seafloor. Down: Theoretical uncertainty of the best backscattering strength estimate $T[\langle \widehat{\mathbf{bs}} \rangle_{\mathrm{SSM}}]$ according to incident angle on the seafloor. From analytical formula 6.47.

of the seafloor echo are then available and they can be corrected from the sonar equation parameter using equation 3.23. In order respect the independence hypothesis of the time-samples, they cannot be all retained. They are therefore taken every pulse length so that there is no overlap in the consecutive instantaneous insonified areas (see details in section 8.3.1). Depending on the beam aperture of the echosounder, the pulse length, the depth and the seafloor slope (i.e. the incidence angle on the seafloor) the seafloor echo length varies and consequently the number of independent time-samples changes. This leads to different uncertainty level according to these parameters. A simulation of the number of independent time-samples that are obtained according to the incident angle on the seafloor was made to give an idea of the magnitude of the uncertainties obtained with EK60 in survey conditions. The choice of the parameters is based on [Eleftherakis et al., 2018] where the authors used Simrad EK60 echosounder at 200 kHz with a pulse length of 256μs for incident angles from 0° to 60°. Effective beam apertures of the echosounder are given in the article as 5.6°x5.7° and the mean depth of the survey is given as 20 m. In this article, the authors decided to process the backscattering strength using time-samples that corresponds to angles close to the beam axis i.e. less than $\pm 1°$ (see section 4.3.1). In the simulation, we take these boundaries to limit the number of seafloor echo time-samples used. Results of the simulation are given figure 6.15 using one ping i.e. $N = 1$ and for different pointing angles. We can observe that for incident angles lower than 28° only one independent time-sample can be available due to the geometry of acquisition, leading to the maximum uncertainty. But when the incident angle

increases, the beam footprint increases leading to much independent time-samples and lower uncertainty levels.

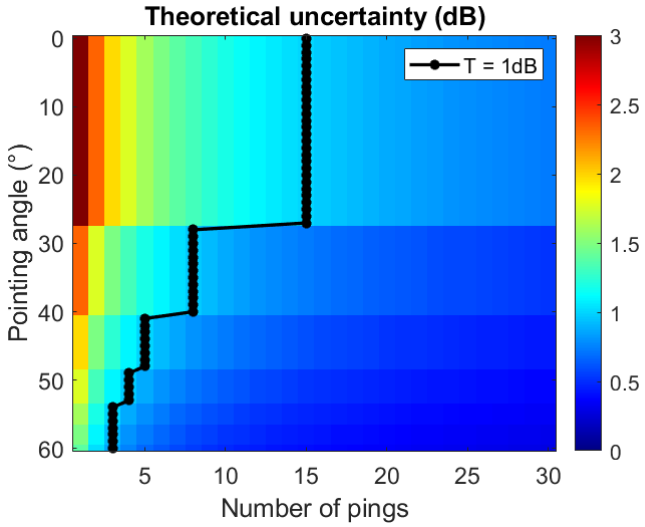

Figure 6.16 – Theoretical uncertainty of the best backscattering strength estimate $T[\langle\widehat{\mathbf{bs}}\rangle_{\mathrm{SSM}}]$ according to incident angle on the seafloor and the number of pings taken into account to process the backscattering strengh. Black curve: limit where the uncertainty levels are equal to 1.0 dB. Simulation of Simrad EK60 beam footprint geometry at 200 kHz with a pulse length of 256μs and for a depth of 20 m. Using analytical formula 6.47.

The results of figure 6.15 are given when only one ping is used to process the backscattering strength. Nevertheless, several pings can be used supposing they are recorded on the same seafloor type. The simulation is then run to give examples of uncertainty levels obtained with Simrad EK60 under the same conditions described above and according to the number of pings taken into account. The results are shown in figure 6.16 as an image where color are uncertainty level in decibels according to the number of pings and the incident angle on the seafloor (i.e. the number of time-samples). As expected we can observe the decrease of the uncertainty level when pings are added. The black curve is the limit where the uncertainty levels are equal to 1.0 dB which is the limit between small and moderated uncertainty according to [Malik et al., 2018]. At near-nadir incidence angles, 15 pings are necessary to reach this level of uncertainty, whereas at 60° only three pings are necessary. In this latter case, the hypothesis of homogeneous seafloor during three pings is easier to suppose.

In conclusion, using singlebeam echosounders data without any further processing leads to a constant theoretical uncertainty level associated to the backscattering strength measurement of 3.0 dB. However, this result can be improved by using more than one ping data to estimate the backscattering strength. In addition, when the echosounder provided enough information to correct the sonar equation parameters, more time-samples are also available which also lead to a decrease of the uncertainty level of the measurements.

6.3.3.2 Multibeam echosounder

In this section data from a multibeam echosounder survey are chosen as an example to apply the theoretical formulation of the uncertainty. One line of a survey made with Kongsberg EM300 is extracted from the project CALIMERO [2] carried out by Ifremer and Shom between 2004 and 2006. Acquisitions were made in the Gulf of Lion in the North-Western part of the Western Mediterranean basin (France).

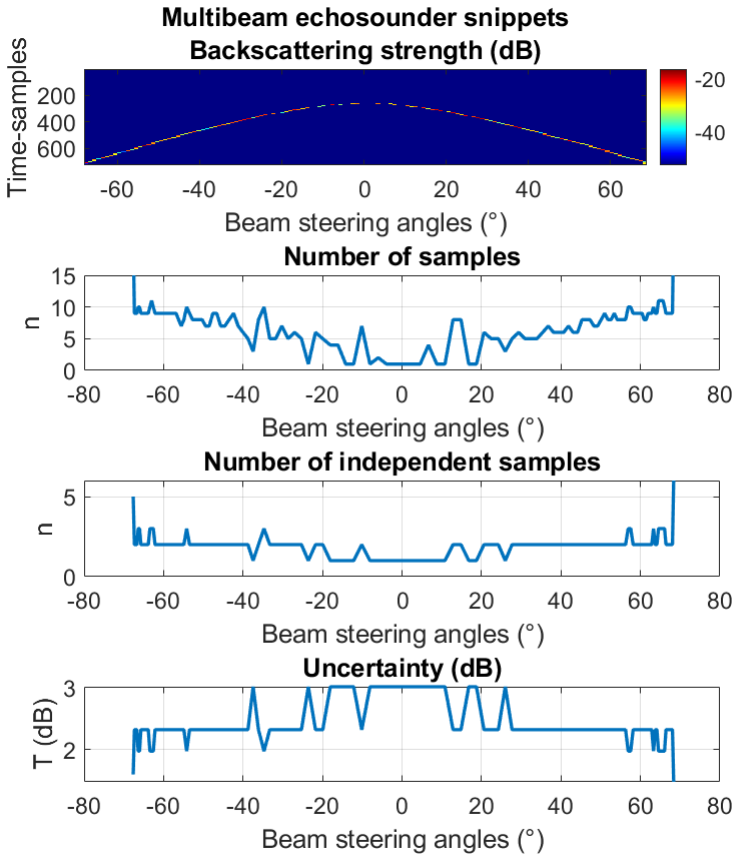

Figure 6.17 – Data from Kongsberg EM300 for one ping. Up: snippets of seafloor echoes recorded in the data given in backscattering strength values for each beam. Second: Number of time-samples inside each beam snippet. Third: number of independent time-samples inside each beam. Down: theoretical uncertainty calculated from analytical formula 6.47.

The survey line chosen as example is composed of more than 7000 pings and corresponds to a mainly flat seafloor of mean depth 45 m. The multibeam echosounder transmitted 135 beams at steering angles ±70°. The pulse length is 1 ms at 30 kHz and the beams aperture is 2°. In the data provided by Kongsberg EM300, corrected time-samples magnitudes of the seafloor echoes are available for every beams. They are given as backscattering strength

2. Details of the project are available in [Augris Claude, 2013] and on `https://doi.org/10.18142/180`.

values in decibels. Only a certain number of time-samples of the seafloor echo are retained in the data which are generally called snippets [Innangi et al., 2015]. The upper graph of figure 6.17 shows these data for one ping. The echosounder algorithm uses these data to compute a backscattering strength value per beam which is associated to the sounding. In each beam a given number of time-samples are therefore available. For the ping data of the example these numbers are shown on the second graph of figure 6.17. In order to compute the uncertainty levels that could correspond to each beam, the time-samples have to respect the independence hypothesis. Therefore, only time-samples separated by the pulse length are retained. The number of remaining time-samples for each beam in given in the third graph of figure 6.17. The associated uncertainty can therefore be obtained. Results are given in the lower graph of figure 6.17. We can observe that the number of independent time-samples is low, mostly due the combination of the narrow beam width and the shallow depths of the survey. Consequently, the resulting uncertainty levels are mainly between 2 dB and 3 dB.

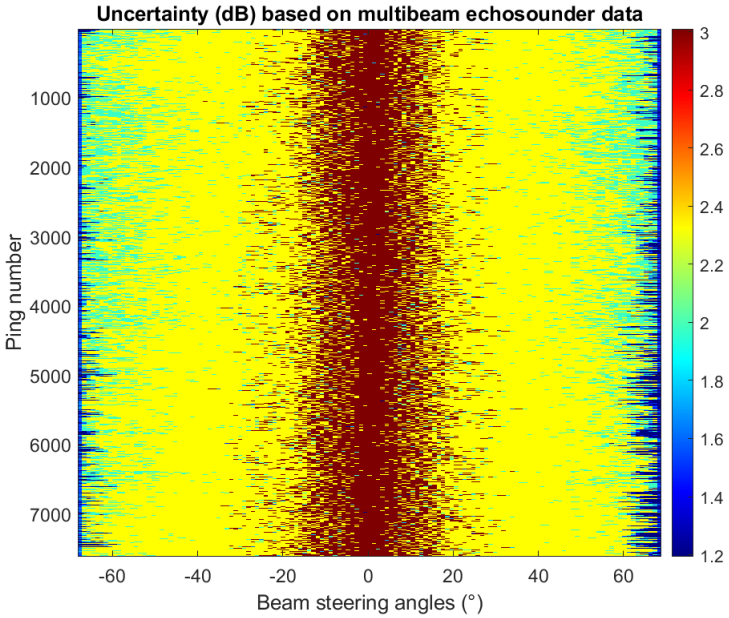

Figure 6.18 – Uncertainty levels calculated from analytical formula 6.47 based on a survey line data of Kongsberg EM300.

The previous result for one ping can be apply to each ping of the survey line chosen as example. For each ping and each beam, an uncertainty level is therefore calculated from the number of independent samples available in the snippets data. The results are given figure 6.18. We retrieve the behaviour observed for one ping i.e. the uncertainty level is close to 3 dB at nadir, and decreases with incident angles. In the conditions of the survey, when using only one ping to calculate the backscattering strength, the uncertainty levels is also observed to never decrease under 1 dB.

A solution to reduce these uncertainty levels is to use several pings to compute the backscattering strength. Based on the data given in figure 6.18 and using the uncertainty formulation

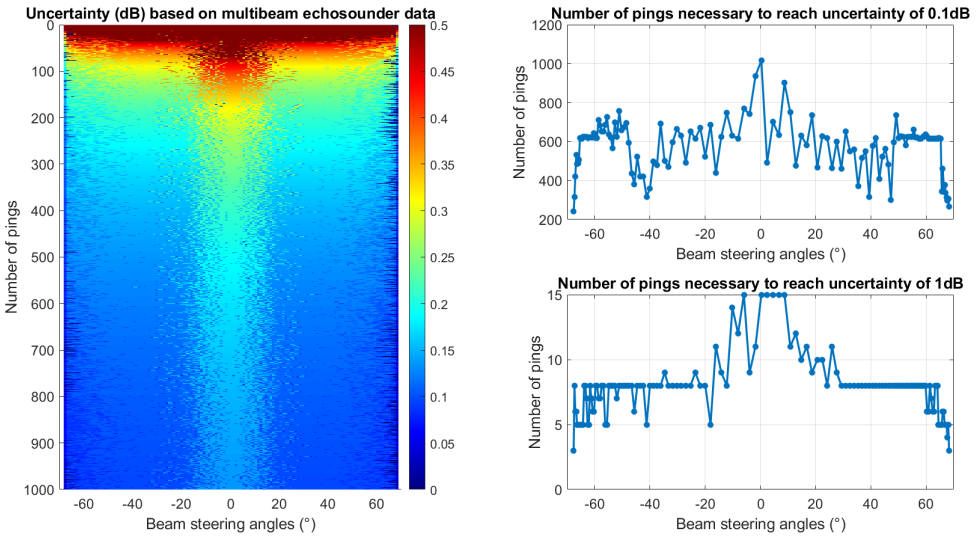

Figure 6.19 – Number of pings necessary to use in order to obtain an uncertainty level of 0.1 dB or 1 dB according to the beam. Based on the number of time-samples of all ping of Kongsberg EM300 data (see figure 6.18). From analytical formula 6.47.

of equation 6.47, the number of pings necessary to reach uncertainty levels of 0.1 dB and 1 dB are calculated for each beam. Results are given in figure 6.19. On the left the uncertainty levels are plotted as an image according to pings and beams. On the right the number of pings necessary to reach 0.1 dB or 1 dB are plotted, they are calculated from the results of the left. As expected, we can observe that the number of pings necessary to reach any of the desired uncertainty levels are higher for near-nadir beams and decreases almost by a factor two for grazing angle beams. Consequently, if these number of pings are used to compute a backscattering strength for example for a digital terrain model (DTM) cell, the resolution of the DTM will be twice lower where measurements are made with near-nadir beams than for other beams. However, the uncertainty level will be ensured constant for all cells of the DTM.

Supposing that the survey is designed so that the beam footprints are contiguous at their -3 dB aperture projection on the seafloor. In the condition of the example survey, pings are therefore spaced by 1.6 m. In order to reach an uncertainty level of 1 dB, 15 pings are necessary to use at nadir (see figure 6.19). They represent a travelled distance of $\sim$ 25 m. However, in order to reach 0.1 dB, 1000 pings are necessary at nadir that represent 1.6 km. In the first case, we can suppose that the seafloor stay homogeneous over 25 m, but in the second case this hypothesis is harder to validate (see section 4.2.2). This result brings to light the compromise that has to be made between the improvement of the uncertainty level and the validity of the fundamental hypothesis of an homogeneous seafloor when dealing with survey data. In this context, a solution to enhance the uncertainty level could be to increase the number of independent time-samples per pings and beams. It implies to choose one or a mix of the two compromises below:

- Decreasing the pulse length: with a smaller pulse length the number of independent

time-samples will increase. However, the hypothesis of a Rayleigh distribution could be at stake because the instantaneous insonified area will decrease which may lead to an insufficient number of scatterers to validate the central limit theorem.

- Increasing the beam aperture: with a larger beam aperture the number of independent time-samples will also increase. However, the hypothesis of an identical Rayleigh distribution for every corrected time-samples magnitudes could be at stake because of the intrinsic variations of the backscattering strength according to angles.

In literature, some recommendations on the number of time-samples and pings to use can be found such as [Eleftherakis et al., 2018] who recommends to retain only time-samples that correspond to a incidence angle of the seafloor of $\pm 1°$ around the sounding (i.e. the center of the beam) and prescribe to use several hundreds of pings (from the same homogenenous seafloor) to estimate the backscattering strength. In another example, [Zhang et al., 2020] assume that the homogeneity of the seafloor on a half-swath of a multibeam echosounder is valid and that several tens of consecutive pings can be supposed to come from the same seafloor type.

6.4 Summary

The aim of this chapter was to compare different methods of estimation of the seafloor acoustic response in order to define which one is the best. Ten estimators were derived based on the four methods of reduction of the information contained in the seafloor echo discussed in the previous chapter. Comparisons were made by simulating corrected time-samples magnitudes as realizations of the same Rayleigh distribution of parameter σ^2. Backscattering strengths were estimated from these realizations based on the bathymetric process described in chapter 5 and represented mathematically by equation 6.2. Criteria of comparison of the estimators are the evolution of their bias and variances according to the number of time-samples and pings taken into account, and their speed of convergence to their expected value.

The ten estimators were analysed in section 6.1. They are based on four descriptors used in literature to reduce the seafloor echo information to a single value: the maximum of the corrected time-samples magnitudes, their median, their sample mean and their square sample mean. In this section, the best estimators of the backscattering strength when using one ping information were identified for each of these descriptors. They are respectively the maximum likelihood estimate of the maximum descriptor distribution $2\hat{\sigma}^2_{\max}$, the unbiased estimate based on the median $\hat{q}^2_{\text{ub}}$, the unbiased estimate based on the samples mean $\hat{\mu}^2_{\text{ub}}$, and the maximum likelihood estimate of the square sample mean descriptor distribution $2\hat{\sigma}^2_{\text{SSM}}$. The latter is also equivalent to the raw descriptor square sample mean $\hat{r}$ and equal to two times the maximum likelihood estimate (MLE) of the Rayleigh distribution parameter. These four estimators were then compared and the best of them was identified based on them expected values and variances (simulated and calculated analytically). It is identified as $2\hat{\sigma}^2_{\text{SSM}}$ i.e. the square sample mean of the corrected time-samples magnitudes. Section 6.1.4.2 demonstrated analytically that this estimator is unbiased and efficient.

In section 6.2, the four estimators of the backscattering strength were derived and compared according to the number time-samples available in a ping but also according to the number of pings available. Based on their computed expected values and variances the best estimator was identified as the square sample mean of the corrected time-samples magnitudes x_{ij} i.e.:

$$\widehat{\mathrm{BS}} = 10\log_{10}\left(\frac{1}{N}\sum_{j=1}^{N} 2\hat{\sigma}^2_{j,\mathrm{SSM}}\right) = 10\log_{10}\left(\frac{1}{nN}\sum_{i=1,j=1}^{n,N} x_{ij}^2\right) \tag{6.48}$$

with i the position of the time-samples in the ping j, n the total number of time-samples available in a ping, and N the number of pings available on the same type of seafloor. This result was expected as the estimator found is twice the maximum likelihood estimate of the Rayleigh distribution parameter which is known as the best estimator of this parameter. Its expected value was calculated as $2\sigma^2$ (see equation 6.42) which was demonstrated to be the definition of the seafloor response therefore the estimator is unbiased. Its variance was calculated as $(2\sigma^2)^2/(nN)$ (see equation 6.43) therefore the variability of the backscattering strength estimate depends on the number of time-samples and pings that are used.

Based on the analytical results of the two first sections, the uncertainty $T_{\widehat{\mathrm{BS}}}$ associated to the best seafloor response estimate was derived analytically in section 6.3 as (in decibels):

$$T_{\widehat{\mathrm{BS}}} = 10\log_{10}\left(1 + \frac{1}{\sqrt{nN}}\right) \tag{6.49}$$

It is therefore only dependent of the number of time-samples n and pings N used in the estimation. Based on this formulation, look-up tables of the uncertainty levels that can be reached according to n and N were processed (see section 6.3.2). They can be used to predict uncertainties that could be obtained during a survey knowing the number of time-samples and pings available on a seafloor region supposed homogeneous. Inversely, they can also be used to maintain a desired uncertainty by calculating the necessary numbers n or N.

Examples of practical uses of the theoretical uncertainty formulation were given in section 6.3.3 in the case of singlebeam and multibeam echosounder surveys. The discussion was based on concrete echosounder parameters and data (Kongsberg EA400, Simrad EK60, and Kongsberg EM300). It was shown that without postprocessing of the data provided by the echosounders the uncertainty levels are generally the higher (3 dB). When post-processing is employed i.e. several time-samples and/or pings are used, this uncertainty level can easily decreased to 1 dB. In order to improve again this value, some compromises have to be made that involve modifications in the echosounder parameters such as the beam apertures and pulse lengths.

All these results are given for the best backscattering strength estimator which is the square sample mean of the corrected time-samples magnitudes. When this estimate is not available, the others can nevertheless be used while being aware that they will not reach the lowest variance and uncertainty and that some of them are biased especially for small number of time-samples and pings.

Conclusion

In this second part of the manuscript, an accurate method of estimating the seafloor acoustic response from single- or multi-beam echosounder data was derived. At first, the definition of the backscattering strength discussed in the first part was refined based on a point-scattering model. This model allowed us to establish a backscattering strength data processing in a stochastic context and also to develop methods of estimation. Ten estimators were analysed based on four methods of reduction of the seafloor echo information. They were compared based on their bias, variances and speed of convergence. From the tens, one estimator was identified as the best estimator of the seafloor response. It is unbiased, has the lower variance and the fastest speed of convergence. For this estimator, an analytical formulation of the uncertainty level associated to the estimation was calculated. Examples of use of this formulation were given based on concrete echosounder data.

The definition of the backscattering strength and of its estimators was derived under specific hypotheses that are listed below:

- Rough seafloor: the seafloor is supposed rough to ensure that the received signal magnitudes are realizations of a random variable.
- Sonar equation perfectly corrected: sonar equations parameters are supposed perfectly known. The recorded time-samples magnitudes are consequently perfectly corrected.
- No other variabilities: only the intrinsic variability of the seafloor response is taken into account. Other variabilities are neglected.
- Rayleigh distribution: the corrected time-samples magnitudes are supposed to be realizations of a Rayleigh distribution.
- Independent time-samples magnitudes: the corrected time-samples magnitudes have to be independent realizations of the Rayleigh distributions.
- Identically distributed time-samples magnitudes: the corrected time-samples magnitudes have to be realizations of the same Rayleigh distributions of parameter σ^2.
- Homogeneous seafloor: recorded data of all pings have to be measured on the same type of seabed i.e. the corrected time-samples magnitudes have to be realizations of the same Rayleigh distribution.

To ensure the corrected time-samples magnitudes to be realizations of a Rayleigh distribution, the number of scatterers inside the instantaneous insonified area $\mathcal{A}$ is assumed large enough for the central limit theorem to be valid (see section 5.1.1). This hypothesis implies specific

characteristics of the echosounder that can be obtained using one or both of the following conditions:

- Large beam aperture
- Long pulse length i.e. narrow band

In addition, the scatterers have to be unrelated and independent, the scattering strengths of the scatterers should bear no relation to their phases and be identically distributed, the scatterers phases should be uniformly distributed on the interval $[-\pi, \pi]$.

Under all these conditions, the backscattering strength was demonstrated analytically to be equal (in expected value) to two times the Rayleigh parameter $2\sigma^2$. σ^2 corresponds to the variance of the real and imaginary parts of the complex backscattering index amplitude which is linked to the number of scatterers in the instantaneous insonified area $\mathcal{A}$ (see equation 5.33). The backscattering strength, or seafloor acoustic response, is therefore directly related to the materials (scatterers index) composing the seafloor and its roughness (scatterers phases).

From this definition and in the context of a bathymetric survey (see figures 4.4 and 4.5), ten estimators of the backscattering strength were compared. The are based on four methods of reduction of the seafloor echo information: the maximum of the corrected time-samples magnitudes, their median, their sample mean and their square sample mean. From these ten estimators, one was identified as the best estimator because it is unbiased, it has the lower variance and it has the faster speed of convergence. This estimator is the square samples mean of the corrected time-samples samples over the number of time-samples in the seafloor echo and the number of pings (see equation 6.48). This result was expected because this estimator is also two times the maximum likelihood estimate of the Rayleigh distribution parameter. It is also efficient.

Based on the analytical formulation of the best estimator of the seafloor response, an analytical formulation of the uncertainty associated to its measurement was derived (see equation 6.49). It showed that the intrinsic uncertainty of the backscattering strength measurement, i.e. the intrinsic variability of the seafloor response, only depends on the number of time-samples and pings used. From this formulation, look-up tables were computed to quantify the uncertainty level obtained with survey data or inversely to adapt the survey according to the uncertainty level desired. Examples were given on survey data from singlebeam echosounders (Kongsberg EA400, Simrad EK60) and multibem echosounder (Kongsberg EM300). The analysis of the uncertainty according to these concrete data sets brings to light that the condition of independence of the time-samples to process the backscattering strength and thus the uncertainty has a major impact on the results. Indeed, the number of time-samples that can be used depends directly on the beam aperture and the pulse length, and the number of pings that can be used depends on the spatial variability of the seafloor. Consequently, a compromise has to be made between these parameters in order to process accurately the seafloor acoustic response.

Part III

Application of the seabed acoustic response estimation method

Preamble

In the two first part of this manuscript an accurate definition of the seafloor acoustic response was established and its best estimator was identified based on simulation of backscattering strength data and analytical calculation. In addition, a formulation of the uncertainty of a backscattering measurement was derived analytically. The aim of this last part of the PhD is to evaluate in practice these theoretical results using singlebeam echosounder data.

One of the main hypotheses made to ensure the calculation of the backscattering strength estimate is that sonar equation parameters are perfectly known and the data perfectly corrected from them. In order to be the closest to this condition, a split-beam singlebeam echosounder was designed and manufactured during the PhD. This way, a precise control of all the system internal parts is available, making possible a rigorous calibration. It also give access to real received data at high sampling frequency i.e. amplitudes and phases of the received signal. The first chapter of this part of the manuscript describes the design and manufacture of the echosounder, its specificities, and its calibration.

In this part of the PhD, the sonar equation employed to measure in practice the backscattering strength BS is based on the theoretical equation 3.10 and inspired from the practical equations 3.19 and 3.23. A calibration gain G_{calib} is added to equation 3.10 to account for the system particularities as:

$$\text{BS} = EL - SL - DI_{\text{Tx}} + 2TL - 10\log_{10}(\mathcal{A}) - G_{\text{calib}} \tag{6.50}$$

where EL is the seafloor echo level received by the echosounder, SL the source level, DI_{Tx} is the directivity index on the echosounder antenna at transmission, TL the transmission loss, and $\mathcal{A}$ the intantaneous insonified area. Among these parameters, some are specific to the echosounder and are constant (e.g. SL, DI_{Tx}, G_{calib}). The objective of the first chapter of this part of the manuscript is to measure precisely these parameters so the backscattering strength measurements of the second chapter could be accurate. Chapter 7 therefore presents the calibration of the echosounder which implies different methods of measurement (e.g. standard hydrophone, calibration sphere, etc.).

It was discussed in section 4.2.4 that the instantaneous insonified area $\mathcal{A}$ is a complex quantity to correct in practice. Indeed, even with splitbeam echosounders, a bias remains when using models of insonified area because of the geometry of acquisition. Consequently, to better correct this parameter, a simulation of the instantaneous insonified area is processed

based on the characteristics of the echosounder measured in the first chapter of this part. This simulation is presented in the second chapter of this part. It gives more precise values of the instantaneous insonified areas with the assumption of a flat seabed.

Besides the system parameters, the sonar equation contains environment parameters (in TL) such as the sound absorption in the sea water that impact backscattering strength measurements. In this part, these environment parameters are measured with dedicated probes in order to be corrected as accurately as possible.

In chapter 8, backscattering strength are computed as the square sample means of the corrected time-samples magnitudes recorded by the echosounder. The bathymetric-like process discussed in the previous part is employed. Different incident angles on the seafloor are reached by tilting the echosounder mechanically. Measurements are made at the University of Bath (United Kingdom) in a fresh water-filled tank with sediments in the bottom, at ENSTA Bretagne (France) in a fresh water-filled tank, and in the harbour of Brest (France) in sea water.

Chapter 7

Design and manufacture of a singlebeam and splitbeam echosounder

In order to correct as precisely as possible sonar equation parameters to estimate accurately the seafloor acoustic response, the system employed should be fully controlled. The objective of this chapter is therefore to develop a singlebeam echosounder that provides perfectly calibrated raw data i.e. an echosounder which characteristics are perfectly known and which raw data are available.

In the first section, the constraints applying on the manufacture of the echosounder are evaluated. They lead to a theoretical design of the system. After manufacturing, measurements of the echosounder characteristics allowed to refine the theoretical calculations. The results are discussed in the second section of this chapter. Finally, the last section present the method of calibration of the echosounder and the resulting characteristics of the system.

7.1 Constraints and dimensioning

We choose to manufacture a singlebeam echosounder that could be titled mechanically at different incidence angles on the seafloor. This echosounder should have the ability to be split-beam i.e. to deliver target position inside its main beam (such as Simrad EK60, see section 3.1.3). Consequently it should be composed of at least four transducers allowing interferometry in both axis of the echosounder. In order to decrease the secondary lobes levels, the system is designed monostatic i.e. the transducers are used as transmitters and also receivers.

The design of the echosounder has to respect two main constraints in the context of the PhD:

1. Transduction should be made with piezoelectric ceramics available at Sorbonne Université (France) which resonate around 100 kHz [Ollivier, 1995].
2. The echosounder should be able to be used in the tank of the university of Bath (United Kingdom) which is 1.50m x 5.0m with 1.40m of water depth above sediments on its floor [Blondel and Pace, 2005] (see figure 7.2).

From the first constraint, the choice of a transmitted frequency of $\mathfrak{f} = 100\,\text{kHz}$ is made as the efficiency of the transducers are better close to their resonance. The second constraint impacts the size of the antenna because measurements have also to respect the far field condition (see section 3.2.1). Therefore the far field distance has to be shorter than the depth of the tank, i.e. with L the size of the antenna, and $\lambda = c/f = 1.5.10^{-2}\text{m}$ the wavelength where $c = 1500\text{m/s}$ is the sound speed in water:

$$\frac{L^2}{\lambda} < 1.4 \Leftrightarrow L < 14\text{cm} \tag{7.1}$$

Consequently, the size of the echosounder antenna cannot exceed 14cm.

7.1.1 Size of the echosounder antenna

The echosounder antenna should be composed of four independent transducers to ensure that interferometry can be process (split-beam) in both axes. A square shape was chosen for the antenna with four square transducers (see figure 7.1).

The transduction is made using piezoelectricity. The piezoelectric ceramics available for the PhD are small cylinders of composite-PZT (lead zirconate titanate) of diameter approximately 8mm. Their polarization and electric field directions are both along their axis, which give a piezoelectric coefficient noted d_{33} in the literature [Rathod, 2020]. Transducers are mounted in the piezocomposite configuration 1-3 connectivity [Bowen et al., 1996] which corresponds to rows of d_{33} piezoelectric cylinders aligned as a matrix. To respect equation 7.1, six rows of height cylinders are juxtaposed to form a transducer of 55mm x 55mm. For mounting purpose, small wedges are added between the row of cylinders. They also ensure the transmitter/receiver face to be a square. A diagram of the antenna is shown figure 7.1. The final size of the antenna speaking area is 110mm x 110mm.

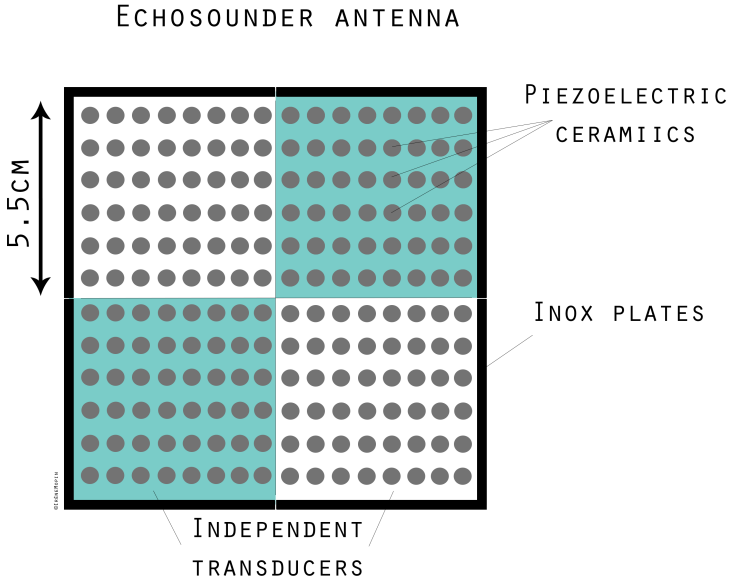

Figure 7.1 – Diagram of the echosounder split-beam antenna.

The theoretical far field range of the antenna is therefore:

$$r_{\text{Far field}} = \frac{L^2}{\lambda} = \frac{(11.10^{-2})^2}{1500/100.10^3} = 81\text{cm} \tag{7.2}$$

7.1.2 Theoretical aperture of the echosounder

In order to evaluate the seabed acoustic response estimates defined in the previous parts of this manuscript, the echosounder is used on concrete seabed types in the harbour of Brest and also in the tank of the university of Bath (see chapter 8). In this tank, different sea sediments are disposed on the bottom as shown in figure 7.2): sand, silt, fine gravel and coarse gravel. In this conditions, in addition to the far field condition that constraints the size of the echosounder antenna for accurate measurements in the tank, another condition on the system geometry appears. The sediments are disposed in trays of 90cm long, consequently, when doing a measurement with the echosounder tilted, its aperture should not be too wide

in order to keep the main lobe on the sediment patch. This condition limits the size of the antenna or the altitude of the echosounder above the seafloor.

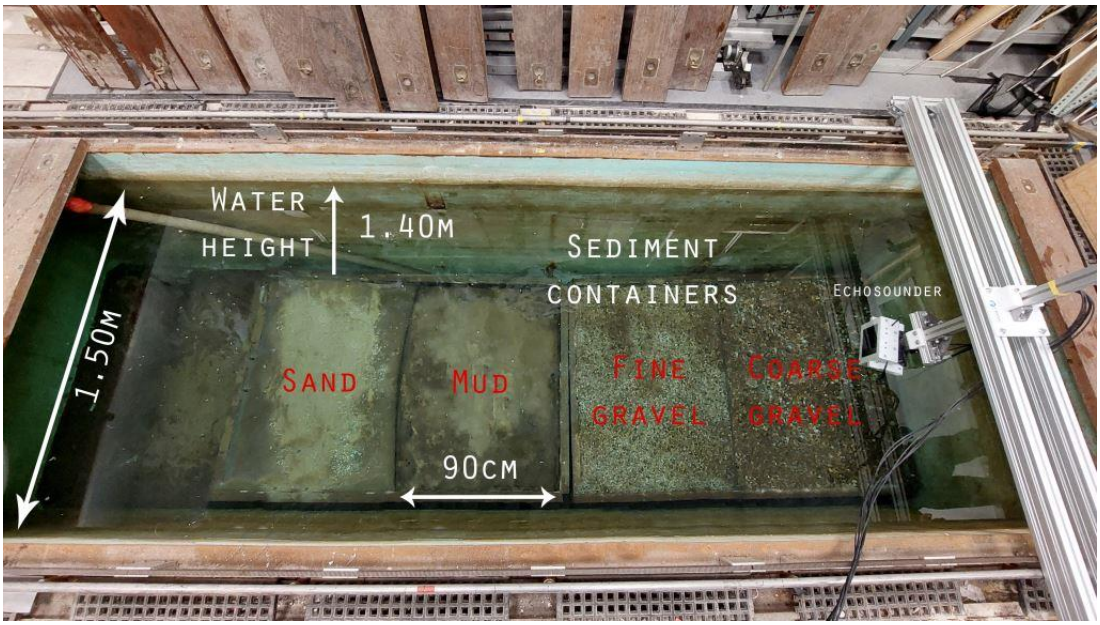

Figure 7.2 – Picture of the sediment trays on the bottom of the tank at the university of Bath (United Kingdom).

Considering the echosounder antenna as a square of size L, its two-way directivity function $\mathcal{D}(\vartheta)$ along one axis is theoretically:

$$D(\vartheta) = \left[\frac{\sin\left(\pi \frac{L}{\lambda} \sin\vartheta\right)}{\pi \frac{L}{\lambda} \sin\vartheta} \right]^4 \tag{7.3}$$

Its theoretical aperture at -3 dB $2\theta_{\text{-3dB}}$ in coupled transmission and reception can be approximated as:

$$2\theta_{\text{-3dB}} = 36.6 \frac{\lambda}{L} = 5.0° \tag{7.4}$$

The largest tilted angle used to measure seafloor response is chosen arbitrarily at 60°. At this angle the projection of the beam footprint of the echosounder (-3 dB aperture) for an altitude above the bottom of 1.4m is 48cm. Consequently, at this altitude, the echosounder beam footprint is ensured to remain inside one sediment tray.

However, in more details, attention could be brought on the entire main beam. Indeed, nulls of the directivity function of equation 7.3, also called directivity nodes, are found when $\sin\left(\pi \frac{L}{\lambda} \sin\vartheta\right) = 0$, i.e. when:

$$\pi \frac{L}{\lambda} \sin\vartheta = n\pi \text{ with } n \neq 0 \tag{7.5}$$

The first node of directivity is therefore positioned at $\sin\vartheta_{\text{null}} = \frac{\lambda}{L}$, i.e. $\vartheta_{\text{null}} = 7.8°$. This value can be also seen as the total width of the main beam of the enchosounder. At this angle, the projection of the total beam footprint $\pm 7.8°$ for an altitude above the bottom of 1.4m is 1.6m. Consequently, when the echosounder is placed at an altitude of 1.4m above the bottom of the tank of the university of Bath, the projection of the total main lobe of directivity exceeds the size of the sediment patch for a tilted angle of 60°. In practice (see chapter 8), the echosounder is placed at a lower altitude above the sediment (1m) to limit this effect while respecting the far field condition.

7.2 Manufacture

The objective of manufacturing an echosounder in this PhD is to be able to control the acquisition chain and specifically the process apply to the received acoustic signals. This way, we can better estimate the sonar equation parameters appearing in the calculation of the seafloor response and better correct the received data. In this section, the different parts composing the echosounder are presented in details.

In the following the echosounder is considered as a system divided in four parts illustrated in figure 7.3:

- **Transduction**: this part of the system transforms the electrical signal into acoustic waves in the medium and reciprocally transforms upcoming acoustic waves into electrical voltages. It is composed of an antenna made of four piezoelectric transducers that transmit acoustic pulses in the water and receive acoustic echoes from underwater targets;
- **Electronics**: the electronic part is the link between the transduction and the acquisition. Its aim is to condition the signals for transmission to the transducers (high voltages $\geq$ 60V) or for reception to the acquisition part (low voltage $\leq$ 1V). It is therefore composed of two separate electronic cards: one specific for transmission and and one specific for reception;
- **Acquisition**: the acquisition part is also separated for transmission and reception. At transmission the digital signal is transformed to analogous signal using the A/D converter, and reversely for reception.
- **Control**: this part of the echosounder corresponds to the user interface where all parameters (frequency, acquisition time, pulse length, etc.) are monitored and where the digital transmitted signal is generated.

In the first part of this manuscript we saw that the backscattering strength depends on the angle of incidence of the transmitted signal on the seafloor. In order to measure this behaviour, the singlebeam echosounder have to be tilted mechanically to reach those incident angles. An external system is used for this purpose. The system is called in the following a Pan & Tilt system (see figure 7.4). It was bought especially for the PhD and allows to tilt the echosounder from 0° to 60° in tank and at sea. A mount was designed at ENSTA Bretagne (France) to fix the square antenna on the Pan & Tilt system, as shown figure 7.4.

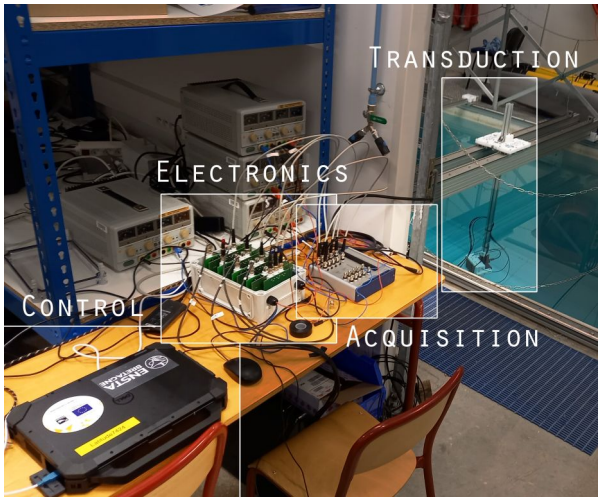

Figure 7.3 – Echosounder parts illustrated during measurements in the tank of ENSTA Bretagne: tranduction, acquisition, electronics and control (computer financially support by the European Union `www.europe.bzh`).

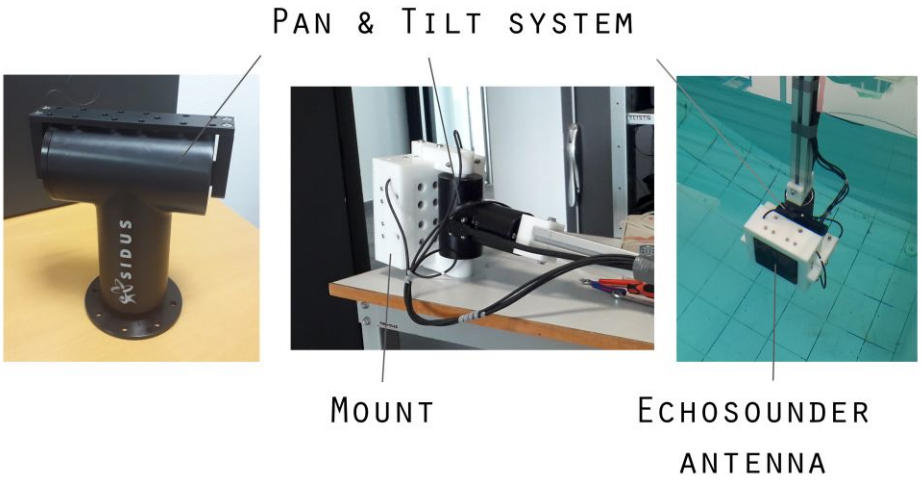

Figure 7.4 – Different views of the Pan & Tilt system, from SIDUS, used to rotate the single beam echosounder (financially support by the European Union `www.europe.bzh`) and the mount designed at ENSTA Bretagne (France) to support the antenna of the echosounder on the Pan&Tilt.

7.2.1 Transduction

As discussed in section 7.1, the echosounder antenna is composed of four square transducers that are made of small cylinders of composite-PZT. Figure 7.5 shows the components of one transducer. We can see on this picture the piezoelectric cylinders connected electrically and mounted on plexiglas matching layers. These layers are used to enhance the efficiency of the transducer when used in water. In effect, characteristic acoustic impedances of the piezoelectric ceramics are high therefore the transmission coefficient $T_{\mathrm{PZT/water}}$ between the

material and the sea water is low:

$$T_{\mathrm{PZT/water}} = \frac{4Z_{\mathrm{PZT}}Z_{\mathrm{water}}}{(Z_{\mathrm{PZT}} + Z_{\mathrm{water}})^2} = 24\% \tag{7.6}$$

with $Z_{\mathrm{water}} = 1.5\mathrm{MRayl}$ the characteristic impedance of the water, and $Z_{\mathrm{PZT}} = \rho c = 22\mathrm{MRayl}$ the characteristic impedance of the PZT [Sherman and Butler, 2007].

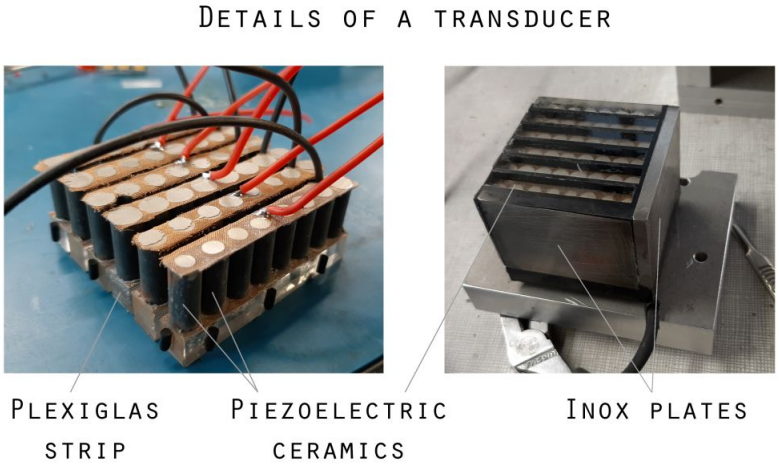

Figure 7.5 – Pictures of the composition of one transducer of the echosounder antenna. Piezoelectric ceramics are connected electrically, mounted on a plexiglas strip and positioned as a square. They are surrounded by inox plates to avoid transmission on the sides of the final antenna. (Photos: C. Ollivon, Institut Jean le Rond ∂'Alembert, France)

To prevent from this low transmission power, a solid material with a characteristic sound speed closer to the sound speed in water is added between the composite-PZT and the water [Ollivier, 1995]. This matching layer does not have any piezoelectric property and is tuned to the frequency of interest (100 kHz) with a thickness of $\lambda/4$. The material used is plexiglas. Compressional sound speed in it is 2690 m/s and its density is $1180\,\mathrm{kg/m^3}$ which gives a characteristic impedance of $Z_{\mathrm{Pl}} = 3\,\mathrm{MRayl}$. In these conditions, the transmission coefficient becomes:

$$T_{\mathrm{PZT/Pl/water}} = \frac{4Z_{\mathrm{PZT}}Z_{\mathrm{water}}}{\left(Z_{\mathrm{Pl}} + \frac{Z_{\mathrm{PZT}}Z_{\mathrm{water}}}{Z_{\mathrm{Pl}}}\right)^2} = 67\% \tag{7.7}$$

This way, the efficiency of the transducer at transmission is close to triple, and therefore so is the efficiency of the echosounder.

In addition to this impedance adaptation, metal plates in inox are added around the antenna to avoid transmission of acoustic signal on the side of the echosounder. Figure 7.5 shows this plates which are positioned on two faces of each transducers after the first moulding in order to surround the final antenna.

At the end, the ensemble of piezoelectric ceramics electrically connected, adaptive layers and inox plates is moulded in a resin acoustically neutral (polyurethane). It ensures the sealing of the transducer. For this operation a mould was specially designed in aluminium.

All transducers of the antenna were manufactured at Sorbonne University, Institut Jean le Rond ∂'Alembert (France).

7.2.2 Electronics

The electronic part of the echosounder is an important element because it represents the link between the transducers and the control panel though which the transmitted and received acoustic signals travel. Electronic components can therefore easily degrade these signals or add some undesired noise. A special attention is consequently given to this part.

A diagram of the electronic part of the echosounder manufactured during this PhD is given figure 7.6. For each of the four transducers, two cards are made: one for transmission and one for reception. Their roles are detailed in the following:

- **Transmission**: in order to transmit a sinusoidal signal at frequency $\mathfrak{f}$ and of length τ, a square signal is generated by the control panel and transmitted to the electronic card in charge of transmission. Before being delivered to the transducer this signal is amplified by a input voltage (60V in these works). Then the signal is transmitted to the transducer which acts as a filter, leading to a sinusoidal signal delivered in water.
- **Reception**: the acoustic signal received by the transducer is directly transmitted to the electronic card in charge of reception. It can be filtered and amplified as desired according to the measurement conditions. The signal is then transmitted to the acquisition part of the echosounder.

Because high voltage are transmitted to the transducer to have enough intensity to reach the seafloor, and on the contrary very low voltage are received, the reception part of the electronics is protected by a diode bridge as illustrated in figure 7.6.

These two cards are made for each transducer of the antenna, therefore height independent electronic cards are used for the echosounder. They were all designed and made at ENSTA Bretagne (France). They are shown in figure 7.3 in the resulting mounting.

7.2.3 Acquisition

The aim of the acquisition part of the echosounder is to link the analogous components (transduction and electronics) to the numerical component (control part). This transformation analogous/digital is made using a specific acquisition card specially bought at ENSTA Bretagne from National Instrument (NIUSB6366) according to the characteristics of the echosounder. This card is used at transmission to transform the digital pulse to an electrical signal (voltage variations) and at reception to record the received electrical signal.

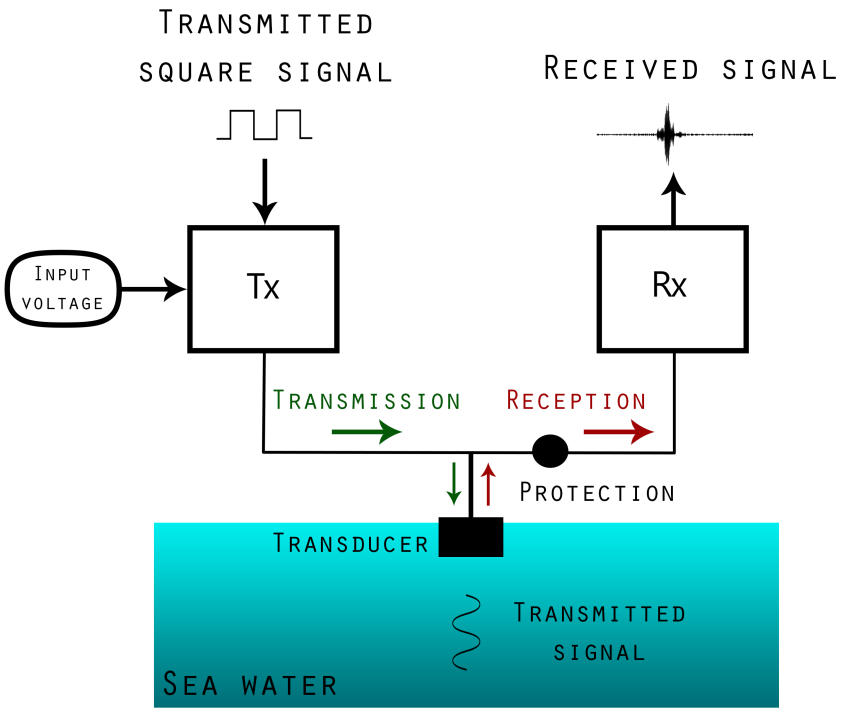

Figure 7.6 – Diagram of the electronic part of the echosounder manufactured at ENSTA Bretagne (France). Tx = Transmission electronic card, Rx = Reception electronic card.

The sampling frequency of the card can be up to 2 MHz which allows to widely respect Shannon criteria for a signal at 100 kHz. For the split-beam purpose of the echosounder, the four received signals from the four transducers of the antenna have to be recorded independently. Consequently, four of the acquisition card inputs are used to convert the received signals from the four transducers to numerical signals. At transmission, only one signal is generated and transmitted to the four transducer simultaneously. All inputs and outputs of the card are synchronous.

7.2.4 Control

The control of the echosounder is made by a dedicated computer (financially support by the European Union `www.europe.bzh`). It generates the digital pulse of frequency 100 kHz and of desired pulse length τ, and records the digital received signals. A part of the processing of the signals is made in real time during acquisition in order to control the measurements. The analysis is then made in post-processing.

7.3 Calibration

All the parts of the echosounder were described in the previous section. Each of them impacts the transmitted and received signals differently. In order to estimate accurately the

seafloor acoustic response we saw in the first parts of this manuscript that the system characteristics have to be perfectly known so that the seafloor echoes time-samples magnitudes could be corrected from the corresponding sonar equation parameters (see equation 6.50). Therefore, impacts of all the components of the echosounder need to be measured and controlled. This is done by calibrating the echosounder in tank and also by controlling this calibration during the campaigns of measurements.

The calibration of the echosounder manufactured during this PhD is carried out in three steps. At first, a control of the good functioning of the four transducers individually is made in the small tank of Sorbonne Université (see figure 7.8). Characteristics of the transducers are then measured such as their impedances and sensitivities. Results are discussed in section 7.3.1. Secondly, the characteristics of the entire antenna are measured. To respect the far field conditions these measurements are made in the larger tank of ENSTA Bretagne (see figure 7.10). In particular, the performances in the coupled transmission and reception of the antenna are evaluated according to frequency. Results are discussed in section 7.3.2. The directivity function of the antenna is also measured. Results are given in section 7.3.3. At the end, the calibration of the echosounder is performed using a specific method (standard sphere target) that allows to estimate all the sonar equation parameters of a monostatic system directly. The method and the results are presented in section 7.3.4. The benefit of this method is that it can be performed in every environment the echosounder is used, which permits to control the calibration any times.

7.3.1 Transducers characteristics measurements

Individual measurements of the transducers characteristics have three major benefits:

1. to verify the proper functioning of each transducer;
2. to evaluate in practice the frequencies at which the manufactured transducers are the most efficient in transmission and in reception;
3. to measure the transducers conductances which are needed to evaluate the electrical power transmitted to the echosounder antenna in the echosounder calibration equation (see section 7.3.4).

These three items can be evaluated by measuring the impedance of the transducers according to frequency, and controlled by measuring the sensitivities of the transducers.

7.3.1.1 Impedance and conductance

Impedance measurements are made with an impedance analyser (financially support by the European Union `www.europe.bzh`). As the impedance Z is a complex value, the measurement provides separately its modulus $|Z|$ and its phase φ_Z. Acquisitions are made for signals of frequencies between 50 kHz and 150 kHz. Measured impedance modulus are given figure 7.7. We can observe a disparity between the different transducers: two of them (#1 and #3) seem equivalent but have higher values of $|Z|$ around 100 kHz, and the two others are slightly different but have the lowest impedance. This divergence between transducers is mostly due to the intrinsic disparity of piezoelectric cylinders they are composed of (see section 7.1) and of the non-perfect repeatability of the mounting. Despite these variations the transducers are considered well.

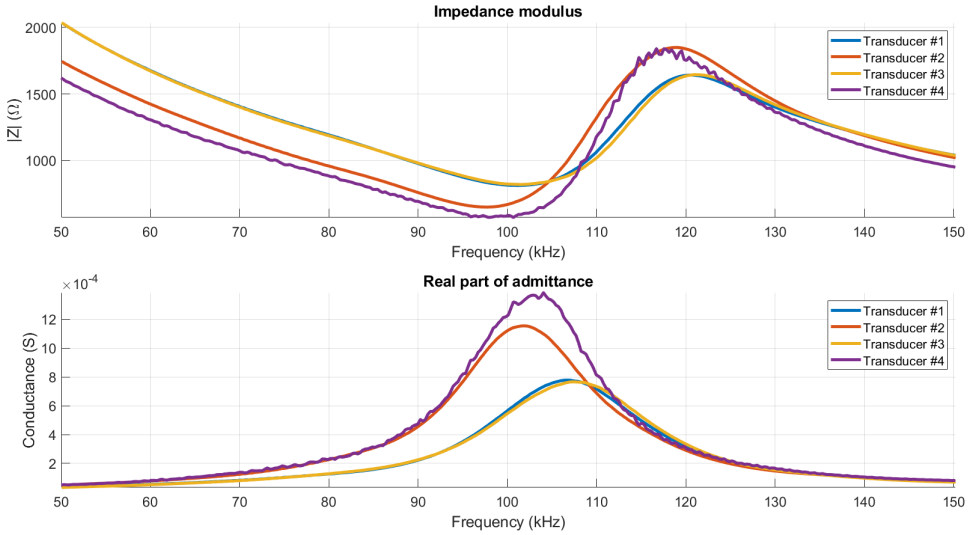

Figure 7.7 – Measured impedance modulus and conductance of the four transducers according to frequency.

Impedance measurements also provide the conductance of the transducers. The conductance G is the real part of the admittance Y which is the inverse of the impedance, i.e.:

$$Y = \frac{1}{Z} = G + jB \tag{7.8}$$

with B the reactance. The conductance is calculated from measurements as:

$$G = 1/|Z| \cos(\varphi_Z) \tag{7.9}$$

The resulting conductances derived from the impedance measurements are given figure 7.7. From these results, at the theoretical frequency of 100 kHz, we can measure the conductances of the four transducers numbered from #1 to #4 as:

$$\begin{cases} G_{\#1}(100\text{kHz}) & = 5.7.10^{-4}\text{S} \\ G_{\#2}(100\text{kHz}) & = 11.2.10^{-4}\text{S} \\ G_{\#3}(100\text{kHz}) & = 5.5.10^{-4}\text{S} \\ G_{\#4}(100\text{kHz}) & = 12.3.10^{-4}\text{S} \end{cases} \tag{7.10}$$

On the results of figure 7.7, we can observe that all transducers do not have exactly the same behaviour according to frequency, therefore the transducers are not precisely the most efficient at the same frequency. Consequently, the frequency at which the final antenna will be the most efficient is included in the range of frequency containing the four maxima of conductance of the four transducers. It gives the range [100, 108] kHz.

7.3.1.2 Sensitivities

The frequency range of efficiency of the four transducers and their proper functioning can be quantify by measuring their transmitting and receiving sensitivities, respectively S_{Tx} and

S_{Rx}, according to frequency. They can be measured in tank using a standard hydrophone (TC4034 from Teledyne/RESON). The measurements were made in the tank of the Institut Jean le Rond ∂'Alembert at Sorbonne Université (France), as shown in figure 7.8.

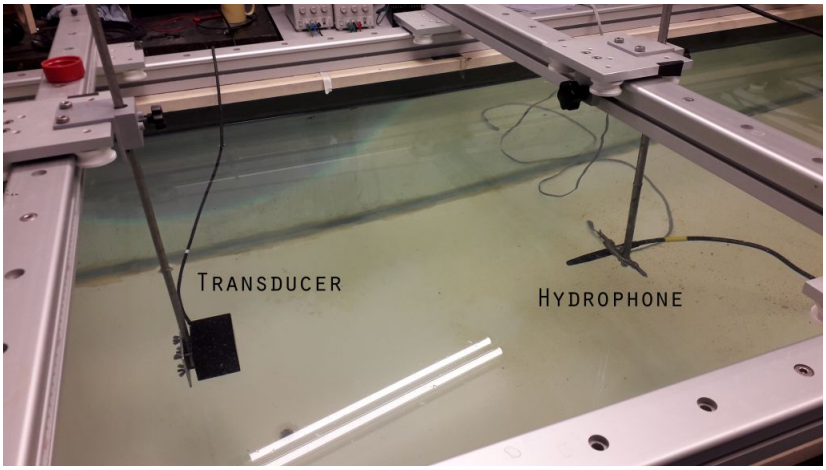

Figure 7.8 – Transducers sensitivity measurements in the tank of the Institut Jean le Rond ∂'Alembert, Sorbonne Université (France) using a standard hydrophone Teledyne/RESON TC4034.

For each measurement, a sonar equation is used to derive the associated sensitivity. The sonar equation associated with the measurement of the transducer receiving sensitivity S_{Rx} was given equation 3.14 and illustrated figure 3.2. The sonar equation associated with the measurement of the transducer transmitting sensitivity S_{Tx} can be derived equivalently as:

$$S_{\mathrm{Tx}} = 10\log_{10}\left(\frac{V_{\mathrm{Rx}}^2}{V_{\mathrm{Tx}}^2}\right) - S_h + TL \tag{7.11}$$

with V_{Rx} the received voltage by the hydrophone, S_h the receiving sensitivity of the hydrophone, V_{Tx} the transmitting voltage to the antenna, and TL the transmission loss between the hydrophone and the echosounder antenna.

Results of the measurements of the transducers sensitivities are given figure 7.9 for a frequency range of [50, 150] kHz. We can observe that the sensitivities trends of the four transducers are quite similar. However, differences (< 3 dB) appear, in particular around the frequency corresponding to their maxima. These differences will impact the shape of the antenna directivity function which probably will not be perfectly symmetrical. This result demonstrates the usefulness of the control of individual transducers that informs on causes of unpredicted variations on the antenna theoretical directivity function. From figure 7.9, we can identify the frequency range where the transducers seem to be the more efficient at transmission as [100, 110] kHz, and at reception as rather [105, 115] kHz. A compromise has therefore to be done between these two results. It can be settled by measuring the antenna characteristics, in particular the coupled transmission/reception sensitivities.

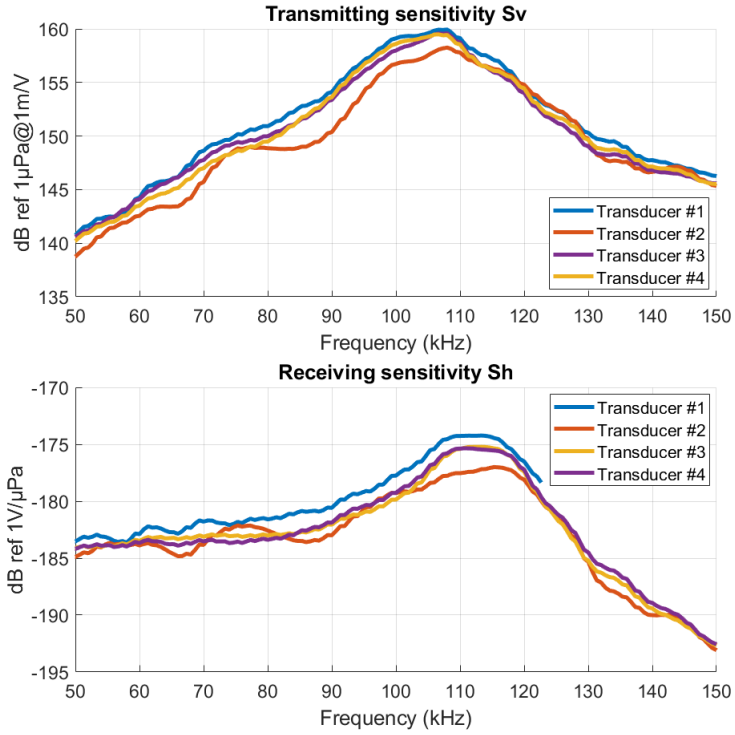

Figure 7.9 – Transmitting and receiving sensitivities of the four transducers according to frequency.

7.3.2 Antenna parameters measurements

The first aim of the measurement of the antenna characteristics is to precisely define the frequency at which the echosounder is the most efficient. This is done by measuring its sensitivities, and particularly its coupled sensitivities. In addition, three specific parameters of the antenna are needed in the following sections to calibrate the echosounder (see equation 7.24): its receiving sensitivity S_{Rx}, its conductance G and its efficiency at transmission β_{Tx}. In this section, the measurement of these three parameters are made and the frequency of the echosounder identified.

7.3.2.1 Sensitivities

The sensitivities of the antenna are measured separately in the tank of ENSTA Bretagne with the standard hydrophone Teledyne/RESON TC4034 as shown in figure 7.10. They are measured on the frequency range $[50,\ 150]$ kHz.

Results of the measurements of the antenna sensitivities at transmission and reception separately are given figure 7.11. As observed on the sensitivities of the individual transducers, the maximum of the transmitting sensitivity is not at the same frequency that the maximum of the receiving sensitivity. Consequently, the optimal choice of the best frequency of the echosounder is to find the maximum of its couple of sensitivities.

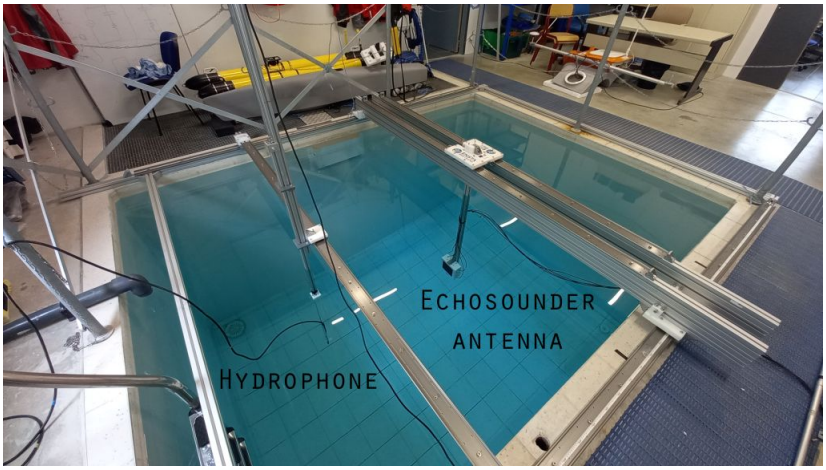

Figure 7.10 – Echosounder antenna sensitivity measurements in the tank of ENSTA Bretagne (France) using a standard hydrophone. (All the mechanical system (frame, bridge, etc.) was mounted during the PhD, and financially support by the European Union `www.europe.bzh`)

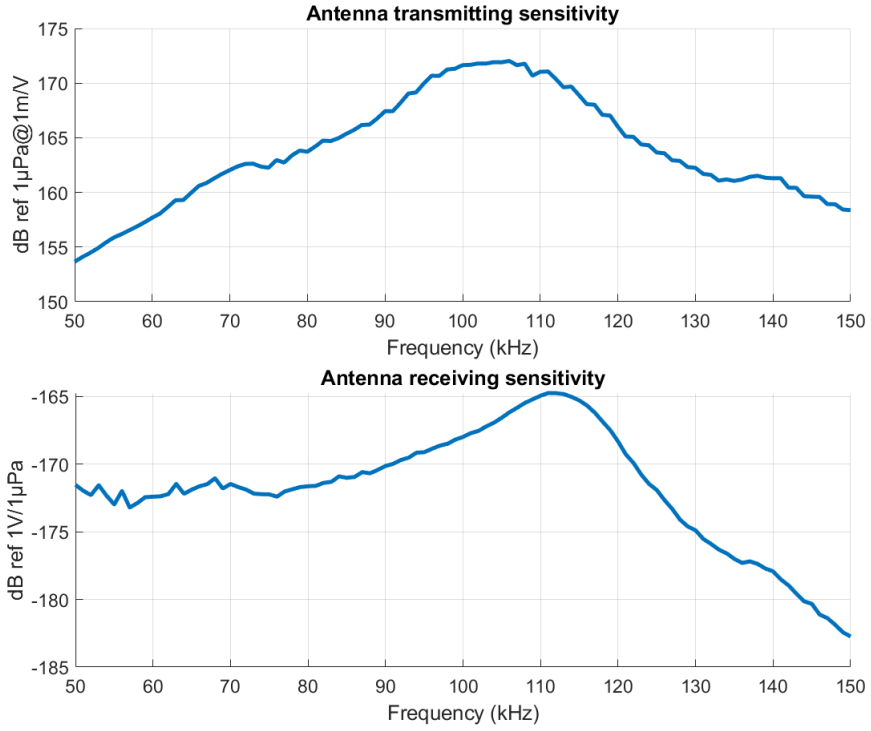

Figure 7.11 – Transmitting and receiving sensitivities of the echosounder antenna, measured in the tank of ENSTA Bretagne (France).

The sum of the transmitting and receiving sensitivities $S_{\mathrm{Rx}} + S_{\mathrm{Tx}}$ is therefore measured, also in the tank of ENSTA Bretagne. This measurement is made available by using a specific target of known target strength TS according to frequency (see section 4.1.1). The target is

chosen as a 25mm diameter tungsten-carbide sphere (details are given in section 7.3.4). The sonar equation associated with this measurement is derived from equation 4.1 as:

$$S_{\mathrm{Rx}} + S_{\mathrm{Tx}} = 10\log_{10}\left(\frac{1}{2}V_{\mathrm{Rx}}^2\right) - 10\log_{10}\left(\frac{1}{2}V_{\mathrm{Tx}}^2\right) + 2TL - TS \tag{7.12}$$

with V_{Rx} the received voltage by the antenna, V_{Tx} the transmitting voltage from the antenna, TL the transmission loss between the target and the echosounder antenna, and TS the target strength.

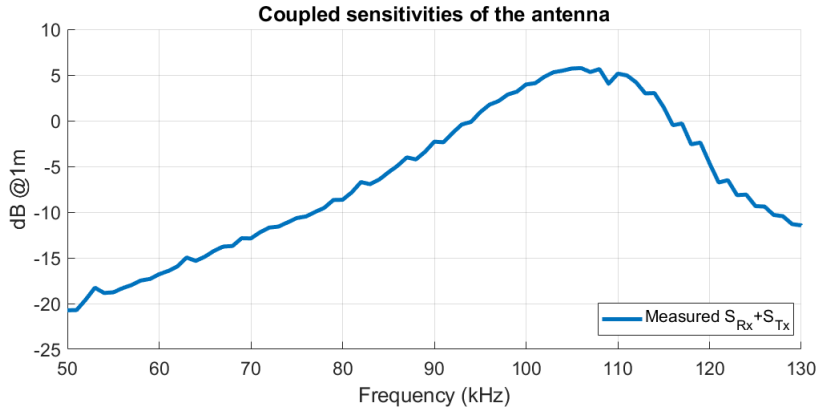

Figure 7.12 – Coupled transmitting and receiving sensitivities of the echosounder antenna measured simultaneously. Measurement are made in the tank of ENSTA Bretagne (France) on a tungsten-carbide sphere of diameter 25mm. Its theoretical target strength according to frequency $TS(\mathfrak{f})$ is given figure 7.17.

Results of the measurements of the coupled sensitivities of the antenna $S_{\mathrm{Rx}} + S_{\mathrm{Tx}}$ according to frequency are given figure 7.12. The maximum of the curve seems to be at 106 kHz therefore the best frequency at which the echosounder should is around this frequency. In order to refine this result, measurements of $S_{\mathrm{Rx}} + S_{\mathrm{Tx}}$ are made in a shorter frequency range (95 kHz to 115 kHz) with a smaller step in frequency (0.1 kHz). The results are given figure 7.13 on the upper graph. On this detailed curve, we can observe strong variations of the coupled sensitivities appearing every 1.8 kHz. This behaviour is correlated to the quantified changes in the sampling frequency shown on the lower graph in orange. In order to create numerically the square signal that is then transmitted to the electronics part of the echosounder (see section 7.2.2), the number of samples inside a period of the signal τ has to be an integer. In order to do so, the sampling frequency of the signal is adapted to the frequency of the transmitted signal. The desired sampling frequency consequently varies according to the frequency. Its variations are plotted on the lower graph of figure 7.13. However, the acquisition card (see section 7.2.3) appears to have a quantification of the sampling frequency larger than the step of sampling frequency desired. Therefore, the sampling frequencies available are less numerous than the desired one. They are also plotted on the lower graph of figure 7.13 in orange. For example, if the transmitted signal is at 105 kHz, the desired sampling frequency is at 1.89 MHz, however the actual sampling frequency will be 1.92 MHz due to the quantification of the acquisition card. The unexpected variations in the measured coupled sensitivities are then due to this quantification of the sampling frequency.

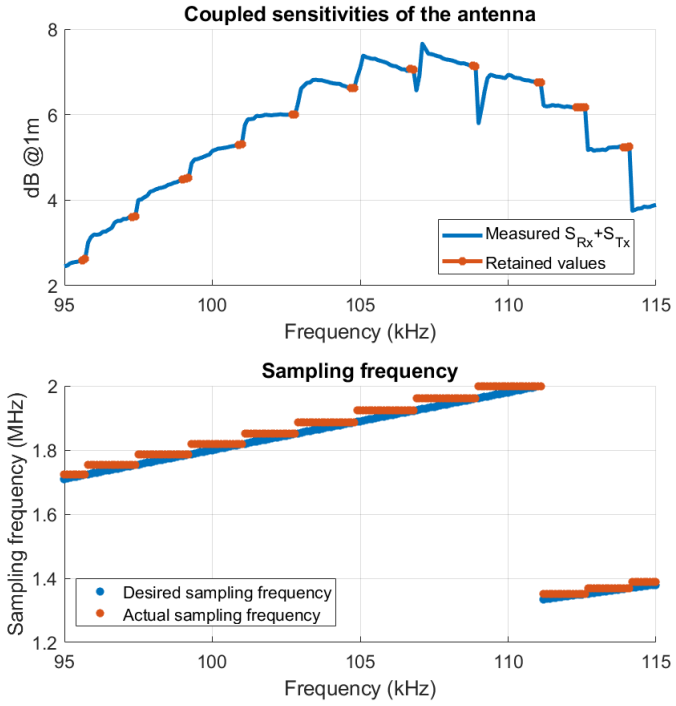

Figure 7.13 – Up: zoom on coupled transmitting and receiving sensitivities measured at the same time with a 0.1 kHz step. Down: sampling frequencies desired and actually employed due to the acquisition card quantification.

The choice of the best operational frequency of the echosounder is then the frequency where the coupled sensitivities have the highest value but also where the actual sampling frequency is the closest to the desired sampling frequency to ensure the actual transmitted signal frequency to be the closest to the desired frequency. The coupled sensitivities measurements that correspond to this latter hypothesis are plotted in orange on the upper graph of figure 7.13. We deduce from this graph that the best frequency at which the echosounder should be used is $\mathfrak{f} = 106.8\,\text{kHz}$.

7.3.2.2 Conductance

The conductance of the antenna can be derived from impedance measurements of the four transducers or directly from impedance measurements of the antenna. At the frequency of the echosounder defined previously, conductances of the four transducers are measured as:

$$\begin{cases} G_{\#1}(106.8\text{kHz}) & = 7.8.10^{-4}\text{S} \\ G_{\#2}(106.8\text{kHz}) & = 9.2.10^{-4}\text{S} \\ G_{\#3}(106.8\text{kHz}) & = 7.6.10^{-4}\text{S} \\ G_{\#4}(106.8\text{kHz}) & = 11.7.10^{-4}\text{S} \end{cases} \tag{7.13}$$

The antenna being constituted of these four transducers mounted in parallel, its conductance is the sum of the individual conductances:

$$G(106.8\text{kHz}) = G_{\#1} + G_{\#2} + G_{\#3} + G_{\#4} = 3.6\text{mS} \tag{7.14}$$

The direct impedance measurement of the antenna gives a conductance at 106.8 kHz of 3.9 ± 0.5 mS which includes the previous result. The value $G = 3.9$ mS is retained in the following.

7.3.2.3 Efficiency

The efficiency of the antenna at transmission β_{Tx} can be estimated from measurements in tank with the standard hydrophone used as a receiver. The acoustic source level generated in front of the antenna in the water can be calculated two ways:

1. From the transmitting chain, the source level SL is given by equation 3.32 as:

$$SL = 170.8 + 10\log_{10}(P_{\text{elec}}) + 10\log_{10}(\beta_{\text{Tx}}) \tag{7.15}$$

   with P_{elec} the electrical power such as [Sherman and Butler, 2007]:

$$P_{\text{elec}} = \frac{1}{2}V_{\text{Tx}}^2 G \tag{7.16}$$

   where V_{Tx} is the 0-peak voltage transmitted to the antenna, and G the conductance of the antenna.

2. From the receiving chain of the hydrophone, the same source level SL is found before it propagates from the face of the antenna in the water toward the hydrophone and then be recorded as the received voltage V_{Rx} i.e. in term of sonar equation:

$$SL = 10\log_{10}\left(\frac{1}{2}V_{\text{Rx}}^2\right) + 20\log_{10}(r) + \alpha r - S_h - G_{\text{hydro}} - DI_{\text{Tx}} \tag{7.17}$$

   where V_{Tx} is the transmitted 0-peak voltage to the antenna during the measurement, r is the range between the antenna and the hydrophone, α is the absorption coefficient, S_h is the hydrophone sensitivity at reception, G_{hydro} is the gain added to the hydrophone signal during the measurement, and DI_{Tx} the directivity index of the antenna at transmission. From equations 3.51 and 3.53, $DI_{\text{Tx}} = 10\log_{10}\left(\frac{4\pi L^2}{\lambda^2}\right)$.

Using these two equations we can derive the transmission efficiency of the echosounder antenna as:

$$\begin{aligned} 10\log_{10}(\beta_{\text{Tx}}) = 10\log_{10}\left(\frac{1}{2}V_{\text{Rx}}^2\right) + 20\log_{10}(r) + \alpha r - S_h - G_{\text{hydro}} \cdots \\ - DI_{\text{Tx}} - 170.8 - 10\log_{10}\left(\frac{1}{2}V_{\text{Tx}}^2 G\right) \end{aligned} \tag{7.18}$$

From the measurements at the echosounder frequency 106.8 kHz, the transmitting efficiency of the echosounder is found as $\beta_{\text{Tx}} = 44\%$.

7.3.3 Antenna directivity measurements

The measurement of the echosounder directivity function is necessary to estimate accurately the seafloor acoustic response. Indeed, two parameters of the sonar equation used to calculate the backscattering strength depend on the directivity function: the beam aperture and the magnitude of the target at any positions inside the beam. These two parameters are mainly found when the sonar equation of the form of equation 3.23 is used. The beam aperture is then a parameter of the model of insonified area (see section 3.2.13). For this purpose the directivity functions that are needed are those on the axes of the square antenna (i.e. the plans orthogonal to the plane of the antenna). We called them 2-D directivity functions in the following.

However, we saw in section 4.2.4 that these model and sonar equation are not sufficient when using several time-samples from the same beam to estimate the backscattering strength. A solution we propose in this PhD is to used the sonar equation 6.50 and to simulate the instantaneous insonified areas $\mathcal{A}$ according to the time of propagation (see chapter 8). This method gives a better estimation of the correction to apply to the seafloor echo magnitudes. For this purpose the entire directivity function (i.e. in 3-D) of the echosounder is required. It is measured in tank and discussed in this section.

7.3.3.1 2-D directivity functions

In order to measure the directivity functions in two dimensions, the pan & tilt system (see figure 7.4) is used to move the antenna in front of the standard hydrophone (see figure 7.14). The hydrophone is used as a receiver therefore the antenna directivity functions are measured at transmission (by reciprocity, they are the same at reception).

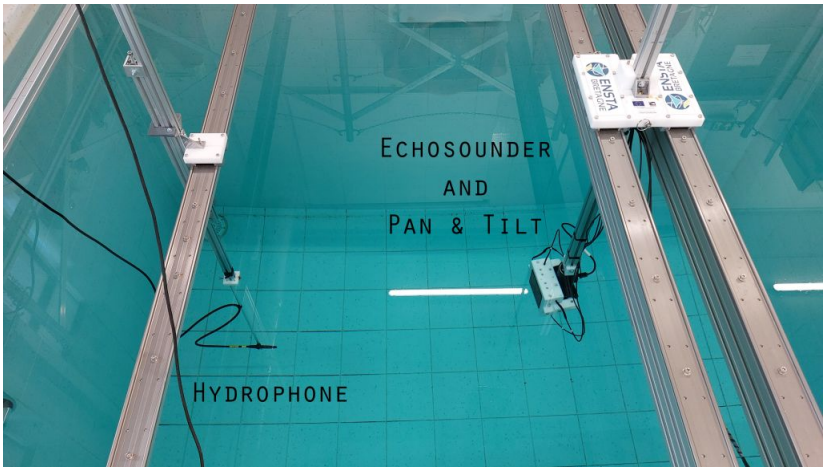

Figure 7.14 – Directivity measurements with the pan & tilt system in the tank of ENSTA Bretagne. (Mechanical system mounted especially for the PhD, financially support by the European Union `www.europe.bzh`)

The two directivity functions on axis (horizontal and vertical) of the antenna are measured every 0.5° from −60° to 60°. Results are given figure 7.15 and compared to the theoretical

directivity function of a linear antenna calculated as:

$$D_{\text{th}}(\vartheta) = \left(\frac{\sin(\pi \frac{L}{\lambda} \sin(\vartheta)}{\pi \frac{L}{\lambda} \sin(\vartheta)} \right)^2 \tag{7.19}$$

where L is the size of the antenna, λ the wavelength, and ϑ the angle from the antenna axis. Both the directivity functions (theoretical and measured) are normalized by their maximum values. We can observe on both graphs of figure 7.15 that the measured main lobe shape is coherent with the theoretical shape, however its aperture is smaller. The total theoretical aperture is 7° where the measured aperture is 6°. This reduction is probably due to the baffle effect generated by the presence of inox plates surrounding the transducers and also by the mount used to support the echosounder. Reduction of the main lobe aperture by definition affects the rest of the directivity function by moving zeros of the function closer to the axis. This is what we observe on the graphs. That said, differences remain on side lobes amplitudes and their relative positions. It could be due to the variations in sensitivities found previously between the transducers (probably caused by variations of piezoelectric ceramic characteristics) and to the irregularities in the mounting (which was made manually).

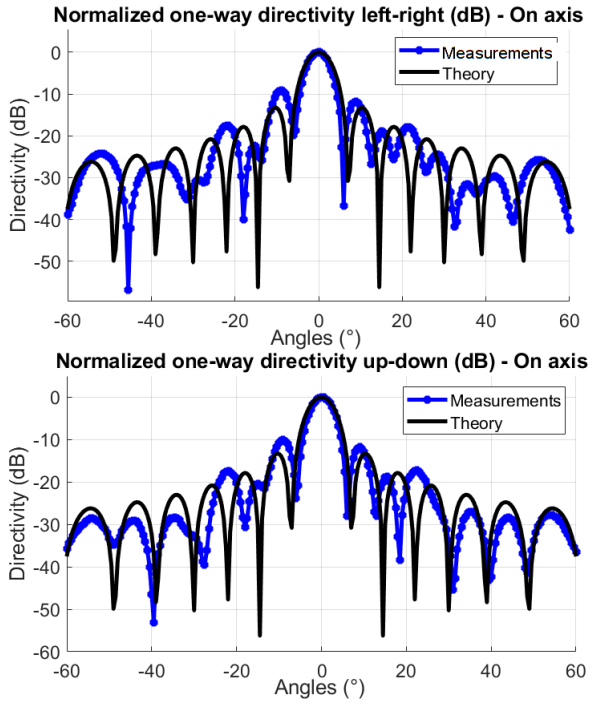

Figure 7.15 – Normalizes 2-D directivity functions of the echosounder measured at transmission and compared to theoretical directivity functions of a linear antenna of length $L = 11\text{cm}$ and a frequency of $\mathfrak{f} = 106.8\,\text{kHz}$.

7.3.3.2 3-D directivity function

The 3-D directivity function of the echosounder antenna in measured using the same mounting as in the previous section and moving the antenna from $-20°$ to $20°$ on all combined directions with a step of 1°. We obtain the pattern on the left of figure 7.16. On the right is added

the theoretical 3-D directivity function calculated by crossing with itself the 2-D directivity function of equation 7.19. The two 3-D directivity functions (theoretical and measured) are normalized by their maximum values.

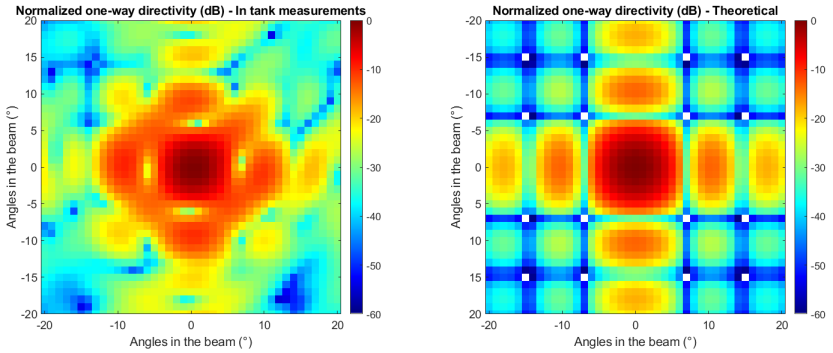

Figure 7.16 – Left: normalized 3-D directivity function of the echosounder at transmission. Right: theoretical directivity function of a square antenna of size $L = 11\,\text{cm}$ and a frequency of $\mathfrak{f} = 106.8\,\text{kHz}$.

As previously, the measured main lobe is slightly sharper than the theoretical one. We also retrieve the differences in the side lobes positions and amplitudes on the crossing axes. However, what remains the biggest difference between the measurement and the theory is the presence of some sorts of links between the four first side lobes. For example, instead of a zeros of directivity at $(-7°, -7°)$ as found theoretically, the measured level at this pair of angles is $-17.8\,\text{dB}$. This effect may be due to the antenna shape with sharp corners inducing more constructive interferences than expected on the edges. This result is another example of the importance of measuring the characteristics of the echosounder antenna to better control the system parameters in the sonar equation.

7.3.4 Echosounder calibration

The objective of this section is to determine the calibration gain specific to the echosounder that appear in the sonar equation 6.50 used to measure the backscattering strength. This is done using the calibration method on a standard target discussed in section 4.1.1 and described in [Foote, 1987]. This way, the measured calibration gain G_{calib} incorporates all the imperfections of the previous measurements of the characteristics of the echosounder components and their connections.

The sonar equation corresponding to the calibration on sphere of an echosounder was presented equation 4.1. It is adpated to the echosounder of the PhD as:

$$EL = SL + DI_{\text{Tx}} - 2TL + TS_{\text{sphere}} + G_{\text{calib}} \tag{7.20}$$

where:

- EL is the echo level received by the echosounder. It can be written in function of the received voltage V_{Rx} and the antenna sensitivity at reception S_{Rx} as:

$$EL = 10\log_{10}\left(\frac{1}{2}V_{\mathrm{Rx}}^2\right) - S_{\mathrm{Rx}} \tag{7.21}$$

- SL is the source level of the echosounder. From equation 3.32, SL is function of the electrical power delivered to the antenna and its efficiency at transmission β_{Tx}. Equation 7.16 gives the electrical power $P_{\mathrm{elec}} = \frac{1}{2}V_{\mathrm{Tx}}^2 G$ with V_{Tx} the transmitted 0-peak voltage and G the conductance of the antenna. Thus:

$$SL = 170.8 + 10\log_{10}(\frac{1}{2}V_{\mathrm{Tx}}^2 G) + 10\log_{10}(\beta_{\mathrm{Tx}}) \tag{7.22}$$

- DI_{Tx} is the directivity index on the antenna at transmission. From equation 3.53, it can be estimated as:

$$DI_{\mathrm{Tx}} \approx 10\log_{10}\left(\frac{4\pi L^2}{\lambda^2}\right) \tag{7.23}$$

  where L is the size of the echosounder antenna with $L = 7.8\lambda$.

- TL is the transmission loss between the echosounder and the target. From equation 3.45 it is equal to $TL = 20\log_{10}(r) + \alpha_{\mathrm{w}} r$ with r the range between the echosounder and the target and α_{w} the absorption coefficient in water.

- G_{calib} is the calibration gain which is the parameter of interest. It combines the gains at transmission and reception described in equation 4.1.

- TS_{sphere} is the target strength (see section 3.2.12) of the standard target. In fishery acoustics, standard targets are generally spheres made of tungsten-carbide [Foote and MacLennan, 1984, Vagle et al., 1996]. For the purpose of the PhD, a sphere of 25mm diameter was bought at Redhill Precision. Its density is given by the manufacturer to be 14947kg/m^3. To derive the target strength of the sphere, its specific sound speeds c_{l} and c_{t}, respectively longitudinal and transverse stress wave speeds, are needed. They were estimated by calculus and measurements in [MacLennan and Dunn, 1984] for a tungsten-carbide sphere of 14900kg/m^3 density which is very close to our sphere characteristic. The authors give its celerities as $c_{\mathrm{l}} = 16853\pm19$m/s and $c_{\mathrm{t}} = 4171\pm7$m/s at 11°C with 95% confidence.

The target strength of the calibration sphere is defined as the ratio of the backscattered intensity from the sphere to the incident intensity (see equation 3.71). Reference analytical calculations of the acoustic response of calibration spheres can be founded in [Hickling, 1962], [Faran, 1951] and [MacLennan, 1981]. In these models, the response of the sphere depends on the ratio of its celerities to the medium celerity (water), the ratio of its density to the density of the water, its radius, and the frequency of the incident acoustic wave. For the sphere of 25mm we use, the model gives the target strengths according to frequency plotted in figure 7.17. From this result, the target strength of the calibration sphere at 106.8 kHz is identified as $TS = -44.6$ dB.

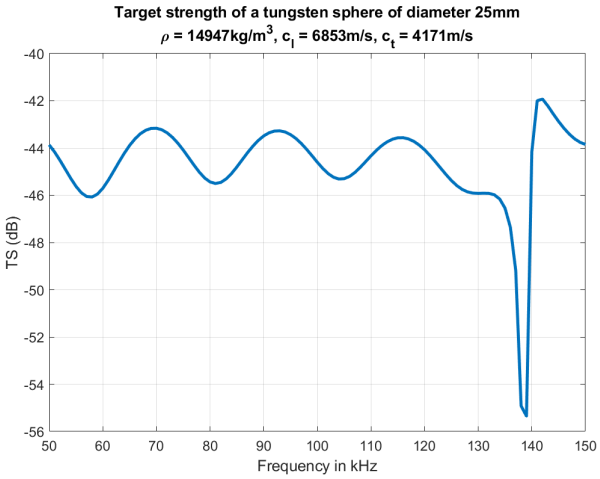

Figure 7.17 – Target strength of a tungsten-carbide sphere of 25mm diameter according to the frequency of the incident acoustic wave. Derived from analytical model in [Hickling, 1962].

Based on equation 7.20, the calibration gain G_{calib} can be derived from measurements as (in decibels):

$$\begin{aligned} G_{\text{calib}} &= EL - SL - DI_{\text{Tx}} + 2TL - TS_{\text{sphere}} \\ &= 10\log_{10}\left(\frac{1}{2}V_{\text{Rx}}^2\right) - S_{\text{Rx}} - 170.8 - 10\log_{10}\left(\frac{1}{2}V_{\text{Tx}}^2 G\right) - 10\log_{10}(\beta_{\text{Tx}}) \cdots \\ &\quad - 10\log_{10}\left(\frac{4\pi L^2}{\lambda^2}\right) + 40\log_{10}(r) + 2\alpha r - TS_{\text{sphere}} \end{aligned} \tag{7.24}$$

with the constant parameters estimated previously at 106.8 kHz as $S_{\text{Rx}} = -165.9$ dB ref. $1\,\text{V}/\mu\text{Pa}$, $G = 3.9$ mS, $\lambda = 1.4$ cm, $TS = -44.6$ dB, $\beta_{\text{Tx}} = 44\%$ and $L = 11$ cm. The absorption coefficient α is calculated for 106.8 kHz using the formula of [Francois and Garrison, 1982]. It results in $\alpha = 2.8$ dB/km in the tank of ENSTA Bretagne filled with fresh water at 17°C.

The calibration gain is measured from the received signal backscattered from the target when it is on axis on the echosounder antenna. During measurements, the transmitted voltage was set to 60V therefore $V_{\text{Tx}} = 60$V. Echo of the sphere is detected on the received signal by computing the inter-correlation between the theoretical sent signal and the recorded signal. The sent signal is a sinusoid of length $\tau \approx 281\mu$s and frequency $f = 106.8$ kHz (CW pulse). The range r between the echosounder and the sphere is measured at the maximum of the inter-correlation, and the received voltage of the sphere V_{Rx} is measured as the envelop amplitude of the received signal at the maximum of the inter-correlation. Finally, using equation 7.24 and all the parameters discussed above, we find a calibration gain equal to $G_{\text{calib}} = 0.7$ dB. This gain will be re-calibrated following the same method in each environment backscattering strength measurement will take place (see chapter 8) in order to control the system and the impact of the environment on it.

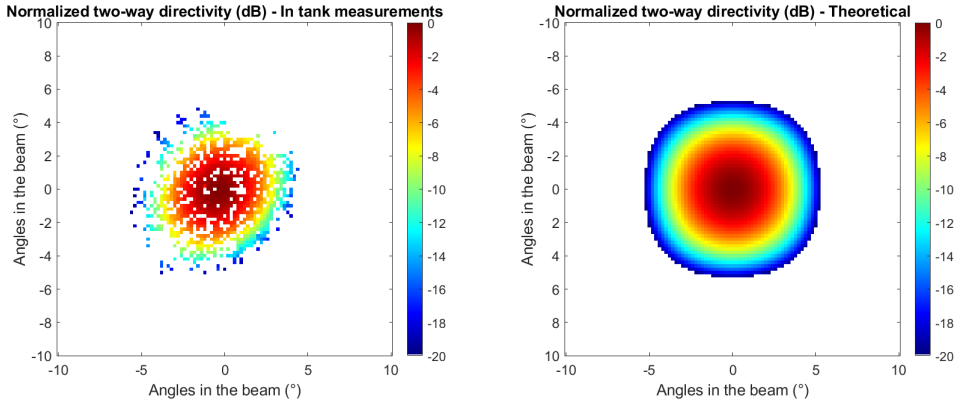

Figure 7.18 – Left: normalized 3-D directivity function of the split-beam echosounder antenna measured on calibration sphere. Right: theoretical directivity function based on equation 7.3.

In addition to the calibration gain on axis, sphere measurements are also used to control the two-way 3-D directivity function of the echosounder. The split-beam characteristic of the antenna allows to measure the positions of the sphere inside the beam of the echosounder together with the sphere responses. By moving the sphere at different positions, the 3-D directivity function can therefore be measured. These measurements were made in the tank of ENSTA Bretagne (France). (Note that the sphere was moved manually). The resulting directivity function is shown on the left of figure 7.18 with on the right the theoretical directivity function calculated from equation 7.3. Except a slight oval shape which is probably due to very small differences in phase between the four transducers, the measured main lobe is coherent with the theoretical one. Figure 7.18 shows a comparison on axis of the measured and theoretical main lobes. They correspond perfectly in shape whereas the axis is very slightly bias of 0.2°. This effect could be due to the differences in sensitivities observed between the transducers in section 7.3.1.2. Beam apertures are measured on both axes as $2\theta_{\text{-3dB}} = 4.2°$.

7.4 Summary

This chapter presented the singlebeam echosounder designed and manufactured during the PhD. Its aim is to measure the seafloor acoustic response using the method and the estimator developed in the second part on this manuscript. For this purpose the echosounder is splitbeam and its characteristics are precisely measured in tank. This way, the parameters of the sonar equation employed in practice to estimate the backscattering strength are precisely known. They appear in the sonar equation 6.50 as detailed below:

$$\begin{aligned} \text{BS} &= EL - SL - DI_{\text{Tx}} + 2TL - 10\log_{10}(\mathcal{A}) - G_{\text{calib}} \\ &= 10\log_{10}\left(\frac{1}{2}V_{\text{Rx}}^2\right) - S_{\text{Rx}} - 170.8 - 10\log_{10}(\frac{1}{2}V_{\text{Tx}}^2 G)\cdots \\ &- 10\log_{10}(\beta_{\text{Tx}}) - 10\log_{10}\left(\frac{4\pi L^2}{\lambda^2}\right) + 20\log_{10}(r) + \alpha_{\text{w}} r - 10\log_{10}(\mathcal{A}) - G_{\text{calib}} \end{aligned} \tag{7.25}$$

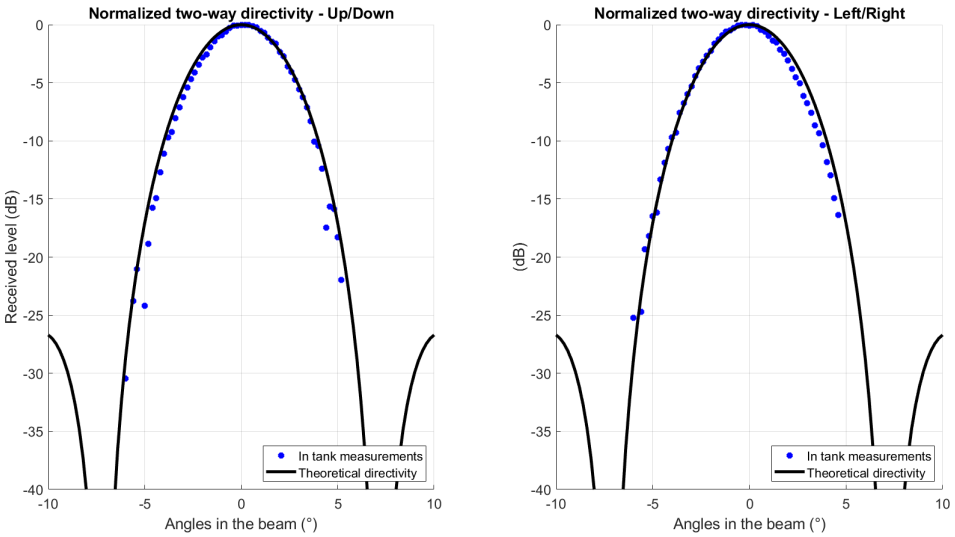

Figure 7.19 – Measured main lobe of the normalized 3-D directivity function of the split-beam echosounder antenna of figure 7.18 and associated theoretical directivity function. Left: vertical axis. Right: horizontal axis.

The system parameters calibrated in this chapter are: the echosounder receiving sensitivity S_{Rx}, the conductance of the antenna G, the efficiency at transmission of the antenna β_{Tx}, the calibration gain G_{calib} and the directivity function that is needed to simulate the instantaneous insonified area $\mathcal{A}$. Their measured values are summed up in table 7.1. This sonar equation will be used in the next chapter to correct the seafloor echo magnitudes.

Parameters	Values
Specificities	Split-beam & single beam echosounder
Type of transmit signal	CW pulse
Antenna geometry	Square of length $L = 11\,\mathrm{cm}$
Operating frequency	$\mathfrak{f} = 106.8\,\mathrm{kHz}$
Signal period	$T = 1/\mathfrak{f} \approx 9.3\,\mu\mathrm{s}$
Signal wave length	$\lambda = c/\mathfrak{f} \approx 1.4\,\mathrm{cm}$
Pulse length (during calibration)	$\tau = 30T \approx 281\,\mu\mathrm{s}$
Far field distance	$r_{\text{Far field}} = L^2/\lambda \approx 86\,\mathrm{cm}$
Receiving sensitivity	$S_{\mathrm{Rx}} = -165.9\,\mathrm{dB}$ ref. $1\,\mathrm{V}/\mu\mathrm{Pa}$
Transmitting sensitivity	$S_{\mathrm{Tx}} = 172.2\,\mathrm{dB}$ ref. $1\,\mu\mathrm{Pa}/1\,\mathrm{V}\ 1\,\mathrm{m}$
Efficiency at transmission	$\beta_{\mathrm{Tx}} = 44\%$
Conductance	$G = 3.9\mathrm{mS}$
Directivity index at transmission	$DI_{\mathrm{Tx}} = 10\log_{10}\left(\frac{4\pi L^2}{\lambda^2}\right) = 28.9\,\mathrm{dB}$
Actual aperture	$2\theta_{\text{-3dB}} = 4.2°$
Calibration gain (on axis)	$G_{\mathrm{calib}} = 0.7\,\mathrm{dB}$

Table 7.1 – Measured characteristics of the split-beam echosounder developed during the PhD

Chapter 8

Analysis of the seafloor response estimation method based on echosounder measurements

In the previous parts of this manuscript, we derived theoretically the best estimator of the seafloor acoustic response and also a formulation of its uncertainty (see chapter 5). In this chapter, these analytical results are validated using singlebeam echosounder measurements and then the backscattering strength estimation method and the uncertainty estimation method are applied to echosounder data from surveys at sea.

Before using singlebeam echosounder data to validate the model of chapter 5, they are pre-processed specifically as described in the second section of this chapter. Origins of the data are given in the first section. The validation of the model is made in two times: at first the hypotheses under which the model is valid are presented and verified independently using the echosounder data, then the uncertainty formulation is verified. For each item, conditions of validity of the model are discussed.

In the last section of this chapter, the method of estimation of the seafloor acoustic response is applied to singlebeam and multibeam echosounder data acquired at sea. In addition, the estimation of the uncertainty levels is also processed from these data and compared to the theoretical results. Information that derived from this comparison are discussed in the context of detecting seafloor changes.

8.1 Origins of data

Data used in this chapter come from three different surveys made with two different echosounders: the singlebeam echosounder developed in this PhD (see chapter 7) and another singlebeam echosounder manufactured during the project S2MF [1] (see appendix C) carried out by Sorbonne Université, ENSTA Bretagne and Ifremer between 2016 and 2018.

The echosounder of the PhD was used in two surveys: one in the tank of the university of Bath (United Kingdom) and one in the harbour of Brest (France), both in 2022. The survey of project S2MF was made in the Bay of Brest in 2018. In this section the three acquisition campaigns are presented together with their characteristics (sound speed, type of water, etc.) and the echosounder parameters.

8.1.1 Tank of the university of Bath (United Kingdom)

Measurements in the tank of the university of Bath (United Kingdom) were made with the echosounder manufactured in this PhD in September 2022. The echosounder was installed on the tank with a mount especially designed at ENSTA Bretagne (France) as shown in figure 8.1. The Pan & Tilt system was used to tilt the echosounder from 0° (vertical) to 60° toward the different sediment trays.

Four sediment types were available: sand (average grain size 1-2 mm), silt (50μm), fine gravel (5 mm) and coarse gravel (20 mm), as shown in figure 7.2 in section 7.1. A careful preparation at the time the trays were installed ensured all sediments were water-saturated

1. Project ANR-14-ASTR-0022 founded by the French research agency (ANR, Agence Nationale de la recherche) and the French armament direction (DGA, Direction Générale de l'Armement)

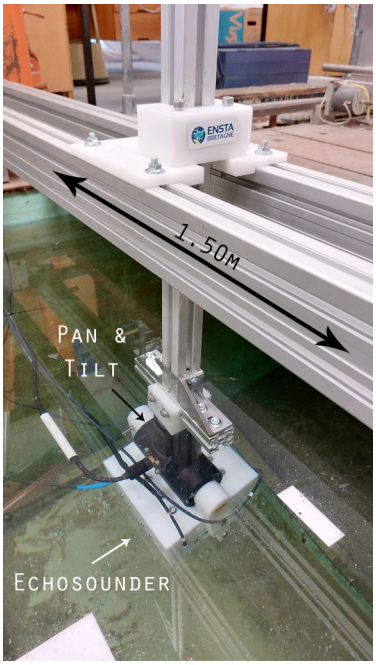

Figure 8.1 – Echosounder mounted for measurements in the tank of the university of Bath (United Kingdom). September 2022.

and their surface smooth and horizontal [Blondel and Pace, 2007][Blondel et al., 2006]. The thickness of the sediments is 14 cm.

In the tank, the water height is limited (1.4 m), therefore the beam footprint is constrained. The pulse length transmitted was thus adjusted as short as possible to obtain several individual pulse lengths inside the beam footprint leading to independent time-samples during seafloor response measurements. For each sediment several measurements were made at different incidence angles. Characteristics of these acquisitions are shown in table 8.1. All measurements were made with the echosounder perfectly still.

Characteristics	Values
Water	Fresh
Sound speed	1474 m/s
Antenna height above sediment H	1.0 m
Transmitted frequency $\mathfrak{f}$	106.8kHz
Transmitted pulse length τ	$5T \approx 31\mu$s

Table 8.1 – Characteristic of seafloor response measurements made in the tank of the university of Bath (United Kingdom) in September 2022 with the echosounder designed during this PhD.

8.1.2 Harbour of Brest (France)

Measurements in the harbour of Brest (France) were also made with the echosounder manufactured in this PhD in July 2022. The echosounder was mounted on the ENSTA Bretagne survey vessel *Panopée* and tilted from nadir to 60° using the Pan & Tilt system as shown in figure 8.2. In order to ensure that the seafloor type remains the same from one ping to another, acquisitions are made with the vessel docked. Nevertheless, movements of the echosounder remained due to the wind and crew displacements that induce respectively rotation of the vessel around the vertical axis (yaw) and small roll. Also, the tide modifies the water height between the seafloor and the echosounder during acquisition, inducing changes in the beam footprint between time-space acquisitions.

Figure 8.2 – Echosounder mounted on the side of ENSTA Bretagne survey vessel in the harbour of Brest (France).

At low tide, during one of the days of acquisition, we could see the seafloor from the vessel, as shown on the picture figure 8.3. On this picture we can observe that the seabed in composed of a seagrass mat upon what seems to be a hard sediment with disperse and large pebbles.

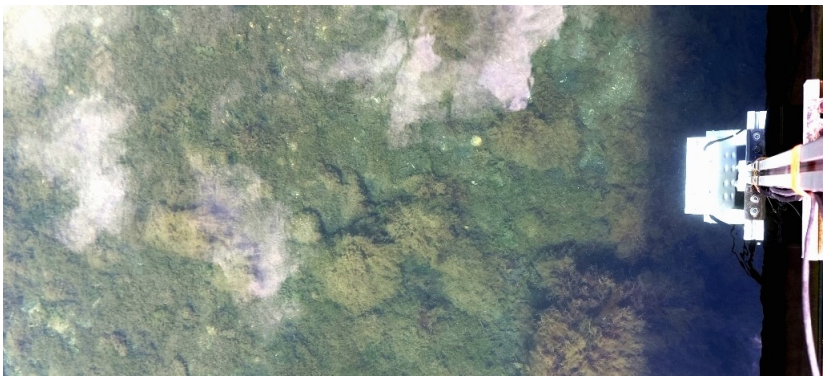

Figure 8.3 – View of the seafloor composition at low tide by transparency during measurements in the harbour of Brest (France) in July 2022.

On the side of the vessel where the measurements were made, the seafloor topography was not flat. Consequently, a first measurement of the bathymetry was done using the Pan & Tilt system to move the echosounder from $-10°$ (under the vessel) to $90°$ (on the external side) with a step of $2°$. The resulting bathymetry is given figure 8.4 with reference (0 m) the water height under the echosounder at the moment of the measurement. We can observe on this figure the slope of the seafloor, and the effect of the large pebbles generating shadows (i.e. holes in the sounding mat) after 6 m across-track.

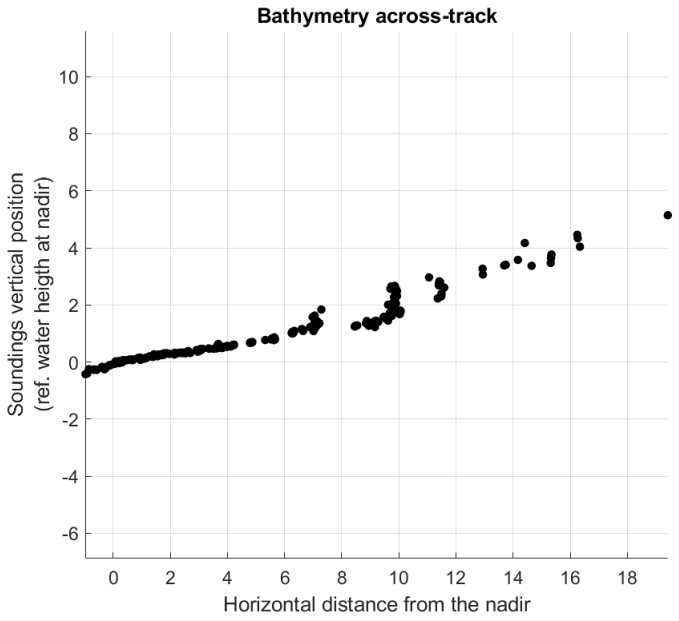

Figure 8.4 – Bathymetry measured across-track of the vessel when docked.

Characteristics of the acquisitions in the harbour are shown in table 8.2.

Characteristics	Values
Water	Sea water
Sound speed	1512 m/s
Antenna height above sediment H	[3 - 6]m
Transmitted frequency $\mathfrak{f}$	106.8kHz
Transmitted pulse length τ	$15T \approx 140\mu$s

Table 8.2 – Characteristic of seafloor response measurements made in the harbour of Brest (France) in July 2022 with the echosounder designed in this PhD.

8.1.3 Bay of Brest (France)

Data from the Bay of Brest (France) used in the following were acquired during project S2MF in May 2018 aboard R/V *Thalia* (Ifremer). The echosounder used was a singlebeam

echosounder manufactured during the project as a prototype of a non-linear multi-frequency echosounder. It was mounted on a pole on the starboard side of the vessel (see figure 8.5). A Pan & Tilt system (larger than the one of this PhD) was used to tilt the echosounder from 0° (nadir) to 60° with a 5° step. At each angle, data were acquired while the vessel was drifting slowly. The calm weather during the survey ensured the vessel to drift for short distances. Measurements were then assumed to be made on the same seafloor type.

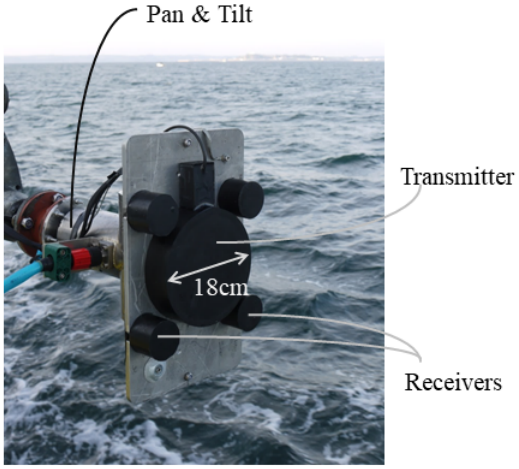

Figure 8.5 – Non-linear multi-frequency singlebeam echosounder of project S2MF, mounted on a Pan & Tilt system, during acquisitions in the Bay of Brest (France) in May 2018. One transmitting cylindrical transducer in the center, and four receivers spaced 20 cm apart. From [Mopin et al., 2022].

The aim of project S2MF was to use non-linearities of the seawater to generate harmonic frequencies of a transmitted single one. The echosounder was therefore made in order to transmit one frequency at a high level (the fundamental, at 100 kHz) and to receive several frequencies from 100 kHz to 400 kHz. The generation of these harmonic frequencies was based on the propagation medium's non-linear properties, producing frequencies multiples of the fundamental frequency transmitted (100 kHz, yielding harmonics at 200 kHz, 300 kHz, etc.). For the purpose of this chapter of the PhD, only the fundamental frequency is used, i.e. 100kHz. Details of the measurements with the other frequencies are given in [Mopin et al., 2022] in the context of seafloor characterisation (see Appendix C).

Three areas with distinct seafloor types were surveyed with the singlebeam echosounder during the project, as shown in figure 4.2 in section 4.2.2. Area 1 on the figure is at the mouth of the small Elorn river. Area 2 is in the so-called "Carré Renard", a plateau in the center of the Bay and also a well-surveyed area for echosounder calibration [Eleftherakis et al., 2018]. Area 3 is at the mouth of another small river, the Aulne. According to the morpho-sedimentological map in [Gregoire, 2016], created from [Gregoire et al., 2016] and [Pluquet and Ehrhold, 2009], Area 1 is composed of sandy mud or muddy sand, Area 2 is mostly composed of gravel with rare pebbles, and Area 3 of gravelly coarse sand with maerl

and episodic rocks. During the survey, videos and photographs of the seafloor were taken in these areas (cf. figure 8.6). They show sand and mud in Area 1, pebbles and brittle-stars in Area 2, and a hard seafloor (rock) and a large amount of shells in Area 3.

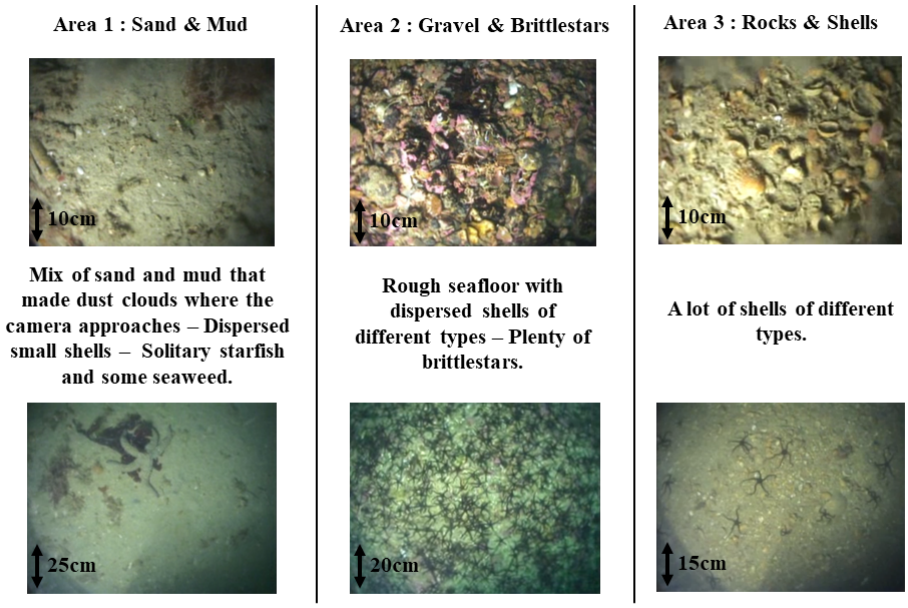

Figure 8.6 – Seafloor photographs in the three areas of the Bay of Brest (France) where acquisitions were made during project S2MF with the multi-frequency echosounder. May 2018. From [Mopin et al., 2022].

As shown in figure 8.5 the echosounder is bi-static i.e. transmitter and receiver are dissociated. The transmitter was an 18 cm-diameter disk formed of the same composite-PZT as the echosounder of this PhD which resonates at 100 kHz (see section 7.2.1). Four wide-band receivers were placed around the transmitter. Their vertical spacing was about 20 cm and was useful for seabed detection through interferometry. Measurements of the characteristics of the system were made in tank during the project, in particular its combined two-way directivities (see Appendix C). The equivalent aperture of the echosounder was thus calculated by integrating the corresponding measured directivity patterns (see section 3.2.14). At 100 kHz, they vary from 6.3^o at a range of 10 m to 6.8^o at a range of 30 m. This variation in range is due to the mechanism of generation of the harmonic frequencies based on the non-linearity of the sea water (see Appendix C).

Characteristics of the singlebeam echosounder of the project S2MF and of the acquisitions in the Bay of Brest are given in table 8.3.

Characteristics	Values
Water	Sea water
Sound speed	1501 m/s
Antenna height above sediment H	[10 - 30]m
Transmitted frequency $\mathfrak{f}$	100 kHz
Transmitted pulse length τ	$60T \approx 600\mu$s
Equivalent beam aperture Φ	[6.3 - 6.8]°

Table 8.3 – Characteristic of seafloor response measurements made in the Bay of Brest (France) in May 2018 during project S2MF with the multi-frequency singlebeam echosounder. Only the fundamental frequency (100 kHz) is used in this manuscript.

8.2 Data pre-processing

In order to apply the seafloor response estimation method discussed in the other parts of this manuscript, the raw data recorded by the echosounders have to be corrected from all sonar equation parameters. For each ping, the resulting corrected magnitudes are then x_i as described in the model of chapter 5 (see equation 5.2.1) where i is the seafloor echo time-samples number.

The sonar equation used for to correct raw data was shown in the preamble of this part (see equation 6.50). The specificity in the data-processing applied in this section is that all time-samples of the seabed echo are retained in order to evaluate the results of the estimation according to the number of time-samples (and ping) taken into account as (see theoretical analyses of chapters 5 and 6). Consequently, parameters that depend on the propagation time t or equivalently the range r, have a different value for each time-sample. In this case, the sonar equation is written as:

$$10\log_{10}\left(x_i^2\right) = EL(t) - SL - DI_{\text{Tx}} + 2TL(t) - 10\log_{10}(\mathcal{A}(t)) - G_{\text{calib}} \tag{8.1}$$

where:

- $EL(t)$ is the echo level received by the echosounder at the time t,
- SL is the source level of the echosounder (see section 3.2.2),
- DI_{Tx} is the directivity index on the antenna at transmission (see section 3.2.3),
- $TL(t)$ is the transmission loss between the echosounder and the seabed at time t (see section 3.2.4),
- G_{calib} is the calibration gain of the echosounder antenna (see section 7.3.4),
- $\mathscr{A}(t)$ is the instantaneous insonified area on the seafloor at time t,
- x_i is a realization of the random variable $|\mathbf{A}|$ at time t. In other words, it corresponds to the corrected seafloor echo time-sample magnitudes in equation 5.2.1 where i is the time index (see illustration in figure 5.7).

In order to process an accurate estimation of the backscattering strength using x_i, parameters of equation 8.1 then need to be measured as precisely as possible. Three of them ensue directly from calibration of the echosounders (SL, DI_{Tx} and G_{calib}). In the case of the echosounder of the PhD, transmission loss ($TL(t)$) are calculated using the model of section 3.2.4. However, in the case of the echosounder of project S2MF, the propagation is non-linear therefore a different approach is used where the transmission loss are estimated in tank during calibration. Details are given in appendix C. The last parameter ($\mathscr{A}(t)$) can be derived using the models of section 3.2.13, but we saw in the previous chapters that this correction is not ideal. Consequently, $\mathcal{A}(t)$ is derived using a simulation in order to get a precise estimation of the instantaneous insonified areas according to the propagation time t. This simulation is based on the directivity functions of the echosounders and on their transmitted pulse envelopes, both measured during calibration.

Details of the calibrations of the echosounder of the PhD during measurements in the tank of the university of Bath and in the harbour of Brest are discussed in the first part of this section. Results of the calibration (in tank) of the echosounder of project S2MF are also shown in this section. Then the simulation of the instantaneous areas is presented, and finally, in the last part of this section, the method of detection and extraction of the seafloor echoes is described. At the end, a list of pings composed of corrected seafloor echo magnitudes is provided for processing in the next section.

8.2.1 Calibration

Three characteristics of the echosounders are needed to be calibrated in order to derived the sonar equation of equation 8.1:

- the calibration gain G_{calib}
- the directivity function $\mathcal{D}(\vartheta)$
- the pulse shape (i.e. the actual transmitted signal envelope).

The last two are employed in the simulation of the instantaneous insonified area (see section 8.2.2).

Calibration of the echosounder gain and pulse shapes were made using the method of the sphere target described in section 7.3.4. With the echosounder of the PhD, in addition to the calibration made in the tank of ENSTA Bretagne (see section 7.3.4), other calibrations were made in the tank of the university of Bath and in the harbour of Brest. This leads to a calibration of the three pulse lengths used with this echosounder (see table 8.4). The standard target used was a tungsten-carbide sphere of diameter 25mm. The echosounder of project S2MF was calibrated in the sea water tank of Ifremer (France) using also a tungsten-carbide sphere but of diameter 38.1mm, chosen because its frequency response have no anti-resonance at the frequencies used in the project (100 kHz, 200 kHz, 300 kHz).

The resulting calibration gains measured using equation 7.24 are given in table 8.4 for the echosounder of the PhD. They are all in the same order of magnitude as the gain measured in the tank of ENSTA Bretagne i.e. < 1 dB. In the case of the echosounder of project S2MF, calibration gains includes all parameters of the sonar equation that vary with range due to the

non-linear propagation. They are consequently variable, which is why they are not appearing in table 8.4. Details are given in Appendix C.

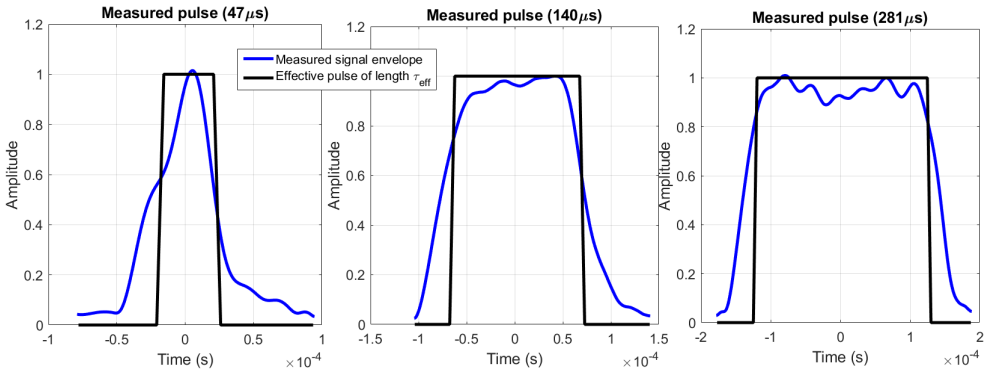

Figure 8.7 – Actual pulse shapes transmitted by the echosounder of the PhD corresponding to three theoretical pulse lengths (left: $5T \approx 47\mu$s, center: $15T = 140\mu$s, right: $30T = 281\mu$s) and equivalent effective pulse length τ_{eff}. Pulse shapes are measured during calibration on sphere in the tank of the university of Bath (United Kingdom) and in the harbour of Brest (France).

	Echosounder of the PhD			Project S2MF
Frequency ƒ	106.8 kHz			100 kHz
Gain G_{calib}	0.0 dB	0.9 dB	0.4 dB	-
Pulse length τ	$5T \approx 47\mu$s	$15T \approx 140\mu$s	$30T \approx 281\mu$s	$60T \approx 600\mu$s
Effective pulse length τ_{eff}	$3.6T \approx 34\mu$s	$13.7T \approx 128\mu$s	$25.9T \approx 242\mu$s	$58.8T \approx 551\mu$s
$2Sa_{\text{corr}}$	−1.4 dB	−0.4 dB	−0.6 dB	−0.37 dB

Table 8.4 – Calibration gains, effective pulse lengths and Sa_{corr} measured during calibration on sphere of the echosounders. Calibration of the echosounder of the PhD were made for a pulse length of $5T$ in the tank of the university of Bath (United Kingdom), for $15T$ and $30T$ in the harbour of Brest (France). Calibration of the echosounder of project S2MF were made in the tank of Ifremer (France) (see Appendix C).

The other parameter measured using the calibration sphere is the actual pulse shape transmitted and received by the echosounders. Figure 8.7 shows the pulse shapes measured for the three different pulse lengths transmitted by the echosounder of the PhD. We can observe that these pulse are not perfectly the squared pulse transmitted to the echosounder antenna. This effect is mainly due to the transducer bandwidth as discussed in section 3.2.15 and also to variations of the sphere TS in the transmitted signal frequency band. From these measured shapes, we can derive the effective pulse length τ_{eff} as the length of the square pulse of unit amplitude that has the same energy as the actual transmitted pulse. The energy of the pulse is computed by integration of the measured signal envelope. Resulting τ_{eff} are calculated from equation 3.80 and given in table 8.4 for each pulse length transmitted with the echosounder of the PhD, and also plotted in figure 8.7. In addition, the correction factor

$2Sa_{\text{corr}}$ corresponding to the loss of acoustic energy from the theoretical pulses to the actual pulses for mono-static systems (see section 3.2.15) are also given in table 8.4.

Directivity functions $\mathcal{D}(\vartheta)$ of the echosounders antennas were measured for both echosounders in tank using a standard hydrophone. For the simulation of the instantaneous insonified areas, 3-D directivity functions are employed. In the case of the echosounder of the PhD, its 3-D directivity function was measured directly using the Pan & Tilt system (see section 7.3.3.2). Results were given in figure 7.16. In the case of the echosounder of project S2MF, the 3-D directivity function is synthetically generated using the 2-D directivity function measured in tank at 100 kHz (see Appendix C). Because of non-linearities, the directivity function changes according to the range. An example is given in figure 8.8 for a range of 27 m.

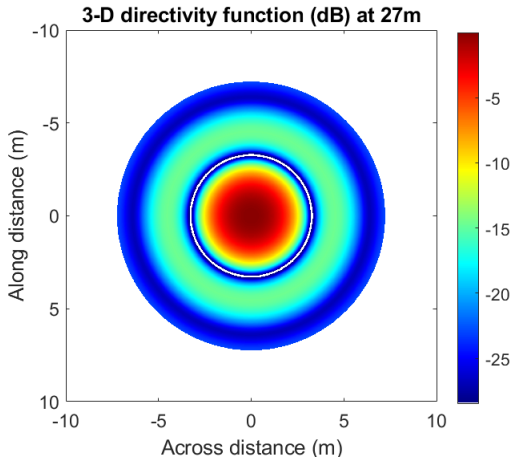

Figure 8.8 – Normalized 3-D directivity function of the echosounder of project S2MF, synthetically generated using the 2-D directivity function measured in tank at 100 kHz (see Appendix C) in 2018.

8.2.2 Simulation of instantaneous insonified areas

The simulation of the instantaneous insonified areas $\mathscr{A}(t)$ is based on the projection of the 3-D directivity function on a flat seafloor. Directivity functions of figure 7.16 and 8.8 are used. Examples of result of that projection are given in figure 8.9 for the echosounder of the PhD and of project S2MF. The simulation is run for different water heights of the echosounders above the seafloor and different tilted angles.

The propagation of the transmitted signal is simulated using the measured pulse shapes described in the previous section. The instantaneous insonified area at time t then corresponds to the area intersecting the pulse shape and the projected directivity function. This area is calculated as the sum of the contributions of each samples of the seafloor whose amplitudes are weighted by the directivity function and the pulse shape.

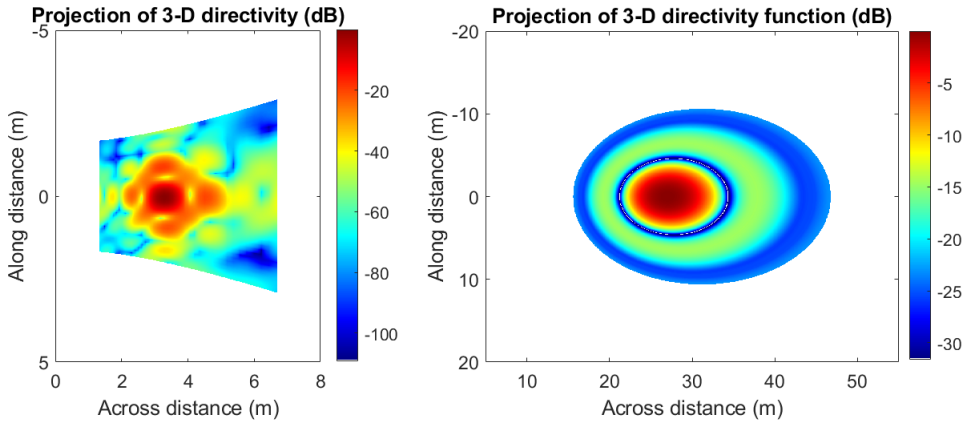

Figure 8.9 – Projection of the directivity functions of the echosounders on a flat seafloor. Left: echosounder of the PhD for a water height of 4.4m and a tilted angle of 36.7°. Right: echosounder of project S2MF for a water height of 27m and a tilted angle of 45°.

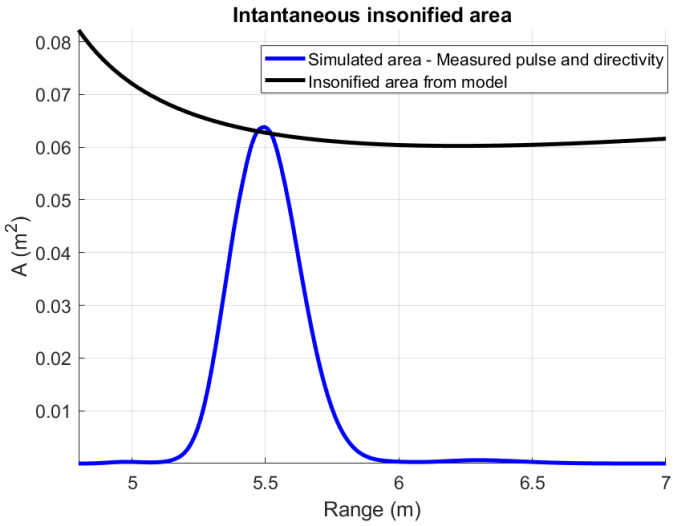

Figure 8.10 – Blue curve: Simulated instantaneous insonified area according the propagation range (or time) for a water height of 4.4m, a tilted angle of 36.7° and the measured pulse shape corresponding to a pulse length of $15T = 140\mu$s transmitted by the echosounder of the PhD. Black curve: Results of model of insonified areas derived from the range. Both for with the characteristics of the echosounder manufactured in this PhD.

An example of a resulting instantaneous insonified area according to time $\mathscr{A}(t)$ is given figure 8.10 (blue curve). The black curve is the insonified areas calculated for the same propagation time (or range) using the model discussed in section 3.2.13. We can see that this model is valid only around the maximum of the instantaneous insonified area i.e. in the center of the beam footprint. This result is expected because this model was designed to compensate the insonified area at the time of the bathymetric sounding which corresponds by definition to the center of the beam footprint i.e. the intersection between the seafloor

and the antenna axis. Using this model to correct the magnitudes of the time-samples away from the center of the beam may consequently induce errors as mentioned earlier in this manuscript and also in [Penrose et al., 2008].

This simulation of the instantaneous insonified area assumes that the seafloor is flat. In the tank of the university of Bath, this hypothesis is valid, however in the harbour of Brest we saw in section 8.1.2 that the terrain is not flat in the area of acquisition. The bathymetry measured with the echosounder and showed in figure 8.4 is therefore used to estimate the incidence angle of the transmitted signals on the seafloor. This incidence angle and the range of the detection of the seafloor echo are then used to derived a synthetic water height assuming the seafloor flat that can be used in the insonified area simulation. In the case of the measurements in the Bay of Brest the seafloor is supposed flat at the scale of the beam footprint even if this hypothesis cannot be verified.

8.2.3 Detection, correction and extraction of the seafloor echoes

In order to apply the estimation method developed in the second part of this manuscript, the seafloor acoustics echoes have to be detected, corrected and extracted from the echosounders data.

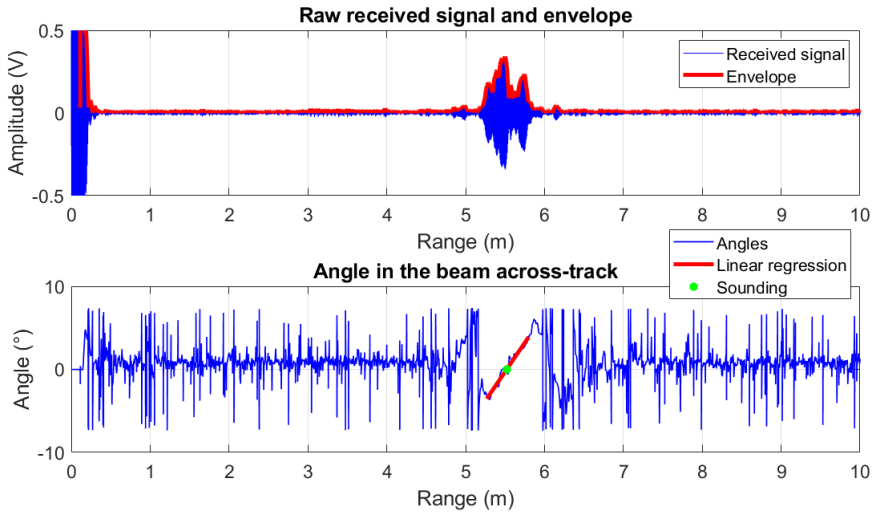

Figure 8.11 – Up: Raw signal received by the echosounder of the PhD for an incidence angle of 40° on the seafloor in the harbour of Brest (France). Down: associated phase angles derived from interferometry.

At first, seafloor echoes are detected using bathymetric methods of sounding detections as discussed in section 1.2: amplitude detection and phase detection. Figure 8.11 shows a representative example of a signal received by the echosounder of the PhD for an incidence angle of 40° on the seafloor. The seafloor echo is found around the maximum of the cross-correlation between the received signal (upper graph) and the theoretical transmitted signal. Then the sounding (green dot) is detected using the angle positions in the beam (lower graph)

that are derived from phase differences between signals received by the upper and lower part of the split-beam antenna. A linear regression of the phase ramp illustrated by the red line in the lower graph is made and the time-sample corresponding to the sounding (i.e. the center of the beam) is found where it crossed zero.

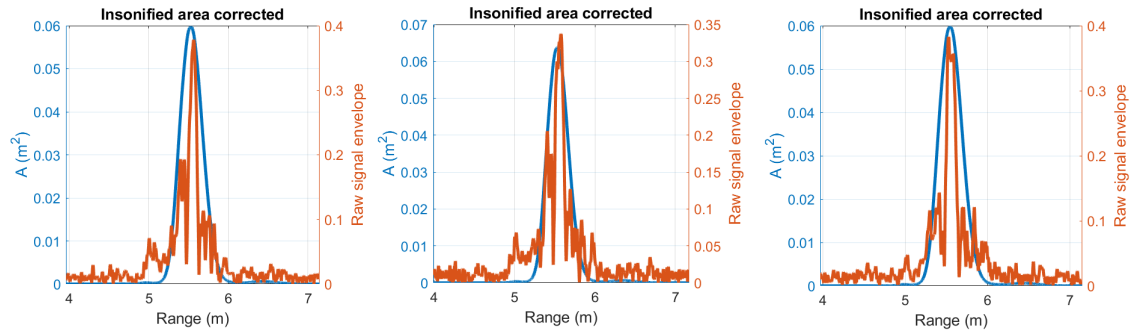

Figure 8.12 – Raw signal envelopes from consecutive pings received by the echosounder of this PhD in the harbour of Brest, and corresponding simulated instantaneous insonified areas. The incidence angle on the seafloor is calculated as 40°.

Once the seafloor echo is detected, a simulated instantaneous insonified area is associated to each time-sample. Figure 8.12 shows raw signal envelopes of three seafloor echoes detected on consecutive pings and their associated insonified area $\mathscr{A}(t)$. The sonar equation can then be applied, leading to corrected time-samples magnitudes. The last step is finally to extract only the time-samples that correspond to the seafloor echo. Because we want to retain the maximum of time-samples, limits of the seabed echo are determined when the insonified area is close to null. In practice this limit is also forced by the ambient noise observed on the signal i.e. limited by the signal to noise ratio.

At the end, seabed acoustic echoes are detected from the raw signals received by the echosounder, corrected from the sonar equation and extracted from the data. These steps are illustrated by figure 8.13 with data from the echosounder of the PhD acquired in the harbour of Brest.

8.3 Validation of the estimation method and its main hypotheses

Echosounder data acquired and prepared for processing as shown in the previous sections are now used to validate the model derived in chapter 5 on which is based the identification of the best estimator of the seafloor response. This model assumed several hypotheses that are discussed in chapter 5 and listed at the beginning of section 6.3.3. In short terms, these hypotheses include the following conditions:

1. The random nature of the seafloor,
2. The sonar equation parameters perfectly corrected,
3. The homogeneity of the seafloor,

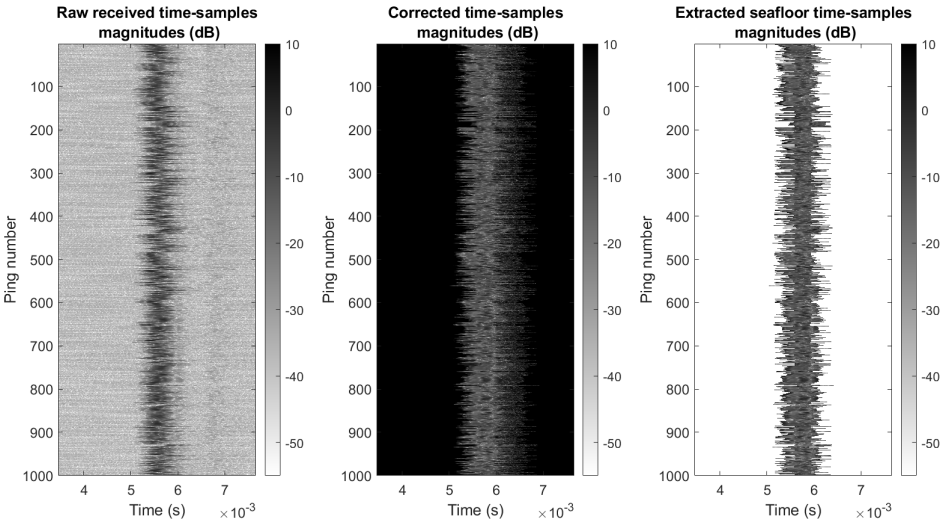

Figure 8.13 – Left: Raw seafloor echo magnitudes. Center: Corrected seafloor echo magnitudes from sonar equation parameters of equation 8.1. Right: extracted and corrected seafloor echo magnitudes. Data from the echosounder manufactured in the PhD and acquired in the harbour of Brest. The incidence angle on the seafloor is 16°.

4. The independence of the time-samples,
5. The corrected time-samples magnitudes following a Rayleigh distribution,
6. The identical distribution of the corrected time-samples magnitudes.

The first hypothesis is validated by making the measurements with the echosounders on true seafloor components, even in tank (see figure 7.2) where sediments are supposed representative of continental margin seabeds [Blondel and Pace, 2007]. Each type of seafloor studied with the three echosounders has its own roughness at the frequency of interest, from the finest (silt in the tank of the university of Bath) to the coarsest (pebbles in the harbour of Brest). The second hypothesis is supposed validated by using the pre-processing method described in section 8.2. Calibration of the echosounders and simulations of the instantaneous insonified areas ensured a precise control of sonar equation parameters. The third hypothesis of homogeneity of the seafloor is perfectly validated for measurements in the tank of the university of Bath where the sediments were prepared carefully in order to ensure their stability and homogeneity [Blondel and Pace, 2007]. In the harbour of Brest, the homogeneity of the seafloor type during measurements with the echosounder was ensured by the fact that the vessel was docked. Even if the seafloor is composed of multiple constituents (seagrass, pebbles...), it is the same mixture that is insonified by every pings. During acquisition in the Bay of Brest (project S2MF), the measurements were assumed on the same seafloor type by the drift of the vessel.

In the following, the validity of the last three hypotheses cited above is discussed.

8.3.1 Independence of successive time-samples

The independence of successive time-samples is controlled inside each ping individually. The received seafloor echo is detected and extracted as explained in section 8.2.3 and the raw time-samples magnitudes are corrected from the sonar equation 8.1 using the calibrated parameters (see section 8.2.1) and the simulated instantaneous insonified areas (see section 8.2.2). This leads to a list of corrected time-samples magnitudes as required by the model of chapter 5 for backscattering strength estimation. However, due to the geometry of the measurements and the method of acquisition, these time-samples are not independent. Indeed, the seafloor area intersected by the pulse during its propagation is insonified multiple times by different part of the pulse. Consecutive recorded time-samples therefore contain the same information as long as they are separated by less than a pulse length. For example, what is insonified by the first part of the pulse is then insonified by the last part of the pulse after a duration equivalent to the pulse length. A solution to avoid this effect is to retain only time-samples that are separated by at least one pulse length [Gensane, 1989]. In the following this method is called sub-sampling the seafloor echo time-samples.

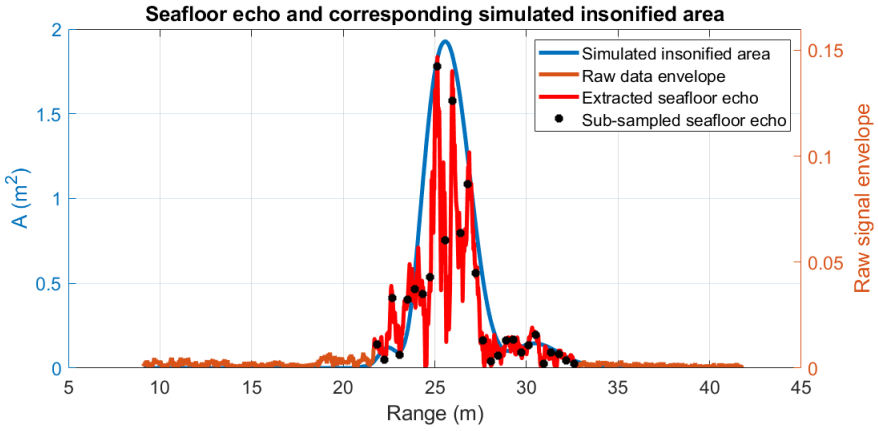

Figure 8.14 – Seafloor echo measured in the Bay of Brest (France) on area 1 of figure 4.2 during project S2MF at an angle of 45° for a water height of 20 m. Orange curve: raw received signal envelope. Blue curve: simulated insonified area. Red curve: extracted seafloor echo. Black dots: retained independent time-samples of the seafloor echo.

Figure 8.14 shows a typical example of a raw received seafloor echo (orange curve), the corresponding simulated insonified area (blue curve), and the time-samples that are finally retained (black dots). We can observe that the number of remaining time-samples is extremely lower than the number of time-samples in the raw signal. This is due to the high sampling frequency used for acquistion (2 MHz) and also the ratio between the beam width and the pulse length. The shorter the pulse, the more time-samples. And on the contrary, the shorter the beam aperture, the less time-samples. In this figure we can also observe the limit chosen to extract the seafloor echo which corresponds to a low insonified area but mostly to the range where the signal to noise ratio is close to unity. In the case of this measurement (with the echosounder of project S2MF), the extracted seafloor echo then includes signals from the main lobe and also the two first secondary lobes (i.e. the small bumps in the insonified area

curve before and after the high main lobe).

The final list of time-samples is consequently a list of independent magnitudes corrected from the sonar equation parameters which is what was assumed in the model of chapter 5 (see equation 5.2.1). The independence between successive time-samples is therefore validated.

8.3.2 Rayleigh hypothesis inside a ping

The Rayleigh distribution of the seafloor time-samples magnitudes is tested using the Kolmogorov-Smirnov statistical test [Saporta, 2006] where the Rayleigh parameter is estimated using the maximum likelihood estimate of the Rayleigh distribution. This test is applied separately on the seafloor echo raw data, on the corrected time-samples magnitudes, and on the corrected and sub-sampled (i.e. independent) time-samples magnitudes. For any seafloor echoes measured in the tank of the university of Bath, in the harbour of Brest, or in the Bay of Brest, the same results are observed:

- raw seafloor echo data are never following a Rayleigh distribution (e.g. for acquisitions made on area 1 during project S2MF 100% of the pings of all incidence angles do not validate Kolmogorov-Smirnov test), which is anticipated because of the non stationary nature of the measurements;
- corrected seafloor echo magnitudes are also not following a Rayleigh distribution (e.g. for acquisitions made on area 1 during project S2MF 100% of the pings of all incidence angles do not validate Kolmogorov-Smirnov test) which is probably due to the high correlation between successive time-samples;
- only corrected and sub-sampled seafloor echo magnitudes are mainly following a Rayleigh distribution (e.g. for acquisitions made on area 1 during project S2MF between 86% and 100% of the pings validate Kolmogorov-Smirnov test, depending of the incidence angle).

These results show the significance of respecting the independence hypothesis in order to validate the Rayleigh distribution hypothesis. The two conditions are then highly linked.

An illustration of these results is given figure 8.15 for one ping measured in the Bay of Brest during project S2MF. We can observe the clear change in the distribution from the raw data to the corrected data. A few time-samples are then retained after sub-sampling but the Rayleigh distribution is validated by the Kolmogorov-Smirnov test.

8.3.3 Identical distribution of all time-samples used

The last hypothesis for the model of chapter 6 to be valid is the identical distribution of all the time-samples used for the estimation. This condition is tested on the echosounder data using also the Kolmogorov-Smirnov test. We saw in the previous section that inside a ping, the corrected time-samples magnitudes follow a unique Rayleigh distribution. In this section, the objective is to test if this condition is still valid when several pings are taken into account. The Kolmogorov-Smirnov test is then applied on groups of corrected and independent samples magnitudes coming from a list of pings on the same seafloor type.

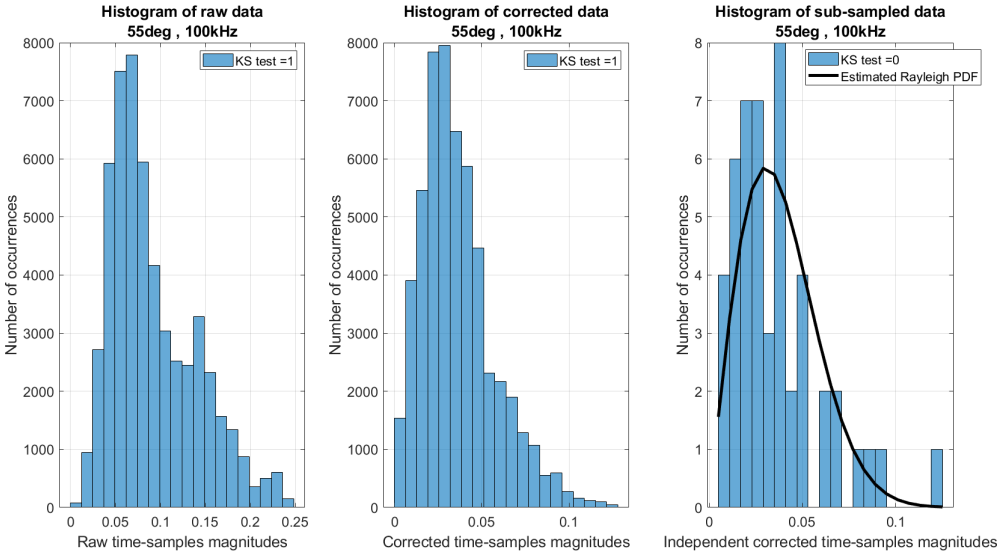

Figure 8.15 – Histograms of an extracted seafloor echo of one ping measured in the Bay of Brest (France) on area 1 of figure 4.2 during project S2MF at an angle of 55° for a water height of 20 m. Left: raw time-samples magnitudes. Center: corrected time-samples magnitudes. Right: corrected and independent time-samples. KS means Kolmogorov-Smirnov parameter: for KS=1 the test of a Rayleigh distribution is not valid (with 5% significance level), for KS=0 the test of a Rayleigh distribution is valid.

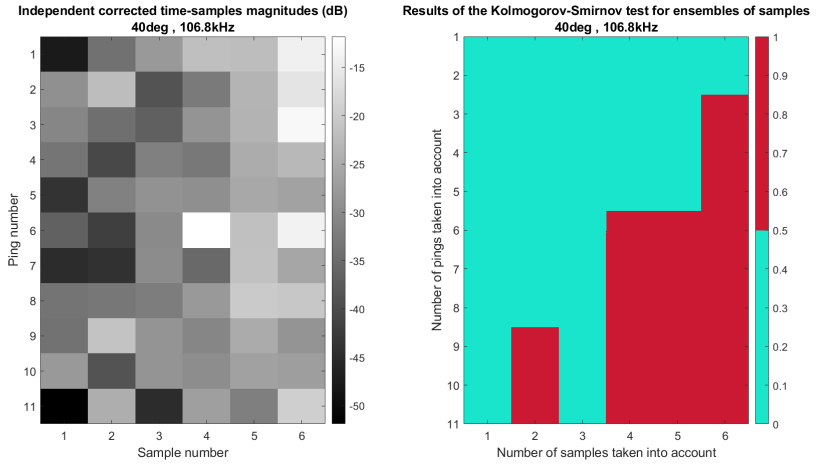

Figure 8.16 – Left: corrected and sub-sampled seafloor echoes measured in the tank of the university of Bath (United Kingdom) on the silt tray with an incidence angle of 40°. Right: results of the Kolmogorov-Smirnov test for groups of samples. When KS=1 (red) the test of a Rayleigh distribution is not valid (with 5% significance level), when KS=0 (green) the test of a Rayleigh distribution is valid.

In order to ensure the homogeneity of the seafloor for one ping to another, measurements were made in the tank of the university of Bath on the silt tray at 40° of incidence. The

independence of the pings was assumed by moving laterally the echosounder of 10cm between successive pings (the width of the projection of the beam footprint in these condition being 7.5 cm at the aperture $2\theta_{-3dB}$). Because of the short size of the tank in this side, only eleven positions were available. The resulting corrected and sub-sampled data are given on the left of figure 8.16. On the right are plotted the results of the Kolmogorov-Smirnov test. Samples are grouped starting by the upper left sample of the matrix, and going down to increase the number of pings. What we can first observe is that, even if the pings are independently following their own Rayleigh distributions (see figure 8.17 center), when they are mixed with each other they loose their rayleighness. Indeed, when all (eleven) pings and all time-samples (six) are taken into account (lower right of the matrix of figure 8.16) the group is not following a Rayleigh distribution. Nevertheless, we also observe on this figure that the more samples are used, the less pings can be used in order to maintain the rayleighness of the group. In the case of these measurements in tank, this effect can hardly be associated to the inhomogeneity of the seafloor as it was designed to be perfectly homogeneous, consequently only remains the following explanations:

- remaining imperfection in the correction of the instantaneous insonified area;
- changes in the backscattering strength from the first time-sample to the last (the first being at an incidence angle of 33° and the last at 47°);
- penetration of the signal inside the sediment generating also interferences between the backscatter signal from the interface and scattered signals from the volume of sediment;
- interference echoes due to the close environment of the measurements.

The first three effects are impacting the data in the horizontal direction (time-sample direction) of the matrix of figure 8.16. Therefore their impact should be lower when grouping only the same sample number of different pings. This is validated on the right of figure 8.17 where groups of samples are made individually for each sample position. Consequently these three effects are very likely impacting the data, even in a controlled environment, but they cannot be separated.

An example of deviation from the unique Rayleigh distribution on *in situ* seafloor is given in figure 8.18 using data acquired in the Bay of Brest during the drift of the vessel on area 2 of figure 4.2. The seafloor is assumed hard (see composition in figure 4.3) and composed mainly of gravel and brittlestars (see figure 8.6). We saw in section 4.2.3 that this terrain area is considered homogeneous and stable in the literature and used as a reference area for echosounder magnitude calibration [Eleftherakis et al., 2018]. Results of the Kolmogorov-Smirnov test are given in the center graph of figure 8.18 using the same method than previously. Samples are then grouped by considering at first the upper left corner of the matrix. We can observe the same pattern than the previous results in tank i.e. when the number of ping increases less samples can be taken into account to ensure the Rayleighness of the group.

Another test of the Rayleighness of the groups is realized by grouping them from the center of the echosounder beam. A group of one sample and several pings is in this case composed only of samples of the center of the beam i.e. of the soundings. Other samples are added symmetrically by moving away from the center to the side-lobes. Results of the Kolmogorov-Smirnov test of these groups are given on the right of figure 8.18. We can observe that groups composed of all time-samples are following a unique Rayleigh distribution using up to

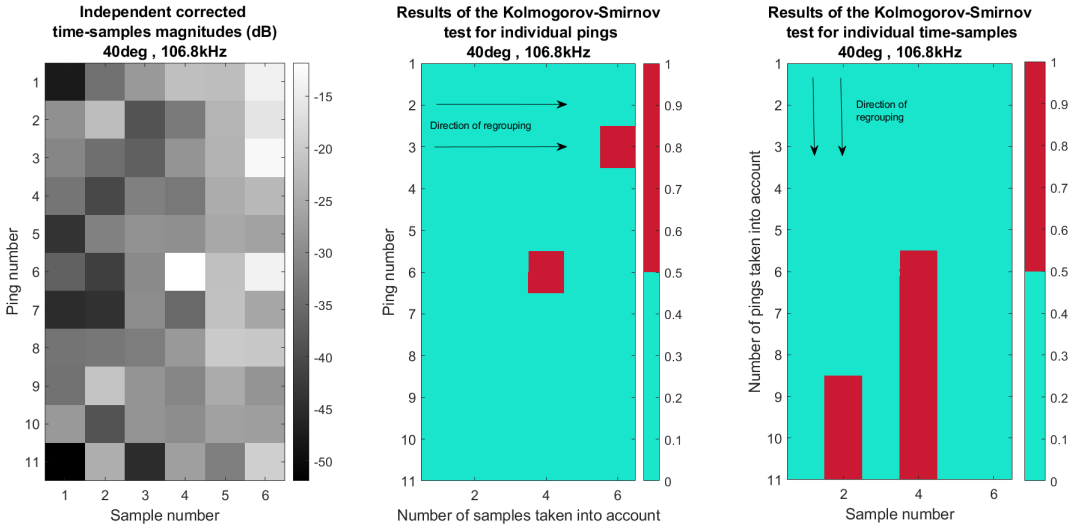

Figure 8.17 – Left: corrected and sub-sampled seafloor echoes measured in the tank of the university of Bath (United Kingdom) on the silt tray with an incidence angle of 40°. Right: results of the Kolmogorov-Smirnov test for groups of samples taken individually for each ping. Right: results of the Kolmogorov-Smirnov test for groups of samples taken only at the position of individual samples. When KS=1 (red) we reject the hypothesis that the distribution is Rayleigh (with 5% significance level), when KS=0 (green) we do not reject the hypothesis that the distribution is Rayleigh.

40 pings. This is almost the same result than when grouping the samples for the upper left corner of the matrix. However, when more pings are used we can observe that the number of samples is limited to a certain value away from the center of the beam. Outside of this limit groups of samples are not following a Rayleigh distribution anymore. This limit is plotted in figure 8.19 (red bars) with the corresponding simulated insonified area employed to correct the time-samples magnitudes. The link between the simulated insonified area and these limits is easily observed, the two red bars being symmetrical around the axis of the beam (i.e. the maximum of the insonified area). In this case, groups of samples are respecting the Rayleigh hypothesis until the end on the main lobe of the echosounder i.e. for a total aperture of 11°. This effect implies that the hypothesis of an identical Rayleigh distribution of the samples used to estimate the backscattering strength using the method derived in chapter 6 is only valid for samples extracted from the main lobe. Its origins can be one of the three explanations discussed above, or a mixture of them.

Results of figure 8.19 are processed for every incidence angles on the same seafloor area. Total apertures for which the groups of samples are still following a Rayleigh distribution for the maximum number of pings are plotted for each incidence in figure 8.20. Close to zero degree of incidence (nadir) the total apertures are null because of the sharpness of the echo. Very few independent time-samples are available for these angles, leading to few possibilities of apertures. On the contrary, for incidence angles larger than 15° the total apertures where the Rayleigh distribution hypothesis is valid are effective. We can observe in figure 8.20 that they are greater or equal to 6° which corresponds to the smallest $2\theta_{\text{-3dB}}$ aperture of the

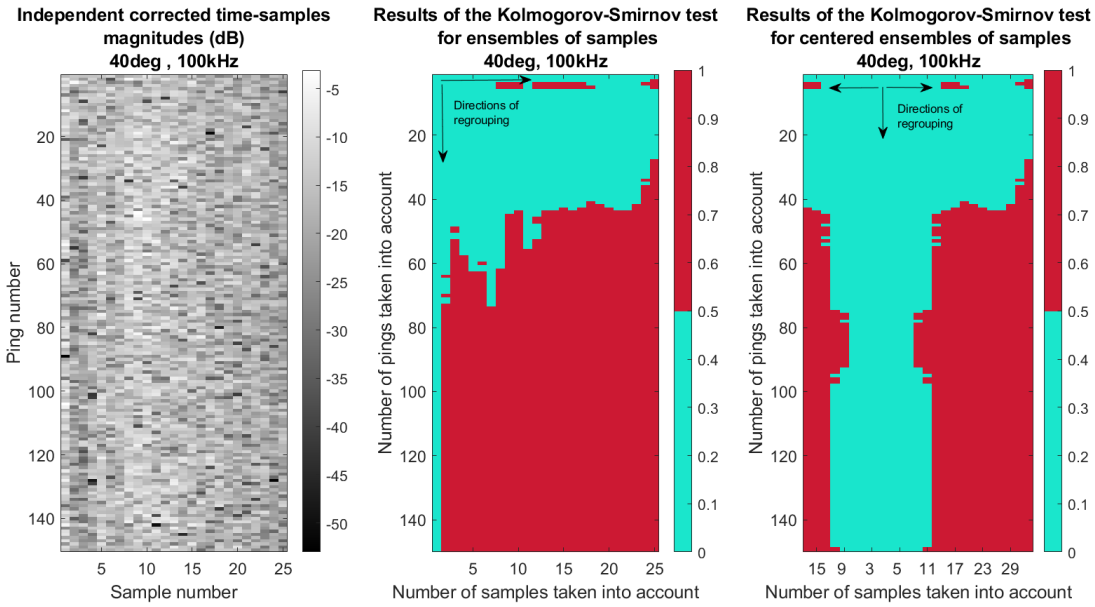

Figure 8.18 – Left: corrected and sub-sampled seafloor echoes measured in the Bay of Brest during project S2MF on area 2 (ravel and brittlestars) for an incidence angle of 40° and a water height of 17.5 m. Right: results of the Kolmogorov-Smirnov test for groups of samples taken by beginning on the upper left corner. Right: results of the Kolmogorov-Smirnov test for groups of samples taken by beginning on the center of the main beam. When KS=1 (red) the test of a Rayleigh distribution is not valid (with 5% significance level), when KS=0 (green) the test of a Rayleigh distribution is valid.

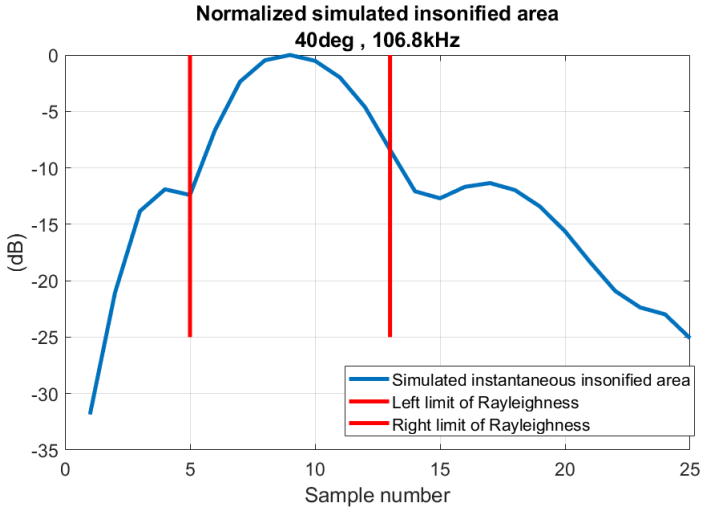

Figure 8.19 – Simulated instantaneous insonified area used to correct time-sample magnitudes for data of the Bay of Brest at an incidence angle of 40° (see figure 8.18). Red bars: limit of the group of samples that follow a unique Rayleigh distribution when the samples are grouped from the center of the beam toward the side-lobes.

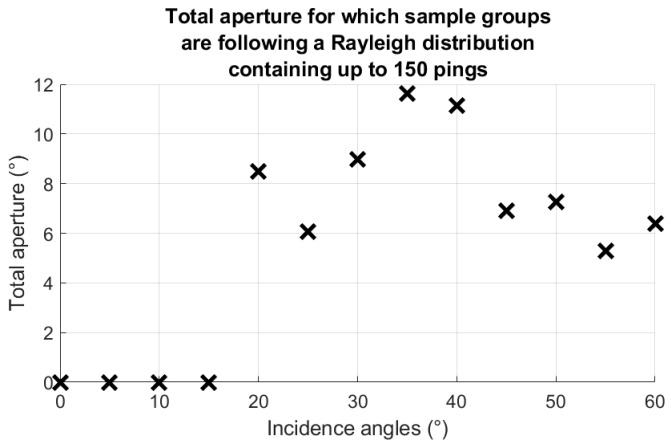

Figure 8.20 – Total aperture from which group of samples including all (150) pings are following a unique Rayleigh distribution according to the incidence angles on the seafloor. Data from area 2 of project S2MF survey at 100kHz.

echosounder at 100 kHz (see Appendix C). The same result is found with data from area 1.

From the results of this section, we can conclude that the identical distribution hypothesis on which is based the seafloor estimation model developed on this PhD is valid but under certain conditions. When a small number of pings is used, all the seafloor echo time-samples can be taken into account in the backscattering strength estimation (whatever the direction of grouping). If the signal to noise ratio is high enough, this can include time-samples originating from the side lobes of the antenna. Nevertheless, when several pings are used, only seafloor echo time-samples which correspond to incident angles included in the $2\theta_{\text{-3dB}}$ aperture of the echosounder can be retained.

8.3.4 Validation of the uncertainty theoretical formulation

The aim of this section is to validate the theoretical formulation of the seafloor response uncertainty developed in section 6.3. This formulation is based on the model of chapter 6 and is valid only for the best estimator of the backscattering strength i.e. the square sample mean of the corrected time-samples magnitudes. In order to verify that the theoretical variations of the uncertainty level according to the number of time-samples and pings taken into account can be retrieve in practice, echosounder data are used.

For validation of the uncertainty formulation, only data respecting the hypothesis under which the model of seafloor response estimation of chapter 6 is valid. In other terms, only time-samples that are corrected from sonar equation and independent are grouped. Then, groups are only retained when they follow a Rayleigh distribution (tests are made using the Kolmogorov-Smirnov test). Data acquired in the tank of the university of Bath while moving the echosounder on the same silt tray every 10 cm are used. This way the homogeneity of the seafloor is ensured.

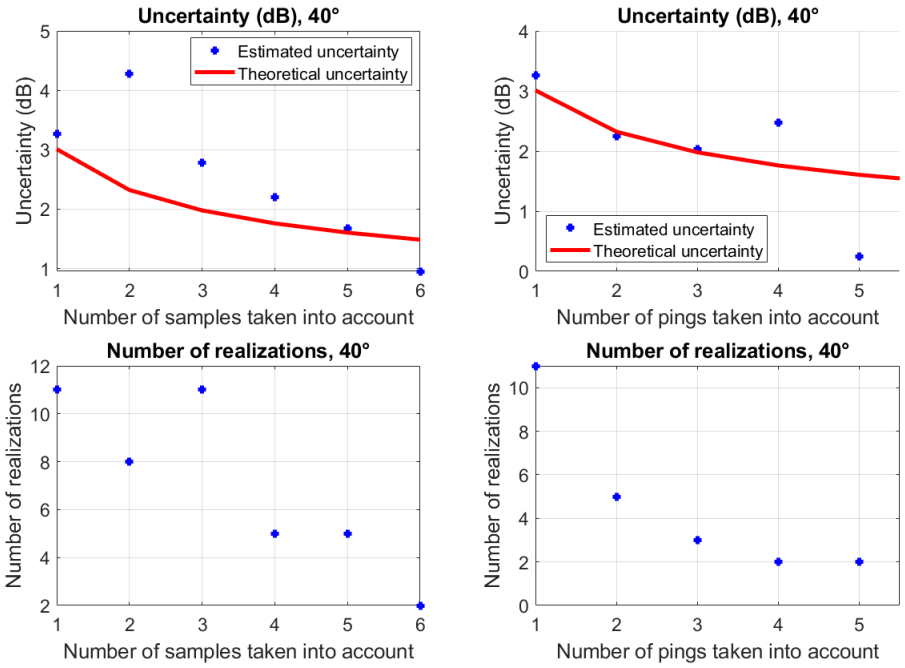

Figure 8.21 – Upper: theoretical and estimated uncertainty levels according (left) to the number of time-samples taken into account (for one ping), (right) to the number of pings taken into account (for one time-samples). Lower: number of realizations used to estimate the uncertainty level. Data at 40° of incidence angle on the silt tray in the tank of the university of Bath. Pings are acquired every 10 cm along the tray.

Uncertainty levels are first processed according to the number of time-samples taken into account. In this case, only one ping is considered. The theoretical uncertainty level is therefore equal to:

$$T_{1\text{ ping}} = 10\log_{10}\left(1+\frac{1}{\sqrt{n\text{x}1}}\right) \tag{8.2}$$

where n is the number of time-samples taken into account. This uncertainty is estimated using the pings recorded every 10 cm on the same tray as independent realizations of the first ping. The resulting estimation of the uncertainty level is given on the upper left of figure 8.21. On the lower left are given the number of realizations used to estimate each level of uncertainty according to the number of time-samples taken into account. Note that when the number of realization is lower than 3, the estimation of the standard deviation is not quite reliable. On these result we can observe that the estimation of the uncertainty is closed to the theoretical formulation, even if the results are highly variable. These variations are supposed due to the small number of realisations available.

The same way, uncertainty levels are processed according to the number of pings taken into account. Only one time-sample is then considered. The theoretical uncertainty level is

therefore equal to:

$$T_{1\text{ sample}} = 10\log_{10}\left(1 + \frac{1}{\sqrt{1\text{x}N}}\right) \tag{8.3}$$

where N is the number of pings taken into account. In this case, the different realizations of a group of pings are generated by using all the pings available. In total, eleven pings are available, therefore, a group of one ping has eleven realizations. A group of two pings has then five realizations, etc. The estimated uncertainty levels are finally given on the upper right of figure 8.21. On the lower right graph are plotted the corresponding number of realizations. Considering the above remark on the standard deviation reliability, only the three first values should be taking into consideration. Consequently, we can observe that the estimated uncertainty levels match to the theoretical formulation.

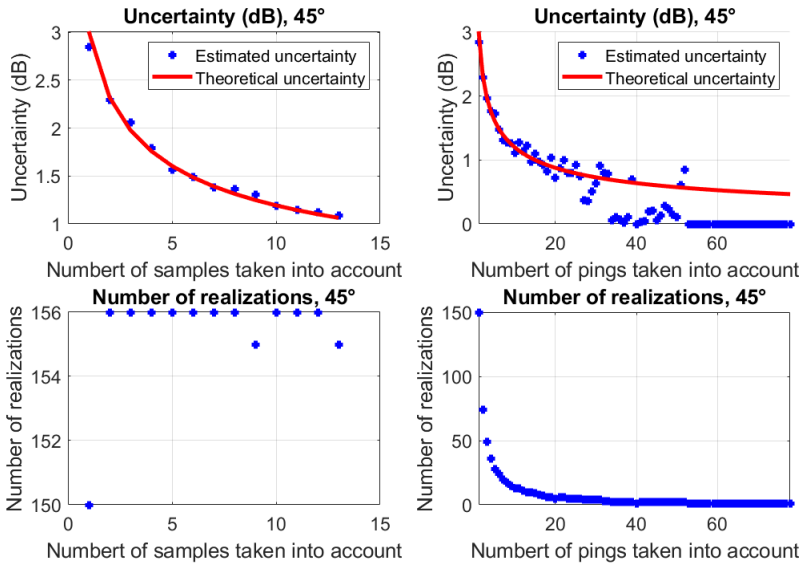

Figure 8.22 – Theoretical and estimated uncertainty levels according (left) to the number of time-samples taken into account (for one ping), (right) to the number of pings taken into account (for one time-samples). Lower: number of realizations used to estimate the uncertainty level. Data at 45° of incidence angle on the seafloor of the harbour of Brest. Pings are acquired every 3 seconds.

The same method is applied to echosounder data acquired in the harbour of Brest with the echosounder developed in this PhD. The resulting estimated uncertainty levels are shown in figure 8.22 according to the number of time-samples taken into account (left) or the number of pings taken into account (right). We observe that until a number of time-samples or pings of 15 the estimated uncertainty levels are perfectly following the theoretical formulation. On the right graph, uncertainty levels are given for numbers of pings above 15. Between 15 and 30 pings taken into account the variability of the results are probably due to the number of realization that decrease with the number of pings. Above 30 pings taken into account, the number of realization is very small, inducing a low reliability on the estimation of the

standard deviation and mean. In particular, when the number of realizations is unity, the standard deviation is null, leading to a null uncertainty level.

In conclusion, results of this section validate the formulation of the uncertainty levels that can therefore be used to estimate an *a priori* uncertainty of the backscattering strength during surveys.

8.4 Application of backscattering strength and uncertainty estimation to echosounder data

In this section we present four examples of application of the seafloor response estimation method developed in this PhD (see chapter 5) which includes the estimation of the backscattering strength and also the uncertainty level associated. The estimation method is based on the bathymetric process: for each ping, a reduction of the seafloor echo information is made using the best backscattering strength estimator identified in chapter 6 i.e. the square sample mean of the corrected time-samples magnitudes. Then all pings values are averaged to get the final estimation of the seafloor response. The uncertainty level is estimated as the ratio of the standard deviation to the mean of these pings values (see equation 6.44). Resulting estimated uncertainty levels are then compared to the theoretical formula 8.2 [2].

Data used in the followings examples are singlebeam echosounder data from project S2MF acquired in the Bay of Brest (France) on area 1 and 2 of figure 4.2 (see details in section 8.1.3 and multibeam echosounder data from project CALIMERO acquired in the Western Mediterranean basin (France) (see details in section 6.3.3.2)). Data from project S2MF are pre-processed using the method described in section 8.2. Data from project CALIMERO are already pre-processed by the echosounder software. However, in both cases, seafloor echo time-samples are sub-sampled in order to respect the independence hypothesis discussed in section 8.3.1.

In the three first parts of this section, data from project S2MF are processed. Because measurements were made while the vessel was drifting, the seafloor can be assumed homogeneous for all pings (150) acquired on both areas and at each incident angle. At first, a small amount of pings (five) is used to estimate the backscattering strength, and all time-samples of the seafloor echoes are used as discussed in section 8.3.3. In a second time, all pings are used (150) which requires to retain only time-samples inside the beam aperture ($2\theta_{\text{-3dB}}$ aperture as discussed in section 8.3.3). Then, in the third part of this section, the seafloor type is not supposed homogeneous any more between pings, and a perspective of identifying seafloor changes based on the estimated backscattering strengths and uncertainties is discussed. Finally, the last part of this section gives an example of resulting backscattering strengths and uncertainty levels obtained using multibeam echosounder data.

2. We use this formula function only of the number of samples because, as no *a priori* is made on the seafloor type and variation, pings cannot be grouped together to estimate the uncertainty according to the number of pings. In other words, realizations of a group of five pings are not available, consequently the uncertainty formulation depending on the number of ping cannot be estimated in practice.

8.4.1 Using a small amount of pings and all seafloor echo time-samples

In this section, only the five first pings recorded by the singlebeam echosounder of project S2MF are taken into account to estimate the backscattering strength, and all time-samples of the seafloor echo are used. Uncertainty levels are then also estimated using the same five pings. Theoretical uncertainties are calculated using formula 8.2 with a number of time-samples depending on the incidence angles. An error bar representation of the uncertainty levels is chosen which allows to use the two sides of the uncertainties T and T_- discussed in section 6.3 (see equations 6.44 and 6.46). We call them respectively positive and negative uncertainties.

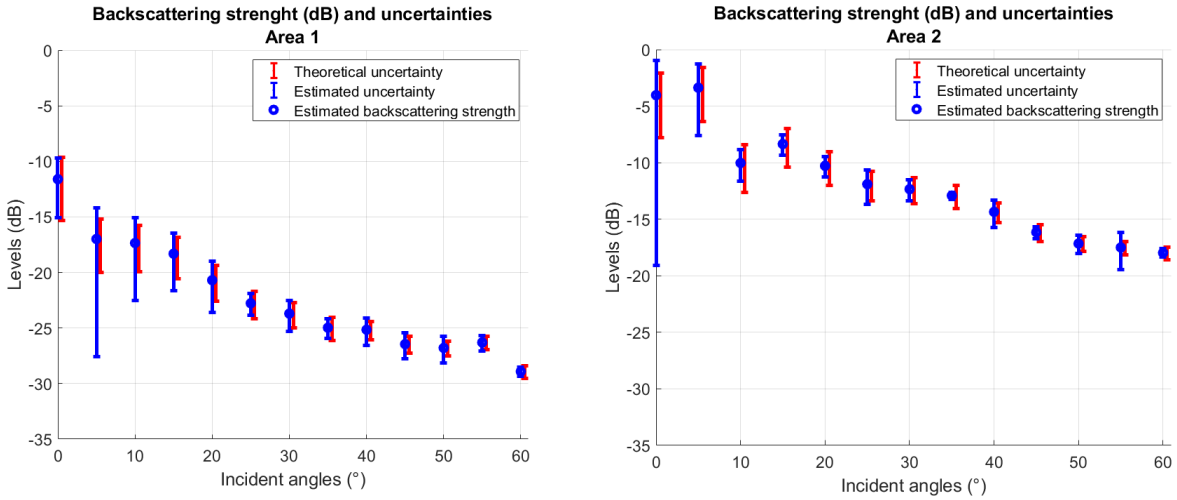

Figure 8.23 – Estimated backscattering strength and uncertainties, and associated theoretical uncertainties according to the incidence angles. Data from project S2MF. Left: area 1 (sand and mud). Right: area 2 (gravel and brittle stars). Five pings are taken into account and all time-samples contained in seafloor echoes.

Backscattering strengths and uncertainties are processed for the two areas and for each incident angles. This leads to angular response curves (ARC) where each backscattering strength estimation has its uncertainty level. Results are given in figure 8.23 where uncertainties are plotted as error bars around the backscattering strength values. At first, we can observe two distinguished ARC corresponding to each seafloor terrain. This result was expected because of the different composition of the seafloor areas and of previous results discussed in appendix C. Regarding the uncertainty levels, we can observe variations of the difference between theoretical and estimated uncertainty, depending on the incidence angle. Uncertainty levels are always close to theory (absolute differences [3] $< -3.8\,\mathrm{dB}$ for area 1 and $< -3.4\,\mathrm{dB}$ for area 2, and mean of these differences respectively -9.5 dB and -8.8 dB). We can also observe that at some angles the estimated uncertainty is higher than the theoretical uncertainty and at other angles the contrary appears. This effect could be related to the deviation of the group of samples from an unique Rayleigh distribution. Indeed, when the group

3. Calculated as $\Delta T_{\mathrm{dB}} = 10\log_{10}\left|10^{(T_{\mathrm{th}}/10)} - 10^{(T/10)}\right|$

of samples deviates from the unique Rayleigh distribution, two trends of the uncertainty levels where sometimes observed on data processed in this PhD:

1. estimated uncertainty level is higher than the theoretical level: samples belong to another distribution (or a mixture of distribution) that can be due to changes in the seafloor type, remaining imperfections in the correction of the sonar equations, penetration of the signal in the sediment, etc. (see discussion in section 8.3.3).
2. estimated uncertainty level is lower than the theoretical level: because the variance of the backscattering strength estimate reaches the Cramer-Rao bound (see section 6.1.4.2), this result is theoretically not possible. Nevertheless, in practice this result was observed when samples used are too correlated. In the case discussed here, the correlation takes place between pings, and can be due to the drift of the vessel that does not ensure the insonified areas to be properly separated.

Based on these observations, the comparison between theoretical and estimated uncertainties may possibly be employed as an indicator of deviation from the unique Rayleigh distribution.

8.4.2 Using all pings and time-samples in the beam width

This time, all pings acquired during measurement with the singlebeam echosounder of project S2MF are taken into account (i.e. 150) but used time-samples are only those contained in the beam aperture of the echosounder. Estimated backscattering strengths and associated uncertainties are plotted figure 8.24 according to the incident angle, for the two areas surveyed.

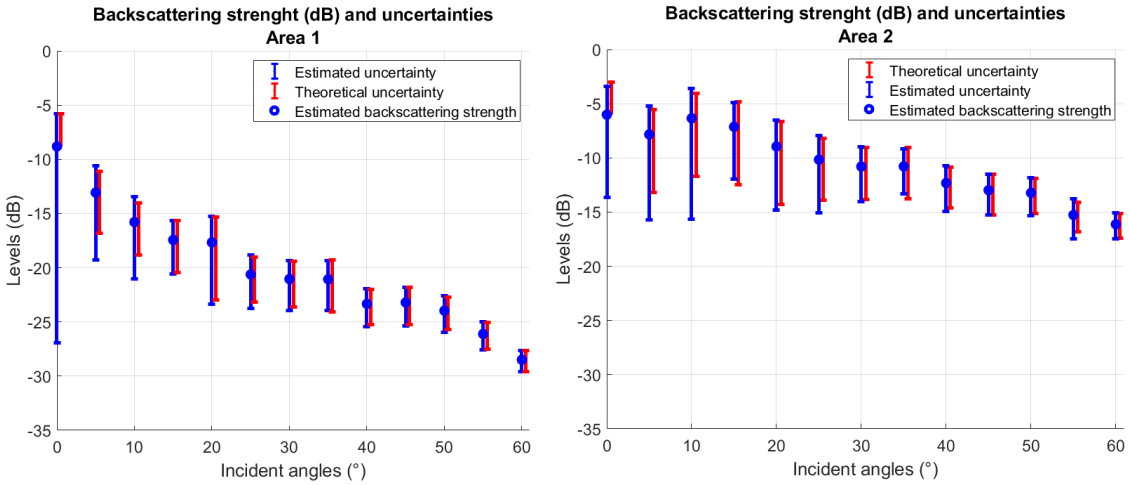

Figure 8.24 – Estimated backscattering strength and uncertainties, and associated theoretical uncertainties according to the incidence angles. Data from project S2MF. Left: area 1 (sand and mud). Right: area 2 (gravel and brittle stars). All pings available (150) are taken into account. Only time-samples contained in the beam aperture ($2\theta_{\text{-3dB}}$) of the echosounder are retained.

As previously, we can observe in figure 8.24 that the ARC are different between the two areas, leading to the possibility to distinguish the seabed types. However, when comparing

these ARC results with the previous ones (see figure 8.25) we observe differences between curves from the same area. In particular, estimated backscattering strengths are mostly lower when using all time-samples of the seabed echo than the ones estimated using only time-samples from the beam aperture. This effect is only due to the incorrect compensation of the directivity function, which is included in the calculated insonified area. Corrected magnitudes of the time-samples away from the center of the beam are in this case lower that the center time-samples, effect that should not appear with a precise correction. Under this effect, the more time-samples taken into account, the lower the estimated backscattering strength is. The variability of the difference between the estimated and theoretical uncertainty levels is probably a marker of this improper correction of the directivity function. We can note that when using data from project S2MF, the perfect correction of sonar equation parameters is sensitive because of the non-linear propagation that impacts the transmission loss of the fundamental frequency (100 kHz) but also its directivity function (see details in appendix C).

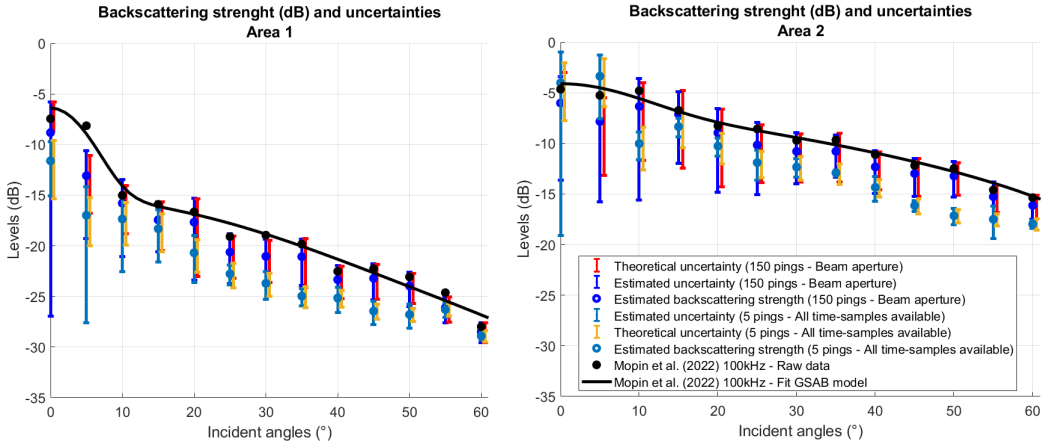

Figure 8.25 – Comparison of estimated backscattering strength and uncertainties according to the incidence angles a) using five pings and all time-samples of the seabed echo or b) using 150 pings and time-samples inside the beam aperture. Black cross and circles are backscattering strengths processed in [Mopin et al., 2022] (see appendix C) and black curves correspond to their angular response curve fitted with GSAB model discussed in section 2.2.4. Data from project S2MF. Left: area 1 (sand and mud). Right: area 2 (gravel and brittle stars).

In figure 8.25 are also plotted backscattering strengths resulting from the processing described in [Mopin et al., 2022] (see appendix C) based on [Eleftherakis et al., 2018]. Corresponding ARC are generated using GSAB model discussed in section 2.2.4. Backscattering strengths are estimated by calculating the mean of the square corrected time-samples magnitudes for each ping and then averaging all ping values. The correction of sonar equation parameters is the same as used in this PhD excepted that a model of insonified area is used (see section 3.2.13) and not a simulation. Time-samples retained from seafloor echoes are only those inside ±1° around the center of the beam. Consequently, two differences remain between the processing of the article and the processing of the PhD:

1. In the article all time-samples in ±1° around the center of the beam are retained for backscattering strength estimation. Thus they are not all independent, and they are

taken in a closer angular range than in the processing of the PhD (the beam aperture is larger than 1°).

2. In the article, the model of insonified area is used, which can lead to bias in the correction of time-samples away from the sounding.

Differences between the ARC of the article and results from the estimation method of this PhD observed in figure 8.25 are mainly induced by the items of the above list.

In term of uncertainty, in the case of using only time-samples from the beam aperture, the estimated uncertainties are almost all equal to the theoretical uncertainties whatever the angle (absolute differences [4] $< -6.9\,\text{dB}$ for area 1 and $< -7.5\,\text{dB}$ for area 2, and mean of these differences respectively -13.0 dB and -11.5 dB). At 0° the negative uncertainty level cannot be represented in decibels because the number $nN = 1$ therefore (from equations 6.46 and 6.47):

$$T_{-} = 10\log_{10}\left(1 - \frac{1}{\sqrt{nN}}\right) \xrightarrow[nN\to 1]{} -\infty \tag{8.4}$$

From these results, we can deduce that grouping only time-samples from the beam aperture of the echosounder almost ensure the validity of the identical Rayleigh distribution hypothesis. Consequently, when doubts remain on the compensation of the directivity function, smaller groups of time-samples could be considered, knowing that the number of pings that is relevant to use depends of the spatial variability of the seafloor.

8.4.3 Application to seafloor changes detection

Among the data acquired on area 2 during project S2MF, a specific behaviour is noticed at the incidence angle of 55° where it seems to appear a change in the seafloor type. In effect, when observing the image of the corrected time-samples magnitudes, a trained user can detect a darker area which probably corresponds to a change in the sediment composition [5]. Figure 8.26 (left) shows this image. The darker area can also be identified on the image of sub-sampled (independent) corrected time-samples magnitudes shown in the center of the figure.

In this part of the section, the processing of backscattering strengths and their associated uncertainties is made by taking groups of five pings composed only of time-samples inside the beam aperture, and moving this window from the first to the last ping (from up to down on the image of figure 8.26). Note that consecutive groups overlap. Results are given according to pings (centers of the group of five) on the right graph of figure 8.26. On this graph we can observe variations of the estimated backscattering strengths all along the pings. However, for most of the groups, these variations are not higher than the uncertainty levels. They can thus be considered as intrinsic variations of the seafloor acoustic response. The same seafloor type can therefore be assumed. Nevertheless, around ping 95 and around ping 115, backscattering strength variations are higher that the uncertainty levels. In this case, we can thus consider

4. Calculated as $\Delta T_{\text{dB}} = 10\log_{10}\left|10^{(T_{\text{th}}/10)} - 10^{(T/10)}\right|$

5. Note that in this case the change of magnitudes can also be due to a variation in the transmitted pulse amplitude or the presence of an obstruction in front of the echosounder (algae, etc.). Nevertheless all hypotheses should be taken into account.

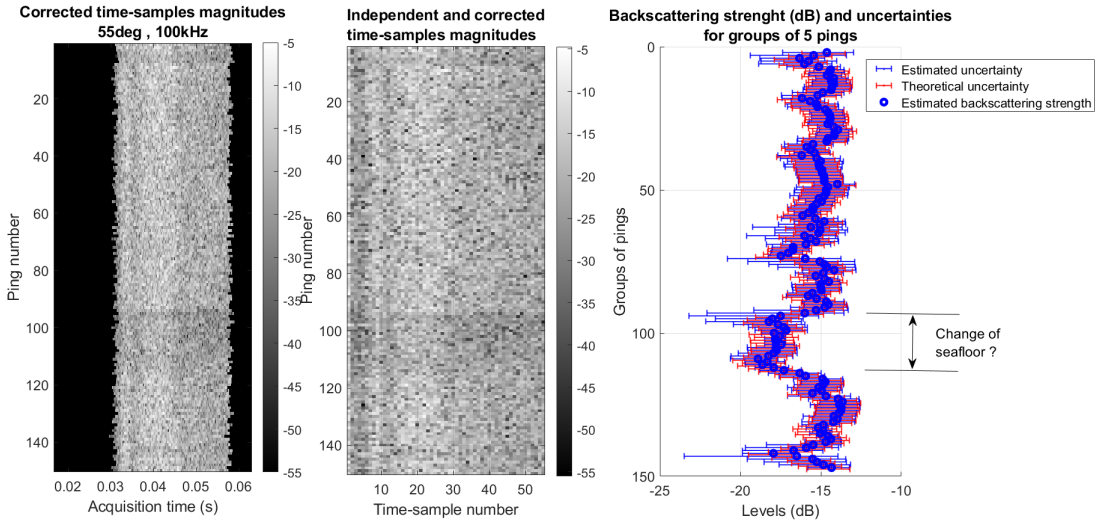

Figure 8.26 – Left: corrected time-samples magnitudes. Center: sub-sampled (i.e. independent corrected time-samples magnitudes. Right: estimated backscattering strengths and associated uncertainty levels (estimated and theoretical) for groups of five pings and only time-samples contained in the beam aperture ($2\theta_{\text{-3dB}}$) of the echosounder. Data from project S2MF acquired on area 2 at a pointing angle of 55°.

that these variations are due to a change of distribution which can be potentially related to a change of seafloor type.

To conclude, the estimated uncertainty levels seem to be useful to identify changes in the seafloor. However, this result should be confirmed by processing echosounder data where seafloor variations are known in order to evaluate the ability of this method to detect concrete terrain modifications and under which conditions.

8.4.4 Application to multibeam echosounder data

In this last section, the method of grouping five pings and move this window along the pings is applied to multibeam echosounder data acquired in survey with Kongberg EM300 during project CALIMERO. The same survey line as discussed in section 6.3.3.2 is used, but only the first 129 pings of the line are processed. Resulting backscattering strengths and estimated uncertainty levels are given figure 8.27. They are calculated for each beam pointing angles of the MBES. Theoretical uncertainty levels are also computed using formula 8.2. We retrieve the same results than figure 6.18. On the right of figure 8.27, an example of estimated backscattering strength and uncertainty levels is plotted for the echosounder beam pointing at $-54°$.

On the left graph of figure 8.27 we can observe a sort of Moiré effect on the image which is due to the overlap of successive groups of pings. In the center-left graph are plotted the estimated uncertainty levels associated to the backscattering strengths estimation of the left graph. These uncertainty levels can also be called *a posteriori* uncertainty levels as they are

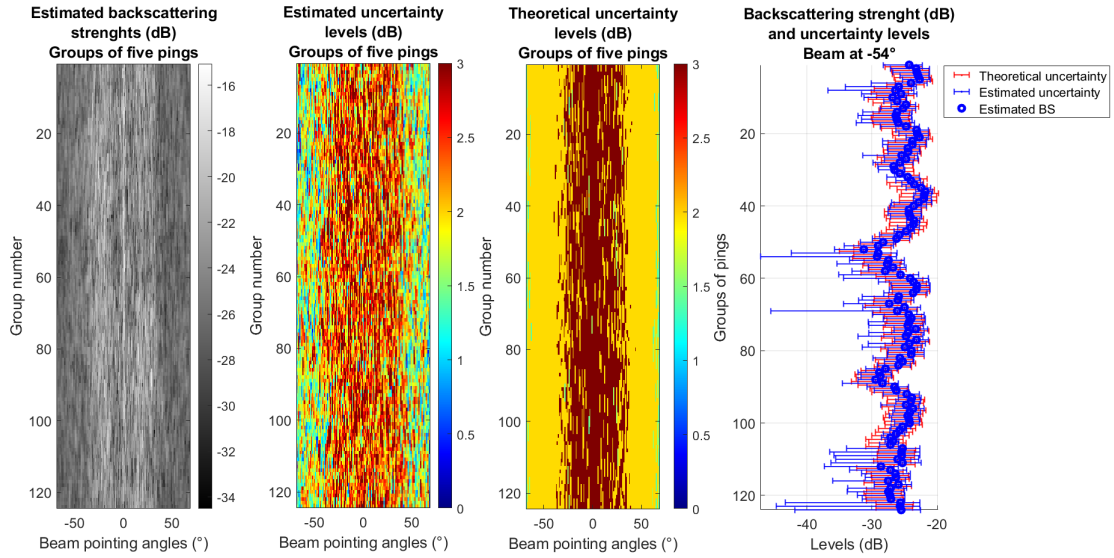

Figure 8.27 – Estimated backscattering strength and uncertainty levels from Kongsberg EM300 multibeam echosounder. Data from project CALIMERO. Pings are grouped by five and composed of available and independent time-samples.

computed from actual measurements. They can be then compared to *a priori* uncertainty levels that are calculated using the theoretical formula and shown on the center-right graph of the figure. Theoretical uncertainty levels show a geometrical pattern were center beams have higher values than grazing angle beams. This is mainly due to the small number of samples available in that area. In practice, we see on the estimated uncertainty levels that this effect is not that strong and that the limits between the two regimes is quite fuzzy.

When comparing *a priori* and *a posteriori* uncertainty levels for all the image of figure 8.27 we found a mean of absolute differences of 0.6 dB with a maximum at 2.5 dB. An example of details of the uncertainty levels is given on the right graph of the figure for the beam at $-54°$. We can observe variations of backscattering strengths but also variations of the differences between theoretical and actual uncertainty levels. As discussed previously, these results can be informative about the quality of the estimation in term of deviation of the group of sample magnitude from the Rayleigh distribution.

8.5 Summary

In this chapter we discussed the validity of the model of chapter 5 on which is based the seafloor acoustic response estimation method. For this purpose, singlebeam echosounder data were employed. They came from two different systems: the echosounder designed and manufactured during this PhD (see chapter 7) and the echosounder manufactured as a prototype of multifrequency echosounder during project S2MF (see appendix C). The advantage of these echosounders is that raw recorded data are available for any processing which led us the opportunity to apply a specific pre-processing as presented in section 8.2. It is composed at first of the calibration of the echosounder, including the measurements of its 3D-directivity

function and the actual transmitted pulse shapes. Then, the instantaneous insonified areas are simulated using these parameters. And finally, detection and extraction of seafloor echoes are computed before correcting each time-samples of the echo from the sonar equation parameters.

Using these pre-processed data, the validation of the model of chapter 5 was first analysed by evaluating the validity of its fundamental hypotheses. Two of them (the random nature of the seafloor and its homogeneity) were assumed valid based on the context of the measurements itself. Indeed, the singlebeam echosounder acquisitions were made in tank (at the university of Bath (UK)), or with the vessel docked (in the harbour of Brest (France)) or drifting (in the Bay of Brest (France)), ensuring little spatial variations of the insonified terrain area. The perfect correction of the sonar equation parameter was also assumed valid, using the previously discussed pre-processing (even if, in the case of project S2MF data, it was shown later that some inaccuracies of the directivity function corrections remain). The last three hypotheses were discussed independently and using the echosounders data for validation. At first the independence of successive time-samples was validated by sub-sampling the data where the separation between two remaining time-samples corresponds to a pulse length (see section 8.3.1). Then the Rayleigh distribution of these time-samples corrected magnitudes was verified based on the Kolmogorov-Smirnov test (see section 8.3.2). And finally, the identical distribution of all retained time-samples corrected magnitudes was studied according to the method of grouping the samples. These results informed us that grouping all the time-samples of the seafloor echo limits the number of pings acceptable under the Rayleigh distribution hypothesis. However, when limiting the number time-samples used, the number of ping could be increased. This effect is mainly due to the remaining imperfections in the instantaneous insonified area corrected, in particular with data from project S2MF echosounder. In that case, we saw in section 8.3.3 that the identical Rayleigh distribution hypothesis is effective when retained time-samples originate from angles inside the beam aperture of the echosounder.

Once these fundamental hypotheses were validated, the uncertainty theoretical formulation of equation 6.49 was evaluated using the same echosounder data. Its variations according to the number of time-samples was estimated using the different pings on the same terrain area as realizations of the list of time-samples. Its variations according to the number of pings used was also evaluated using the different pings but by grouping them by a changing number. Accurate results were found with echosounder data from the tank of the university of Bath and from the harbour of Brest.

In the last section of this chapter, different examples of application of the method of estimation of the backscattering strength and its uncertainty level developed in this PhD were given. Data from measurements in the Bay of Brest (France) with the singlebeam echosounder of project S2MF (tilted mechanically) were used to illustrate the backscattering strength estimation using in the one hand a small amount of pings and all seafloor echo time-samples and in the other hand all pings but time-samples in the beam aperture of the echosounder. Angular response curves were computed and compared. Uncertainty levels estimated were in both cases and whatever the incidence angle inferior to 1.1 dB, with an improvement 0.55 dB when the limit of the beam aperture is used. The results of these

analyses informed us about the remaining imperfection of the directivity function correction with these data.

A particular set of data from Project S2MF was also used in section 8.4.3 to evaluate the usefulness of the uncertainty levels in detecting seafloor changes. We observed that these levels can be informative of changes when the variability of the backscattering strengths exceeds the uncertainty level. This was noticed on the example presented but more results need to be added to validate this assumption. In particular using data were actual seafloor changes are known. The uncertainty levels were also observed ections 8.4.1 and 8.4.2 to be indicative of the validity of the Rayleigh distribution hypothesis when compared to the theoretical uncertainty levels. This can contain information about the inhomogeneities of the seafloor terrain or, on the contrary, about the excess of correlation between successive pings (e.g. due to the stationarity of the vessel).

At the end of this chapter, the estimation method is applied to multibeam echosounder data from project CALIMERO that were discussed in section 6.3.3.2. Backscattering strengths and uncertainty levels were estimated for each beam by grouping five pings after sub-sampling the data provided by the echosounder (note that the pre-processing was not modified). In this case, uncertainty levels were higher ($< 2.5\,\mathrm{dB}$) which is mainly due to the small number of independent samples remaining for each beam. Differences with theoretical uncertainty levels were however of $0.6\,\mathrm{dB}$ in average. These results allow to conclude that the method developed in this manuscript can be accurately applied to MBES survey data. In this case, the number of pings to group should be chosen wisely as a compromise between the resolution of the resulting map (or digital terrain model DTM) and the desired uncertainty level. In addition, attention should be brought to the spatial variability of the seafloor that can provoke deviation from the Rayleigh distribution hypothesis.

Conclusion

The objective of this last part of the PhD was to apply the method of estimation of the seafloor acoustic response on data from echosounders. For this purpose, a specific singlebeam and splitbeam echosounder was designed and manufactured during the PhD. After a precise calibration in tank, this echosounder was used to acquired data in the harbour of Brest (France) and in the tank of the university of Bath (United Kingdom) where sea sediment are disposed in the bottom in different trays. These data were used to verify the validity of the fundamental hypotheses on which is based the proposed backscattering strength estimation method. To complement, data from a singlebeam echosounder manufactured during project S2MF (2018) were used. They were also employed to evaluate the usefulness of the backscattering strength uncertainty formulation. At the end, an example of results using multibeam echosounder data from project CALIMERO (2005) was presented.

The echosounder manufactured in this PhD was designed under two dimensioning constraints: 1) employing piezoelectric ceramics available at Sorbonne University (France) as component of the transducers and 2) the echosounder could be used in the tank of the university of Bath. In order to increase the precision of the correction of sonar equation parameters during data pre-processing, the echosounder was also chosen to be splitbeam. Under these conditions, the echosounder was designed as a square antenna of length 11 cm, and its main transmission frequency was evaluated as 106.8 kHz. Its total beam aperture is 4.2 ° and its far field distance 86 cm (all characteristics of the echosounder are given in table 7.1). Calibration of the echosounder was performed in the tank of ENSTA Bretagne (France). All sonar equation parameters were estimated from measurements, including the 3D-directivity function (see section 7.3). This parameter was then used to simulate the instantaneous insonified area (see section 8.2.2). Because the transmitted pulse length changed between acquisitions in tank and in the harbour, sphere calibrations were also performed during each measurement campaigns (see section 8.2.1). Calibration gain were therefore controlled and adjusted to measurement conditions.

Data acquired during the PhD and during project S2MF were used to verify the validity of the hypotheses made to derive the backscattering strength estimation method (see section 8.3). In particular, three assumptions were analysed: the independence of the seafloor echo time-samples used to estimate the backscattering strength, their magnitudes (corrected from sonar equation parameters) following a Rayleigh distribution, and the identical distribution of grouped samples magnitudes. From these studies, we concluded that the independence of the

time-samples can be obtained by sub-sampling the seafloor echo time-sampling by at least a pulse length. In that case we observed that for a ping, corrected time-samples magnitudes are in most of the cases following a Rayleigh distribution. However, when grouping pings together to estimate backscattering strengths, we noticed that restraining the group of time-samples to the aperture of the echosounder ensured to respect the identical Rayleigh distribution hypothesis. This effect was observed when using data from project S2MF. It is very likely due to remaining imperfections of the directivity pattern correction which is included in the simulation of insonified areas. Because of the prototype nature of project S2MF echosounder and in particular the non-linear generation and propagation of the signals, limits of this type appeared in the correction of sonar equation parameters. The development of an echosounder during this PhD was, inter alia, dedicated to avoid these limits. Acquisitions with this echosounder were planned in the Bay of Brest, however, unexpected delays (e.g. global pandemic) impacted the manufacture, leaving less time for measurements at sea at the end of the PhD. Further investigations should therefore be informative of the impact of a precise correction of sonar equation parameters on the validity of the identical Rayleigh distribution according to the number of ping employed and the position of samples in the beam.

Following the validation of the model hypotheses, the theoretical uncertainty formulation was verified on the same data set (see section 8.3.4). Comparisons between analytical results and estimated uncertainty levels were presented. They show good agreement according to the number of pings and time-samples taken into account. Limits of this results were discussed, in particular the impact of the number of realizations available to estimate the uncertainty levels.

The backscattering strength estimation method being validated, it was then applied to *in situ* data acquired during project S2MF on two different terrains: a hard seafloor composed of gravel and brittlestars, and a soft seafloor composed of sand and mud. Backscattering strengths were estimated for several incident angles, leading to angular response curves (ARC). These curves allowed to identify the two different terrains. Results were compared to a classical method of estimation used in [Mopin et al., 2022] (see appendix C). In addition to backscattering strengths, uncertainty levels associated to the results were calculated. We observed that this parameter can provide information about the deviation of sample groups from the Rayleigh distribution when compared with theoretical results. It was also noticed that the uncertainty level could potentially be an additional parameter to detect seafloor changes. Indeed, variations larger that the intrinsic variability of the seafloor response can be located using the uncertainty level associated to the backscattering strength estimation. Note that the uncertainty formulation that is used in this context of application only depends of the number of time-samples (see equation 8.2) as no realization of a ping on the exact same terrain is technically measurable.

At the end of this part, the seafloor response estimation method was applied to multibeam echosounder data (see section 8.4.4). The feasibility of this application was demonstrated with also the ability to process the uncertainty levels associated to backscattering strength estimations. In further works, this part could be developed and extended to estimation of the seafloor response for digital terrain model (DTM). In this case, the general uncertainty formulation including the number of time-samples and also the number of pings (see equation

6.49) should be used because several estimations of the backscattering strength are used to process the result of a DTM cell, the same way that several soundings are used to process the bathymetric value of a DTM cell. In this context, the seafloor is consequently supposed homogeneous inside each DTM cell, and the uncertainty level decreases with the number of pings used to evaluate the backscattering strength. A compromise is therefore to be made between a low uncertainty and high DTW resolution.

Chapter 9

Conclusions and perspectives

Historically, the seafloor nature is an important feature used by navigators to locate their ship as a complement to the water height. In addition to soundings, seafloor type had thus appeared on nautical charts since the 19th century. At this time, soundings were measured manually using a lead line and so was the seabed composition. Later, following the development of underwater acoustics, echosounders were designed for navigation safety and then used in hydrographic surveys. Soundings were therefore measured by acoustics and charts mostly based on these measurements. The extraction of seafloor type information from these measurements came consequently naturally to complement the soundings. Nowadays, numerical soundings are mostly all associated with a seabed related attribute, calculated from the seafloor acoustic echo and called the seafloor acoustic response. Beyond nautical charts, this response is used also in various marine applications such as seabed characterisation, seabed classification, habitat mapping, seafloor monitoring, sonar performance modelling, or acoustic propagation modelling. The objective of this PhD was to characterise accurately the seafloor acoustic response, without any link to a specific application but the identification of the seabed. Nevertheless, the context was restrained to the use of singlebeam and multibeam echosounders (respectively SBES and MBES) in hydrography. Developments were therefore based on the bathymetric method employed in practice and in literature were a sounding is evaluated for each ping and beam of the echosounder and then grouped with other soundings to generate a digital terrain model (DTM). In this context, the seafloor acoustic response is usually called backscattering strength, namely because of the operation geometry of SBES and MBES which is based on the scattering of the acoustic signal from the seafloor back to the echosounder.

Accurate characterisation of seafloor acoustic response to improve seabed identification

When examining the title of this PhD in detail, five concepts emerged: the seafloor, its acoustic response, the characterisation of this response, the specificity of this characterisation to be accurate, and the usage of it in practice in the context of seafloor identification. They led directly to the following questions:

1. What is the seafloor?
2. What is the seafloor acoustic response?
3. How to characterise the seafloor acoustic response?
4. What defines an accurate characterisation of the seafloor acoustic response?
5. What is the practical method to calculate seafloor acoustic responses from survey data?
6. What information can improve seabed identification?

These questions represent the basis of this PhD. They yield to several studies linking theory and practice. The first question was discussed in the introduction of this manuscript, describing the seafloor composition and its variability at different scales. A definition of the seafloor was derived, on which was based all the following analyses. The second question was the subject matter of the first part of this manuscript. A definition of the seafloor acoustic response was inferred based on a semantic analysis of the literature, on a study of theoretical models, on practical usages of computing the seafloor acoustic response (using sonar equations), and

on an analyse of its observed variability. From this definition, a theoretical model of the seafloor response was developed in the second part of this manuscript. The aim of this model was to answer the last four questions of the list. A method of characterisation of the seafloor acoustic response was therefore derived, taking into account theoretical and operational assumptions discussed in the first part and also deterministic and stochastic perspectives. This method was based on the estimation of the seafloor response from bathymetric echosounder data (SBES or MBES). The accuracy of the characterisation was ensured by comparing different estimators using their expected values and variances and identifying the best of them. In addition, an analytical formulation of the intrinsic uncertainty of the seafloor response was derived to obtain a measure of this accuracy. The last part of this manuscript validated the estimation method and the uncertainty formulation using SBES data from the echosounder manufactured during this PhD, and also brought to light the usefulness of *a priori* and *a posteriori* uncertainty levels for seabed identification and detection of changes.

9.1 Overview

Answers to the previous questions are discussed and summed up in the following and perspectives of applications and future developments are proposed in the last section.

9.1.1 Definition of the seafloor

The question of the definition of the seafloor was discussed in the introduction of this manuscript. In a first approximation, we saw that it can be considered as an interface between the sea water and the geophysical substrate. However, due to several external phenomena (e.g. sedimentation, benthos, currents), this interface is generally blur. In most of the cases a mixture of different components (mineral, animal, etc.) forms a layer between the substrate and the water. The surface of this layer can be hard to describe as it can filled with sea water. Consequently we defined the seafloor as an interface between to fluid media: the sea water and what we called the sediment medium which is composed of all types of materials and organisms and also water.

Due to its constitution and to external phenomena impacting the interface, it is considered rough at three different scales: the large scale (bathymetry), the medium scale (beam footprint), and the fine scale (wavelength). In addition, spatial and temporal variabilities of the sea bottom are also observed at several scales. Nevertheless, temporal variations were neglected in the works this PhD i.e. the interface was considered stable in time.

In the context of SBES and MBES measurements, the seafloor corresponds to a strong energetic echo that has the length of the beam footprint. This length can be larger or smaller than the transmitted pulse length, depending on the geometry of acquisition. In this manuscript, the strong hypothesis that the two media (sea water and sediment) are homogeneous at the pulse length scale was assumed. It allows to group the corresponding parts of the seafloor echo during processing.

9.1.2 Definition of the seafloor acoustic response

The primary subject of this PhD is the seafloor acoustic response. It was therefore convenient to study this subject regarding the literature and also practical usages of it. This was made based on four types of analysis: semantic, based on theoretical models, based on practical usages, and the analysis of the subject variability. All were discussed in the first part of this manuscript. Resulting from these analyses, the seafloor acoustic response was found to be a single value, specific to a seafloor type, and which depends on the frequency $\mathfrak{f}$ and the incidence angle θ_i of the transmitted signal on the seafloor. Because we retrained the study to SBES and MBES that are monostatic, the term used to describe the seafloor acoustic response in this manuscript was chosen among all terms found in literature as the backscattering strength. It corresponds physically to the ratio BS (in decibels) of the scattered acoustic intensity from the seafloor in direction of the echosounder to the incident acoustic intensity. It can be written in function of its parameters as $\mathrm{BS}(\theta_\mathrm{i}, \mathfrak{f})$.

Under this form, the seafloor response is modelled theoretically (see chapter 2) using physical or heuristic models, and is also used in practice through sonar equations (see chapter 3). In the latter case, it can then be computed during SBES or MBES surveys from seafloor acoustic echoes. However, literature observations and examples of SBES measurements made during this PhD bring to light the actual variability of the backscattering strength. Origins of this variability were discussed in chapter 4 together with two contradictory ensembles of applications where, on the one hand this variability tends to be reduced, and on the other hand it is of interest due to its informative relevance to detect changes in seafloor type. Consequently, with the aim to reduce measurements of the seafloor response at its lower standard deviation or, on the contrary, in order to detect changes in seafloor type, the intrinsic variability of backscattering strength measurements needed to be identified. This was the purpose of the second part of this manuscript, which analytical results were then validated using SBES data in the third part of the manuscript.

The seafloor acoustic response, or backscattering strength, was consequently defined as a single value BS (in decibels) but that is computed from a random variable **bs** which realisations can be found in seafloor echoes from every pings acquired on the same seafloor type. It therefore corresponds to the expected value of this random variable as:

$$\mathrm{BS} = 10 \log_{10} \left(\mathrm{E} \left[\mathbf{bs} \right] \right) \tag{9.1}$$

Attention should be made that this equality is valid in practice only when all other phenomena impacting the variability of the measurement are corrected or avoided. Only the intrinsic variability of the backscattering strength should remain.

9.1.3 Model and link to the seafloor acoustic response

In order to study the intrinsic variability of the seafloor response, a stochastic model was derived in chapter 5 assuming the seafloor (i.e. the interface) to be composed of several point scatterers i of random amplitudes a_i and phases ϕ_i. The seafloor echo amplitude $\mathbf{A}$ received by the echosounder and perfectly corrected from all sonar equation parameters is therefore also a complex random variable. Under the hypotheses that:

- the amplitude a_i and phase ϕ_i of the i$^{\text{th}}$ scatterer are statistically independent of each other and of the amplitudes and phases of all other scatterers,
- the amplitude a_i are identically distributed,
- the phase ϕ_i are uniformly distributed on the interval $(-\pi, \pi)$,
- the number of scatterers in the instantaneous insonified area is large,

the seafloor echo amplitude module $|\mathbf{A}|$ was demonstrated to be following a Rayleigh distribution which parameter was noted σ^2.

Based on the definition of the backscattering strength **bs** as the ratio of acoustic intensities, it was shown to be linked to the seafloor echo (corrected) amplitude module $|\mathbf{A}|$ by the formula:

$$10 \log_{10} (\mathbf{bs}) = 10 \log_{10} \left(|\mathbf{A}|^2 \right) \tag{9.2}$$

which led to the direct relationship between the backscattering strength and the Rayleigh parameter:

$$\mathrm{BS} = 10 \log_{10} \left(2\sigma^2 \right) \tag{9.3}$$

The Rayleigh parameter was shown to be connected to the variance of the real and imaginary parts of the seafloor echo corrected amplitude, consequently, from an acoustic point of view, the backscattering strength corresponds to a description of the variability of the interface roughness and the change of impedance.

9.1.4 Estimators of the seafloor acoustic response

Using the previous result and under the condition of bathymetric measurements with SBES or MBES, estimators of the backscattering strength were derived in chapter 5 and compared in chapter 6. The bathymetric method applied to seafloor response estimation was defined as the reduction of each seafloor echo magnitude of a ping to a single value (after correction of sonar equation parameters) followed by the mean of successive ping values if desired. Four reduction methods found in literature and used in practice were discussed:

- the maximum value of the n corrected time-samples magnitudes x of a seafloor echo,
- the median of the n corrected time-samples magnitudes x of a seafloor echo,
- the sample mean of the n corrected time-samples magnitudes x of a seafloor echo,
- the square sample mean of the n corrected time-samples magnitudes x of a seafloor echo.

These values were called descriptors (of the variability of the seafloor echo magnitude).

From these reduction methods, ten estimators of $2\sigma^2$ were derived including:

- the descriptors themselves i.e. directly the maximum, median, mean, and square sample mean of the corrected seafloor echo magnitudes,
- the estimators derived from the maximum likelihood of the descriptor probability function,
- the unbiased descriptors.

They were compared by simulating corrected seafloor echo magnitudes as realisations of a Rayleigh distribution of known parameter. The comparison was based on calculations of the estimators bias, variances, and speed of convergence. The analyses were made according to the number of time-samples n from seafloor echoes taken into account in the backscattering strength calculation, and the number of pings N.

The best estimator of the seafloor acoustic responses identified from the comparison was half the square sample mean of the corrected seafloor echo magnitudes x i.e.:

$$\widehat{\mathrm{BS}} = 10\log_{10}\left(\frac{1}{nN}\sum_{i=1,j=1}^{n,N} x_{ij}^2\right) \tag{9.4}$$

where n is the number of seafloor echo time-samples and N the number of pings. This estimate is unbiased, has the minimum variance and converges to a given variance faster than the nine other ones in term of number of samples and pings taken into account. It is also equal to twice the maximum likelihood estimate (MLE) of the Rayleigh distribution parameter, result that was expected as the MLE is known to be an accurate estimator. Analytical calculations confirmed the estimator is unbiased and also demonstrated that its variance reaches the Cramer-Rao bound which makes it an efficient estimator. The latter is equal to $\frac{(\sigma^2)^2}{nN}$.

When, for any reasons, the square sample mean reduction method is not available, the best estimator is therefore not achieved. However, an accurate estimation of the seafloor response can be obtained using the other reduction methods being aware that their variance are not the lower that can be obtained and that they can be biased. Using the maximum descriptor leads to:

$$\widehat{\mathrm{BS}}_{\max} = 10\log_{10}\left(\frac{1}{N}\sum_{j=1}^{N}\max(x_{ij})\right) \tag{9.5}$$

This estimator is biased. Using the median descriptor leads to:

$$\widehat{\mathrm{BS}}_{\mathrm{med}} = 10\log_{10}\left(\frac{1}{N}\sum_{j=1}^{N}\mathrm{med}(x_{ij})\right) + 1.6 \tag{9.6}$$

This estimator is unbiased but its speed of convergence is low, which leads to bias when a small number of seafloor echo time-samples n are taken into account. And finally, using the sample mean descriptor leads to:

$$\widehat{\mathrm{BS}}_{\mathrm{mean}} = 10\log_{10}\left(\frac{1}{nN}\sum_{i=1,j=1}^{n,N} x_{ij}\right) + 1.0 \tag{9.7}$$

This estimator is unbiased but with also a low speed of convergence.

9.1.5 Validity of the fundamental hypotheses

The point scattering model and the results presented previously are based on several fundamental hypotheses that were assumed for theoretical analyses. In the last part of this

manuscript, the validity of these hypotheses in practice was discussed, based on SBES measurements. For this purpose, specific acquisitions were made using the echosounder designed and manufactured during the PhD (see chapter 7). The list of assumptions is given below with the conditions under which they were demonstrated to be valid in practice (see chapter 8):

- Random nature of the seafloor: the seafloor was theoretically supposed rough to ensure that the received signal magnitudes to be realizations of a random variable. In order to ensure this condition during SBES acquisitions the measurements were made only on concrete seabed sediments in the harbour or the Bay of Brest (France) and in the tank of the university of Bath (United Kingdom) where sediment trails are disposed in the tank bottom.
- Sonar equation parameters perfectly corrected: sonar equations parameters were supposed perfectly known in the theoretical analyses leading to seafloor echo time-samples magnitudes perfectly corrected. In practice, this assumption was ensure by the precise calibration (on sphere) of the echosounder performed in the tank of ENSTA Bretagne (France) and also by a specific pre-processing of the data including the simulation of the instantaneous insonified area.
- No other variabilities: only the intrinsic variability of the seafloor response was taken into account in the model, other variabilities (spatial, temporal, and sparse) were neglected. To avoid these other variabilities, measurements were made in tank where the sediments are perfectly stable, in the harbour with the vessel at dock (ensuring a low spatial variability), and in the Bay of Brest but with the vessel drifting slowly (limiting the spatial variability and also the temporal variability as a small number of pings (150) were acquired successively).
- Independence of seafloor echo time-samples: in the model, the corrected time-samples magnitudes were independent. This condition was ensured by sub-sampling time-samples of seabed echoes by the transmitted pulse length.
- Rayleigh distribution: the corrected seafloor echo time-samples magnitudes were supposed theoretically to be realizations of a Rayleigh distribution. This assumption was verified using data from SBES (the echosounder manufactured during the PhD and the echosounder of project S2MF (2016-2018)). It was shown that seafloor echo time-samples magnitudes are following a Rayleigh distribution if and only if they are independent and corrected from sonar equation parameters.
- Identically distributed time-samples magnitudes: in the theoretical model, the corrected time-samples magnitudes of all pings were assumed to be realizations of the same Rayleigh distributions of parameter σ^2. In practice, this assumption is the hardest to be ensure. Indeed, we showed that when taking pings individually, seafloor echo time-samples magnitudes (corrected and independent) generally respect the Rayleigh distribution hypothesis, and so are the time-samples of a short list of pings taken at the same propagation time. However, when mixing these two axes, groups of samples magnitudes are not always longer following a unique Rayleigh distribution. This effect was shown to be mostly due to remaining imperfection in the correction of the instantaneous insonified area (linked to the directivity function), but can also come from changes in the backscattering strength from the first sample of the echo to the last (because of the angular variation of BS), from the penetration of the signal inside

the sediment, or from interference echoes (particularly with measurements in tank). A solution, demonstrated in chapter 8, was to use all time-samples of seafloor echoes but a small number of pings, or to use a large amount of pings but a small number of time-samples i.e. those inside the beam aperture of the echosounder.

9.1.6 Seafloor acoustic response estimation results

The fundamental hypotheses of the model being validated, the estimation of the seafloor acoustic response was applied to SBES data acquired during project S2MF in the Bay of Brest (France) in 2018 (see appendix C). The best estimator of BS was used to derive angular response curves (ARC) on two different terrains composed in the one hand of sand and mud and on the other hand of gravel and brittle stars. The sonar equation employed to correct raw seafloor echo data was the following:

$$10\log_{10}\left(x_i^2\right) = EL(t) - SL - DI_{\mathrm{Tx}} + 2TL(t) - 10\log_{10}(\mathcal{A}(t)) - G_{\mathrm{calib}} \tag{9.8}$$

where:

- $EL(t)$ is the echo level received by the echosounder at the time t,
- SL is the source level of the echosounder,
- DI_{Tx} is the directivity index on the antenna at transmission,
- $TL(t)$ is the transmission loss between the echosounder and the seabed at time t,
- G_{calib} is the calibration gain of the echosounder antenna,
- $\mathscr{A}(t)$ is the simulated instantaneous insonified area on the seafloor at time t,
- x_i is a realization of the random variable $|\mathbf{A}|$ at time t. In other words, it corresponds to the corrected seafloor echo amplitude module in equation 9.4 where i is the time index i.e. the seafloor echo time-sample number in a ping.

All specific parameters of the echosounder were measured in the tank of Ifremer (France) in 2018 during sphere calibration.

The ARC calculated from the two set of data were found of different shapes which confirmed the fact that seafloor acoustic response could be used to identify different type of terrain. They were also compared to ARC derived in [Mopin et al., 2022] using the same estimator of the backscattering strength (square sample mean) but a shorter number of time-samples.

9.1.7 Usefulness of the seafloor acoustic response uncertainty

As the objective of the PhD was to improve this terrain identification using an accurate characterisation of the seafloor acoustic response in practice, the estimation of the measurement accuracy was made by calculating its uncertainty. Based on the theoretical development of the best backscattering strength estimator and its probability density function, the uncertainty level T associated to this estimation was derived as

$$T = 10\log_{10}\left(1 + \frac{1}{\sqrt{nN}}\right) \tag{9.9}$$

where n is the number of time-samples and N the number of pings taken into account in the measurement of the backscattering strength.

This analytical formulation was validated using SBES data described previously. It was shown that, for example, when $N = 1$ the formula can be used in the case of ARC estimation, and the complete formula according to n and N can be used in the case where several pings values are averaged in a digital terrain model (DTM) cell. These are two non-exhaustive examples of applications of the uncertainty formulation.

A comparison between the theoretical uncertainty levels and the actual uncertainty levels computed from the SBES data brought to light the information that can contained this uncertainty. In addition to be a measure of the distance (in term of resemblance) between two measurements of the backscattering strength, the difference between theoretical and actual uncertainty levels appeared to give information about the deviation of the group of samples from the Rayleigh distribution. Based on these two results, it may be useful to detect seafloor changes in the acoustic point of view, and probably informative of the seafloor homogeneity.

In chapter 6 the uncertainty formulation was applied to MBES data from project CALIMERO (2004-2006) as an *a priori* estimation of the uncertainty that can be obtained with the echo-sounder in the given geometry of acquisition. In practice, these results can be, for example, used to modify the survey plan to ensure a minimum level of uncertainty. In chapter 8, *a posteriori* uncertainty levels were calculated from the same MBES data. Results showed good agreements with the theoretical uncertainty levels, leading to the validation of the application of the uncertainty level formulation to MBES data.

9.2 Conclusion

To conclude, results of this PhD provide an detailed description of the seafloor acoustic response metrology. Empirical methods developed practically by users, softwares or echo-sounder manufacturers to compute the backscattering strength were confronted to theoretical statements from literature. The link between the two domains was made using a stochastic model based on the bathymetric processing of SBES and MBES. From this model, an accurate definition of the seafloor acoustic response was proposed and an analytical estimator of the backscattering strength was derived. Some of the results were therefore expected (e.g. the best estimator being the square sample mean), and some of them clarified heuristic and usual assumptions (e.g. the link between the Rayleigh distribution and the backscattering strength, or the restriction to the beam aperture). Finally, a measure of the accuracy of backscattering strength acquisitions with SBES or MBES was proposed, based on the uncertainty of the measurements. This uncertainty can be used as an *a priori* information about the quality of a planned survey, or as an *a posteriori* indication of precision of the seafloor response measurements.

9.3 Perspectives

Different aspects of the developments presented in this manuscript could be analysed in details in future works. For example, ten estimators of the seafloor acoustic response were discussed, among which only one was retained as the best estimator. A study of the behaviour

of these other estimators may be of interest, in particular when measurements conditions are not perfect (e.g. the median estimator could be found robust in presence of outliers). The impact of the backscattering strength variations according to the incident angles could also be studied in regard to the deviation of the group of sample from the Rayleigh distribution. On some terrain these variations are observed small especially at grazing angles (e.g. hard and very rough seafloor) so that their impact could probably be neglected in the beam footprint, but on the contrary, some terrains have strong ARC variations (e.g. sand or soft seafloor) that could induce quantifiable changes in the seafloor echo samples distribution along the beam footprint.

In the last part of this manuscript, the potential of the estimation of the backscattering strength uncertainty to indicate seafloor changes or deviations from the Rayleigh distribution hypothesis was demonstrated. This succinct analysis should be developed, with in particular an application to specific data where seafloor changes are known to appear. The sensitivity of the method could therefore be studied.

9.3.1 What is an homogeneous seafloor?

In the analyses of the model hypotheses and the validation of the uncertainty formulation, the echosounder data used were supposed acquired on homogeneous seafloors. However, we saw during the study of the conditions of validity of the unique Rayleigh distribution hypothesis and also during the comparison of theoretical and actual uncertainty levels, that even when the seafloor is assumed homogeneous in term of macroscopic composition, deviations from the Rayleigh hypothesis can appeared. These deviations were observed of two forms:

- the actual uncertainty levels are higher than the theoretical ones i.e. the distribution is different from Rayleigh. This implies, e.g., that the identical distribution of the scatterers amplitudes inside the instantaneous insonified area is not respected.
- the actual uncertainty levels are lower than the theoretical ones i.e. the samples are too correlated. This implies that the seafloor echo samples or the pings are not independent.

The second point is mainly due to the geometry of the survey or the post-processing. Nevertheless, the first point is directly linked to the homogeneity assumption, and followed a couple of questions: is the deviation from the Rayleigh distribution a mark of presence of inhomogeneities in the seafloor? From which scale of physical inhomogeneities can this deviation be identified from echosounder data? Does the homogeneity of the seafloor imply the seabed echo samples to be identically distributed? A particular attention should therefore be given in future works to the definition of an homogeneous seafloor in term of acoustic measurements.

9.3.2 Application to reflectivity maps

The seafloor response estimator described in this manuscript was demonstrated to be applicable to MBES bathymetric data. The intrinsic uncertainty levels associated to the measurements can then be derived from the data if the conditions of validity of the model are verified (e.g. independence of seafloor echo samples, pings, etc.). By employing the equivalent of the TPU (total propagated uncertainty) used for bathymetric soundings (see [Malik et al., 2018]) in addition to these resulting intrinsic uncertainties, a total uncertainty of the

reflectivity survey can be obtained. An uncertainty map could therefore be computed in complement to the reflectivity map (*a priori* and *a posteriori*).

Appendix

Appendix A

Appendix: List of phrases describing the seafloor acoustic response

Phrases
Volume roughness scattering
Diffuse and specular scattering
Reflectivity
Scattering strength
Seabed acoustic response
Scattering coefficient
Bottom loss
Pressure reflection coefficient
Plane wave reflection coefficient
Seabed/bottom scattering
Backscattering strength
Backscattering of sound from a natural bottom
Backscatter of wave radiation
Backscattering from the bottom
Bottom scattering coefficient
Scattering strength from measurement of the reflection
Underwater reverberation
Backscattering index
Scattering from the bottom
Backscattering coefficient
Sonar reverberation
Coherent reflection coefficient
Reverberation
Scattering cross-section
Backscatter strength
Seafloor/bottom reverberation
Reverberation strength
Backscattering cross-section
Scattering constant of the bottom

Seafloor reverberation index
Lambert parameter
Mackenzie's constant
Lambert constant
Lambert coefficient
Degree of reflectivity of the sediment interface
Bottom reverberation strength
Scattering function
Rayleigh reflection coefficient
Pressure reflection coefficient from smooth surface
Rayleigh bottom reflection coefficient
Reflection loss
Bottom reflection coefficient
Backscatter
Reverberation
Backscattering
Bottom backscattering coefficient
Bottom backscattering cross-section
Reflected signal
Backward scattering
Differential backscattering cross section
Acoustic scattering from the ocean bottom
Bottom backscattering
Acoustic response of the seafloor
Scattering amplitude
Plane wave scattering amplitude
Bottom scattering strength
Backscattering amplitude
Acoustic backscatter from the seafloor
Cross-section
Boundary reverberation
Geacoustic model
Total loss due to bottom
Bottom reverberation at the transducer
Ocean boundaries scattering
Bottom interaction model
Backscatter of sound from a rough boundary
Reflection coefficient

Appendix B

Appendix: List of papers and conferences

Articles

- **Comparison of methods employed to extract information contained in seafloor backscatter**, Mopin,Irène, Le Chenadec,Gilles, Legris,Michel, Blondel,Philippe, Marchal,Jacques, Zerr Benoît, Proceedings of Meetings on Acoustics, 070036, 44, 2021, Acoustical Society of America, https://asa.scitation.org/doi/abs/10.1121/2.0001509

Abstract: Seabed maps are based on quantities extracted from measurements of the seafloor's acoustic response by sonar systems such as single-beam echo-sounders (SBES), multi-beam echo-sounders (MBES) or sidescan sonars (SSS). In this paper, a comparison of various strategies to estimate the backscattering strength (BS) from recorded time-series, i.e. seabed echoes extracted from pings, is presented. The work hypotheses are based on processed data from a SBES designed to be tilted mechanically. Ideal survey conditions are taken into account and the seafloor is supposed to be rough so that BS is assumed to be equivalent to the Rayleigh probability density function parameter. Classical methods such as averaging corrected (sonar equation) backscattered single values over a set of pings to estimate BS are compared to other methods exploiting several time-samples being part of pings. Simulated data is considered to estimate BS in different situations (several estimators, natural/squared values, number of samples and pings). The best estimator to reach a 0.1dB uncertainty is proposed, and a formula governing the number of time-samples and pings needed to reach an accurate BS estimation according to the measurement conditions is derived.

- **Design and field testing of a non-linear single-beam echosounder for multi-frequency seabed characterization**, Irène Mopin, Jacques Marchal, Michel Legris, Gilles Le Chenadec, Philippe Blondel, Benoît Zerr, Applied Acoustics, Volume 187, 2022, 108490, ISSN 0003-682X, https://doi.org/10.1016/j.apacoust.2021.108490

Abstract: Seabed mapping and characterization are best performed using several frequencies and several angles of incidence. This is often an issue because of the need to employ different sonars, with distinct frequencies but co-located as much as possible to image the same patch of seafloor. This article presents the design, calibration and field testing of a multiple-frequency single-beam echosounder (SBES), mounted on a mechanical pan-and-tilt

head. It uses very high transmitting levels to produce non-linear effects and generate harmonics of a 100 kHz fundamental frequency. PZT transducers are used to transmit high acoustic powers and PDVF transducers enable the reception of scattering levels over a very broad frequency band (for the different harmonics). Tank experiments are used to verify effective harmonic generation. The shock distance (at which harmonics are at their maximum level) is measured as 2 m from the transmitter and recommended as the minimum far-field range. Non-linear transmission losses (distinct from linear losses) are calibrated using a full metal sphere 38.1 mm in diameter and of known frequency response, up to ranges commensurate with the depths expected in the field ($\geqslant$30m). The -3dB beamwidth varies from 5.8° at 100 kHz to 2.8° at 300 kHz. Harmonics are used to resolve phase ambiguities in detecting seabed depths. Backscattering strengths BS are matched to the Generic Seafloor Acoustic Backscatter (GSAB) model to derive the best-fitting parameters. Field validation took place in the Bay of Brest (France) in May 2016, over three different types of seafloor (namely: sandy mud; gravel; gravelly coarse sand with maerl). Additional in situ calibration was used. The echosounder was pointed at angles from 0° (nadir) to 60° by 5° steps. One of the areas surveyed ("Carré Renard"), commonly used for instrument calibration and comparison with other measurements, showed differences <1dB at 200 kHz. Videos and photographs of the seafloor were used to ground truth interpretations of the BS curves. The results show that these BS curves measured with the echosounder are relevant for seabed classification and characterization. The different shapes and levels of BS when compared to ground truth are coherent with the Jackson model. The main limit of this prototype of echosounder is the signal to noise ratio, in particular for high frequency harmonics ($\geqslant$400 kHz). The in situ calibration is unavoidable because of the nonlinear parameter variations with water characteristics (temperature, salinity...). Calibrated BS curves from 100 kHz to 300 kHz can be directly compared to other measurements, for example to calibrate other instruments.

Talks on conferences

- **Statistical estimation of seafloor backscattering strength and its intrinsic uncertainty using bathymetric echosounders**, Irène Mopin, Gilles Le Chenadec, Michel Legris, Philippe Blondel, Jacques Marchal, Benoît Zerr, Hydrographic conference HYDRO2022, Monaco, December 2022.

Abstract: Echosounders are the key instruments to accurately measure bathymetry. They can also provide detailed seabed reflectivity information, measuring the seafloor acoustic response as a function of time and angles. For each ping and beam, a backscattering strength BS is estimated and associated to the sounding. This BS value is determined from the recorded time-series (pings) by using one or several time samples (snippets) and transforming their magnitudes into a reflectivity level, according to the sonar equation. At the end, several BS values from consecutive pings are generally averaged to minimise the variability of successive measurements. How they are calculated, and how they are averaged, is often open to interpretation. We present and compare different methods to process the reflectivity level. Its uncertainty, generated by the intrinsic variability of the seabed, is derived analytically and its mathematical formulation applied to survey data from a tilted split-beam echosounder at 106.8 kHz. This is illustrated with a BS curve in dB according to incident angles, and complemented with associated curves of uncertainties (theoretical and estimated). Finally, the uncertainty formula is applied to bathymetric echosounders data, resulting in an uncertainty

mosaic associated with the reflectivity mosaic.

- **Etude de la réponse acoustique des fonds marins**, Irène Mopin, Séminaire APy, Université de Bordeaux, Juin 2022

Abstract: Les sondeurs utilisés en hydrographie pour la cartographie des fonds marins fournissent aujourd'hui, en plus de l'information bathymétrique, l'intensité rétrodiffusée par le fond. Une sonde est donc dans la plupart des cas associée à un niveau acoustique reçu correspondant à l'écho du fond. Pour plusieurs applications telles que la classification ou la caractérisation des fonds, il est nécessaire de transformer ce niveau reçu en une quantité absolue appelée réponse acoustique du fond. Elle est spécifique à un type de fond (sable, vase, roche...) et dépend de la fréquence du signal émis et de son angle d'incidence. De nombreuses méthodes sont utilisées par les constructeurs et utilisateurs de sondeurs pour réduire l'information contenue dans une trame temporelle reçue (ping) et en déduire la réponse du fond. Dans cette présentation les principaux traitements seront comparés à l'aide d'outils statistiques. Des conseils de bonnes pratiques seront proposés, associés à une formulation théorique du rapport nombre de pings / nombre d'échantillons temporels à utiliser pour obtenir une valeur de réponse du fond pertinente.

- **Application of seafloor backscattering strength estimators to echosounder measurement at sea**, Irène Mopin, Gilles Le Chenadec, Michel Legris, Philippe Blondel, Jacques Marchal, Benoît Zerr, International Conference of Underwater Acoustic ICUA 2022

Abstract: Echosounders are ubiquitously used to measure bathymetry; they can also provide seabed reflectivity maps based on the measurement of the seafloor acoustic response and its variations. For each ping and beam, the backscattering strength BS is estimated and associated to the sounding. This single BS value is determined from the recorded time-series (pings) by using one or several time samples and transforming their magnitudes into a reflectivity level, according to the sonar equation. At the end, several BS values from consecutive pings or beams are generally averaged to minimise the variability of successive measurements. How they are calculated, and how (and why) they are averaged, is however open to interpretation. Different methods are presented to reduce the time-series information to a single BS value in the context of Rayleigh scattering. To anchor these theoretical considerations to actual applications, the processes are applied to field data from a single beam echosounder designed at Sorbonne University and used on well-constrained seafloor patches in the Bay of Brest (France) in 2016. The echosounder was tilted mechanically from nadir to 60° and it transmitted a 100 kHz sine wave of 600 μs duration on the different terrains. The issue of the insonified area compensation of several time-samples is discussed, and inferred backscattering strengths are compared relatively and with ground-truth.

- **Research Sounding Competition, The sound of the seafloor**, Irène Mopin, Webinar of the United Kingdom Acoustics Network, March 2022

- **Etude de la réponse acoustique des fonds marins**, Irène Mopin, Matinée Son, Trégor Sonore, Janvier 2022

Abstract: Les sondeurs utilisés en hydrographie pour la cartographie des fonds marins fournissent aujourd'hui, en plus de l'information bathymétrique, l'intensité rétrodiffusée par le fond. Une sonde est donc dans la plupart des cas associée à un niveau acoustique reçu

correspondant à l'écho du fond. Pour plusieurs applications telles que la classification ou la caractérisation des fonds, il est nécessaire de transformer ce niveau reçu en une quantité absolue appelée réponse acoustique du fond. Elle est spécifique à un type de fond (sable, vase, roche...) et dépend de la fréquence du signal émis et de son angle d'incidence. De nombreuses méthodes sont utilisées par les constructeurs et utilisateurs de sondeurs pour réduire l'information contenue dans une trame temporelle reçue (ping) et en déduire la réponse du fond. Dans cette présentation les principales procédures seront comparées à l'aide d'outils statistiques. Des conseils de bonnes pratiques seront proposés, associés à une formulation théorique du rapport nombre de pings / nombre d'échantillons temporels à utiliser pour obtenir une valeur de réponse du fond pertinente.

- **Comparison of methods employed to extract information contained in seafloor backscatter**, Irène Mopin, Gilles Le Chenadec, Michel Legris, Philippe Blondel, Jacques Marchal, Benoît Zerr, Underwater Acoustic Conference & Exhibition series UACE 2021

Abstract: Echosounders are ubiquitously used to measure bathymetry; they can also provide seabed reflectivity maps based on the measurement of the seafloor acoustic response and its variations. For each ping and beam, the backscattering strength BS is estimated and associated to the sounding. This single BS value is determined from the recorded time-series (pings) by using one or several time samples and transforming their magnitudes into a reflectivity level, according to the sonar equation. At the end, several BS values from consecutive pings or beams are generally averaged to minimise the variability of successive measurements. How they are calculated, and how (and why) they are averaged, is however open to interpretation. Different methods are presented to reduce the time-series information to a single BS value in the context of Rayleigh scattering. To anchor these theoretical considerations to actual applications, the processes are applied to field data from a single beam echosounder designed at Sorbonne University and used on well-constrained seafloor patches in the Bay of Brest (France) in 2016. The echosounder was tilted mechanically from nadir to 60° and it transmitted a 100kHz sine wave of 600μs duration on the different terrains. The issue of the insonified area compensation of several time-samples is discussed, and inferred backscattering strengths are compared relatively and with ground-truth.

- **Marine observations with a harmonic single-beam echo-sounder**, Irène Mopin, Jacques Marchal, Michel Legris, Philippe Blondel, Benoît Zerr, Gilles Le Chenadec, e-Forum Acusticum 2020

Abstract: Seabed maps are based on measurements of acoustic backscatter, generally made by different systems: single-beam echo-sounders (SBES), multibeam echo-sounders (MBES) and sidescan sonars (SSS) to name the main ones. According to the practical application, the seafloor acoustic echo is extracted by data processing that implies several hypotheses. All are based on the theoretical sonar equation, but in practice they differ from one to another in their computations of each parameter. The acoustic intensity reflected from the seafloor, called "backscattering strength" (BS), is therefore slightly different between the real-time values provided by the sonar according to the manufacturer's proprietary computing methods, and the improved values provided by any post-processing algorithm. This might affect subsequent analyses, like seafloor characterisation or target detection. Our presentation summarises the state of the art of the sonar equation parameters applied to seafloor characterisation. This summary is followed with a comparison of BS processing methods used in both real and de-

ferred time. Advantages and limitations of each method are discussed, in particular looking at the compound determination of the ensonification area/volume, the effective pulse length (Sacorr), and calibration gains. Conclusions taken from this study and combined with previous works on real data will be used as a base for a new research project.

- **Marine observations with a harmonic single-beam echo-sounder**, Irène Mopin, Jacques Marchal, Michel Legris, Philippe Blondel, Benoît Zerr, Gilles Le Chenadec, Sea Tech Week 2020

Abstract: To characterise the seabed or water-column targets with acoustics, it is common to use multiple frequencies and therefore several sonar transducers or echo-sounders. The single beam echo-sounder we present here is able, thanks to non-linearity of the sea water, to generate more than three harmonics above its fundamental transmitted frequency, in effect producing four distinct frequencies with a single echo-sounder. In addition, all transmitted signals are perfectly in phase because they are carried by the same pulse, which has obvious benefits for further processing of the echoes. In this presentation, after a short review of the entire system, its application to seabed characterisation using the reflectivity level (acoustic backscattering strength from the seafloor) will be exposed. Further developments of plans to use this echo-sounder for fishery acoustics will then be highlighted, based on datasets recently acquired in the Bay of Brest (France). (Project funded by ANR and DGA / ANR-14-ASTR-0022-00).

- **Fine-tuning seabed backscatter level estimation with bathymetric echo-sounders in complex terrains**, Irène Mopin, Philippe Blondel, Benoît Zerr, Gilles Le Chenadec, Jacques Marchal, Internation Conference of Underwater Acoustic ICUA 2020

Abstract: Seabed reflectivity maps are based on the measurement of the acoustic backscattering strength (BS) of the bottom and are generally supplied by different systems such as single-beam echo-sounders (SBES) or multi-beam echo-sounders (MBES). For one ping, the sounder records a time series of acoustic power or intensity values received along each beam. Each of these time series traditionally results in a single value of BS (along each beam), and this value is used to create the reflectivity map associate to the bathymetric map. To determine one BS-value from a time series, a usual way mostly used in real-time in single-beam echo-sounders is to detect the sample whose power value is maximum and transform it to a reflectivity level with the sonar equation. Then, a mean of several BS-values from consecutive pings is generally done to get a more stable result. But this BS-level estimation based on the maximum level of the time-series and a ping-mean is not the only way to estimate the bottom backscattering strength. Several methods can be employed that rely on various assumptions or choices made either by the manufacturer or by the end-users. In this paper, we propose different estimation methods of the 1-ping BS-value, such as keeping and averaging a defined number of samples in the echo and computing BS histograms, or using moments (mean, median) in the ping-space to average data. An evaluation and a comparison of these methods on real backscatter data from a single-beam echo-sounder are presented.

Appendix C

Appendix: Article Applied Acoustics (2022)

Applied Acoustics 187 (2022) 108490

Contents lists available at ScienceDirect

Applied Acoustics

journal homepage: www.elsevier.com/locate/apacoust

Design and field testing of a non-linear single-beam echosounder for multi-frequency seabed characterization

Irène Mopin [a,*], Jacques Marchal [b], Michel Legris [a], Gilles Le Chenadec [a], Philippe Blondel [c], Benoît Zerr [a]

[a] ENSTA Bretagne, UMR 6285, Lab-STICC, STIC-PRASYS, 2 rue François Verny, 29806 Brest Cedex 09, France
[b] Sorbonne Université, UMR 7190, Institut Jean le Rond D'Alembert, 2 Place de la Gare de Ceinture, 78210 Saint Cyr L'École, France
[c] University of Bath, Department of Physics, Claverton Down, Bath BA2 7AY, United Kingdom

ARTICLE INFO

Article history:
Received 19 February 2021
Received in revised form 1 July 2021
Accepted 21 October 2021

Keywords:
Underwater acoustics
Non-linear acoustics
Backscatter strength (BS)
Seabed characterization
Single-beam echosounder (SBES)

ABSTRACT

Seabed mapping and characterization are best performed using several frequencies and several angles of incidence. This is often an issue because of the need to employ different sonars, with distinct frequencies but co-located as much as possible to image the same patch of seafloor. This article presents the design, calibration and field testing of a multiple-frequency single-beam echosounder (SBES), mounted on a mechanical pan-and-tilt head. It uses very high transmitting levels to produce non-linear effects and generate harmonics of a 100 kHz fundamental frequency. PZT transducers are used to transmit high acoustic powers and PDVF transducers enable the reception of scattering levels over a very broad frequency band (for the different harmonics). Tank experiments are used to verify effective harmonic generation. The shock distance (at which harmonics are at their maximum level) is measured as 2 m from the transmitter and recommended as the minimum far-field range. Non-linear transmission losses (distinct from linear losses) are calibrated using a full metal sphere 38.1 mm in diameter and of known frequency response, up to ranges commensurate with the depths expected in the field ($\leqslant$30 m). The -3 dB beamwidth varies from 5.8° at 100 kHz to 2.8° at 300 kHz. Harmonics are used to resolve phase ambiguities in detecting seabed depths. Backscattering strengths *BS* are matched to the Generic Seafloor Acoustic Backscatter (GSAB) model to derive the best-fitting parameters. Field validation took place in the Bay of Brest (France) in May 2016, over three different types of seafloor (namely: sandy mud; gravel; gravelly coarse sand with maerl). Additional *in situ* calibration was used. The echosounder was pointed at angles from 0° (nadir) to 60° by 5° steps. One of the areas surveyed ("Carré Renard"), commonly used for instrument calibration and comparison with other measurements, showed differences $<$1 dB at 200 kHz. Videos and photographs of the seafloor were used to ground truth interpretations of the *BS* curves. The results show that these *BS* curves measured with the echosounder are relevant for seabed classification and characterization. The different shapes and levels of BS when compared to ground truth are coherent with the Jackson model. The main limit of this prototype of echosounder is the signal to noise ratio, in particular for high frequency harmonics ($\geqslant$ 400 kHz). The *in situ* calibration is unavoidable because of the non-linear parameter variations with water characteristics (temperature, salinity...). Calibrated *BS* curves from 100 kHz to 300 kHz can be directly compared to other measurements, for example to calibrate other instruments.

1. Introduction

Single-beam echosounders (SBES) have been used since the 20th century primarily for hydrographic purposes. Their first aim was to achieve bathymetric requirements such as reliable detections of the seabed and precise positioning of the soundings. More recently, they have also become reference systems for seabed characterization and classification mostly because of their usability (straightforward technology, lightweight and portable), their ability to be fully calibrated using a sphere target [1] and their versatility in frequencies (available from 10 kHz to 500 kHz). Different algorithms have been developed to address the challenges, for example received pulse envelope alteration [2,3], or signal echo modification according to frequency [4]. However, seabed acoustic response depends on the frequency as well as the incidence angle [5–8]. Therefore, to be discriminant, the acoustic response of the seafloor

* Corresponding author.
E-mail address: irene.mopin@ensta-bretagne.org (I. Mopin).

https://doi.org/10.1016/j.apacoust.2021.108490
0003-682X/

must be measured according to several incident angles θ and transmitted frequencies f. This yields reflectivity or backscattering strengths $BS(f,\theta)$ specific of a seabed type [9].

In the context of traditional SBES, the angular issue is solved by mechanically tilting the system even if, obviously, the use of multi-beam echosounders would be more appropriate [10]. As for frequencies, transmitting a large diversity of frequencies implies the use of several systems (single- or multi-beams) on the same vessel, requiring larger vessels and increasing survey costs. Where the angular measurements are practicable, multi-frequency measurements are most often limited by space requirements on board [11]. In the case of MBES, new systems are able to transmit signals at different frequencies, but require either to run several acquisitions on the same survey line or to transmit alternatively one ping at one frequency at any single time. Signals are consequently not perfectly synchronised. Another method used for SBES is to transmit a signal containing several frequencies i.e. a frequency modulated (FM) signal. However, frequencies are also not in-phase and the bandwidth of a single head SBES is generally limited, restraining the diversity of frequency measurements available with one echo-sounder. The SBES presented in this paper is a compromise between the number of frequencies desired, the space available and the cost of the survey. Its ability to generate several spread frequencies (100 kHz apart) perfectly synchronised and with only one transducer head makes it efficient for seabed characterization or classification surveys and very economical of space.

The system is mechanically tilted to reach angles from 0° (nadir) to 60°, and designed to generate multiple frequencies perfectly simultaneously with a unique transducer head. The generation of these harmonic frequencies is based on the propagation medium's non-linear properties [12–14], producing frequencies multiples of the fundamental frequency transmitted (100 kHz, yielding harmonics at 200 kHz, 300 kHz, etc.). This approach is widely used in medical acoustics and non-destructive inspection [15] but seldom in underwater acoustics, even though the feasibility of characterizing underwater targets thanks to harmonic frequencies was demonstrated e.g. in [16].

Section 2 summarises the underlying theory and presents how it informed the design of transmitter and receivers, whose non-linear properties are measured in tanks and at sea. Section 3 explains how acoustic data is processed to get accurate seabed backscattering strengths $BS(f,\theta)$. Section 4 presents sea trials in the Bay of Brest (France) and compares the results with reference measurements from [17] and with established seabed response models like [18]. Finally, Section 5 discusses the need for *in situ* calibration and envisageable improvements.

2. Theory, design and validation of a harmonic single-beam echosounder

The non-linear properties of acoustic wave propagation in water [12,14] are used to generate multiple frequencies with a system classically employed in underwater acoustics: the SBES. The echosounder described in this paper is able to generate several isolated frequencies, harmonics of the lower one, perfectly simultaneous in time and space.

2.1. Using non-linearities in an underwater acoustics context

To generate several frequencies within a single transmitter, we take advantage of the non-linear propagation of acoustic waves in sea water [12,14]. The principle is based on the 3-D quadratic non-linear equation for fluids in terms of the acoustic potential $\mathbf{\Phi}(\boldsymbol{X},t)$ [19,20]:

$$\Delta\mathbf{\Phi}(\boldsymbol{X},t)-\frac{1}{c_0^2}\frac{\partial^2\mathbf{\Phi}}{\partial t^2}=\frac{2}{c_0}\mathcal{A}\left(\frac{\partial\mathbf{\Phi}}{\partial t}\right)+\frac{1}{c_0^2}\frac{\partial}{\partial t}\left[(\nabla\mathbf{\Phi})^2+(\beta-1)\frac{1}{c_0^2}\left(\frac{\partial\mathbf{\Phi}}{\partial t}\right)^2\right] \tag{1}$$

where $\boldsymbol{X}$ are the 3-D coordinates and t the propagation time (omitted from the later expressions of $\mathbf{\Phi}$, to simplify the equation); c_0 is the sound speed in the given fluid (water), and β the non-linear coefficient [21,22]. $\mathcal{A}(*)$ is a linear operator related to attenuation. In water, it takes into account the thermoviscous attenuation $-\frac{b}{2\rho_0 c_0^3}\frac{\partial^2 *}{\partial t^2}$ [23], in which b is the viscosity coefficient and ρ_0 the density of the medium, and it also accounts for the relaxation [19,24].

As the acoustic wave propagates through water, non-linear processes will transfer some energy from the fundamental frequency to its harmonics [14,25,26]. To observe these non-linear phenomena, the power transmitted needs to be much higher than with traditional echosounders. This constraint is often a limitation to using non-linear acoustics. Previous studies and the model by [19,27] helped us to improve the development and design of the echosounder, making it efficient in terms of acoustic energy for each harmonic frequency.

2.2. Constraint on the transmitter: high power

According to [14], harmonic frequencies appear in the signal during its propagation through the medium, when only one single frequency is actually transmitted by the transducer. The main constraint, in practice, is that a very high acoustic level must be transmitted into the water, at the transducer head. Electronic components have therefore to be able to generate a high amplitude signal and the transducer itself must be designed to support such a high pressure variation on its surface, while avoiding cavitation and the generation of third harmonic when the transmitted signal is not sinusoidal. The transmitter (Tx) developed for this purpose is an 18 cm-diameter disk formed with composite-PZT [28], which resonates at 100 kHz (see Fig. 1). Its composition and large surface are enough to support high power at 100 kHz, allowing this fundamental frequency to be transmitted. The harmonic frequencies generated during propagation are therefore 200 kHz, 300 kHz, etc. The source level estimated from linear measurements of the transmitter sensitivity is 228.5 dB re. 1 μPa @ 1 m.

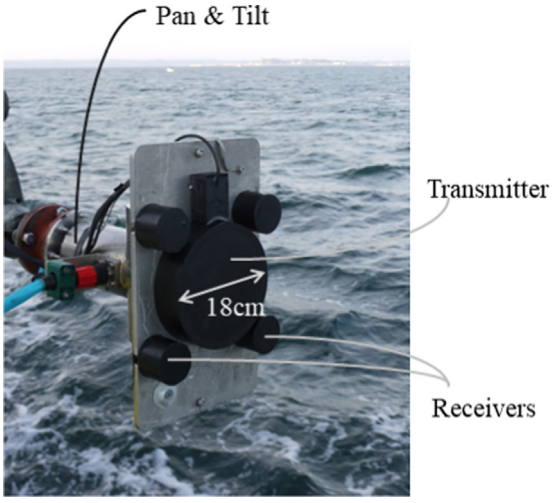

Fig. 1. Multi-frequency SBES before a survey, with one transmitting cylindrical transducer in the center, and four receivers spaced 20 cm apart.

2.3. Constraints on the receiver(s): the spread of frequencies

To receive all harmonic frequencies, the receivers must be wide-band. They also have to be very sensitive because the harmonic levels could be quite low (received seabed echo amplitude of the 300 kHz harmonic could be lower than 20 mV at 30 m range for a tilted angle of 60°), especially at very high frequencies. PVDF (Polyvinylidene fluoride) technology [29] respects these criteria and was consequently selected. We can note that with a suitable receiver sensitivity the range of the system is only limited by the level of the higher intended harmonic compared to the received noise level. The receivers (Rx) are in our case made of one layer of PVDF, with a backing formed by a layer of vinyl and a large syntactic foam as backing. They have the shape of a small disk 3 cm in diameter to optimise the sensitivity/aperture constraints at high frequencies. Four receivers are placed around the Tx transducer as shown on Fig. 1. Their vertical spacing is about 20 cm and is useful for seabed detection through interferometry.

2.4. Validation of harmonic frequencies generation

The effective generation of harmonic frequencies with the selected transducer shape and material is done by measuring the harmonic levels at several ranges from the transmitter in fully-controlled environments. These measurements were done in two tanks: one 10 m-long and filled with fresh water (at Sorbonne University, Paris, France), and one 35 m-long filled with sea water (at Ifremer, Brest, France). The experiments both consisted in emitting a continuous wave (CW) with the Tx transducer of Fig. 1 and receiving the direct-signal with a calibrated hydrophone Reson TC4034. Measurements were obtained every 2 or 3 meters in the small tank, and every 5 meters in the large tank. The level $L(r)$ of each harmonic, depending on the range r, is calculated after using a band-pass filter. Results are shown on Fig. 2. We can perfectly observe the creation of the harmonic along the range before the shock distance L_c [19] (around 2 m) where their levels are increasing. After the shock, the levels decrease with range, i.e. it is a transmission loss, mainly due to the geometrical divergence of the signal within the medium. The attenuation is close to negligible on these short distances (around 3 dB/km in fresh water and 33 dB/km in salt water). We can notice a minute inflection at 10 m. This is explained by the different water conditions between each tank. The respective characteristics of these two environments are contrasted with conditions during the sea survey in Table 1.

These different sets of measurements show that, in each environment, the transmitter effectively and efficiently creates harmonic frequencies. The results also show the importance of knowing where the shock appears, i.e. when the harmonics are at their maximum levels. This is as important as knowing the far-field distance, in an operational point of view. Indeed, for ranges lower than L_c, measurements are not recommended as all the harmonic frequencies are not fully generated. This distance is therefore a characteristic of the multi-frequency echosounder and needs to be kept in mind by future users.

2.5. Directivity patterns and equivalent beam apertures

To estimate the reflectivity level of the seafloor at different incidence angles, we need to know the directivity pattern $D(f, r, \varphi)$ of the echosounder to calculate its equivalent beam aperture $\phi(f, r)$ for each frequency. The combined two-way directivity $10\log(D(f, r, \varphi))$ is measured in the tanks for different ranges r from the echosounder and pointing angles $\varphi \in [-15°; +15°]$, and they are calculated for each frequency f. Fig. 3 shows the directivity patterns at $r = 20\ m$ for the fundamental frequency of 100 kHz and the first harmonics at 200 kHz and 300 kHz. We can observe the variations of the main beams' apertures according to frequency [31], and also asymmetries of the side-lobes, mainly due to the layout of the PZT component of the transducer (in spiral).

The equivalent aperture $\phi(f, r)$ of the echosounder is calculated for each frequency by integrating the corresponding measured directivity patterns [32] (Fig. 3). When measuring the directivity patterns for different r and plotting their equivalent apertures $\phi(f, r)$ we obtain the results of Fig. 4, showing the increase of beamwidths with range. At 100 kHz, they vary from 6.3° at 10 m to 6.8° at 30 m, at 200 kHz from 4.0° at 10 m to 4.6° at 30 m and at 300 kHz from 3.1° at 10 m to 3.9° at 30 m.

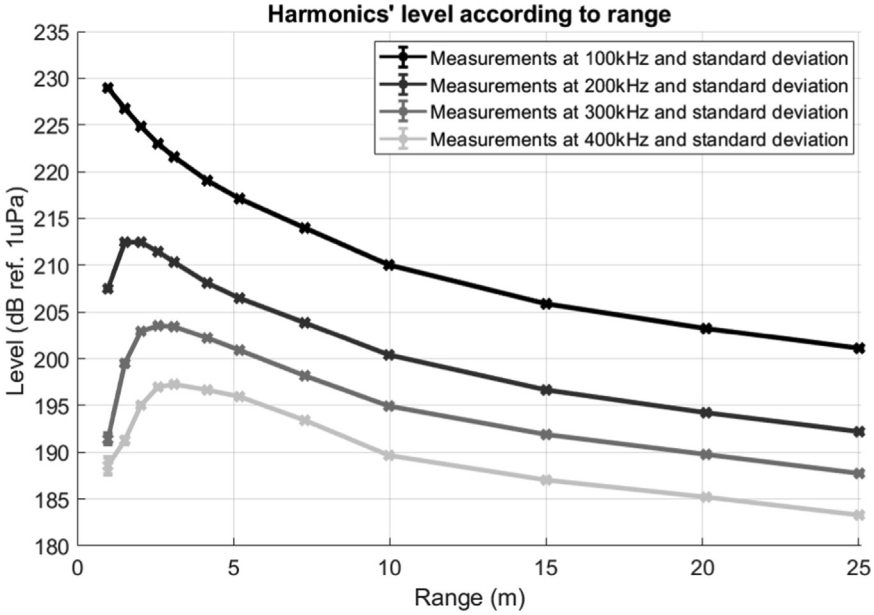

Fig. 2. Measurements of the generation of harmonic frequencies in a small (< 10 m) freshwater tank and in a large ($\geqslant 10$ m) salt water tank, according to the range from the transmitter with the maximum level at emission. At each range, 100 measurements are averaged. Associated standard deviations are not very noticeable because they are all < 0.9 dB.

Table 1
Characteristics of the water in the tanks and during the sea trials, measured *in situ*. The non-linear coefficient β is estimated with the empirical Blackstock formula [27,30] from the measurements of temperature and salinity. Because acoustics measurements in tanks were done horizontally i.e. the SBES axis crossed only one layer of water, the non-linear coefficient is constant during propagation. However, at sea, measurements are done vertically or while tilting the SBES, therefore its axis crossed several layers of water of different composition. The non-linear coefficient consequently varies during the propagation, and it is therefore given as a range of values.

	Small tank	Large tank	Survey at sea
Type of water	Fresh water	Salt water	Salt water
Sound speed (c_0)	1450 m/s	1498 m/s	[1500.8; 1503.0] m/s
Water density	1000 kg/m^3	1028 kg/m^3	[1026; 1027] kg/m^3
Temperature	9.8 °C	11.8 °C	[13.1; 13.8] °C
Salinity	0 psu	37 psu	[34.6; 35.4] psu
Particles in suspension	None Clear water	None Clear water	A lot Turbid water
β (dimensionless)	3.35	3.59	[3.59; 3.60]

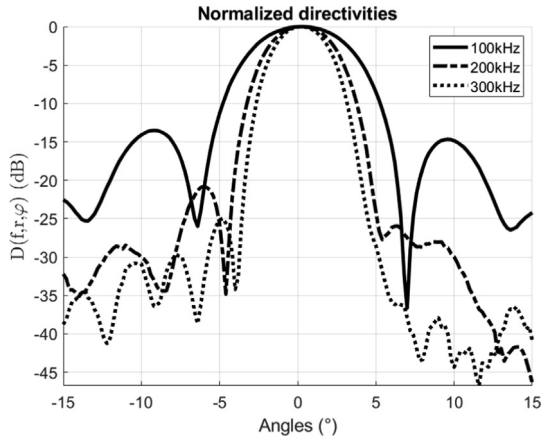

Fig. 3. Measured directivity patterns $10\log(D(f,r,\varphi))$ at $r = 20$ m for f = 100 kHz, f = 200 kHz, f = 300 kHz. At each angle, 4 measurements are averaged. Standard deviations σ stand in the following interval for each frequency: $\sigma_{100\text{ kHz}}(\varphi) \in [2.6; 6.1]$ dB, $\sigma_{200\text{ kHz}}(\varphi) \in [2.0; 7.3]$ dB, $\sigma_{300\text{ kHz}}(\varphi) \in [2.3; 6.7]$ dB.

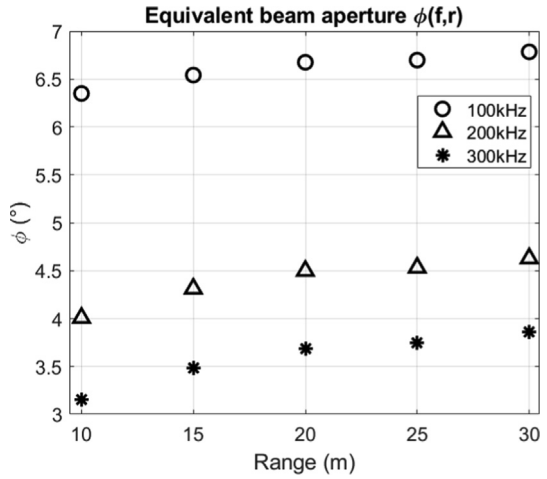

Fig. 4. Equivalent beam apertures $\phi(f,r)$ of the main lobe according to range and frequency, calculated from the directivity patterns measured between 10 m and 30 m.

2.6. Measurements of the operating gain and range variations

The echosounder aims to measure the absolute acoustic response of the seabed. It is therefore essential to evaluate: 1) its total operating gain according to frequency, $G(f)$, due to electrical connections, processing, etc., and: 2) the transmitted level to which is directly related a specific decrease of each harmonic with range as observed in Section 2.4. In the case of backscatter measurements, we include both the transmit level and its decrease during two-way propagation, expressed as a variable noted $\mathcal{L}(f,r)$. Indeed, because of non-linear propagation, acoustic forward transmission losses $TL_{fw}(f,r)$ to the target differ from the classical, linear model (proportional to $20\log r + \alpha r$ [32] with α the linear attenuation coefficient). Likewise, the operating gain cannot be calculated either with linear theoretical formulae [33].

For practical use, we propose to create look-up tables of each gain and frequency level according to the range: $G(f) + \mathcal{L}(f,r)$, that will be used to calculate the seabed response (sonar equation) in place of all the unknown parameters (see Eq. 2). This can be achieved with measurements on a calibrated target [34,1], moved along the axis of the echosounder. The principle is to compare the received backscattering level of the controlled point target with its actual target strength $TS(f)$ whose frequency spectrum is perfectly known [35]. The target used for our measurements is a full-metal sphere (tungsten, carbide and cobalt) of diameter 38.1 mm, chosen because its frequency responses have no anti-resonance at the frequencies we use (respectively 100 kHz, 200 kHz, 300 kHz). The final outcomes are look-up tables of $G(f) + \mathcal{L}(f,r)$ according to range and frequency. For our objective, the sphere is moved from 10 m to 30 m range which gives a sufficient range of look-up tables for surveys in the Bay of Brest (depths $\leqslant 30\,m$) (for larger ranges, the calibration should increase to similar ranges or, if the measurements could not be made because of practical reasons, an estimation of $G(f) + \mathcal{L}(f,r)$ variations for r greater than 30 m should be proposed, based on measurements at r lower than 30 m). For this experimental setup, the associated sonar equation is:

$$\begin{aligned} 20\log(V_{Rx}(f,r)) &= 20\log(V_{Tx}(f)) + S_h(f) + S_v(f) \\ &\quad +10\log(D(f,r,\varphi)) - TL_{fw}(f,r) \\ &\quad -TL_{bw}(f,r) + TS(f) + G_o(f) \end{aligned} \tag{2}$$

with f the harmonic frequency, V_{Rx} and V_{Tx} respectively the received and transmitted voltages, S_h and S_v respectively the receiver and transmitter sensitivities, $D(f,r,\varphi)$ is the combined directivity function at transmission and reception, φ the angle in the beam (i.e $D(f,r,\varphi = 0°) = 1$ on the beam-axis), TL_{fw} and TL_{bw} respectively the transmission losses forward (from the transmitter to the sphere) and backward (from the sphere to the receiver), and $G_o(f)$ encompasses the electrical gains. Because of the non-linear operation of the echosounder, the perfectly known parameters are only $V_{Rx}(f,r)$, the target strength of the sphere $TS(f)$ (i.e. its backscattering cross section [36]) and $D(f,r,\varphi)$. Measurements on the target are done on the axis of the echosounder so that $10\log(D(f,r,\varphi)) = 0$. Consequently, we can define the difference $20\log(V_{Rx}(f,r)) - TS(f)$ as the sum of an operating gain $G(f)$ and a level range variations $\mathcal{L}(f,r)$ such as:

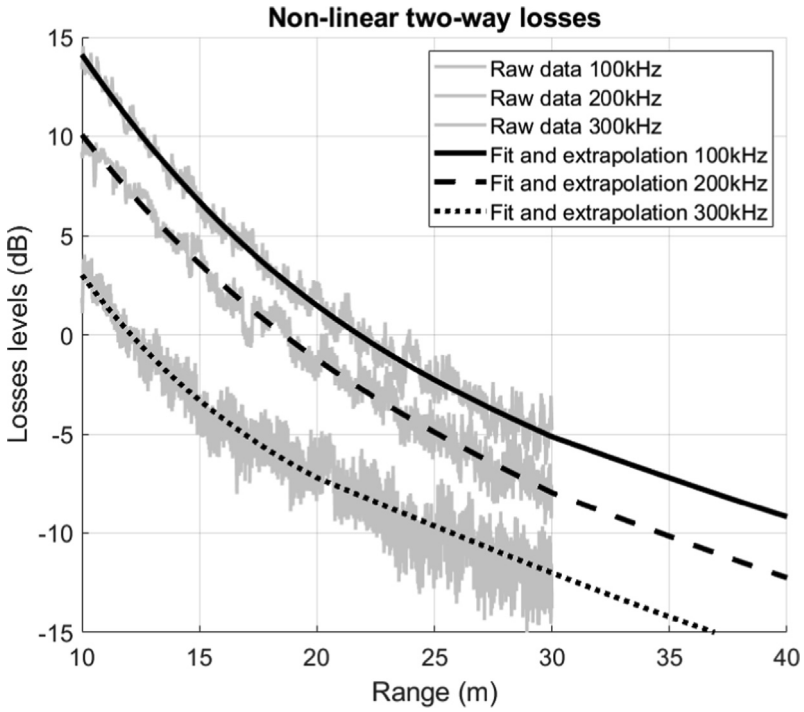

Fig. 5. Grey: measurements of $G(f)+\mathcal{L}(f,r)$ in the large tank of Ifremer (sea water) according to the range from the echosounder in operational mode (i.e. with the maximum level at emission). Black: best-fitting curves used as look-up tables.

$$G(f)+\mathcal{L}(f,r)=20\log\left(V_{Rx}(f,r)\right)-TS(f) \tag{3}$$

Measured $G(f)+\mathcal{L}(f,r)$ and their corresponding best-fitting curves used as look up tables are shown for the fundamental frequency and its 2 first harmonics on Fig. 5. Finally, $G(f)+\mathcal{L}(f,r)$ contains the propagation losses, Tx and Rx sensitivities, the fixed transmit level $20\log\left(V_{Tx}(f)\right)$, electrical gains, and signal processing gains of the echosounder we wished to estimate, and that will be useful for seafloor reflectivity calculations.

3. Seabed reflectivity processing

Raw data from the multi-frequency echosounder are time-sampled values of received levels $20\log\left(V_{Rx}(r)\right)$, with $r=ct/2$, in which t is the listening time, i.e. the time after emission of the signal. Signals for each harmonic frequency are extracted thanks to a band-pass filter and noted $20\log\left(V_{Rx}(f,r)\right)$. The transmit signal, also called pulse, is a 100-kHz sine wave of duration T. Each harmonic received signal is perfectly in-phase and investigated separately. From these received time signals, the echo of the seabed is detected and its reflectivity index, or backscattering strength $BS(f,\theta)$, is computed (in decibels) as:

$$\begin{aligned}BS(f,\theta)=&\,20\log\left(V_{Rx}(f,r)\right)-20\log\left(V_{Tx}(f)\right)-S_h(f)-S_v(f)\\&-10\log\left(D(f,r,\varphi)\right)+TL_{fw}(f,r)+TL_{bw}(f,r)-G_o(f)\\&-10\log(A(f,\theta))\end{aligned} \tag{4}$$

with θ the incidence angle on the seabed, $D(f,r,\varphi)$ the directivity (combining Tx and Rx) of the echosounder for the frequency f at the range r taken at the angle $\varphi=\cos^{-1}(h/r)$ the angle of the sample in the beam (with h the water height at nadir on a supposed flat seabed), $TL_{fw}(f,r)$ and $TL_{bw}(f,r)$ respectively the transmission losses forward (from the transmitter to the seabed) and backward (from the seabed to the receiver), and $A(f,\theta)$ the insonified area on the seafloor (see Section 3.2). Directivity patterns of the echosounder $D(f,\varphi)$ for each frequency are also measured in the tanks with hydrophones, at varying range (their apertures slightly change during propagation). Using the look-up tables of $G(f)+\mathcal{L}(f,r)$ computed in Section 2.6, we can write:

$$BS(f,\theta)=G(f)+\mathcal{L}(f,r)-10\log\left(D(f,r,\varphi)\right)-10\log(A(f,\theta)) \tag{5}$$

where $r=h/\cos(\theta)$ is the flat seabed approximation linking r and θ.

3.1. Bottom echo detection

The sounding (i.e. the time-sample of the seafloor-echo coming from the center of the echo-sounder beam) is detected with two methods, depending on the incidence angle [17]: 1) on the center of gravity computed on the intensity values for angles near the nadir, 2) from phase differences, thanks to the receivers vertically aligned for other angles. The sounding range is noted r_s and its equivalent received time $t_s=2r_s/c$. We can note that the seafloor echoes of the harmonic frequencies are in some cases very useful to improve detection (for example in case of phase ambiguities, due to the relatively large distance between two receivers). Indeed, the phase ramps at high frequencies are shorter and steeper than that of the fundamental frequency, because of their shorter beamwidths. Around the sounding sample, indexed by i, several time-samples are retained (this is the equivalent of the "snippets" of multibeam echosounders [37,38]). They are averaged to compute $BS(f,\theta)$ for one ping. As in [17], samples i are retained when the condition $\varphi_i\in[-1^\circ;+1^\circ]$ is valid with φ the angle of the samples in the beam.

3.2. Insonified area

The insonified area is calculated thanks to a geometrical model using the echosounder equivalent along-track ϕ_{al} and across-track ϕ_{ac} beam apertures [32], the incidence angle θ, and the effective pulse length T_{eff} (defined below) which takes into account the signal loss of energy during transmission. In our case, ϕ_{al} and ϕ_{ac} both

equal the equivalent beam aperture measured in Section 2.5 because of the SBES symmetry, i.e. $\phi_{al} = \phi_{ac} = \phi(f,r)$. The insonified area model is composed of two regimes, near-nadir and oblique-angle, such as [39] (assuming the slope along-track is flat):

$$A(f,\theta) = \min\left(\pi\frac{r^2}{\cos\theta}\left(\frac{\phi(f,r)}{2}\right)^2, \frac{cT_{\text{eff}}(f)}{2\sin\theta}.r.\phi(f,r)\right) \quad (6)$$

The effective pulse lengths are computed for each frequency by measuring the difference of acoustic energy between the desired rectangular pulse and the pulse actually transmitted by the echosounder. Indeed, when the pulse is transmitted by the Tx transducer, its bandwidth creates transitory effects on the shape of the signal. The energy of the signal actually transmitted is therefore lower than the perfect rectangular pulse energy given electronically to the transducer. This difference of acoustic energy is taken into account by using an effective pulse length T_{eff} whose amplitude is unity and whose energy is proportional to the theoretical pulse energy by a factor called Sa_{corr} in [17,35], defined as:

$$10\log(T_{\text{eff}}(f)) = 10\log(T(f)) + Sa_{\text{corr}}(f) \quad (7)$$

with $T(f)$ the theoretical signal duration chosen by the user at $T(100\,kHz) = 600$ µs. Values of $Sa_{\text{corr}}(f)$ and $T_{\text{eff}}(f)$ are given in Table 2 for the fundamental frequency (100 kHz) and the first two harmonics (200 kHz and 300 kHz).

3.3. Resulting $BS(f,\theta)$ measurements

To estimate the backscattering strength (i.e. the $BS(f,\theta)$ curves) of a given seabed, the SBES has to be tilted mechanically to reach discrete incidence angles $\theta_j \in [0°, 5°, 10°, \ldots, 60°]$. This is obtained with the pan & tilt device shown in Fig. 1. On a given surveyed area, 150 pings are recorded for each tilting angle. As recommended in [17], seabed samples i of each ping are retained to be part of a $BS(f,\theta_j)$ value (average) when their incidence angle on the seafloor $\theta_i = \theta_s + \varphi_i + \gamma_s$ is included in the interval $[-1°; +1°]$ around the desired angles θ_j, i.e.:

$$BS(f,\theta_j) = 10\log\left(\frac{1}{N}\sum_{i=1}^{N}\sigma_{BS}(f,\theta_i)\right) \text{if} \theta_i \in [\theta_j - 1°; \theta_j + 1°] \text{ where } \theta_i = \theta_s + \varphi_i + \gamma_s \quad (8)$$

with $\sigma_{BS}(f,\theta_i) = 10^{BS(f,\theta_i)/10}$, θ_s the incidence angle of the sounding on the seafloor ($\cos\theta_s = h/r_s$), φ_i the angle of the time-sample i in the beam (with respect to the axis), γ_s the roll values at the time of the sounding s, and N the number of samples i that respect the condition $\theta_i \in [\theta_j - 1°; \theta_j + 1°]$.

During our survey, the sea was perfectly calm (World Meteorological Organisation Sea State Code 0) and the roll of the ship was always $< \pm 1°$ so that almost all values were averaged. We consequently obtain $BS(f,\theta)$ values for all incidence angles θ_j from 0° to 60° with a step of 5°.

3.4. Fitting the $BS(f,\theta)$ curves

In the following, the discrete measurements $BS(f,\theta_j)$ are fitted with the heuristical model GSAB (Generic Seafloor Acoustic Backscatter) for seafloor backscattering strength [40], to get seabed $BS(f,\theta)$ curves that can be analysed in Section 4. The model describes the BS into three parts thanks to six parameters [41]:

$$BS(\theta) = 10\log\left(A.\exp\left(-\frac{\theta^2}{2B^2}\right) + C.\cos^D(\theta) + E.\exp\left(-\frac{\theta^2}{2F^2}\right)\right) \quad (9)$$

with A regulating the specular amplitude, B controlling the angular width of the specular regime, C giving the average backscatter level at oblique incidence, D being the angular decrement of the backscatter (equal to 2 for Lambert law), E the transitory maximum level and F its angular half-extent.

Table 2
Proportionality coefficient $Sa_{\text{corr}}(f)$ between the theoretical pulse energy and the effective pulse energy, measured in the tanks for the fundamental frequency (100 kHz) and the first two harmonics (200 kHz and 300 kHz). Effective pulse lengths are associated to these values.

Frequencies	100 kHz	200 kHz	300 kHz
$Sa_{\text{corr}}(f)$	−0.37 dB	−0.49 dB	−1.03 dB
$T_{\text{eff}}(f)$	551 µs	536 µs	473 µs

4. Sea trials and results

Sea trials took place in the Bay of Brest (France) in May 2016 aboard R/V *Thalia* of Ifremer. Three areas with distinct seafloor types (see Section 4.1) were surveyed in order to demonstrate the feasibility of discriminating seabeds with our echosounder. The SBES was mounted on a pole on the starboard side of the vessel (see Fig. 1). A pan&tilt system was used to tilt the sounder at several angles, from 0°(nadir) to 60°, with a 5° step. At each angle, data were acquired while the vessel was drifting slowly. This drift ensured a minimum of acoustic noise from the vessel's engines or electrical on-board devices, because the sounder was a prototype and therefore not fully fitted with filters against other types of acoustic noise. The calm weather during the survey ensured the vessel drifted for a distance short enough to assume the seafloor is the same for all pings.

4.1. Area descriptions

Measurements were done onto three areas of the Bay of Brest chosen for their distinct seabed types (see map on Fig. 6). Area 1 is at the mouth of the small Elorn river. Area 2 is in the so-called "Carré Renard", a plateau in the center of the Bay and also a well-surveyed area for echosounder calibration [17]. Finally, Area 3 is at the mouth of another small river, the Aulne. According to the morpho-sedimentological map in [42], created from [43,44], Area 1 is composed of "sandy mud" or "muddy sand", Area 2 is mostly composed of "gravels" with rare pebbles, and Area 3 is composed of "gravelly coarse sand" with maerl and episodic rocks. During the survey, videos and photographs of the seafloor were taken in these areas (cf. Fig. 7). They show sand and mud in Area 1, pebbles and brittle-stars in Area 2, and a hard seafloor (rock) and a large amount of shells in Area 3.

4.2. Raw results

The raw results take the form of several $BS(f,\theta)$ curves for frequencies of 100 kHz and above, for all 3 areas surveyed. At first, we compare on Fig. 8 the results at the fundamental frequency (100 kHz) for the different areas. Crosses, triangles and circles show the raw measurements (averages of acoustic intensity values) and lines show the fit of the GSAB model to these measurements. We observe differences in shape and level according to the areas, as expected. Area 3 has a hard and rough seafloor; correspondingly, the $BS(f,\theta)$ curve has a generally low level and is flattened at the nadir angles. Conversely, the curve of Area 1 (sandy/muddy seafloor) has a very large range of levels, from −6.4 dB at 0° to −26.8 dB at 60°, and a high specular level. The curve of Area 2 is in between those two descriptions, with a high global BS level but a medium range of BS values according to incidence angles and a visible specular regime, not as strong as Area 1. These effects of specular flattening are commonly observed [45–

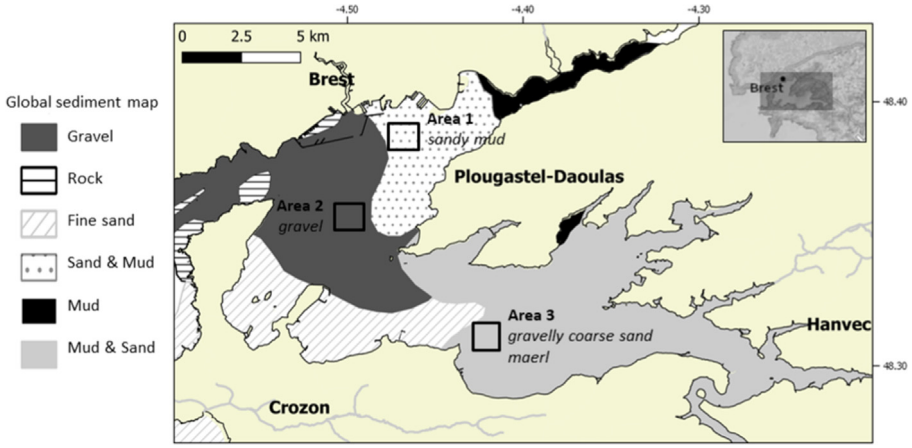

Fig. 6. Areas surveyed in the Bay of Brest (France). The global sediment map comes from data.shom.fr (www.shom.fr/HOM/GEOL_SEDIM_MONDIALE) and land information come from geo.data.gouv.fr. At the time of the survey, the water heights were constant for all pings: $h = 20.5\ m$ for Area 1, $h = 17\ m$ for Area 2, and $h = 31\ m$ for Area 3.

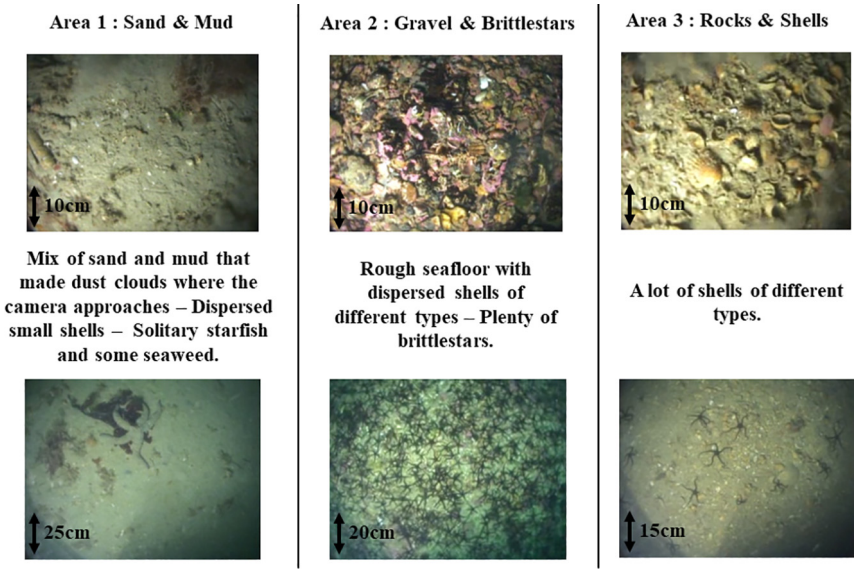

Fig. 7. Seafloor photographs in the three areas studied, taken during the survey, with visual descriptions. Data collected by the authors.

47] when the seabed rugosity changes from structures finer than the wavelength (like sand or mud at 100 kHz) to macro-structures close or larger than the wavelength (like pebbles or rocks). The specular shape can disappear, like for Area 3, on hard seafloor, as demonstrated e.g. by [18] (roughness effect).

We can also compare (see Fig. 9) raw results in one area for the fundamental frequency (100 kHz) with two of its harmonic frequencies (namely 200 kHz and 300 kHz). We observe frequency variations where, in particular, the shapes of the $BS(f,\theta)$ curves are modified, mostly on the specular parts which decrease with frequency and where Bragg backscattering [32] for grazing angles inversely increases.

4.3. Calibration on reference Area 2 ("Carré Renard")

Data were acquired in area 2 because it is a known reference area for echosounder calibration [17], and it was therefore possible to compare our results to reference curves noted $BS_{\text{ref}}(f,\theta)$. Our Ifremer colleagues kindly shared two reference curves at 200 kHz and 333 kHz, reported in [17]. Their 200-kHz curve $BS_{\text{ref}}(200\ \text{kHz},\theta)$ can be usefully compared to our measurements of $BS(200\ \text{kHz},\theta)$. The 333-kHz curve can be used with caution to compare with our measurements at 300 kHz. The comparison is plotted as the difference $BS_{\text{ref}}(f,\theta) - BS(f,\theta)$ according to incidence angles for 200 kHz and 300 kHz respectively on Figure 10. We see that those differences follow a curve whose shape can be explained by several biases. The first one is visible in the range variations $(\mathcal{L}(f,r))$ estimated in Section 2.6, which can appear because of a difference in water composition (salinity) or turbidity between the measurements in the tanks and *in situ* (see Table 1) that may impact the generation of non-linearities [48,49] and therefore the levels of harmonic frequencies. The second bias is due to the difference of variation of β during the propagation. Indeed, the Tx signal propagates horizontally in the tanks and vertically or obliquely during the survey. Thus, whereas the non-linear coefficient is constant along the propagation in tank, it is variable *in situ*, introducing modification in the harmonic generation and sustain. A last bias comes from slight errors in the operating gain $G(f)$, from *in situ* sensitivity variations, electronics or processing adjustments. Thanks to the references curves, these biases can be quantified *in situ* and properly accounted for. Thus, the difference between the reference curve $BS_{\text{ref}}(f,\theta)$ and the raw-results for each inci-

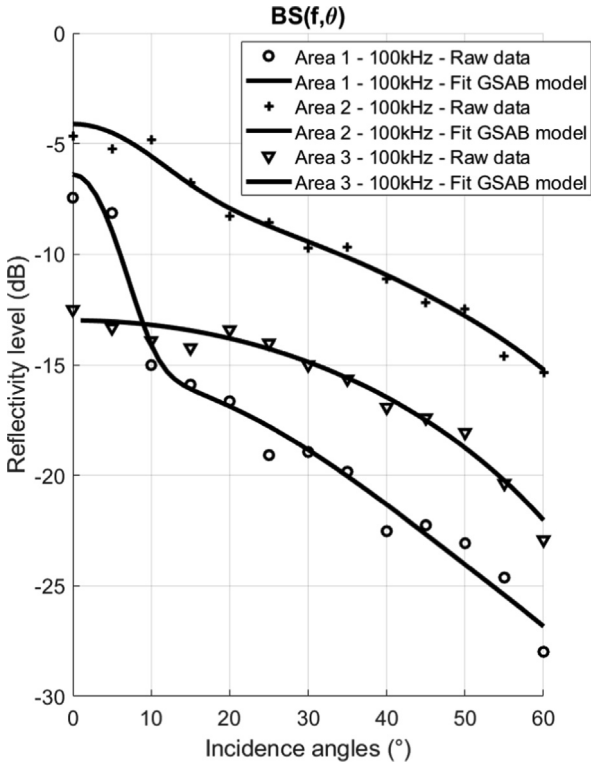

Fig. 8. $BS(f,\theta)$ curves of the fundamental frequency 100 kHz on the three areas surveyed: (1) sand & mud, (2) pebbles & brittle-stars, (3) hard seafloor (rocks) & shells. The raw measurements are respectively indicated with crosses, triangles and circles. The lines correspond to the respective GSAB model fits.

dence angle $BS(f,\theta)$, noted $G_{\text{corr}}(f) + \mathcal{L}_{\text{corr}}(f,\theta) = BS_{\text{ref}}(f,\theta) - BS(f,\theta)$, is a correction which added to the $BS(f,\theta)$ calculation in Eq. 5, gives:

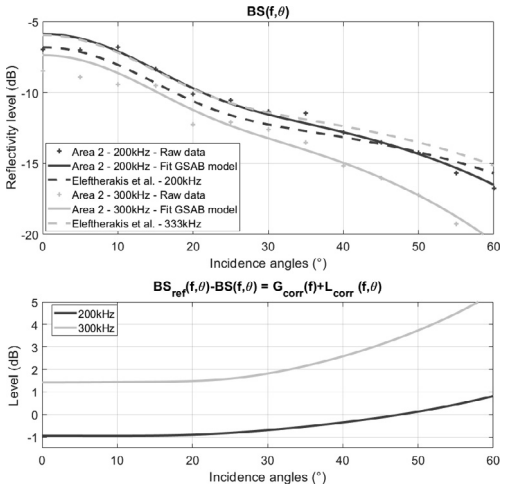

Fig. 10. Top: $BS(f,\theta)$ curves for harmonic frequency 200 kHz and 300 kHz on Area 2 (pebbles & brittle-stars). Raw measurements are indicated with crosses; the full line shows the GSAB model fit [32]; the dashed line corresponds to $BS_{\text{ref}}(200kHz,\theta)$ and $BS_{\text{ref}}(333kHz,\theta)$ curves from [17] on the same area. Bottom: gain and range variation corrections, i.e. differences $BS_{\text{ref}}(f,\theta) - BS(f,\theta) = G_{\text{corr}}(f) + \mathcal{L}_{\text{corr}}(f,\theta)$ between the reference reflectivity curve and the raw results.

$$\begin{aligned} BS_{\text{calib}}(f,\theta) \quad &= G(f) + G_{\text{corr}}(f) + \mathcal{L}(f,\theta) + \mathcal{L}_{\text{corr}}(f,\theta) \\ &\quad -10\log\left(D(f,h/\theta,\varphi)\right) - 10\log(A(f,\theta)) \end{aligned} \tag{10}$$

The value $BS_{\text{calib}}(f,\theta)$ obtained after calibration on Area 2 is the absolute reflectivity level of this area. This calibration is done for the two frequencies of which reference reflectivity curves are available: 200 kHz and 300 kHz.

To apply the calibration to the other areas, we have to transform incidence angles to range, thanks to the measurements of echo-sounder altitude (i.e. the range h at nadir): $r = h/\cos(\theta)$. This gives a correction $G_{\text{corr}}(f) + \mathcal{L}_{corr}(f, r = h/\cos(\theta))$, function of range, and we can therefore calibrate the $BS(f,\theta)$ curves of each area by doing

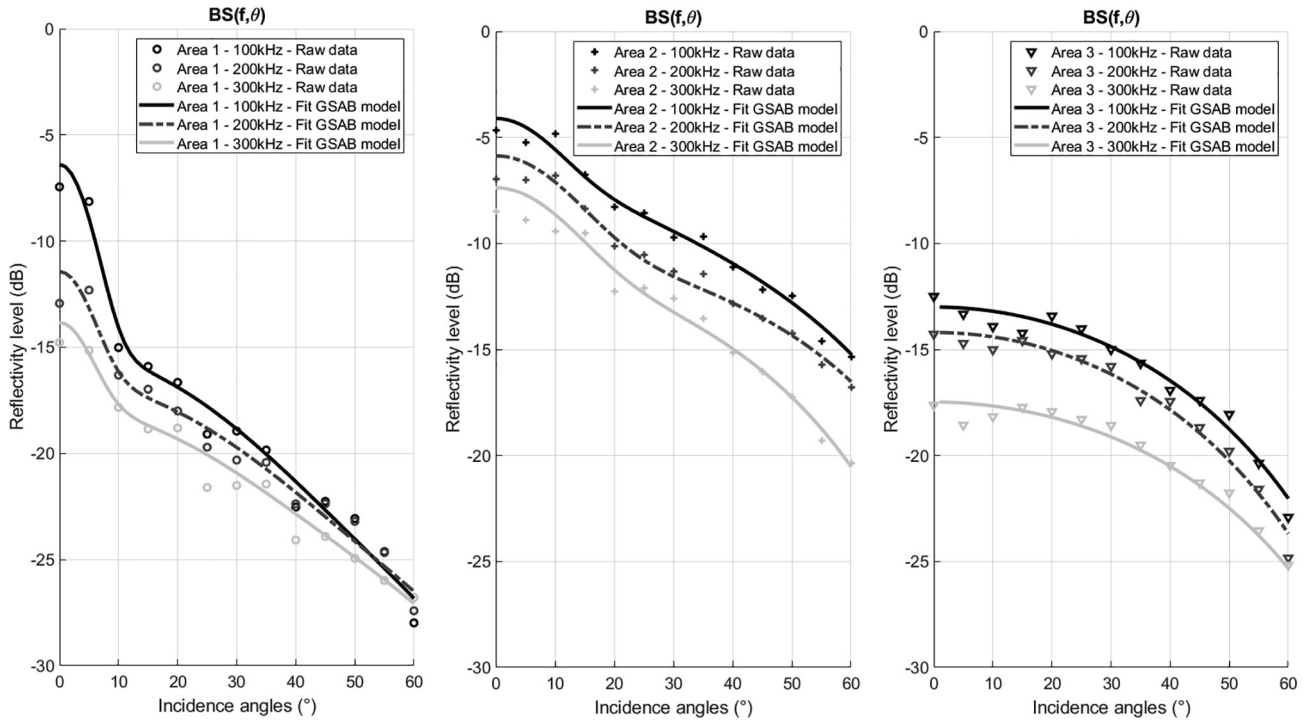

Fig. 9. $BS(f,\theta)$ curves of the fundamental frequency (100 kHz) and two harmonics (200 kHz and 300 kHz) on the three areas (left: sand & mud, center: pebbles & brittle-stars, right: hard seafloor (rocks) & shells). Raw measurements are indicated with circles and the GSAB model fits with lines.

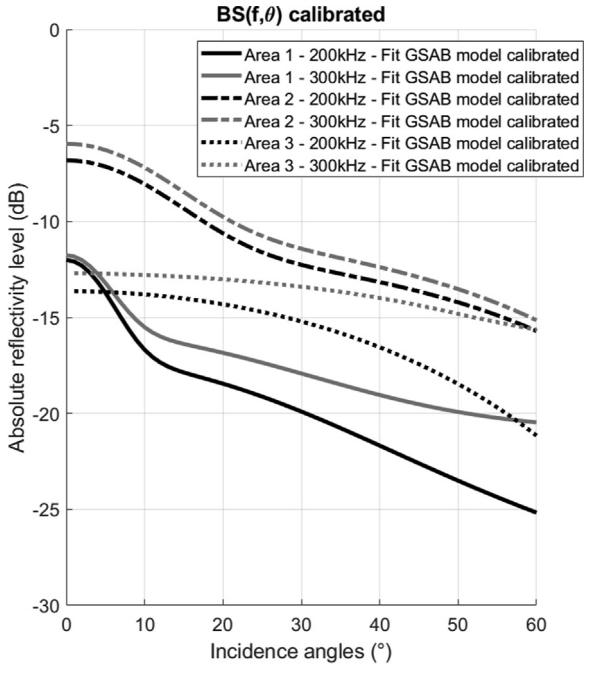

Fig. 11. Absolute $BS_{\text{calib}}(f,\theta)$ curves after calibration for the 3 areas and the two first harmonics 200 kHz and 300 kHz.

the same transformation. At the end, we obtain calibrated reflectivity curves of the three areas, shown in Fig. 11. We can see that the shapes of the curves discriminate clearly between the different seafloor types, and also that the variations of those shapes for one area with frequency is not the same for each seabed type.

The raw results (Figs. 8 and 9) and the calibrated results (Fig. 11) allow us to conclude that the curves $BS_{\text{calib}}(f,\theta)$ obtained with the harmonic frequencies are able to discriminate seabed responses according to incidence angles and their absolute levels. Indeed, clear differences are observed between responses of seabed from the 3 areas surveyed that correspond to variations of the seabed composition. Also, modifications of the curve shape are observed between frequency responses like in Area 1 (sand & mud). These results clearly show the interest of multi-frequency single-beam echosounders for seafloor characterization. They also demonstrate the importance of clearly mapping the characteristics of the instrument, in controlled tank environments and through a full and thorough calibration *in situ*.

5. Discussion

5.1. In situ calibration

The results of the calibration on the reference area show the clear necessity of a calibration *in situ* to obtain absolute reflectivity levels. Preliminary tank measurements are essential to characterise the entire instrument through parameters like its directivity, the effective pulse length, electrical gains, essential to calculate the backscattering strength. In our case, they were also extremely useful to validate the generation of harmonics, and determine the shock distance. The calibration is imperative to measure the true seafloor acoustic responses of multiple areas, and ultimately this harmonic echosounder can be used as a reference system to calibrate other sounders, from single-beam to multibeam. An *in situ* calibration could be performed periodically in order 1) to check the validity of the last calibration results according to the new area surveyed, and 2) to detect potential technical issues with the system (defective transducer, aging electronic, etc.).

5.2. Seafloor acoustic characterization and classification

Our prototype multi-frequency SBES uses non-linear acoustics to generate several harmonic frequencies. The seafloor reflectivity variations presented in Section 4 as a function of incidence angles and for several frequencies are consistent with the physical considerations responses studied and modeled by Jackson in [47,50], even if the frequencies used is this article are mostly beyond the original validity domain of this model (up to 100 kHz) – other studies (e.g. [51,52]) already show it can be safely extended up to 240 kHz -: the acoustic response of a sandy-muddy seabed cover a large range of *BS* values from the nadir to the grazing angles and generate a strong specular effect, whereas a hard and rough seabed like rock has a flat response with a specular nonexistent. These variations are found in our results (see Fig. 12) and give us confidence that classification and characterization of seabed types are feasible solutions with the harmonic single-beam echosounder. The frequency variations of the seabed responses are a major point for classification because it adds a lot of information. The possibility to measure several frequency responses simultaneously and therefore perfectly on the same seabed is a real asset of this type of echosounder.

5.3. Improving the non-linear echosounder

This multi-frequency SBES allows the concurrent use of three frequencies at once (central frequency of 100 kHz and two harmonics at 200 kHz and 300 kHz respectively), using a CW signal at transmission. By improving the system and specifically its signal-to-noise ratio, our next improvements will aim to access higher harmonics at 400 kHz, 500 kHz etc., providing more information on seabed types. The use of much higher frequencies (and therefore access to much smaller wavelengths) will also prove an asset for the imaging of less reflective targets like marine vegetation. Some types of macrophytes have limited gas content in their leaves and blades, but are detectable by using higher frequencies ($\geqslant$ 400 kHz). This multi-frequency SBES, augmented with its pan & tilt system, can therefore prove very useful for studies of marine vegetation (in particular the mapping of canopy heights and the quantification of biomass) [53]. It can also be advantageously used for fisheries application, using the frequency–response of particular fish species or plankton (e.g [54,55]). Other small-scale targets would also become more accessible, like gas bubbles in the water column above gas seeps or small oil inclusions in oil spills.

To be more efficient in measuring seabed acoustic responses curves, we can think, in future developments, about a system which could be able to generate beams simultaneously at a series of incident angles, such as a multi-beam echosounder [46], and following the first works at low frequency of [56,57].

6. Conclusion

The use of different technologies have enabled the development of a multi-frequency single-beam echo-sounder (SBES), using non-linear acoustics to transmit several harmonic frequencies. Our design generates a fundamental frequency at 100 kHz and several harmonic frequencies at 200 kHz and 300 kHz in particular. Bespoke, wide-band receivers were built to maximise backscatter measurements over ranges $\leqslant$ 30 m, commensurate with the depths expected in field surveys. The generation of harmonic frequencies was checked and quantified through tank experiments.

A complete processing methodology was presented, enabling to fully calibrate the echosounder, and we showed the importance of *in situ* calibration to account for variability in the marine environments. Mounted on a pan & tilt unit, the SBES is able to measure absolute seafloor reflectivity $BS_{\text{calib}}(f,\theta)$, according to incident angles and to different frequencies, at the same time and for the exact same patch of seabed. The multi-frequency SBES was tested in a survey in the Bay of Brest (France), measuring different types of seabed concurrently imaged with seafloor photographs and videos. One of the areas ("Carré Renard") benefited from previous measurements, and we were able to demonstrate the consistency of the different measurements, matching seabed types and differences. These results prove that acoustic seafloor characterization and classification is possible with this kind of instrument.

Declaration of Competing Interest

The authors declare that they have no known competing financial interests or personal relationships that could have appeared to influence the work reported in this paper.

Acknowledgments

This research was supported by the Direction Générale de l'Armement (DGA) and Agence Nationale de la Recherche (ANR) in France (project ANR-14-ASTR-0022). IM's PhD studentship is funded by the Agence Innovation Défense (AID) in France and the Defence Science Technology Laboratory (DSTL) in the UK (project #2018632). We would like to thank Ifremer for their help with the tank measurements and the survey with R/V *Thalia*.

References

[1] Demer DA, Berger L, Bernasconi M, Bethke E, Boswell K, Chu D, et al. Calibration of acoustic instruments. ICES Cooper Res Rep 2015;326(133). https://doi.org/10.25607/OBP-185.
[2] Pouliquen E, Lurton X. Seabed identification using echo-sounder signals. In: European Conference on Underwater Acoustics, Elsevier Applied Science, London and New York; vol. 535. 1992, p. 14–8.
[3] Snellen M, Siemes K, Simons DG. Model-based sediment classification using single-beam echosounder signals. J Acoust Soc Am 2011;129(5):2878–88. https://doi.org/10.1121/1.3569718.
[4] Hamilton L, Mulhearn P, Poeckert R. Comparison of ROXANN and QTC-View acoustic bottom classication system performance for the Cairns area, Great Barrier Reef, Australia. Continental Shelf Res 1999;19(12):1577–97. https://doi.org/10.1016/S0278-4343(99)00020-5.
[5] De Moustier C. Beyond bathymetry: Mapping acoustic backscattering from the deep seafloor with Sea Beam. J Acoust Soc Am 1986;79(2):316–31. https://doi.org/10.1121/1.393570.
[6] Clarke JH, Danforth B, Valentine P. Areal seabed classification using backscatter angular response at 95khz. High Frequency Seafloor Acoustics 1997; SACLANTCEN Conference Proceedings CP-45:243–250.
[7] Brown CJ, Blondel P. Developments in the application of multibeam sonar backscatter for seafloor habitat mapping. Appl Acoust 2009;70(10):1242–7. https://doi.org/10.1016/j.apacoust.2008.08.004. the Application of Underwater Acoustics for Seabed Habitat Mapping.
[8] Hughes Clarke J. Toward remote seafloor classification using the angular response of acoustic backscattering: a case study from multiple overlapping gloria data. IEEE J Ocean Eng 1994;19(1):112–27. https://doi.org/10.1109/48.289456.
[9] Innangi S, Barra M, Di Martino G, Parnum I, Tonielli R, Mazzola S. Reson seabat 8125 backscatter data as a tool for seabed characterization (central mediterranean, southern italy): Results from different processing approaches. Appl Acoust 2015;87:109–22. https://doi.org/10.1016/j.apacoust.2014.06.014.
[10] Fezzani R, Berger L. Analysis of calibrated seafloor backscatter for habitat classification methodology and case study of 158 spots in the Bay of Biscay and Celtic Sea. Mar Geophys Res 2018;39(1–2):169–81.
[11] Pouliquen E, Zerr B, Pace NG, Spina F. Seabed segmentation using a combination of high frequency sensors. In: Oceans '99. MTS/IEEE. Riding the Crest into the 21st Century. Conference and Exhibition. Conference Proceedings (IEEE Cat. No.99CH37008); vol. 2. 1999, p. 888–93. doi: 10.1109/OCEANS.1999.804991.
[12] Bulanov V, Korskov I, Popov P. Measurements of the nonlinear acoustic parameter of sea water via a device using reflected pulses. Instrum Exp Technol 2017;60(3):414–7.
[13] Endo H. Calculation of nonlinearity parameter for seawater. J Acoust Soc Am 1984;76(1).
[14] Rudnick I. On the attenuation of finite amplitude waves in a liquid. J Acoust Soc Am 1958;30(6):564–7. https://doi.org/10.1121/1.1909686.
[15] Bjørnø L. Forty years of nonlinear ultrasound. Ultrasonics 2002;40(1):11–7. https://doi.org/10.1016/S0041-624X(02)00084-7.
[16] Prieur F, Nasholm SP, Austeng A, Tichy F, Holm S. Feasibility of second harmonic imaging in active sonar: Measurements and simulations. IEEE J Ocean Eng 2012;37(3):467–77. https://doi.org/10.1109/JOE.2012.2198933.
[17] Eleftherakis D, Berger L, Le Bouffant N, Pacault A, Augustin JM, Lurton X. Backscatter calibration of high-frequency multibeam echosounder using a reference single-beam system, on natural seafloor. Mar Geophys Res 2018;39(1–2):55–73.
[18] Jackson D. APL-UW high-frequency ocean environmental acoustic models handbook. Tech. Rep. 102; University of Washington; 1994.
[19] Di Marcoberardino L, Marchal J, Cervenka P. Nonlinear multi-frequency transmitter for seafloor characterization. Acta Acust united Acust 2011;97(2):202–8.
[20] Hamilton MF, Blackstock DT. Nonlinear acoustics. Academic Press; 1997.
[21] Fox FE, Wallace WA. Absorption of finite amplitude sound waves. J Acoust Soc Am 1954;26(6):994–1006. https://doi.org/10.1121/1.1907468.
[22] Beyer RT. Parameter of nonlinearity in fluids. J Acoust Soc Am 1960;32(6):719–21. https://doi.org/10.1121/1.1908195.
[23] Kuznetsov V. Equations of nonlinear acoustics. Sov Phys Acoust 1971;16:467–70.
[24] Pierce AD. Acoustics: An introduction to its physical principles and applications. 1989 Edition. Acoustical Society of America; 1990.
[25] Enflo BO, Hedberg CM. Theory of nonlinear acoustics in fluids, vol. 67. Springer Science & Business Media; 2006.
[26] Beyer RT. Nonlinear acoustics. Phys Acoust 2012;2(Part B):231–332.
[27] Marchal J. Acoustique non linéaire: contribution théorique et expérimentale à l'étude de l'émission paramétrique (Non-linear acoustics: theoretical and experimental contribution to the parametric transmission research). Ph.D. thesis; Paris 6; 2002.
[28] Ting RY. A review on the development of piezoelectric composites for underwater acoustic transducer applications. IEEE Trans Instrum Meas 1992;41(1):64–7. https://doi.org/10.1109/19.126633.
[29] Woodward B, Chandra R. Underwater acoustic measurements on polyvinylidene fluoride transducers. Electrocomponent Sci Technol 1978;5. https://doi.org/10.1155/APEC.5.149.
[30] Blackstock DT. Basic research in nonlinear acoustics. Texas Univ., Austin Report; 1975.
[31] Blackstock DT. Nonlinear acoustics: Propagation in a periodic waveguide, scattering of sound by sound, propagation through a three-layer fluid, and nonlinearity parameters of sea water. Tech. Rep.; Texas Univ. at Austin Applied Reseach Labs; 1991.
[32] Lurton X. An Introduction to Underwater Acoustics. Principles and Applications. Springer; 2010.
[33] Sherman CH, Butler JL. Transducers and arrays for underwater sound, vol. 4. Springer; 2007.
[34] Simmonds J, MacLennan DN. Fisheries acoustics: theory and practice. John Wiley & Sons; 2008.
[35] Ona E, Mazauric V, Calibration LNA. methods for two scientific multibeam systems. ICES J Mar Sci 2009;66:1326–34.
[36] Foote KG. Optimizing two targets for calibrating a broadband multibeam sonar. In: OCEANS 2006. p. 1–4. https://doi.org/10.1109/OCEANS.2006.306944.
[37] Schimel AC, Beaudoin J, Parnum IM, Le Bas T, Schmidt V, Keith G, et al. Multibeam sonar backscatter data processing. Mar Geophys Res 2018;39(1):121–37.
[38] Lucieer V, Picard K, Siwabessy J, Jordan A, Tran M, Monk J. Seafloor mapping field manual for multibeam sonar [Version 1]. Field Manuals for Marine Sampling to Monitor Australian Waters, Version 1 2018;Canberra, Australia, NESP Marine Biodiversity Hub:42–64. https://doi.org/10.11636/9781925297669.
[39] Malik M, Lurton X, Mayer L. A framework to quantify uncertainties of seafloor backscatter from swath mapping echosounders. Mar Geophys Res 2018;39(1–2):151–68.
[40] Lamarche G, Lurton X, Verdier AL, Augustin JM. Quantitative characterisation of seafloor substrate and bedforms using advanced processing of multibeam backscatter – Application to Cook Strait, New Zealand. Continental Shelf Research 2011;31(2, Suppl):S93–S109. doi: 10.1016/j.csr.2010.06.001; geological and Biological Mapping and Characterisation of Benthic Marine Environments.
[41] Lurton X, Lamarche G, Brown C, Lucieer V, Rice G, Schimel A, et al. Backscatter measurements by seafloor-mapping sonars: guidelines and recommendations. In: A collective report by members of the GeoHab Backscatter Working Group.
[42] Gregoire G. Dynamique sédimentaire et évolution holocène d'un système macrotidal semi-fermé: l'exemple de la rade de Brest. (Sedimentary dynamics and holocen evolution of a macrotidal half-closed system: the example of the bay of Brest)). Ph.D. thesis; Institut français de recherche pour l'exploitation de la mer; 2016. URL:http://www.theses.fr/2016BRES0103.
[43] Gregoire G, Ehrhold A, Roy PL, Jouet G, Garlan T. Modern morpho-sedimentological patterns in a tide-dominated estuary system: the Bay of Brest (west Britanny, france). J Maps 2016;12(5):1152–9. https://doi.org/10.1080/17445647.2016.1139514.

[44] Pluquet F, Ehrhold A. Une nouvelle stratégie d'étude des habitats marins littoraux au moyen de la vedette acoustique V/O Haliotis. (A new study strategy of coastal marine habitats with research vessel R/V Haliotis). Tech. Rep.; Ifremer/DYNECO/EB/09-02/FP; 2009.
[45] Kloser R, Penrose J, Butler A. Multi-beam backscatter measurements used to infer seabed habitats. Continental Shelf Res 2010;30(16):1772–82. https://doi.org/10.1016/j.csr.2010.08.004.
[46] Fonseca L, Brown C, Calder B, Mayer L, Rzhanov Y. Angular range analysis of acoustic themes from stanton banks ireland: A link between visual interpretation and multibeam echosounder angular signatures. Appl Acoust 2009;70(10):1298–304. https://doi.org/10.1016/j.apacoust.2008.09.008 [the Application of Underwater Acoustics for Seabed Habitat Mapping].
[47] Jackson DR, Winebrenner DP, Ishimaru A. Application of the composite roughness model to high-frequency bottom backscattering. J Acoust Soc Amer 1986;79(5):1410–22. https://doi.org/10.1121/1.393669.
[48] Kim BN, Yoon SW. Nonlinear parameter estimation in water-saturated sandy sediment with difference frequency acoustic wave. Ultrasonics 2009;49 (4):438–45. https://doi.org/10.1016/j.ultras.2008.11.002.
[49] Akulichev V, Bulanov V. Acoustical nonlinearity, sound absorption, and scattering in bubble-saturated seawater. In: Doklady Earth Sciences; vol. 479. Springer; 2018, p. 375–8.
[50] Jackson DR, Baird AM, Crisp JJ, Thomson PAG. High-frequency bottom backscatter measurements in shallow water. J Acoust Soc Am 1986;80 (4):1188–99. https://doi.org/10.1121/1.393809.
[51] Choi JW, Na J, Seong W. 240-khz bistatic bottom scattering measurements in shallow water. IEEE J Oceanic Eng 2001;26(1):54–62. https://doi.org/10.1109/48.917926.
[52] Blondel P, Dobbins PF, Jayasundere N, Cosci M. High-frequency bistatic scattering experiments using proud and buried targets. In: Acoustic Sensing Techniques for the Shallow Water Environment. Springer; 2006. p. 155–70.
[53] Tegowski J, Kruss A, Tatarek A, Wiktor J, Blondel P. Spatial distribution of macroalgae along the shores of Kongsfjorden (West Spitsbergen) using acoustic imaging. online; 2017. doi: 10.1515/popore-2017-0009.
[54] Stanton TK, Chu D, Jech JM, Irish JD. New broadband methods for resonance classification and high-resolution imagery of fish with swimbladders using a modified commercial broadband echosounder. ICES J Mar Sci 2010;67(2):365–78. doi: 10.1093/icesjms/fsp262. arXiv:https://academic.oup.com/icesjms/article-pdf/67/2/365/29136431/fsp262.pdf.
[55] Lavery AC, Chu D, Moum JN. Measurements of acoustic scattering from zooplankton and oceanic microstructure using a broadband echosounder. ICES J Mar Sci 2009;67(2):379–94. doi: 10.1093/icesjms/fsp242. arXiv:https://academic.oup.com/icesjms/article-pdf/67/2/379/29135889/fsp242.pdf.
[56] Marchal J, Cervenka P. Modeling of the parametric transmission with the spatial Fourier formalism. Optimization of a parametric antenna. Acta Acustica united with Acustica 2004;90(1):49–61.
[57] Foulon M, Amate M, Burlet N, Penven P, Cervenka P, Marchal J. Experimentations and sonar development for buried objects detection and classification. Tech. Rep.; Institut Jean Le Rond D'Alembert; 2011.

Bibliography

[Abraham and Lyons, 2002] Abraham, D. and Lyons, A. (2002). Novel physical interpretations of K-distributed reverberation. IEEE Journal of Oceanic Engineering, 27(4):800–813.

[Abramowitz and Stegun, 1964] Abramowitz, M. and Stegun, I. A. (1964). Handbook of mathematical functions with formulas, graphs, and mathematical tables, volume 55. US Government printing office.

[Aja-Fernandez et al., 2008] Aja-Fernandez, S., Alberola-Lopez, C., and Westin, C. (2008). Noise and signal estimation in magnitude MRI and Rician distributed images: A LMMSE approach. IEEE Transactions on Image Processing, 17(8):1383–1398.

[Aja-Fernández and Vegas-Sánchez-Ferrero, 2016] Aja-Fernández, S. and Vegas-Sánchez-Ferrero, G. (2016). Statistical analysis of noise in MRI. Switzerland: Springer International Publishing.

[Aktaş, 2011] Aktaş, S. (2011). Quantile function for Rayleigh distribution Kapasitans-Voltaj (C-V). Afyon Kocatepe Universitesi (Turkey).

[Alexandrou et al., 1992] Alexandrou, D., de Moustier, C., and Haralabus, G. (1992). Evaluation and verification of bottom acoustic reverberation statistics predicted by the point scattering model. The Journal of the Acoustical Society of America, 91(3):1403–1413.

[Amiri-Simkooei et al., 2009] Amiri-Simkooei, A., Snellen, M., and Simons, D. G. (2009). Riverbed sediment classification using multi-beam echo-sounder backscatter data. The Journal of the Acoustical Society of America, 126(4):1724–1738.

[Appel-Hansen, 1979] Appel-Hansen, J. (1979). Accurate determination of gain and radiation patterns by radar cross-section measurements. IEEE Transactions on Antennas and Propagation, 27(5):640–646.

[Audric, 2004] Audric, M. (2004). Gaps, a new concept for USBL [global acoustic positioning system for ultra short base line positioning]. In Oceans' 04 MTS/IEEE Techno-Ocean'04 (IEEE Cat. No. 04CH37600), volume 2, pages 786–788. IEEE.

[Augris Claude, 2013] Augris Claude, Agin Gregory, e. a. (2013). Seabed substrate database from a compilation of sediment samples taken during oceanographic campaigns carried out in the Gulf of Lion by Ifremer, CEFREM, IRSN, CEREGE, FOB, MIO, LECOB, The Conseil Général de l'Hérault and Rhône-Méditerranée-Corse Water Agency. Ifremer.

[Augustin and Lurton, 2005] Augustin, J. . and Lurton, X. (2005). Image amplitude calibration and processing for seafloor mapping sonars. In Europe Oceans 2005, volume 1, pages 698–701 Vol. 1.

[Barrett et al., 2020] Barrett, J., Chase, Z., Zhang, J., Holl, M. M. B., Willis, K., Williams, A., Hardesty, B. D., and Wilcox, C. (2020). Microplastic pollution in deep-sea sediments from the great australian bight. Frontiers in Marine Science, 7.

[Beaulieu, 1990] Beaulieu, N. C. (1990). An infinite series for the computation of the complementary probability distribution function of a sum of independent random variables and its application to the sum of rayleigh random variables. IEEE Transactions on Communications, 38(9):1463–1474.

[Becker, 2004] Becker, K. (2004). Effect of various surface-height distribution properties on acoustic backscattering statistics. IEEE Journal of Oceanic Engineering, 29(2):246–259.

[Beckmann, 1965] Beckmann, P. (1965). Shadowing of random rough surfaces. IEEE Transactions on Antennas and Propagation, 13(3):384–388.

[Beckmann and Spizzichino, 1987] Beckmann, P. and Spizzichino, A. (1987). The scattering of electromagnetic waves from rough surfaces. 511 p., Artec House, Norwood, MA, USA.

[Berman and Berman, 1962] Berman, H. G. and Berman, A. (1962). Effect of correlated phase fluctuation on array performance. The Journal of the Acoustical Society of America, 34(5):555–562.

[Biffard et al., 2007] Biffard, B. R., Preston, J. M., and Chapman, N. R. (2007). Acoustic classification with single-beam echosounders: Processing methods and theory for isolating effects of the seabed on echoes. In OCEANS 2007, pages 1–8. IEEE.

[Billon et al., 1981] Billon, D., Joseph, J., and Le Gall, J. (1981). Simulation des images du fond marin obtenues par un sonar detecteur ou classificateur d'objets. In 8° Colloque sur le traitement du signal et des images, FRA, 1981. GRETSI, Groupe d'Etudes du Traitement du Signal et des Images (France).

[Blomqvist, 1979] Blomqvist, A. (1979). Figures of merit of windows for power density spectrum estimation with the DFT. Proceedings of the IEEE, 67(3):438–439.

[Blondel et al., 2006] Blondel, P., Dobbins, P. F., Jayasundere, N., and Cosci, M. (2006). High-frequency bistatic scattering experiments using proud and buried targets. In Acoustic Sensing Techniques for the Shallow Water Environment, pages 155–170. Springer.

[Blondel and Pace, 2007] Blondel, P. and Pace, N. (2007). High-frequency bistatic scattering on seabed and targets: Comparison of scaled and full-scale experiments with sea trials. Proc. IOA, 29(6):147–154.

[Blondel and Pace, 2005] Blondel, P. and Pace, N. G. (2005). Scaled tank experiments: Seabed and target scattering at high frequencies. Proc. 1st UAM. Heraklion.

[Blondel et al., 2015] Blondel, P., Prampolini, M., and Foglini, F. (2015). Acoustic textures and multibeam mapping of shallow marine habitats–examples from eastern malta. Proceedings of the Institute of Acoustics, 37(1):250–257.

[Bobber, 1970] Bobber, R. J. (1970). Underwater electroacoustic measurements. Naval research laboratory.

[Bouffaut, 2019] Bouffaut, L. (2019). Detection and classification in passive acoustic contexts: Application to blue whale low-frequency signals. PhD thesis, IRENav, France.

[Bourret, 1961] Bourret, R. C. (1961). Directivity of a linear array in a random transmission medium. The Journal of the Acoustical Society of America, 33(12):1793–1797.

[Bouvet, 1992] Bouvet, M. (1992). Traitements des signaux pour les systèmes sonar. Masson Paris.

[Bowen et al., 1996] Bowen, L., Gentilman, R., Fiore, D., Pham, H., Serwatka, W., Near, C., and Pazol, B. (1996). Design, fabrication, and properties of SonoPanel(TM) 1–3 piezocomposite transducers. Ferroelectrics, 187(1):109–120.

[Brede et al., 1990] Brede, R., Kristensen, F. H., Solli, H., and Ona, E. (1990). Target tracking with a split-beam echo sounder. International Symposium on Fisheries Acoustics, Seattle (USA), 189:254–263.

[Brekhovskikh et al., 1991] Brekhovskikh, L. M., Lysanov, Y. P., and Beyer, R. T. (1991). Fundamentals of ocean acoustics. Acoustical Society of America.

[Brown, 1962] Brown, J. L. (1962). Variation of array performance with respect to statistical phase fluctuations. The Journal of the Acoustical Society of America, 34(12):1927–1928.

[Bunchuk and Zhitkovskii, 1980] Bunchuk, A. and Zhitkovskii, Y. Y. (1980). Sound scattering by the ocean bottom in shallow-water regions. Soviet Physics Acoustics (Engl. Transl.), USA, 26(5).

[Buratti et al., 1989] Buratti, R., Rio, J., and Witlin, M. (1989). Use of multicolor displays for sonar detection. In Underwater Acoustic Data Processing, pages 539–544. Springer.

[Burckhardt, 1978] Burckhardt, C. B. (1978). Speckle in ultrasound b-mode scans. IEEE Transactions on Sonics and Ultrasonics, 25(1):1–6.

[Burdic and Bartram, 1984] Burdic, W. S. and Bartram, J. F. (1984). Underwater acoustic system analysis. Acoustical Society of America.

[Buscombe et al., 2014] Buscombe, D., Grams, P. E., and Kaplinski, M. A. (2014). Characterizing riverbed sediment using high-frequency acoustics: 1. spectral properties of scattering. Journal of Geophysical Research: Earth Surface, 119(12):2674–2691.

[Calderon, 1964] Calderon, M. (1964). Probability density analysis of ocean ambient and ship noise. Technical report, Navy Electronics Lab San Diego (California).

[Canepa and Pace, 2000] Canepa, G. and Pace, N. (2000). Seafloor segmentation from multibeam bathymetric sonar. In Proceedings of the fifth European conference on underwater acoustics, Lyon, France, pages 361–366.

[Caprais and Lombardi, 1996] Caprais, P. and Lombardi, A. (1996). Development of a SACLANTCEN MCM sonar performance model. Technical report, NATO. SACLANTCEN.

[Caruthers and Novarini, 1993] Caruthers, J. W. and Novarini, J. C. (1993). Modeling bistatic bottom scattering strength including a forward scatter lobe. IEEE Journal of Oceanic Engineering, 18(2):100–107.

[Charlot, 2019] Charlot, D. (2019). Sea bottom sound velocity estimation using high resolution multiswath multibeam bathymetric echosounder. In AGU Fall Meeting Abstracts, volume 2019, pages OS13B–1533.

[Charlot et al., 2019] Charlot, D., Eddadsi, J., Geoffroy, G., and Legris, M. (2019). Real-time correction of sound refraction errors in bathymetric measurements using multiswath multibeam echosounder. In OCEANS 2019 - Marseille, pages 1–7.

[Chotiros et al., 1985] Chotiros, N. P., Boehme, H., Goldsberry, T. G., Pitt, S. P., Lamb, R. A., Garcia, A. L., and Altenburg, R. A. (1985). Acoustic backscattering at low grazing angles from the ocean bottom. part ii. statistical characteristics of bottom backscatter at a shallow water site. The Journal of the Acoustical Society of America, 77(3):975–982.

[Chou et al., 2021] Chou, E., Southall, B. L., Robards, M., and Rosenbaum, H. C. (2021). International policy, recommendations, actions and mitigation efforts of anthropogenic underwater noise. Ocean & Coastal Management, 202:105427.

[Christensen et al., 1943] Christensen, R. J., Raitt, R. W., Parker, C. H., Schafer, T. H. S., Frautschy, J. D., and Sheehy, M. J. (1943). The discrimination of transducers against reverberation. Technical report, Reverberation group. University of California Division of War Research At the U. S. Navy Radio and Sound Laboratory. San Diego, California.

[Clarke et al., 2012] Clarke, J. H., Michael, Z., Christopher, R., and Philip, R. (2012). Optimal use of multibeam technology in the study of shelf morphodynamics. In Sediments, Morphology, and Sedimentary Processes on Continental Shelves: Advances in Technologies, Research, and Applications, pages 1–28. Blackwell.

[Clay and Medwin, 1977] Clay, C. S. and Medwin, H. (1977). Acoustical oceanography: principles and applications. New York, NY (USA) Wiley-Interscience.

[Dacol and Berman, 1988] Dacol, D. K. and Berman, D. H. (1988). Sound scattering from a randomly rough fluid–solid interface. The Journal of the Acoustical Society of America, 84(1):292–302.

[Davies, 1954] Davies, H. (1954). The reflection of electromagnetic waves from a rough surface. Proceedings of the IEE-Part IV: Institution Monographs, 101(7):209–214.

[Dawe, 1997] Dawe, R. L. (1997). Detection threshold modelling explained. Technical report, Defence science and technology organisation, Canberra (Australia).

[Dawe and Galbreath, 1997] Dawe, R. L. and Galbreath, E. R. (1997). Enhancement using colour for sonar displays. Fifth international congress on sound and vibrations, Adelaide, South Australia.

[Del Balzo et al., 1997] Del Balzo, D. R., Leclere, J. H., and Collins, M. J. (1997). Critical angle and seabed scattering issues for active-sonar performance predictions in shallow water. High Frequency Seafloor Acoustics (SACLANTCEN Conference Proceedings CP-45), pp. 123-130.

[Demer et al., 2017] Demer, D., Andersen, L., Bassett, C., Berger, L., Chu, D., Condiotty, J., and Cutter, G. (2017). Evaluation of a wideband echosounder for fisheries and marine ecosystem science. ICES Cooperative Research Report, n°336.

[Desharnais and Ellis, 1997] Desharnais, F. and Ellis, D. D. (1997). Data-model comparisons of reverberation at three shallow-water sites. IEEE Journal of Oceanic Engineering, 22(2):309–316.

[Dolan and Lucieer, 2014] Dolan, M. F. J. and Lucieer, V. L. (2014). Variation and uncertainty in bathymetric slope calculations using geographic information systems. Marine Geodesy, 37(2):187–219.

[Dosso and Holland, 2006] Dosso, S. E. and Holland, C. W. (2006). Geoacoustic uncertainties from viscoelastic inversion of seabed reflection data. IEEE Journal of Oceanic Engineering, 31(3):657–671.

[Duncan et al., 2013] Duncan, A. J., Parnum, I. M., and Henley, P. J. (2013). Efficient modelling of mid to high frequency underwater acoustic propagation. In Proceedings of acoustics.

[Eleftherakis et al., 2012] Eleftherakis, D., Amiri-Simkooei, A., Snellen, M., and Simons, D. G. (2012). Improving riverbed sediment classification using backscatter and depth residual features of multi-beam echo-sounder systems. The Journal of the Acoustical Society of America, 131(5):3710–3725.

[Eleftherakis et al., 2018] Eleftherakis, D., Berger, L., Le Bouffant, N., Pacault, A., Augustin, J.-M., and Lurton, X. (2018). Backscatter calibration of high-frequency multibeam echosounder using a reference single-beam system, on natural seafloor. Marine Geophysical Research, 39(1-2):55–73.

[Ellis and Crowe, 1991] Ellis, D. D. and Crowe, D. V. (1991). Bistatic reverberation calculations using a three-dimensional scattering function. The Journal of the Acoustical Society of America, 89(5):2207–2214.

[Ellis and Franklin, 1987] Ellis, D. D. and Franklin, J. (1987). The importance of hybrid ray paths, bottom loss, and facet reflection on ocean bottom reverberation. In Progress in Underwater Acoustics, pages 75–84. Springer.

[Essen, 1994] Essen, H. H. (1994). Scattering from a rough sedimental seafloor containing shear and layering. The Journal of the Acoustical Society of America, 95(3):1299–1310.

[Faran, 1951] Faran, J. J. (1951). Sound scattering by solid cylinders and spheres. The Journal of the Acoustical Society of America, 23(4):405–418.

[Ferrara et al., 2011] Ferrara, G., Migliaccio, M., Nunziata, F., and Sorrentino, A. (2011). Generalized-k (gk)-based observation of metallic objects at sea in full-resolution synthetic aperture radar (SAR) data: A multipolarization study. IEEE Journal of Oceanic Engineering, 36(2):195–204.

[Ferretti et al., 2015] Ferretti, R., Fumagalli, E., Caccia, M., and Bruzzone, G. (2015). Seabed classification using a single beam echosounder. In OCEANS 2015 - Genova, pages 1–5.

[Fezzani and Berger, 2018] Fezzani, R. and Berger, L. (2018). Analysis of calibrated seafloor backscatter for habitat classification methodology and case study of 158 spots in the bay of biscay and celtic sea. Marine Geophysical Research, 39(1):169–181.

[Fezzani et al., 2021] Fezzani, R., Berger, L., le Bouffant, N., Fonseca, L., and Lurton, X. (2021). Multispectral and multiangle measurements of acoustic seabed backscatter acquired with a tilted calibrated echosounder. The Journal of the Acoustical Society of America, 149(6):4503–4515.

[Foldy, 1946] Foldy, L. L. (1946). Basic methods for the calibration of sonar equipment. Technical report, Office of Scientific Research and Development, National Defense Research Committee, Divison 6., Washington D.C. (USA).

[Fonseca et al., 2021] Fonseca, L., Lurton, X., Fezzani, R., Augustin, J.-M., and Berger, L. (2021). A statistical approach for analyzing and modeling multibeam echosounder backscatter, including the influence of high-amplitude scatterers. The Journal of the Acoustical Society of America, 149(1):215–228.

[Fonseca and Mayer, 2007] Fonseca, L. and Mayer, L. (2007). Remote estimation of surficial seafloor properties through the application angular range analysis to multibeam sonar data. Marine Geophysical Researches, 28(2):119–126.

[Foote, 1982] Foote, K. G. (1982). Optimizing copper spheres for precision calibration of hydroacoustic equipment. The Journal of the Acoustical Society of America, 71(3):742–747.

[Foote, 1983] Foote, K. G. (1983). Maintaining precision calibrations with optimal copper spheres. The Journal of the Acoustical Society of America, 73(3):1054–1063.

[Foote, 1987] Foote, K. G. (1987). Calibration of acoustic instruments for fish density estimation: A practical guide. int. coun. explor. Sea Coop. Res. Rep., 144:1–69.

[Foote, 2014] Foote, K. G. (2014). Discriminating between the nearfield and the farfield of acoustic transducers. The Journal of the Acoustical Society of America, 136(4):1511–1517.

[Foote et al., 2005] Foote, K. G., Chu, D., Hammar, T. R., Baldwin, K. C., Mayer, L. A., Hufnagle, L. C., and Jech, J. M. (2005). Protocols for calibrating multibeam sonar. The Journal of the Acoustical Society of America, 117(4):2013–2027.

[Foote and MacLennan, 1984] Foote, K. G. and MacLennan, D. N. (1984). Comparison of copper and tungsten carbide calibration spheres. The Journal of the Acoustical Society of America, 75(2):612–616.

[Francois and Garrison, 1982] Francois, R. E. and Garrison, G. R. (1982). Sound absorption based on ocean measurements. part ii: Boric acid contribution and equation for total absorption. The Journal of the Acoustical Society of America, 72(6):1879–1890.

[Fromm, 2020] Fromm, A. R. (2020). Spatial distribution and directionality of acoustic scattering in rocky environments. Technical report, Naval postgraduate school, Monteray, California (USA).

[Fuhs, 1982] Fuhs, A. E. (1982). Radar cross section lectures. Technical report, Naval postgraduate school, Monterey, California, USA.

[Gabella, 2014] Gabella, M. (2014). Variance of fluctuating radar echoes from thermal noise and randomly distributed scatterers. Atmosphere, 5(1):92–100.

[Gallaudet, 2001] Gallaudet, T. C. (2001). Shallow water acoustic backscatter and reverberation measurements using a 68-kHz cylindrical array: a dissertation. Calhoun.

[Galloway, 2008] Galloway, J. L. (2008). Systematic acoustic seafloor habitat mapping of the British Columbia coast. Marine habitat mapping technology for Alaska. Alaska Sea Grant College Program, University of Alaska Fairbanks.

[Garlan and Demoulin, 1997] Garlan, T. and Demoulin, X. (1997). Sedimentological acoustics: an attempt to reduce the gap between acoustical modeling and sedimentological survey. High Frequency Seafloor Acoustics (SACLANTCEN Conference Proceedings CP-45), pp. 163-170.

[Gensane, 1989] Gensane, M. (1989). A statistical study of acoustic signals backscattered from the sea bottom. IEEE Journal of Oceanic Engineering, 14(1):84–93.

[Goff et al., 2004] Goff, J. A., Kraft, B. J., Mayer, L. A., Schock, S. G., Sommerfield, C. K., Olson, H. C., Gulick, S. P., and Nordfjord, S. (2004). Seabed characterization on the New Jersey middle and outer shelf: correlatability and spatial variability of seafloor sediment properties. Marine Geology, 209(1):147–172.

[Goodman, 1975] Goodman, J. W. (1975). Statistical Properties of Laser Speckle Patterns, pages 9–75. Springer Berlin Heidelberg, Berlin, Heidelberg.

[Gorska et al., 2018] Gorska, N., Kowalska-Duda, E., Pniewski, F., and Latała, A. (2018). On diel variability of marine sediment backscattering properties caused by microphytobenthos photosynthesis: Impact of environmental factors. Journal of Marine Systems, 182:1–11.

[Gregoire, 2016] Gregoire, G. (2016). Dynamique sédimentaire et évolution holocène d'un système macrotidal semi-fermé : l'exemple de la rade de Brest. PhD thesis, Institut français de recherche pour l'exploitation de la mer (Ifremer), Brest.

[Gregoire et al., 2016] Gregoire, G., Ehrhold, A., Roy, P. L., Jouet, G., and Garlan, T. (2016). Modern morpho-sedimentological patterns in a tide-dominated estuary system: the Bay of Brest (west Britanny, france). Journal of Maps, 12(5):1152–1159.

[Hare, 2001] Hare, R. (2001). Error budget analysis for US Naval Oceanographic Office (NAVOCEANO) hydrographic survey systems. University of Southern Mississippi, Hydrographic Science Research Center for the Naval Oceanographic Office.

[Hare et al., 1995] Hare, R., Godin, A., and Mayer, L. (1995). Accuracy estimation of canadian swath (multibeam) and sweep (multitransducer) sounding systems. Canadian Hydrographic Service Internal Report.

[Harris, 1978] Harris, F. (1978). On the use of windows for harmonic analysis with the discrete Fourier transform. Proceedings of the IEEE, 66(1):51–83.

[Hickling, 1962] Hickling, R. (1962). Analysis of echoes from a solid elastic sphere in water. The Journal of the Acoustical Society of America, 34(10):1582–1592.

[Hiroji, 2016] Hiroji, A. (2016). Extracting sonar relative beam patterns for multi-sector multibeam sonar. PhD thesis, University of New Brunswick (Canada).

[Holden, 2014] Holden, A. (2014). Acoustical terminology in the sonar modelling handbook. The Journal of the Acoustical Society of America, 136(4):2217–2217.

[Howell, 2000] Howell, H. R. (2000). Inferring bottom acoustic properties from AN/SQQ-32 sonar reverberation data. Technical report, Naval postgraduate school, Monterey, California, USA.

[Huang et al., 2013] Huang, Z., Siwabessy, J., Nichol, S., Anderson, T., and Brooke, B. (2013). Predictive mapping of seabed cover types using angular response curves of multibeam backscatter data: Testing different feature analysis approaches. Continental Shelf Research, 61-62:12–22.

[Hughes Clarke et al., 1997] Hughes Clarke, J. E., Danforth, B., and Valentine, P. (1997). Areal seabed classification using backscatter angular response at 95kHz. High Frequency Seafloor Acoustics (SACLANTCEN Conference Proceedings CP-45), pp. 243-250.

[Ierodiaconou et al., 2018] Ierodiaconou, D., Schimel, A. C., Kennedy, D., Monk, J., Gaylard, G., Young, M., Diesing, M., and Rattray, A. (2018). Combining pixel and object based image analysis of ultra-high resolution multibeam bathymetry and backscatter for habitat mapping in shallow marine waters. Marine Geophysical Research, 39(1-2):271–288.

[Innangi et al., 2015] Innangi, S., Barra, M., Di Martino, G., Parnum, I., Tonielli, R., and Mazzola, S. (2015). Reson Seabat 8125 backscatter data as a tool for seabed characterization (Central Mediterranean, Southern Italy): Results from different processing approaches. Applied Acoustics, 87:109–122.

[Ishimaru, 1977] Ishimaru, A. (1977). Theory and application of wave propagation and scattering in random media. Proceedings of the IEEE, 65(7):1030–1061.

[Ishimaru, 1978] Ishimaru, A. (1978). Wave propagation and scattering in random media, volume 2. Academic Press New York.

[Ivakin and Lysanov, 1981] Ivakin, A. and Lysanov, Y. P. (1981). Underwater sound scattering by volume inhomogeneities of a bottom medium bounded by a rough surface. Sov. Phys. Acoust, 27(3):212–215.

[Jackson and Richardson, 2007] Jackson, D. and Richardson, M. (2007). High-frequency seafloor acoustics. Springer Science & Business Media.

[Jackson et al., 2009] Jackson, D. R., Richardson, M. D., Williams, K. L., Lyons, A. P., Jones, C. D., Briggs, K. B., and Tang, D. (2009). Acoustic observation of the time dependence of the roughness of sandy seafloors. IEEE Journal of Oceanic Engineering, 34(4):407–422.

[Jackson et al., 1986] Jackson, D. R., Winebrenner, D. P., and Ishimaru, A. (1986). Application of the composite roughness model to high-frequency bottom backscattering. The Journal of the Acoustical Society of America 97, 1410.

[Jakeman and Pusey, 1976] Jakeman, E. and Pusey, P. (1976). A model for non-rayleigh sea echo. IEEE Transactions on Antennas and Propagation, 24(6):806–814.

[Jakeman and Tough, 1987] Jakeman, E. and Tough, R. J. A. (1987). Generalized k distribution: a statistical model for weak scattering. J. Opt. Soc. Am. A, 4(9):1764–1772.

[Jao and Elbaum, 1978] Jao, J. K. and Elbaum, M. (1978). First-order statistics of a non-rayleigh fading signal and its detection. Proceedings of the IEEE, 66(7):781–789.

[Jenserud et al., 2001] Jenserud, T., Simons, D., and Cristol, X. (2001). Rumble project-scattering index models. Norwegian Defence Research Establishment (Norway).

[Jumars et al., 1996] Jumars, P. A., Jackson, D. R., Gross, T. F., and Sherwood, C. (1996). Acoustic remote sensing of benthic activity: A statistical approach. Limnology and Oceanography, 41(6):1220–1241.

[Karoui et al., 2015] Karoui, I., Quidu, I., and Legris, M. (2015). Automatic sea-surface obstacle detection and tracking in forward-looking sonar image sequences. IEEE Transactions on Geoscience and Remote Sensing, 53(8):4661–4669.

[Kluyver, 1905] Kluyver, J. C. (1905). A local probability problem. Koninklijke Nederlandse Akademie van Wetenschappen Proceedings Series B Physical Sciences, 8:341–350.

[Kuo, 1964] Kuo, E. Y. T. (1964). Wave scattering and transmission at irregular surfaces. The Journal of the Acoustical Society of America, 36(11):2135–2142.

[Ladroit et al., 2018] Ladroit, Y., Lamarche, G., and Pallentin, A. (2018). Seafloor multibeam backscatter calibration experiment: comparing 45 degres-tilted 38-kHz split-beam echosounder and 30-kHz multibeam data. Marine Geophysical Research, 39(1):41–53.

[Lamarche et al., 2011] Lamarche, G., Lurton, X., Verdier, A.-L., and Augustin, J.-M. (2011). Quantitative characterisation of seafloor substrate and bedforms using advanced processing of multibeam backscatter — application to Cook Strait, New Zealand. Continental Shelf Research 31.

[Le Chenadec, 2004] Le Chenadec, G. (2004). Analyse de descripteurs énergétiques et statistiques de signaux sonar pour la caractérisation des fonds marins. PhD thesis, Université de Bretagne Occidentale, France.

[Le Deunf et al., 2020] Le Deunf, J., Debese, N., Schmitt, T., and Billot, R. (2020). A review of data cleaning approaches in a hydrographic framework with a focus on bathymetric multibeam echosounder datasets. Geosciences, 10(7).

[Lehmann and Casella, 2006] Lehmann, E. L. and Casella, G. (2006). Theory of point estimation. Springer Science & Business Media.

[Listewnik, 2013] Listewnik, K. (2013). Sound silencing problem of underwater vehicles. In Solid State Phenomena, volume 196, pages 212–219. Trans Tech Publ.

[Lord and Murphy, 1964] Lord, G. E. and Murphy, S. R. (1964). Reception characteristics of a linear array in a random transmission medium. The Journal of the Acoustical Society of America, 36(5):850–854.

[Lucieer et al., 2018] Lucieer, V., Roche, M., Degrendele, K., Malik, M., Dolan, M., and Lamarche, G. (2018). User expectations for multibeam echo sounders backscatter strength data-looking back into the future. Marine Geophysical Research, 39(1):23–40.

[Lurton, 2010] Lurton, X. (2010). An introduction to underwater acoustics: principles and applications. Springer Science & Business Media.

[Lurton and Augustin, 2010] Lurton, X. and Augustin, J.-M. (2010). A measurement quality factor for swath bathymetry sounders. IEEE Journal of Oceanic Engineering, 35(4):852–862.

[Lurton et al., 2018] Lurton, X., Eleftherakis, D., and Augustin, J.-M. (2018). Analysis of seafloor backscatter strength dependence on the survey azimuth using multibeam echosounder data. Marine Geophysical Research, 39(1-2):183–203.

[Lurton et al., 2015] Lurton, X., Lamarche, G., Brown, C., Lucieer, V., RIce, G., Schimel, A., and Weber, T. (2015). Backscatter measurements by seafloor-mapping sonars: guidelines and recommendations. A collective report by members of the GeoHab Backscatter Working Group, pages 1–200.

[Lysanov and Brekhovskikh, 1982] Lysanov, Y. and Brekhovskikh, L. (1982). Fundamentals of ocean acoustics, volume 8. Springer.

[Mackenzie, 1961] Mackenzie, K. V. (1961). Bottom reverberation for 530 and 1030cps sound in deep water. The Journal of the Acoustical Society of America, 33(11):1498–1504.

[MacLennan, 1981] MacLennan, D. (1981). The theory of solid spheres as sonar calibration targets. Scottish Fish. Res. Rep., 22.

[MacLennan and Dunn, 1984] MacLennan, D. and Dunn, J. (1984). Estimation of sound velocities from resonance measurements on tungsten carbide calibration spheres. Journal of Sound and Vibration, 97(2):321–331.

[MacLennan et al., 2002] MacLennan, D. N., Fernandes, P. G., and Dalen, J. (2002). A consistent approach to definitions and symbols in fisheries acoustics. ICES Journal of Marine Science, 59(2):365–369.

[Majcher et al., 2021] Majcher, J., Quinn, R., Plets, R., Coughlan, M., McGonigle, C., Sacchetti, F., and Westley, K. (2021). Spatial and temporal variability in geomorphic change at tidally influenced shipwreck sites: The use of time-lapse multibeam data for the assessment of site formation processes. Geoarchaeology, 36(3):429–454.

[Malik et al., 2018] Malik, M., Lurton, X., and Mayer, L. (2018). A framework to quantify uncertainties of seafloor backscatter from swath mapping echosounders. Marine Geophysical Research, 39(1-2):151–168.

[Malik et al., 2019] Malik, M., Schimel, A. C., Masetti, G., Roche, M., Le Deunf, J., Dolan, M. F., Beaudoin, J., Augustin, J.-M., Hamilton, T., and Parnum, I. (2019). Results from the first phase of the seafloor backscatter processing software inter-comparison project. Geosciences, 9(12):516.

[Manik, 2012] Manik, H. M. (2012). Seabed identification and characterization using sonar. Advances in Acoustics and Vibration, 2012.

[Mansour et al., 2013] Mansour, A., Leblond, I., Hamad, D., and Artigas, L. F. (2013). Wireless sensor networks for ecosystem monitoring & port surveillance. In 2nd Symposium on Wireless Sensor and Cellular Networks 2013 (WSCN 2013).

[Marandino, 1987] Marandino, D. (1987). Low-frequency reverberation measurements with an activated towed array: Scattering strengths and statistics. Technical report, SACLANT ASW research centre, La Spezia (Italy).

[Mayer, 2006] Mayer, L. A. (2006). Frontiers in seafloor mapping and visualization. Marine Geophysical Researches, 27(1):7–17.

[McKinney and Anderson, 1964] McKinney, C. and Anderson, C. (1964). Measurements of backscattering of sound from the ocean bottom. The Journal of the Acoustical Society of America, 36(1):158–163.

[Middleton et al., 1960] Middleton, D., of Electrical, I., and Engineers, E. (1960). An introduction to statistical communication theory, volume 960. McGraw-Hill New York.

[Millar, 2011] Millar, R. B. (2011). Maximum likelihood estimation and inference: with examples in R, SAS and ADMB. John Wiley & Sons.

[Montereale-Gavazzi et al., 2019] Montereale-Gavazzi, G., Roche, M., Degrendele, K., Lurton, X., Terseleer, N., Baeye, M., Francken, F., and Van Lancker, V. (2019). Insights into the short-term tidal variability of multibeam backscatter from field experiments on different seafloor types. Geosciences, 9(1):34.

[Mopin et al., 2021] Mopin, I., Chenadec, G. L., Legris, M., Blondel, P., Marchal, J., and Zerr, B. (2021). Comparison of methods employed to extract information contained in seafloor backscatter. Proceedings of Meetings on Acoustics, 44(1):070036.

[Mopin et al., 2022] Mopin, I., Marchal, J., Legris, M., Chenadec, G. L., Blondel, P., and Zerr, B. (2022). Design and field testing of a non-linear single-beam echosounder for multi-frequency seabed characterization. Applied Acoustics, 187:108490.

[Narayanan et al., 1994] Narayanan, V., Shankar, P., and Reid, J. (1994). Non-rayleigh statistics of ultrasonic backscattered signals. IEEE Transactions on Ultrasonics, Ferroelectrics, and Frequency Control, 41(6):845–852.

[Nicolaescu and Oroian, 2001] Nicolaescu, L. and Oroian, T. (2001). Radar cross section. In 5th International Conference on Telecommunications in Modern Satellite, Cable and Broadcasting Service. TELSIKS 2001. Proceedings of Papers (Cat. No.01EX517), volume 1, pages 65–68 vol.1.

[Nolle et al., 1963] Nolle, A. W., Hoyer, W. A., Mifsud, J. F., Runyan, W. R., and Ward, M. B. (1963). Acoustical properties of water filled sands. The Journal of the Acoustical Society of America, 35(9):1394–1408.

[Novarini and Caruther, 1998] Novarini, J. C. and Caruther, J. W. (1998). A simplified approach to backscattering from a rough seafloor with sediment inhomogeneities. IEEE Journal of Oceanic Engineering, 23(3):157–166.

[Novarini and Caruthers, 1994] Novarini, J. C. and Caruthers, J. W. (1994). The partition wavenumber in acoustic backscattering from a two-scale rough surface described by a power-law spectrum. IEEE Journal of Oceanic Engineering, 19(2):200–207.

[Nurlatifah et al., 2021] Nurlatifah, Yamauchi, T., Nakajima, R., Tsuchiya, M., Yabuki, A., Kitahashi, T., Nagano, Y., Isobe, N., and Nakata, H. (2021). Plastic additives in deep-sea debris collected from the western north pacific and estimation for their environmental loads. Science of The Total Environment, 768:144537.

[Ocheltree and Frizzel, 1989] Ocheltree, K. and Frizzel, L. (1989). Sound field calculation for rectangular sources. IEEE Transactions on Ultrasonics, Ferroelectrics, and Frequency Control, 36(2):242–248.

[Ogilvy, 1988] Ogilvy, J. A. (1988). Computer simulation of acoustic wave scattering from rough surfaces. Journal of Physics D: Applied Physics, 21(2):260–277.

[Ogilvy and Merklinger, 1991] Ogilvy, J. A. and Merklinger, H. M. (1991). Theory of wave scattering from random rough surfaces. Acoustical Society of America.

[Ollivier, 1995] Ollivier, F. (1995). Conception et réalisation d'un sonar latéral bathymétrique à haute résolution avec voies préformées compensées en attitude. Theses, Université Pierre et Marie Curie (UPMC Paris 6), France.

[Ona et al., 2009] Ona, E., Mazauric, V., and Andersen, L. N. (2009). Calibration methods for two scientific multibeam systems. ICES Journal of Marine Science, 66(6):1326–1334.

[Papoulis and Pillai, 2002] Papoulis, A. and Pillai, S. U. (2002). Probability, random variables, and stochastic processes. Tata McGraw-Hill Education.

[Patterson, 1963] Patterson, R. B. (1963). Backscatter of sound from a rough boundary. The Journal of the Acoustical Society of America, 35(12):2010–2013.

[Pearson, 1906] Pearson, K. (1906). Drapers company research memoirs, biometric series, iii. 1905, pages 1–54.

[Penrose et al., 2008] Penrose, J. D., Gavrilov, A., and Parnum, I. M. (2008). Statistics of seafloor backscatter measured with multibeam sonar systems. Journal of the Acoustical Society of America, 123(5):3628–3628.

[Petillot et al., 2010] Petillot, Y., Pailhas, Y., Sawas, J., Valeyrie, N., and Bell, J. (2010). Target recognition in synthetic aperture and high resolution side-scan sonar. In Proc. European Conference on Underwater Acoustics, pages 99–106.

[Petillot et al., 2001] Petillot, Y., Tena Ruiz, I., and Lane, D. (2001). Underwater vehicle obstacle avoidance and path planning using a multi-beam forward looking sonar. IEEE Journal of Oceanic Engineering, 26(2):240–251.

[Pluquet and Ehrhold, 2009] Pluquet, F. and Ehrhold, A. (2009). Une nouvelle stratégie d'étude des habitats marins littoraux au moyen de la vedette acoustique V/O Haliotis. (*A new study strategy of coastal marine habitats with research vessel R/V Haliotis*). Technical report, Ifremer/DYNECO/EB/09-02/FP.

[Pouliquen and Lurton, 1992] Pouliquen, E. and Lurton, X. (1992). Identification de la nature du fond de la mer à l'aide de signaux d'écho-sondeurs. Le Journal de Physique IV, 2(C1):C1–941.

[Prampolini et al., 2018] Prampolini, M., Blondel, P., Foglini, F., and Madricardo, F. (2018). Habitat mapping of the maltese continental shelf using acoustic textures and bathymetric analyses. Estuarine, Coastal and Shelf Science, 207:483–498.

[Preston, 2009] Preston, J. (2009). Automated acoustic seabed classification of multibeam images of Stanton Banks. Applied Acoustics, 70(10):1277–1287. The Application of Underwater Acoustics for Seabed Habitat Mapping.

[Pusey et al., 1974] Pusey, P. N., Schaefer, D. W., and Koppel, D. E. (1974). Single-interval statistics of light scattered by identical independent scatterers. Journal of Physics A: Mathematical, Nuclear and General, 7(4):530–540.

[Rathod, 2020] Rathod, V. T. (2020). A review of acoustic impedance matching techniques for piezoelectric sensors and transducers. Sensors, 20(14):4051.

[Rayleigh, 1907] Rayleigh, L. (1907). On the dynamical theory of gratings. Proceedings of the Royal Society of London. Series A, Containing Papers of a Mathematical and Physical Character, 79(532):399–416.

[Rivet et al., 2007] Rivet, B., Girin, L., and Jutten, C. (2007). Log-rayleigh distribution: A simple and efficient statistical representation of log-spectral coefficients. IEEE Transactions on Audio, Speech, and Language Processing, 15(3):796–802.

[Rohou et al., 2019] Rohou, S., Jaulin, L., Mihaylova, L., Le Bars, F., and Veres, S. M. (2019). Reliable robot localization: a constraint-programming approach over dynamical systems. John Wiley & Sons.

[Samaran et al., 2019] Samaran, F., Berne, A., Leroy, E. C., Moreira, S., Stafford, K. M., Maia, M., and Royer, J.-Y. (2019). Antarctic blue whales (balaenoptera musculus intermedia) recorded at the equator in the atlantic ocean. Marine Mammal Science, 35(2):641–648.

[Saporta, 2006] Saporta, G. (2006). Probabilités, analyse des données et statistique. Editions technip.

[Savage and Meredith, 1996] Savage, K. D. and Meredith, R. W. (1996). Modeled high-frequency acoustic backscattered levels from range-independent and simplistic range-dependent sand bottoms. Technical report, Naval research lab, Stennis Space Center, Mississippi (USA).

[Scanlon et al., 1996] Scanlon, G. A., Bourke, R. H., and Wilson, J. H. (1996). Estimation of bottom scattering strength from measured and modeled mid-frequency sonar reverberation levels. IEEE Journal of Oceanic Engineering, 21(4):440–451.

[Sevaldsen, 2002] Sevaldsen, E. (2002). Bottom reverberation predictions with the acoustic model Lybin-a comparison between three bottom backscattering algorithms. Norwegian Defence Research Establishment (Norway).

[Shepherd and Milnarich, 1973] Shepherd, W. L. and Milnarich, P. (1973). Basic relations between a rayleigh-distributed randomly varying voltage and a decibel record of the voltage. Proceedings of the IEEE, 61(12):1765–1766.

[Sherman and Butler, 2007] Sherman, C. H. and Butler, J. L. (2007). Transducers and arrays for underwater sound, volume 4. Springer.

[Siddiqui, 1964] Siddiqui, M. (1964). Statistical inference for rayleigh distributions. Journal of Research of the National Bureau of Standards, Sec. D, 68(9):1007.

[Siddiqui, 1962] Siddiqui, M. M. (1962). Some problems connected with rayleigh distributions. Journal of Research of the National Bureau of standards, 66(2):167–174.

[Simmonds and MacLennan, 2008] Simmonds, J. and MacLennan, D. N. (2008). Fisheries acoustics: theory and practice. John Wiley & Sons.

[Simons and Snellen, 2009] Simons, D. G. and Snellen, M. (2009). A Bayesian approach to seafloor classification using multi-beam echo-sounder backscatter data. Applied Acoustics, 70(10):1258–1268.

[Snellen et al., 2011] Snellen, M., Siemes, K., and Simons, D. G. (2011). Model-based sediment classification using single-beam echosounder signals. The Journal of the Acoustical Society of America, 129(5):2878–2888.

[Stanic and Kennedy, 1992] Stanic, S. and Kennedy, E. (1992). Fluctuations of high-frequency shallow-water seafloor reverberation. The Journal of the Acoustical Society of America, 91(4):1967–1973.

[Stanton and Clay, 1986] Stanton, T. and Clay, C. (1986). Sonar echo statistics as a remote-sensing tool: Volume and seafloor. IEEE Journal of Oceanic Engineering, 11(1):79–96.

[Stanton et al., 2018] Stanton, T. K., Lee, W.-J., and Baik, K. (2018). Echo statistics associated with discrete scatterers: A tutorial on physics-based methods. The Journal of the Acoustical Society of America, 144(6):3124–3171.

[Stanton et al., 1994] Stanton, T. K., Wiebe, P. H., Chu, D., Benfield, M. C., Scanlon, L., Martin, L., and Eastwood, R. L. (1994). On acoustic estimates of zooplankton biomass. ICES Journal of Marine Science, 51(4):505–512.

[Stockhausen, 1963] Stockhausen, J. H. (1963). Scattering from the volume of an inhomogeneous half-space. The Journal of the Acoustical Society of America, 35(11):1893–1893.

[Strutt and Rayleigh, 1945] Strutt, J. W. and Rayleigh, B. (1945). The theory of sound. Dover Publications.

[Stutzman, 1998] Stutzman, W. (1998). Estimating directivity and gain of antennas. IEEE Antennas and Propagation Magazine, 40(4):7–11.

[Taraldsen et al., 2015] Taraldsen, G., Berge, T., Haukland, F., Lindqvist, B. H., and Jonasson, H. (2015). Uncertainty of decibel levels. The Journal of the Acoustical Society of America, 138(3):EL264–EL269.

[Trevorrow, 2004] Trevorrow, M. V. (2004). Statistics of fluctuations in high-frequency low-grazing-angle backscatter from a rocky sea bed. IEEE Journal of Oceanic Engineering, 29(2):236–245.

[Trzcinska et al., 2021] Trzcinska, K., Tegowski, J., Pocwiardowski, P., Janowski, L., Zdroik, J., Kruss, A., Rucinska, M., Lubniewski, Z., and Schneider von Deimling, J. (2021). Measurement of seafloor acoustic backscatter angular dependence at 150 kHz using a multibeam echosounder. Remote Sensing, 13(23):4771.

[Tsang and Kong, 2004] Tsang, L. and Kong, J. A. (2004). Scattering of electromagnetic waves: advanced topics, volume 26. John Wiley & Sons.

[Tuthill et al., 1988] Tuthill, T., Sperry, R., and Parker, K. (1988). Deviations from rayleigh statistics in ultrasonic speckle. Ultrasonic Imaging, 10(2):81–89.

[Urgeles et al., 2002] Urgeles, R., Locat, J., Schmitt, T., and Clarke, J. E. H. (2002). The july 1996 flood deposit in the saguenay fjord, quebec, canada: implications for sources of spatial and temporal backscatter variations. Marine Geology, 184(1-2):41–60.

[Urick, 1954] Urick, R. J. (1954). The backscattering of sound from a harbor bottom. The Journal of the Acoustical Society of America, 26(2):231–235.

[Urick, 1966] Urick, R. J. (1966). Correlative properties of ambient noise at bermuda. The Journal of the Acoustical Society of America, 40(5):1108–1111.

[Urick, 1983] Urick, R. J. (1983). Principles of underwater sound 3rd edition. Peninsula Publishing Los Altos, California (USA).

[Vagle et al., 1996] Vagle, S., Foote, K., Trevorrow, M., and Farmer, D. (1996). A technique for calibration of monostatic echosounder systems. IEEE Journal of Oceanic Engineering, 21(3):298–305.

[van Walree et al., 2005] van Walree, P. A., Tęgowski, J., Laban, C., and Simons, D. G. (2005). Acoustic seafloor discrimination with echo shape parameters: A comparison with the ground truth. Continental Shelf Research, 25(18):2273–2293.

[Velegrakis et al., 2010] Velegrakis, A. F., Ballay, A., Poulos, S. E., Radzevičius, R., Bellec, V. K., and Manso, F. (2010). European marine aggregates resources: Origins, usage, prospecting and dredging techniques. Journal of Coastal Research, pages 1–14.

[Vickery, 1998] Vickery, K. (1998). Acoustic positioning systems. a practical overview of current systems. In Proceedings of the 1998 Workshop on Autonomous Underwater Vehicles (Cat. No. 98CH36290), pages 5–17. IEEE.

[Wackerly et al., 2014] Wackerly, D., Mendenhall, W., and Scheaffer, R. L. (2014). Mathematical statistics with applications. Cengage Learning.

[Wagner et al., 1983] Wagner, R., Smith, S., Sandrik, J., and Lopez, H. (1983). Statistics of speckle in ultrasound b-scans. IEEE Transactions on Sonics and Ultrasonics, 30(3):156–163.

[Ward, 1981] Ward, K. (1981). Compound representation of high resolution sea clutter. Electronics letters, 17(16):561–563.

[Watson and McGirr, 1972] Watson, W. and McGirr, R. (1972). An Active Sonar Performance Prediction Model, volume 286. Naval Undersea Research and Development Center.

[Weinberg, 1982] Weinberg, H. (1982). Generic sonar model. In OCEANS 82, pages 201–205.

[Williams, 1951] Williams, A. O. (1951). The piston source at high frequencies. The Journal of the Acoustical Society of America, 23(1):1–6.

[Zerr et al., 2005] Zerr, B., Mailfert, G., Bertholom, A., and Ayreault, H. (2005). Sidescan sonar image processing for AUV navigation. In Europe Oceans 2005, volume 1, pages 124–130 Vol. 1.

[Zhang et al., 2020] Zhang, K., Li, Q., Zhu, H., Yang, F., and Wu, Z. (2020). Acoustic deep-sea seafloor characterization accounting for heterogeneity effect. IEEE Transactions on Geoscience and Remote Sensing, 58(5):3034–3042.

[Zhu et al., 2014] Zhu, S., Tang, G., Xiong, L., and Zhang, G. (2014). Uncertainty of slope length derived from digital elevation models of the Loess Plateau, China. Journal of Mountain Science, 11(5):1169–1181.

[Zrnic, 1975] Zrnic, D. S. (1975). Moments of estimated input power for finite sample averages of radar receiver outputs. IEEE Transactions on Aerospace and Electronic Systems, AES-11(1):109–113.

Titre : Caractérisation précise de la réponse acoustique du fond marin pour l'amélioration de l'identification des fonds

Mots clés : Rétrodiffusion, incertitude, échosondeur, hydrographie, acoustique sous-marine

Résumé : Les échosondeurs sont aujourd'hui largement utilisés en hydrographie pour mesurer la bathymétrie ; ils fournissent une information de réflectivité du fond à partir de la mesure de la réponse acoustique du fond marin.
L'objectif de cette thèse est de proposer une description détaillée de la métrologie de la réponse acoustique des fonds fondée sur les états de l'art théoriques et opérationnels. Les méthodes empiriques pour calculer l'index de rétrodiffusion, développées en opération par les utilisateurs, logiciels, ou les fabricants d'échosondeurs, sont confrontées aux considérations de la littérature. Le lien entre les deux domaines est fait en utilisant un modèle stochastique se basant sur le traitement bathymétrique des sondeurs mono- et multi-faisceaux.
À partir de ce modèle, une définition précise de la réponse acoustique du fond marin est proposée et des estimateurs de l'index de rétrodiffusion sont calculés. Le meilleur estimateur est ensuite identifié par comparaison des biais, variances et rapidité de convergence.
Enfin, une mesure de la précision de l'acquisition des index de rétrodiffusion avec des sondeurs mono- et multi-faisceaux est proposée, basée sur l'incertitude de la mesure. Cette incertitude peut être utilisée en tant qu'information *a priori* sur la qualité d'un levé planifié, ou comme une indication *a posteriori* sur la précision de la mesure de la réponse du fond marin.

Title: Accurate characterisation of seafloor acoustic response to improve seabed identification

Keywords: Backscatter, uncertainty, echosounder, hydrography, underwater acoustics

Abstract: Echosounders are commonly used in hydrography to measure bathymetry; they can also provide seabed reflectivity information based on the measurement of the seafloor acoustic response.
The aim of the PhD is to provide a detailed description of the seafloor acoustic response metrology based on both theoretical and practical states of the art. Empirical methods to compute the backscattering strength, developed in operations by users, softwares or echosounder manufacturers, are confronted to theoretical statements from literature. The link between the two domains is made using a stochastic model based on the bathymetric processing of singlebeam and multibeam echosounders (respectively SBES and MBES).
From this model, an accurate definition of the seafloor acoustic response is proposed and estimators of the backscattering strength are derived. The best estimator is then identified by comparing their bias, variances, and speeds of convergence.
Finally, a measure of the accuracy of backscattering strength acquisitions with SBES or MBES is proposed, based on the uncertainty of the measurements. This uncertainty can be used as an *a priori* information about the quality of a planned survey, or as an *a posteriori* indication of precision of the seafloor response measurements.